# On the evaluation of time-dependent fluid-dynamic forces on bluff bodies

Thesis by

Flavio Noca

In Partial Fulfillment of the Requirements

for the Degree of

Doctor of Philosophy

California Institute of Technology

Pasadena, California

1997

(Submitted May 20, 1997)

# Acknowledgements

I would first like to thank my wife Muriel, as well as my mom, my dad, and my sister Patrizia, who have always been supportive throughout my college education.

I would like to extend my thanks to the people that were directly involved with the development of this work, my advisor Anatol Roshko, Mory Gharib, Anthony Leonard, Ron Henderson, Doug Shiels and Dave Jeon. I would also like to thank the remaining members of my committee, Hans Hornung and Chris Brennen.

My thanks are also directed towards the people who provided help and advice with the practical aspects of my laboratory projects, especially Pavel Svitek, Joe Haggerty, and Derek Lisoski.

Finally, I would like to thank all the friends who turned these graduate years into a very pleasant experience, in order of increasing sanity, Petros Koumoutsakos, Don Kendrick, Guillaume Vendroux, Jacques Bélanger, Patrick Germain, Philippe Geubelle, Rob Mallet, Mark Walter, Philippe Adam, Sid Valluri, Patrice and Ping, Eric and Sylviane, Raymond and Claire, the members of the soccer club, as well as all the people whom I am now forgetting.

This research was supported by the Office of Naval Research, ONR Grant No. N00014-93-1144 and N00014-94-1-0793, and the Jet Propulsion Laboratory Supercomputing Project (funded from the Nasa Offices of Mission to Planet Earth).

# Abstract

We present some *exact* expressions for the evaluation of time-dependent forces on a body in an incompressible and viscous cross-flow which only require the knowledge of the velocity field (and its derivatives) in a finite and arbitrarily chosen region enclosing the body.

Given a control volume $V$ with external surface $S$ which encloses an arbitrary body, the fluid-dynamic force $\mathbf{F}$ on the body can be evaluated from one of the following three expressions (in abbreviated form):

$$\begin{aligned}
\mathbf{F} &= -\frac{1}{\mathcal{N}-1}\frac{d}{dt}\int_V \mathbf{x}\wedge\boldsymbol{\omega}\,dV + \oint_S \hat{\mathbf{n}}\cdot\boldsymbol{\Upsilon}_1\,dS + \text{body motion terms},\\
\mathbf{F} &= -\frac{d}{dt}\int_V \mathbf{u}\,dV + \oint_S \hat{\mathbf{n}}\cdot\boldsymbol{\Upsilon}_2\,dS + \text{body motion terms},\\
\mathbf{F} &= \text{no volume integral terms} + \oint_S \hat{\mathbf{n}}\cdot\boldsymbol{\Upsilon}_3\,dS + \text{body motion terms},
\end{aligned}$$

where $\mathcal{N}$ is the space dimension, $\mathbf{u}$ is the flow velocity, $\boldsymbol{\omega}$ is the vorticity, $\mathbf{x}$ is the position vector, and the tensors $\boldsymbol{\Upsilon}_1$, $\boldsymbol{\Upsilon}_2$, $\boldsymbol{\Upsilon}_3$ depend only on the velocity field $\mathbf{u}$ and its (spatial and temporal) derivatives.

The first equation is already known for either simply connected domains or inviscid flows. We re-derive it here for viscous flows in doubly connected domains (i.e. domains which include a body). We then obtain the second and third equation through a simple algebraic manipulation of the first equation.

These expressions are particularly useful for experimental techniques like Digital particle Image Velocimetry (DPIV) which provide time sequences of 2D velocity fields but not pressure fields.

They are tested experimentally with DPIV on two-dimensional, low Reynolds number circular cylinder flows. Both steady and unsteady motions are studied.

# Contents

# List of Figures

# Chapter 1 Introduction

## 1.1 Extrinsic vs. intrinsic force measurements

When a bluff body is submerged into a moving fluid, it experiences a force. The existence of such a force has been demonstrated long before the emergence of the science of fluid mechanics. Any wild animal such as a horse who attempts to cross a flowing river knows well the tremendous entraining power of water despite the fact that he knows little about the discoveries of Leonardo da Vinci, Daniel Bernoulli, and Leonhard Euler. Such awareness is the result of an *extrinsic* measurement: the horse "measures" the force of the stream from the strength it has to exert to walk or swim through the water.

On the other hand, if Leonardo, Daniel, or Leonhard were riding the animal, they would observe a vortical, perhaps turbulent, flowfield downstream of the animal and would probably be able to deduce the force exerted by the fluid (the river) on the bluff body (the horse) by applying the equations of fluid mechanics to the observed flow configuration: they would be performing an *intrinsic* measurement.

But let's not get ahead of our horses. We will first examine briefly how *extrinsic* measurements are performed, and we will then expand on *intrinsic* techniques in the remainder of this monograph.

## 1.2 Extrinsic force measurement techniques

### 1.2.1 Local measurements

Before a horse decides to cross the river, he could just put one of his hoofs into the stream and test the streaming power of the water. He would thus be performing a *local* measurement on a part of his body.

In laboratories, fluid dynamic forces can be measured in a similar way by paving the body with an array of pressure and shear stress sensors. Summing the contribution of each signal from each sensor over the surface of the body yields effectively the force on the body (Figure 1.1). Often, it may be unpractical to have such a large array of sensors on the surface of the body, and one has to resort to some other method.

Note though that this local technique is the only one thus far available for the measurement of *sectional forces*. As a matter of fact, if one desires to measure the force only on a section of a straight cylinder instead of on the whole cylinder, then one could place an array of pressure (and

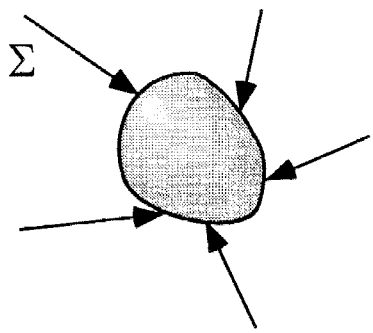


Figure 1.1: Sketch showing local stresses on body surface.

shear) sensors around the periphery of the desired section, and integrate the pressure signal[1]. We will see that intrinsic techniques may yet be an alternative method for measuring sectional forces.

### 1.2.2 Global measurements

When the horse finally makes up its mind and immerges itself into the river, he will not be able to sense the water pressure and shear on each individual part of its body separately. Instead, he will get a feel for the *global* force, which is the next topic in our story.

As mentioned in the preamble, an extrinsic technique can yield a fluid force without any a priori knowledge of fluid mechanics. Consider a body of mass $m$ whose center of mass follows a trajectory $\mathbf{x} = \mathbf{x}(t)$ with respect to an inertial frame of reference (Figure 1.2). Then, if the body is embedded in a fluid, the force exerted by the fluid upon the body can be evaluated from the relation:

$$\mathbf{F}_{\text{fluid}} = -m\ddot{\mathbf{x}} + \mathbf{F}_{\text{ext}}, \tag{1.1}$$

where $\mathbf{F}_{\text{fluid}}$ is the fluid force to be measured and $\mathbf{F}_{\text{ext}}$ is a force as imposed by an external agency.

For the horse crossing the river, the acceleration $\ddot{\mathbf{x}}$ is essentially zero (if the horse is still on its feet), and the fluid force is nothing but equal and opposite to the force exerted by the ground on the horse, or equivalently, the fluid force is equal to the force exerted by the horse onto the ground to counteract the current.

If the horse loses its grip, and decides to hang on to the branch of a tree extending from the river bank, he would then be connected to a spring system for which the external force is:

$$\mathbf{F}_{\text{ext}} = -\zeta\dot{\mathbf{x}} - k(\mathbf{x} - \mathbf{x}_0), \tag{1.2}$$

where $\zeta$ is the damping coefficient, $k$ the spring constant, and $\mathbf{x}_0$ the rest position of the spring. As such, the spring system acts as a *force balance*. A knowledge of the motion $\mathbf{x} = \mathbf{x}(t)$ of the horse's

[1]Szepessy S. & Bearman P. W., Aspect ratio and end plate effects on vortex shedding from a circular cylinder, *Journal of Fluid Mechanics* **234** (1992) 191-217.

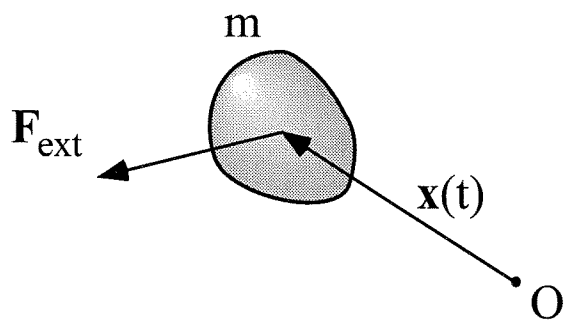


Figure 1.2: Sketch showing external global force on body.

center of mass supplies all the information needed to measure the fluid force:

$$\mathbf{F}_{\text{fluid}} = -m\ddot{\mathbf{x}} - \zeta\dot{\mathbf{x}} - k(\mathbf{x} - \mathbf{x}_0). \tag{1.3}$$

A strain gauge, for example, is nothing but a spring system with a displacement $\mathbf{x} - \mathbf{x}_0$ much smaller than the characteristic body dimension.

Now, if the branch breaks and if the river is just so deep that the horse's feet are not touching the river floor anymore, then the horse would have to swim. This would be the case of a self-propelling body immersed in a fluid, such as a fish or a bird, for which the external force is simply null:

$$\mathbf{F}_{\text{ext}} = 0. \tag{1.4}$$

Thus, for a self-propelling body moving at constant speed, the fluid force is absent:

$$\mathbf{F}_{\text{fluid}} = 0. \tag{1.5}$$

This result may seem surprising to the reader, but it just happens that the swimming horse contorts itself just enough not to feel any net fluid dynamic force. In engineering, one would introduce the concepts of *thrust* and *drag* and say that the horse produces just enough fluid dynamic *thrust* to balance the fluid dynamic *drag*. The concepts of thrust and drag are very useful engineering tools to determine the characteristics of a ship or an aircraft, just because for these man-made devices, thrust mechanisms are often distinct from drag mechanisms. An engine produces thrust while the fuselage produces drag. End of story. However, from a rigorous point of view, thrust and drag are arbitrary concepts, and often it is impossible to distinguish the separate contributions from drag and thrust, especially for flexible organisms such as fish or birds (or swimming horses).

Finally, if the poor horse runs out of steam, then he would become a free falling object, for which

the external force is provided by gravity:

$$\mathbf{F}_{\text{ext}} = m\mathbf{g}, \tag{1.6}$$

where $\mathbf{g}$ is the gravitational acceleration. Thus, the hydrodynamic force on the sinking horse can be inferred simply by tracing the motion of its center of gravity and using:

$$\mathbf{F}_{\text{fluid}} = -m\ddot{\mathbf{x}} + m\mathbf{g}. \tag{1.7}$$

The conclusion of the story is that the force on the horse can be evaluated straightforwardly in many situations despite the enormous complexity of the flow pattern around it. However, extrinsic methods do not provide any insight on the relation between the fluid force $\mathbf{F}_{\text{fluid}}$, the flow structure, and the possible motion of the body $\mathbf{x}(t)$.

## 1.3 Motivation for an intrinsic force measurement technique based on flowfield information

### 1.3.1 Brief description

An intrinsic technique measures the force on a body just from a knowledge of the flowfield around the body (Figure 1.3), without any need for a force balance or similar external devices:

$$\mathbf{F}_{\text{fluid}}(t) = \mathcal{L}_{\mathbf{x}}\left[\mathbf{u}(\mathbf{x},t), \frac{\partial \mathbf{u}}{\partial \mathbf{x}}, \frac{\partial \mathbf{u}}{\partial t}, \frac{\partial^2 \mathbf{u}}{\partial \mathbf{x}\partial \mathbf{x}}, \ldots; \Phi(\mathbf{x},t), \frac{\partial \Phi}{\partial \mathbf{x}}, \ldots\right], \tag{1.8}$$

where $\mathbf{u}(\mathbf{x},t)$ is the velocity field and $\Phi(\mathbf{x},t)$ is the thermodynamic field described by the pressure $p$, the density $\rho$, and the temperature $T$:

$$\Phi(\mathbf{x},t) = \left[p(\mathbf{x},t), \rho(\mathbf{x},t), T(\mathbf{x},t)\right]. \tag{1.9}$$

The operator $\mathcal{L}_{\mathbf{x}}$ converts the spatial and temporal flow information around a bluff body into an actual time dependent force $\mathbf{F}_{\text{fluid}}(t)$. It does so through a manipulation of the (Navier-Stokes) equations which govern the flow under study. In practical situations, however, it may be difficult to measure the instantaneous thermodynamic field $\Phi(\mathbf{x},t)$. It will be shown, though, that for *incompressible flows*, fluid dynamic forces can actually be extracted from a simple quadrature of the velocity field and its derivatives:

$$\mathbf{F}_{\text{fluid}}(t) = \mathcal{L}_{\mathbf{x}}\left[\mathbf{u}(\mathbf{x},t), \frac{\partial \mathbf{u}}{\partial \mathbf{x}}, \frac{\partial \mathbf{u}}{\partial t}, \frac{\partial^2 \mathbf{u}}{\partial \mathbf{x}\partial \mathbf{x}}, \ldots\right], \tag{1.10}$$

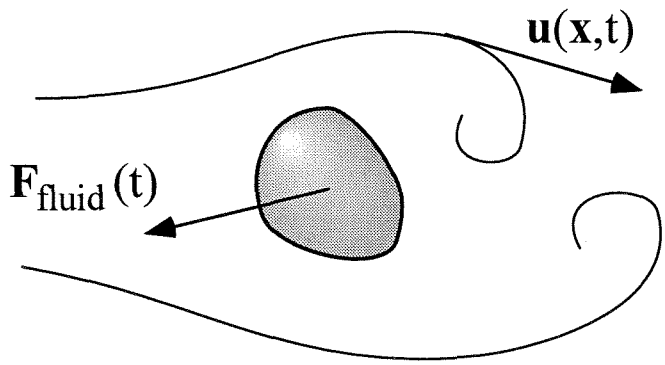


Figure 1.3: Sketch showing fluid-dynamic forces and local flowfields.

where $\mathcal{L}_{\mathbf{x}}$ is a spatial integral operator. Present experimental techniques such as Digital Particle Image Velocimetry[2] (DPIV) do indeed provide time series of velocity field data, and thus are well suited for a practical implementation of intrinsic methods.

### 1.3.2 Practical motivations

**Measurement of sectional vs. spanwise-averaged forces** If Leonardo, Daniel and Leonhard decide to rescue the ill-fated horse, they may try to throw a line into the stream hoping that the horse would get a hold of it. The line does not remain straight, however, and assumes a very contorted topology because the fluid dynamic forces are uneven along the length of the cable. Attaching a force balance at one end of the rope (which yields a *spanwise-averaged* force) certainly does not describe the force that each section of the rope is feeling. Moreover, paving the rope with sensors is certainly not a simple task. An intrinsic measurement thus becomes the only alternative for an effective measurement of the *sectional* force.

**Measurement of small force levels** In order to reduce the amount of wiggling in their cable, Leonardo, Daniel, and Leonhard may reduce its diameter, and may also realize that now even a force balance is unable to pick up the small force levels generated by the flow on their line. That is because the Reynolds number based on the section of the rope is very small, and forces at small Reynolds numbers are hardly measurable in a water medium. Given a rope diameter of $d = 1$ cm and a flow speed of $U = 1$ cm/s, the Reynolds number based on the diameter of the rope turns out to be:

$$Re = \frac{Ud}{\nu} = 100, \tag{1.11}$$

[2]Willert C. & Gharib M., Digital Particle Image Velocimetry, *Experiments in Fluids* **10** (1991) 181-193.

where $\nu$ is the kinematic viscosity of water. The force level on a line of length $L = 1$ m would then be:

$$F = \frac{1}{2} C_D \rho U^2 L d \approx 5.0 \times 10^{-4} \text{ N}, \tag{1.12}$$

where the coefficient of drag $C_D$ has been taken approximately equal to unity. This corresponds to a force level of less than one-tenth of a gram ($\approx 0.05$ gram) which is hardly measurable. An intrinsic method which uses flowfield information to measure forces would certainly circumvent this problem.

**Measurement of fluid forces in natural situations** Before trying to pull the horse with the rope, Leonardo, Daniel, and Leonhard may want to make sure that the current force on the horse is not too strong to avoid breaking the rope or getting drenched. Obviously, the horse, who is unconscious, cannot give them the information (this is a talking horse). A force balance is unsuitable since the animal is lying on the river floor, and a strain gauge is useless for the body is already strained under the water current. However, an intrinsic analysis based on the flowfield around the body could provide the necessary information to evaluate the fluid force acting on the animal.

Such situations may be encountered quite frequently, not only for man-made structures (hydro- and aero-dynamic forces on offshore stations, buildings, bridges, etc...) where the use of extrinsic methods may be unpractical, but also in Nature. It is not uncommon to see dragonflies or bumblebees "glued" down to a force balance for the study of their flight energetics. We believe that the study would be more trustworthy if the animals were allowed to fly or swim freely and the forces acting on the animal wings or fins were measured though the use of a non-intrusive, intrinsic technique.

### 1.3.3 Scientific motivation

Despite all the practical advantages that intrinsic methods may have over extrinsic methods, none may be as prominent as the scientific viewpoint.

As Leonardo, Daniel, and Leonhard are hoisting up their horse with a line, they may notice that the quadruped is engaging himself into a wild oscillation transverse to the river current. Sure, they may rig up a force balance to their line and quantify the oscillating force to which the animal is subject. However, the three fellows will not possibly reach any new insight on the details of this oscillation unless they start examining the flow structure around the animal. Realizing that vortex shedding is at the source of the oscillation may not be sufficient to quantify the frequency and amplitude of the oscillation.

An intrinsic method may yield a quantitative functional relationship between the periodic transverse force and the vorticity patterns in the near wake of the object. It may thus shed some light on the relation between the force acting on a cylinder in forced vibration and the various forms of

vortex patterns observed in the wake of a cylinder in forced oscillation[3]. It may also help relating wake structure to the frequency and amplitude of a freely oscillating cylinder in a cross flow.

The method should also apply to a more general class of flows which involve vortex-structure interactions. Examples are biomechanical flows connected with animal flight and swimming, and geophysical flows (tornadoes).

### 1.3.4 Master plan

Intrinsic techniques thus have the potential of measuring forces in situations where the use of extrinsic methods may be unpractical or fail altogether. They may also yield the direct link between the flow structure around a body and the force acting on it.

In this monograph, the equations that can be used for the implementation of an intrinsic technique will first be derived. It will be shown that these equations can be put in various forms, some of which may be more practical than others. From the start, we will specialize to the incompressible flow case, since it is the case that can actually be implemented with present day experimental techniques.

The method will be first validated numerically for the flow past a cylinder oscillating in an arbitrary fashion. The technique will then be applied to actual experimental situations. The two-dimensional flow past a cylinder at $Re \sim 100$ will be used as a test bench. Both steady and unsteady cylinder motions will be investigated.

By work end, we hope to make our horse realize that in wild flow situations, it is better to use our instinct than our intellect.

[3]Williamson C. H. K. & Roshko A., Vortex formation in the wake of an oscillating cylinder, *Journal of Fluids and Structures* **2** (1988) 355.

# Chapter 2 Traditional expressions for fluid-dynamic forces

In Paragraph 2.1, the most fundamental equations for the evaluation of fluid-dynamic forces on a bluff body will be derived. We will see that these equations involve a pressure term which needs to be evaluated or measured. Since present day experimental techniques cannot yield a pressure field directly, it has to be inferred from the velocity field (which can be measured).

In Paragraph 2.2, some simple, though approximate, methods for dealing with the pressure term will first be presented. In particular, mention will be made of the Kutta-Zhukovsky Theorem, and some wake survey techniques will be presented.

The remainder of the Chapter will be dedicated to exact methods.

In Paragraph 2.3, we derive an expression for the fluid-dynamic force in terms of two successive integrations of the velocity field and its derivatives.

In Paragraph 2.4, the "impulse equation" for an *infinite domain* will be derived in two different ways, one which uses the body as a kinematical domain of integration, and one that preserves the body identity.

In Paragraph 2.5, the "impulse equation" for a *finite, simply connected domain* will be presented. It will be derived classically, with the body considered as a fluid-dynamical entity.

In Chapter 3, the latter equation will be revisited through a derivation in a *doubly connected* domain which keeps the body and fluid as separate entities.

## 2.1 Conservation of momentum equation for a finite control volume

### 2.1.1 Formulation

The starting point is the integral formulation for the conservation of momentum principle in continuum mechanics[1]. Consider a material control volume $V_m(t)$ bounded by a material surface[2] $S_m^*(t)$.

[1]The following derivation is very much along the lines of the one in Dimotakis P., *Laser Doppler velocimetry momentum defect measurements of cable drag at low to moderate Reynolds numbers*, NCBC Report R541, 1977.

[2]The asterisk has been added for notation convenience, as shown later.

Conservation of momentum can be written as[3]:

$$\frac{d}{dt}\int_{V_m(t)} \rho \mathbf{u}\, dV = \oint_{S_m^*(t)} \hat{\mathbf{n}} \cdot \boldsymbol{\Sigma}\, dS, \tag{2.1}$$

where $\rho$ is the medium density, $\mathbf{u}$ its velocity, and $\boldsymbol{\Sigma}$ the stress tensor. Here, $V_m(t)$ is a material control volume enclosed by the surface $S_m^*(t)$ with unit outward normal $\hat{\mathbf{n}}$. For a Newtonian fluid, we have:

$$\boldsymbol{\Sigma} = -p\mathbf{I} + \mathbf{T}, \tag{2.2}$$

where $p$ is the pressure and $\mathbf{T}$ is the viscous stress tensor:

$$\mathbf{T} = \lambda(\boldsymbol{\nabla} \cdot \mathbf{u})\mathbf{I} + \mu(\boldsymbol{\nabla}\mathbf{u} + \boldsymbol{\nabla}\mathbf{u}^T). \tag{2.3}$$

As seen in Figure 2.1, the surface $S_m^*(t)$ can be decomposed into the surface of the body $S_b(t)$ (with outward normal pointing *into* the body), the exterior surface[4] $S_m(t)$, and the surface of the umbilicus (or "branch cut") $S_u(t)$ which joins the exterior surface to the body surface, that is:

$$S_m^*(t) = S_m(t) \oplus S_b(t) \oplus S_u(t), \tag{2.4}$$

such that:

$$\oint_{S_m(t)\oplus S_b(t)\oplus S_u(t)} \Phi\, dS = \int_{S_m(t)} \Phi\, dS + \int_{S_b(t)} \Phi\, dS + \int_{S_u(t)} \Phi\, dS. \tag{2.5}$$

Let us look closely at the surface integral over the umbilicus. If the umbilicus is chosen to be of infinitesimal cross section, then the integrand varies only with the longitudinal coordinate of the umbilicus. In other words, it can be approximated to be constant along the perimeter of the umbilicus. By slicing the umbilicus into rings of infinitesimal area $\delta S_u(t)$, and taking the surface

[3]The equation should have another term on the right-hand side to include volume forces:

$$\int_{V_m(t)} \rho \mathbf{f}\, dV.$$

Here, $\mathbf{f}$ is the volume force per unit mass (of gravitational or electromagnetic origin, for example). An *a priori* knowledge of it is needed to carry on the algebra. Each case needs to be dealt with separately. In electromagnetics, the coupling between fluid flow and electromagnetic forces is quite intricated. Even in the case of a gravitational field, only a few cases lend themselves to further simplifications, as in the case of a fluid of uniform and constant density. For the rest of the article, *it will be assumed that the volume force $\rho\mathbf{f}$ is independent of the flow.* In other words, it can be measured in advance when the flow is turned off, and can be subtracted from the forces measured when the flow is turned on (in constant and uniform density flows, this procedure would be equivalent to removing buoyancy forces). Therefore, without too much loss in generality, the term in volume force is excluded from the rest of the discussion.

[4]Now the reader should understand the reason for the asterisk. The exterior surface will play a dominant role and will appear in most of the results. As such, we did not want to carry along any additional cumbersome notation to express the fact that $S_m(t)$ is an exterior surface.

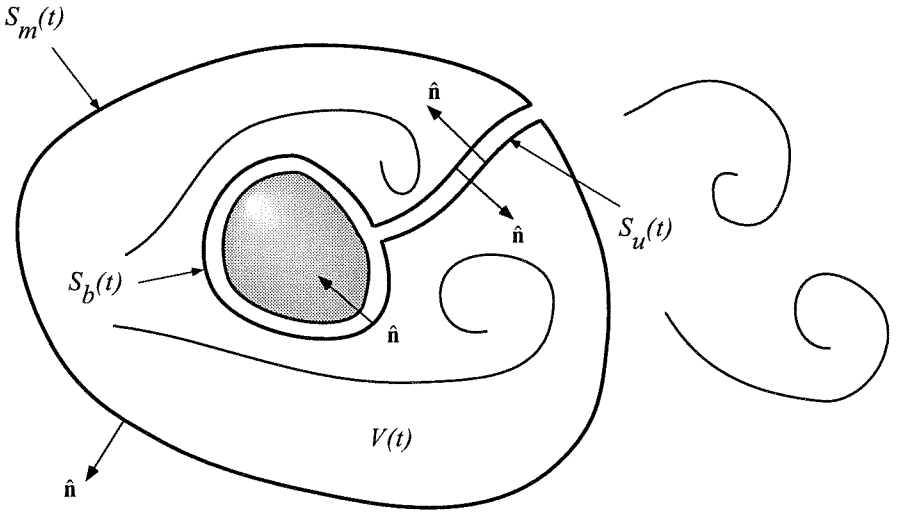


Figure 2.1: Control volume analysis.

integral over one of these rings, one obtains:

$$\int_{\delta S_u(t)} \hat{\mathbf{n}} \cdot \boldsymbol{\Sigma}\, dS \approx \boldsymbol{\Sigma}^T[\delta S_u(t)] \cdot \int_{\delta S_u(t)} \hat{\mathbf{n}}\, dS, \tag{2.6}$$

where $\boldsymbol{\Sigma}^T[\delta S_u(t)]$ is the value of the integrand $\boldsymbol{\Sigma}^T$ at the longitudinal position of the ring $\delta S_u(t)$. Since:

$$\int_{\delta S_u(t)} \hat{\mathbf{n}}\, dS = 0, \tag{2.7}$$

the integration over the umbilicus does not contribute to the total surface integral, and we can write:

$$\oint_{S_m(t)\oplus S_b(t)\oplus S_u(t)} \Phi\, dS = \oint_{S_m(t)} \Phi\, dS + \oint_{S_b(t)} \Phi\, dS, \tag{2.8}$$

where it is to be remembered that the unit normal $\hat{\mathbf{n}}$ over $S_b(t)$ is *into* the body.

Now, let us look at the surface integral over the body:

$$\oint_{S_b(t)} \hat{\mathbf{n}} \cdot \boldsymbol{\Sigma}\, dS = \oint_{S_b(t)} \hat{\mathbf{n}} \cdot (-p\mathbf{I} + \mathbf{T})\, dS. \tag{2.9}$$

This integral is, by *definition*, the force exerted by the body on the fluid. The *force of the fluid on the body* is then:

$$\mathbf{F} = -\oint_{S_b(t)} \hat{\mathbf{n}} \cdot \boldsymbol{\Sigma}\, dS. \tag{2.10}$$

Introducing this definition into the conservation of momentum equation yields:

$$\mathbf{F} = -\frac{d}{dt}\int_{V_m(t)} \rho\mathbf{u}\, dV + \oint_{S_m(t)} \hat{\mathbf{n}} \cdot (-p\mathbf{I} + \mathbf{T})\, dS. \tag{2.11}$$

In practical applications, one prefers to use an arbitrary volume instead of a material volume. Assume that at time $t$, the material volume $V_m(t)$ coincides with an arbitrary volume $V(t)$. Then, we can use Reynolds Theorem[5]:

$$\frac{d}{dt}\int_{V_m(t)} \Phi\, dV = \frac{d}{dt}\int_{V(t)} \Phi\, dV + \oint_{S^*(t)} \hat{\mathbf{n}}\cdot(\mathbf{u}-\mathbf{u}_S)\,\Phi\, dS, \tag{2.12}$$

where $S^*(t) = S^*_m(t)$ and $\mathbf{u}_S$ is the velocity of the surface $S^*(t)$. As a result, the force exerted by the fluid on the body is:

$$\begin{aligned}\mathbf{F} &= -\frac{d}{dt}\int_{V(t)} \rho\mathbf{u}\, dV - \oint_{S^*(t)} \hat{\mathbf{n}}\cdot(\mathbf{u}-\mathbf{u}_S)\,\rho\mathbf{u}\, dS \\ &\quad + \oint_{S(t)} \hat{\mathbf{n}}\cdot(-p\mathbf{I}+\mathbf{T})\, dS.\end{aligned} \tag{2.13}$$

Note that the second integral in Equation 2.13 is taken over the whole surface $S^*(t)$ whereas the third one is taken over only the exterior surface $S(t)$. The surface integral over $S^*(t)$ can be decomposed, as before, into three surface integrals, and by making the surface integral over the umbilicus to vanish, we obtain:

$$\oint_{S^*(t)} \hat{\mathbf{n}}\cdot(\mathbf{u}-\mathbf{u}_S)\,\rho\mathbf{u}\, dS = \oint_{S_b(t)} \hat{\mathbf{n}}\cdot(\mathbf{u}-\mathbf{u}_S)\,\rho\mathbf{u}\, dS + \oint_{S(t)} \hat{\mathbf{n}}\cdot(\mathbf{u}-\mathbf{u}_S)\,\rho\mathbf{u}\, dS. \tag{2.14}$$

The final result is:

$$\begin{aligned}\mathbf{F} &= -\frac{d}{dt}\int_{V(t)} \rho\mathbf{u}\, dV \\ &\quad + \oint_{S(t)} \hat{\mathbf{n}}\cdot[-p\mathbf{I}-(\mathbf{u}-\mathbf{u}_S)\,\rho\mathbf{u}+\mathbf{T}]\, dS \\ &\quad - \oint_{S_b(t)} \hat{\mathbf{n}}\cdot(\mathbf{u}-\mathbf{u}_S)\,\rho\mathbf{u}\, dS.\end{aligned} \tag{2.15}$$

This is the most general expression for the hydrodynamic force acting on a body.

### 2.1.2 Boundary conditions on body surface

We see that Equation 2.15 involves an integral over the body surface. The motion of the body surface as well as the behavior of the flow velocity at the body surface is an important feature of bluff body flows hydrodynamics. A myriad of boundary conditions are possible, and here, only the main ones will be mentioned.

1. Fluid flow conditions at the body surface

[5] Candel S.: *Mécanique des fluides*, p.86, Dunod, 1990.

- No through flow condition:

$$(\mathbf{u} - \mathbf{u}_S) \cdot \hat{\mathbf{n}} \,|_b = 0. \tag{2.16}$$

- No slip condition:

$$(\mathbf{u} - \mathbf{u}_S) \,|_b = 0. \tag{2.17}$$

2. Wall velocity conditions:

- Rigid body motion:

$$\mathbf{u}_S \,|_b = \mathbf{f}(t) + \mathbf{x}_b \wedge \mathbf{g}(t), \tag{2.18}$$

  where $\mathbf{f}(t)$ is the *translational* velocity of the body and $\mathbf{g}(t)$ is the *angular* velocity.

- Body motion with sliding walls:

$$\mathbf{u}_S \wedge \hat{\mathbf{n}} \,|_b = \mathbf{f}[\mathbf{x}_b(t), t], \tag{2.19}$$

$$\mathbf{u}_S \cdot \hat{\mathbf{n}} \,|_b = \mathbf{g}(t). \tag{2.20}$$

### 2.1.3 Incompressible case

For simplicity, the rest of this monograph will be specialized to the case where the density $\rho$ is constant in time and uniform in space. Thereafter, the density will be set equal to unity (in dimensionless units):

$$\rho = 1. \tag{2.21}$$

As a result, the starting equation for the rest of the analysis will be (see Equation 2.15):

$$\begin{aligned} \mathbf{F} \;=\; & -\frac{d}{dt}\int_{V(t)} \mathbf{u}\, dV \\ & + \oint_{S(t)} \hat{\mathbf{n}} \cdot [-p\mathbf{I} - (\mathbf{u} - \mathbf{u}_S)\,\mathbf{u} + \mathbf{T}]\, dS \\ & - \oint_{S_b(t)} \hat{\mathbf{n}} \cdot (\mathbf{u} - \mathbf{u}_S)\,\mathbf{u}\, dS. \end{aligned} \tag{2.22}$$

An additional relation which may be of use in later sections is the continuity equation:

$$\boldsymbol{\nabla} \cdot \mathbf{u} = 0. \tag{2.23}$$

Also, for incompressible flow, the integral involving the viscous tensor $\mathbf{T}$ can be written as:

$$\oint_{S(t)} \hat{\mathbf{n}} \cdot \mathbf{T}\, dS = \oint_{S(t)} \mu\, \hat{\mathbf{n}} \cdot \boldsymbol{\nabla}\mathbf{u}\, dS = -\oint_{S(t)} \mu\, \hat{\mathbf{n}} \wedge \boldsymbol{\omega}\, dS, \tag{2.24}$$

where $\boldsymbol{\omega}$ is the vorticity vector.

At this point, several options are possible, depending on how one wishes to use this expression for force measurements. The possibilities will be reviewed in the following sections.

### 2.1.4 The pressure problem

Let us examine closely each term in Equation 2.22. The equation can be decomposed into three major terms, depending on the domain of integration (see Figure 2.2):

1. A volume integral over the fluid enclosed in an arbitrary control volume $V(t)$:

$$-\frac{d}{dt}\int_{V(t)} \mathbf{u}\, dV. \tag{2.25}$$

   A knowledge of the velocity field $\mathbf{u}(\mathbf{x},t)$ is sufficient to determine this term. Because of the time derivative, a single snapshot of the flow (i.e. , $\mathbf{u}(\mathbf{x})$) does not provide enough information for the evaluation of instantaneous forces. A time series of the velocity field is needed.

2. A surface integral over the bounding surface $S(t)$ of the control volume:

$$\oint_{S(t)} \hat{\mathbf{n}} \cdot [-p\mathbf{I} - (\mathbf{u} - \mathbf{u}_S)\,\mathbf{u} + \mathbf{T}]\, dS. \tag{2.26}$$

   This integral requires a knowledge of both the pressure field $p(\mathbf{x})$ and the velocity field $\mathbf{u}(\mathbf{x})$. The viscous terms can be readily evaluated from the velocity field and its derivatives.

3. A surface integral over the body surface $S_b(t)$:

$$-\oint_{S_b(t)} \hat{\mathbf{n}} \cdot (\mathbf{u} - \mathbf{u}_S)\,\mathbf{u}\, dS. \tag{2.27}$$

   For a no-through flow condition at the body surface, this term vanishes. Otherwise, it can be evaluated in a straightforward manner according to the flow conditions at the body surface (please refer to Paragraph 2.1.2).

Thus, as it is, Equation 2.22 may yield the instantaneous fluid-dynamic force acting on the body from a knowledge of both the velocity field $\mathbf{u}(\mathbf{x},t)$ over the arbitrary volume $V(t)$, and the pressure field along the arbitrary, exterior bounding surface $S(t)$.

Also, the equation involves only a *single quadrature* of the pressure and velocity field (and its derivatives). This means that a knowledge of the pressure field $p(\mathbf{x})$ and the velocity field $\mathbf{u}(\mathbf{x},t)$ (and its derivatives) yields the fluid-dynamic forces with *one single integration.*

From what has just been said, the usefulness of Equation 2.22 relies on a knowledge of the pressure field $p(\mathbf{x},t)$ over the arbitrary surface $S(t)$. Present day experimental techniques such

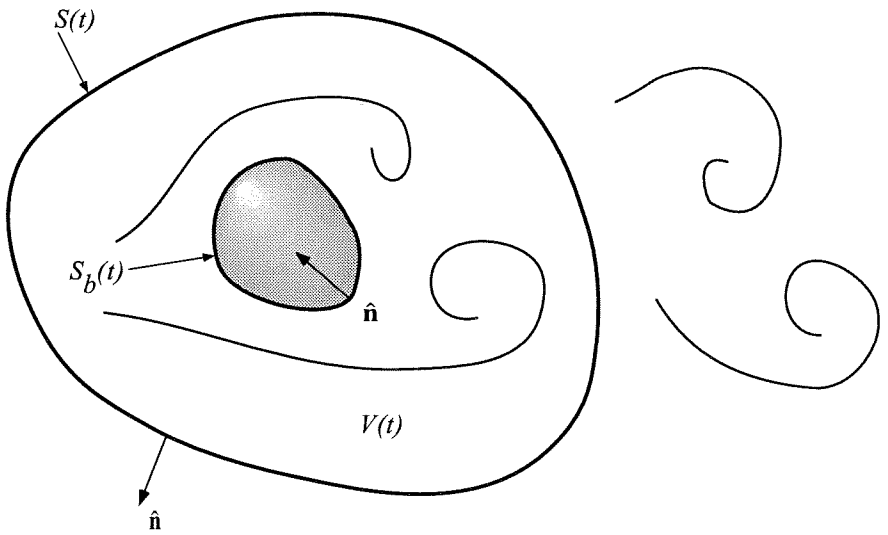


Figure 2.2: Domain of integration for the evaluation of fluid-dynamic forces on a bluff body.

as Digital Particle Image Velocimetry[6] (DPIV) certainly produce time sequences of velocity fields $\mathbf{u}(x,t)$. However, no technique is yet available for the direct experimental evaluation of the pressure field. This last point strongly undermines the utility of Equation 2.22 for the measurement of forces.

Nonetheless, several methods exist to circumvent the pressure problem. In Paragraph 2.2, we will start with some approximate methods.

In Paragraph 2.3, we will then present an exact method which will yield the force as a *double quadrature* of the velocity field (and its derivatives) only. This latter method will thus eliminate the need for the pressure field, albeit at the expense of an additional quadrature.

In Paragraph 2.4, we will derive the "impulse equation" and will show that the fluid-dynamic force can actually be expressed in terms of a *single quadrature* of the velocity field (and its derivatives), as long as the domain is *infinite*.

In Paragraph 2.4, an "impulse equation" will be presented for a domain which is finite, but *simply connected*, in which the body is considered as part of the fluid. In Chapter 3, we will show that the expression thus obtained is actually perfectly valid even in a *doubly connected* domain, where the body is taken separate from the fluid.

[6]Willert C. & Gharib M., Digital Particle Image Velocimetry, *Experiments in Fluids* **10** (1991) 181-193.

## 2.2 Approximate methods for the evaluation of pressure

### 2.2.1 The Kutta-Zhukovsky Theorem

If the flow is steady (non-time dependent) and if the surface $S(t)$ lies wholly in vorticity-free regions, then the total pressure $p_T$ may be taken as constant[7] over the surface $S(t)$:

$$p_T|_{S(t)} = p + \frac{1}{2}u^2\Big|_{S(t)} = \text{const.} \tag{2.28}$$

Equation 2.22, which can be rewitten as follows:

$$\begin{aligned} \mathbf{F} \;=\; & -\frac{d}{dt}\int_{V(t)} \mathbf{u}\, dV \\ & + \oint_{S(t)} \hat{\mathbf{n}} \cdot [-(p + \tfrac{1}{2}u^2)\mathbf{I} + \tfrac{1}{2}u^2\mathbf{I} - (\mathbf{u} - \mathbf{u}_S)\,\mathbf{u} - \mu\mathbf{I} \wedge \boldsymbol{\omega}]\, dS \\ & - \oint_{S_b(t)} \hat{\mathbf{n}} \cdot (\mathbf{u} - \mathbf{u}_S)\,\mathbf{u}\, dS, \end{aligned} \tag{2.29}$$

then becomes:

$$\begin{aligned} \mathbf{F} \;=\; & \oint_{S(t)} \hat{\mathbf{n}} \cdot [\tfrac{1}{2}u^2\mathbf{I} - (\mathbf{u} - \mathbf{u}_S)\,\mathbf{u}]\, dS \\ & - \oint_{S_b(t)} \hat{\mathbf{n}} \cdot (\mathbf{u} - \mathbf{u}_S)\,\mathbf{u}\, dS. \end{aligned} \tag{2.30}$$

If the no-through flow condition applies at the body surface, and if the bounding surface $S(t)$ is taken as being fixed (time-independent) such that $\mathbf{u}_S = 0$, then the fluid-dynamic force on the body is given by:

$$\mathbf{F} = \oint_S \hat{\mathbf{n}} \cdot (\tfrac{1}{2}u^2\mathbf{I} - \mathbf{u}\,\mathbf{u})\, dS. \tag{2.31}$$

We have finally arrived at an expression which can effectively be used for the measurement of forces. However, it is very limited in scope since it requires the flow to be stationary (time-independent) and the surface $S$ to lie wholly in vorticity-free flow.

Note that this expression can be turned into a well known relation by expressing it as a volume integral through a vector identity:

$$\oint_S \hat{\mathbf{n}} \cdot (\tfrac{1}{2}u^2\mathbf{I} - \mathbf{u}\,\mathbf{u})\, dS = \int_{V+V_b} \mathbf{u} \wedge \boldsymbol{\omega}\, dV, \tag{2.32}$$

where the body has now be included as part of the fluid. Saffman[8] calls the term $\mathbf{u} \wedge \boldsymbol{\omega}$ the vortex force, and attributes the concept to Prandtl (1918). In a two-dimensional space, a potential vortex

[7] For inviscid flows, the surface $S(t)$ may lie in vortical regions as long as the surface $S(t)$ is a streamsurface, in which case the total pressure is also constant over the surface.

[8] Saffman P.E., *Vortex dynamics*, p. 46, Cambridge University Press, 1993.

can be placed within the body volume $V_b$ (a "phantom vortex" as it is called by Wu & Wu[9]) such that:

$$\boldsymbol{\omega} = \boldsymbol{\Gamma}\delta(\mathbf{x}), \tag{2.33}$$

where $\boldsymbol{\Gamma}$ is the circulation vector (normal to the two-dimensional plane). The fluid-dynamic force on the body is then:

$$\begin{aligned} \mathbf{F} &= \int_{V+V_b} \mathbf{u} \wedge \boldsymbol{\omega}\, dV \\ &= \int_{V+V_b} \mathbf{u} \wedge \boldsymbol{\Gamma}\delta(\mathbf{x})\, dV \\ &= \mathbf{u}_0 \wedge \boldsymbol{\Gamma}, \end{aligned} \tag{2.34}$$

which is commonly known as the Kutta-Zhukovsky Theorem (1902).

The volume integral of $\mathbf{u} \wedge \boldsymbol{\omega}$ (or its equivalent surface integral given in Equation 2.31) will recur quite often in the next chapters, and we will usually refer to it as either the *vortex force* or the *Kutta-Zhukovsky* force.

### 2.2.2 Wake surveys for time-averaged flows

In some drag measurement procedures, it is desired to measure the average drag of a body by measuring quantities on the surface of the control volume only. The starting point is Equation 2.22 which we reproduce here for clarity:

$$\begin{aligned} \mathbf{F} = & -\frac{d}{dt}\int_{V(t)} \mathbf{u}\, dV \\ & + \oint_{S(t)} \hat{\mathbf{n}} \cdot [-p\mathbf{I} - (\mathbf{u} - \mathbf{u}_S)\,\mathbf{u} + \mathbf{T}]\, dS \\ & - \oint_{S_b(t)} \hat{\mathbf{n}} \cdot (\mathbf{u} - \mathbf{u}_S)\,\mathbf{u}\, dS. \end{aligned} \tag{2.35}$$

It is customary (and practical) in wake surveys to have the exterior surface of the control volume fixed. The volume $V(t)$ can still be a function of time because the body can be deformable or be moving around as a solid body[10].

[9] Wu J. Z. & Wu J. M., Vorticity dynamics on boundaries, *Advances in Applied Mechanics*, §VI.A, **32** (1996) 119.

[10] One way to see this would be to expand the time derivative of the integral as follows:

$$\begin{aligned} \frac{d}{dt}\int_{V(t)} \mathbf{u}\, dV &= \int_{V(t)} \frac{\partial \mathbf{u}}{\partial t}\, dV \\ &\quad + \oint_{S_b(t)} \hat{\mathbf{n}} \cdot \mathbf{u}_S\, \mathbf{u}\, dS + \oint_{S(t)} \hat{\mathbf{n}} \cdot \mathbf{u}_S\, \mathbf{u}\, dS, \end{aligned}$$

where the surface integral over $S$ vanishes if the surface is fixed. If the volume $V(t)$ had not been a function of time, the surface integral over $S_b(t)$ would not have been there. A sufficient (although not necessary) condition for this surface integral to vanish is for $\mathbf{u}_S \cdot \hat{\mathbf{n}}$ to be equal to zero.

We will now assume that the body motion coupled with the flow is stochastically periodic with average period $T$. By this statement, we mean that:

$$\lim_{N\to\infty} \sum_{n=-N}^{n=N} \int_{t+nT}^{t+(n+1)T} \left(\frac{d}{dt}\int_{V(t)} \rho \mathbf{u}\, dV\right) dt \equiv 0, \tag{2.36}$$

or, in abbreviated notation:

$$\left\langle \frac{d}{dt}\int_{V(t)} \rho \mathbf{u}\, dV \right\rangle \equiv 0. \tag{2.37}$$

In other words, wake surveys allow drag measurements of time-averaged flows only. Note that the time averaging was necessary to remove the integral over the volume $V(t)$. Finally:

$$\begin{aligned} \langle \mathbf{F} \rangle \;=\; & \oint_S \langle \hat{\mathbf{n}} \cdot (-\mathbf{u}\,\mathbf{u} + \boldsymbol{\Sigma}) \rangle\, dS \\ & - \left\langle \oint_{S_b(t)} \hat{\mathbf{n}} \cdot (\mathbf{u} - \mathbf{u}_S)\, \mathbf{u}\, dS \right\rangle. \end{aligned} \tag{2.38}$$

Moreover, if it is assumed that the no-through flow condition at the body surface is satisfied, then we have, by construction:

$$\hat{\mathbf{n}} \cdot (\mathbf{u} - \mathbf{u}_S)\,|_b \equiv 0, \tag{2.39}$$

and the surface integral over the body vanishes[11].

Finally:

$$\langle \mathbf{F} \rangle = \oint_S \hat{\mathbf{n}} \cdot \langle -\mathbf{u}\,\mathbf{u} + \boldsymbol{\Sigma} \rangle\, dS. \tag{2.40}$$

Equation 2.40 cannot be used as yet without further assumptions regarding the value of the stress tensor $\boldsymbol{\Sigma}$ on the surface $S$. If the surface lies some distance away from the body, the viscous stress tensor $\mathbf{T}$ becomes negligible, and only the pressure term remains.

$$\langle \mathbf{F} \rangle = \oint_S \hat{\mathbf{n}} \cdot \langle -\mathbf{u}\,\mathbf{u} - p\mathbf{I} \rangle\, dS. \tag{2.41}$$

Since wake surveys involve only flow velocity measurements on the surface $S$, the pressure has to be inferred. In general, it is assumed that the pressure in the far wake of the body is equal to the pressure outside the wake of the body, where we know Bernoulli's equation can be effectively used[12] (similar to a boundary layer assumption). This assumption is in general valid only far downstream of the body. Other possibilities exist for inferring this pressure with more precision[13].

To conclude, traditional wake survey methods can be used only for time-averaged forces, and

[11] This term would be present in the case of flows with surface injection, but it could be evaluated in a straightforward manner.

[12] Schlichting H., *Boundary Layer Theory*, McGraw Hill, 1987.

[13] Dimotakis P., *Laser Doppler velocimetry momentum defect measurements of cable drag at low to moderate Reynolds numbers*, NCBC Report R541, 1977.

have to be applied several body diameters away from the body, where further assumptions about pressure can be made.

## 2.3 Fluid-dynamic forces from a *double quadrature* of the velocity field (and its derivatives)

As mentioned in the previous sections, the only troublesome term in Equation 2.22 is:

$$\oint_{S(t)} \hat{\mathbf{n}} \cdot (-p\mathbf{I})\, dS = -\oint_{S(t)} p\hat{\mathbf{n}}\, dS. \tag{2.42}$$

In this Paragraph, we will show that it can be evaluated in a straightforward manner from the velocity field (and its derivatives).

### 2.3.1 Formulation

This term can actually be expressed in terms of the velocity field (and its derivatives) through the use of the Navier-Stokes equations in differential form:

$$\boldsymbol{\nabla} p = -\frac{\partial \mathbf{u}}{\partial t} - \mathbf{u} \cdot \boldsymbol{\nabla}\mathbf{u} + \boldsymbol{\nabla} \cdot \mathbf{T}. \tag{2.43}$$

The right-hand side of this equation can be readily evaluated from a knowledge of the velocity field $\mathbf{u}(\mathbf{x}, t)$.

At a given time $t$, let us pick an arbitrary point $\mathbf{x}_0$ within the control volume $V(t)$ (see Figure 2.3). Then, the pressure $p(\mathbf{x}, t)$ at any location $\mathbf{x}$ on the surface $S(t)$ is given by:

$$\begin{aligned} p(\mathbf{x},t) &= p(\mathbf{x}_0,t) + \int_{\mathbf{x}_0}^{\mathbf{x}} d\hat{\mathbf{l}} \cdot \boldsymbol{\nabla} p \\ &= p(\mathbf{x}_0,t) + \int_{\mathbf{x}_0}^{\mathbf{x}} \hat{\mathbf{l}} \cdot (-\frac{\partial \mathbf{u}}{\partial t} - \mathbf{u} \cdot \boldsymbol{\nabla}\mathbf{u} + \boldsymbol{\nabla} \cdot \mathbf{T})\, dl, \end{aligned} \tag{2.44}$$

where the line integration is performed along any *arbitrary* path (defined by the unit tangential vector $\hat{\mathbf{l}}$) joining $\mathbf{x}_0$ to $\mathbf{x}$. Since the velocity field is generally known *inside* the control volume, the path should be chosen to lie wholly within the control volume $V(t)$ or on the surface $S(t)$.

Thus, the pressure $p(\mathbf{x}, t)$ on the surface $S(t)$ can be evaluated to within an arbitrary constant $p(\mathbf{x}_0, t)$. This constant is actually irrelevant, because what we are after is not the pressure itself, but the surface integral of the pressure over the bounding surface $S(t)$:

$$-\oint_{S(t)} p(\mathbf{x},t)\hat{\mathbf{n}}\, dS = -\oint_{S(t)} p(\mathbf{x}_0,t)\hat{\mathbf{n}}\, dS - \oint_{S(t)} \left[\int_{\mathbf{x}_0}^{\mathbf{x}} \hat{\mathbf{l}} \cdot (-\frac{\partial \mathbf{u}}{\partial t} - \mathbf{u} \cdot \boldsymbol{\nabla}\mathbf{u} + \boldsymbol{\nabla} \cdot \mathbf{T})\, dl\right] \hat{\mathbf{n}}\, dS, \tag{2.45}$$

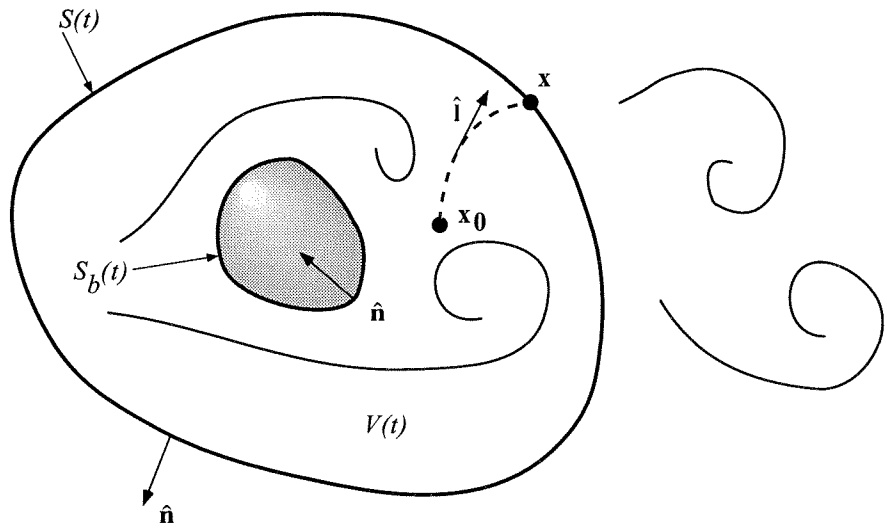


Figure 2.3: Arbitrary path $\mathbf{x}_0 - \mathbf{x}$ along which the line integration is performed to evaluate the pressure difference between points $\mathbf{x}$ and $\mathbf{x}_0$.

and using the fact that:

$$\oint_{S(t)} p(\mathbf{x}_0, t)\hat{\mathbf{n}}\, dS = p(\mathbf{x}_0, t) \oint_{S(t)} \hat{\mathbf{n}}\, dS \equiv 0, \tag{2.46}$$

we finally obtain:

$$-\oint_{S(t)} p(\mathbf{x}, t)\hat{\mathbf{n}}\, dS = \oint_{S(t)} \left[ \int_{\mathbf{x}_0}^{\mathbf{x}} \hat{\mathbf{l}} \cdot \left(\frac{\partial \mathbf{u}}{\partial t} + \mathbf{u} \cdot \boldsymbol{\nabla}\mathbf{u} - \boldsymbol{\nabla} \cdot \mathbf{T}\right) dl \right] \hat{\mathbf{n}}\, dS. \tag{2.47}$$

The left-hand side of this equation is independent of $\mathbf{x}_0$, and so should the right-hand side. At the moment, we cannot remove the explicit $\mathbf{x}_0$ dependence from the right-hand side. We will see in Chapter 4 how it can be done.

As it is, this equation is nonetheless perfectly usable to evaluate fluid forces from a knowledge of the velocity field $\mathbf{u}(\mathbf{x}, t)$ only. The final expression is:

$$\begin{aligned} \mathbf{F} \;=\; & -\frac{d}{dt}\int_{V(t)} \mathbf{u}\, dV \\ & + \oint_{S(t)} \hat{\mathbf{n}} \cdot \tilde{\boldsymbol{\Upsilon}}_{\mathbf{p}}\, dS \\ & - \oint_{S_b(t)} \hat{\mathbf{n}} \cdot (\mathbf{u} - \mathbf{u}_S)\, \mathbf{u}\, dS. \end{aligned} \tag{2.48}$$

where the tensor[14] $\tilde{\boldsymbol{\Upsilon}}_{\mathbf{p}}$ is given by:

$$\tilde{\boldsymbol{\Upsilon}}_{\mathbf{p}} = \left[ \int_{\mathbf{x}_0}^{\mathbf{x}} \hat{\mathbf{l}} \cdot \left(\frac{\partial \mathbf{u}}{\partial t} + \mathbf{u} \cdot \boldsymbol{\nabla}\mathbf{u} - \boldsymbol{\nabla} \cdot \mathbf{T}\right) dl \right] \mathbf{I} - (\mathbf{u} - \mathbf{u}_S)\, \mathbf{u} + \mathbf{T}. \tag{2.49}$$

[14]The tensor $\tilde{\boldsymbol{\Upsilon}}_{\mathbf{p}}$ has been written with the index $\mathbf{p}$ because it enters an equation based on the flow momentum. We will see in later chapters the relevance of this notation.

In Chapter 4, we will show that the integrand $\tilde{\boldsymbol{\Upsilon}}_{\mathbf{p}}$ can be expressed explicitly, without quadratures.

### 2.3.2 Forces from the velocity field (and its derivatives) at the body surface

The analysis in the previous paragraph can help us evaluate forces from information on the body surface only. All we have to do is shrink the control volume such that the volume reduces to zero and the surface $S(t)$ coincides with the surface $S_b(t)$. The original force equation given by Equation 2.22 then becomes:

$$\mathbf{F} = \oint_{S_b(t)} \hat{\mathbf{n}} \cdot (-p\mathbf{I} + \mathbf{T})\, dS \tag{2.50}$$

Note that the unit vector $\hat{\mathbf{n}}$ now points outward from the body surface, and that the term expressing through flow, $\hat{\mathbf{n}} \cdot (\mathbf{u} - \mathbf{u}_S)\mathbf{u}$, has disappeared[15]. This equation states that the force on the body is just the surface integral of the pressure and the shear stress over the body surface. This should not be surprising since it was our definition for the force to start with. The integral of the pressure can be evaluated from the analysis given in the previous paragraph, thus yielding:

$$\mathbf{F} = \oint_{S_b(t)} \hat{\mathbf{n}} \cdot \tilde{\boldsymbol{\Upsilon}}_b\, dS, \tag{2.51}$$

where:

$$\tilde{\boldsymbol{\Upsilon}}_b = \left[\int_{\mathbf{x}_0}^{\mathbf{x}} \hat{\mathbf{l}} \cdot (\frac{\partial \mathbf{u}}{\partial t} + \mathbf{u} \cdot \nabla\mathbf{u} - \nabla \cdot \mathbf{T})\, dl\right] \mathbf{I} + \mathbf{T}. \tag{2.52}$$

The line integration is again perfomed along an arbitrary path. For the particular case of a body in steady motion with a no-slip boundary condition at the surface, the tensor $\tilde{\boldsymbol{\Upsilon}}_b$ assumes the simple form:

$$\tilde{\boldsymbol{\Upsilon}}_b = -\left[\int_{\mathbf{x}_0}^{\mathbf{x}} \hat{\mathbf{l}} \cdot (\nabla \cdot \mathbf{T})\, dl\right] \mathbf{I} + \mathbf{T}. \tag{2.53}$$

where the line integration is now performed along the body surface and $\mathbf{x}_0$ is any fixed point on the body surface.

This equation says that the fluid-dynamic force on the body can be evaluated from a knowledge of the viscous shear $\hat{\mathbf{n}} \cdot \mathbf{T}$ and the viscous force $\nabla \cdot \mathbf{T}$ (which is related to the pressure gradient) along the body surface. In Chapter 4, $\tilde{\boldsymbol{\Upsilon}}_b$ will be given explicitly, without line integrations.

From a practical point of view, this equation is slightly prohibitive because it asks for the flow velocity profile at the body surface. The resolution of the boundary layer is not as yet possible with present whole-field techniques such as DPIV. Nonetheless, if the viscous shear and viscous force over the body surface can somehow be determined by some alternative technique, this equation would be of potential use (even more so the equivalent equation given in Chapter 4).

[15]This does not mean that there is no through flow.

## 2.4 "Impulse equation" for an infinite domain

The "impulse equation", which relates a fluid-dynamic force to the time derivative of the fluid-dynamic impulse, has been known for a long time[16]. The popularity of this equation stems from the simple interpretation that can be made of the force due to a vortex. Since the equation requires the vorticity over the whole domain, it has found its way in computational vortex methods where the vorticity is always confined to a finite domain. As a result, we will often term the equation either the "impulse equation" or the vortex method equation[17].

In this Paragraph, we will give the common, but *incorrect*, derivation of the equation. In Chapter 3, we will present the correct version of the derivation.

### 2.4.1 A vector identity

Most of the transformations that will be used in the next sections rely on the following identity:

$$\int_V \mathbf{x} \wedge \boldsymbol{\nabla} \wedge \mathbf{a}\, dV = (\mathcal{N}-1) \int_V \mathbf{a}\, dV + \oint_S \mathbf{x} \wedge (\hat{\mathbf{n}} \wedge \mathbf{a})\, dS, \tag{2.54}$$

where $\mathbf{a}$ is an arbitrary vector and $\mathcal{N}$ is the dimension of the space ($\mathcal{N} = 3$ in 3D and $\mathcal{N} = 2$ in 2D for example). Most workers do not use this identity literally, and prefer a procedure involving *integration by parts*[18] which ultimately leads to Equation 2.54.

### 2.4.2 The kinematical fluid body

To carry on volume integrations involving *velocity* and *vorticity* fields, some authors[19] extend the velocity and vorticity fields *into* the body. This procedure is perfectly valid since it is kinematical in nature. The picture that now emerges is the one shown in Figure 2.4, in which an imaginary envelope separates the fluid body of volume $V_b(t)$ from the external fluid of volume $V(t)$. On the envelope (which is nothing but the actual body surface $S_b(t)$), any of the boundary conditions listed in Paragraph 2.1.2 can be imposed. The exterior surface $S(t)$ thus bounds the volumes $V(t)$ and $V_b(t)$. In this picture, the fluid body only acts as an intermediate step, and the final answer should not explicitly contain volume integrations over the body volume. Nevertheless, in simple situations

[16] Lamb H., *Hydrodynamics*, §152, Dover, 1945; actually, Lamb mentions that J. J. Thomson had already derived an equation for the impulse in 1883 in a memoir entitled *On the motion of vortex rings.*

[17] Some authors in the world of fluid-structure interactions refer to it as the Lighthill equation. This is because Lighthill, in a 1979 paper, mentioned that the "impulse equation" could be most useful for the evaluation of forces on offshore structures. See Lighthill M. J., Waves and hydrodynamic loading, *Proc. Int. Conf. Behav. Off-Shore Struct.*, 2nd, **1** (1979) 1.

[18] Lamb H., *Hydrodynamics*, §152, Cambridge University Press, 1924; Batchelor G. K., *An introduction to fluid dynamics*, §7.2, Cambridge University Press, 1967; Leonard A., Computing incompressible flows with vortex elements, lecture notes from *Numerical methods in fluid mechanics*, Ae 232, Caltech, 1989, and *Particle methods in fluid mechanics*, Ecole d'été d'analyse numérique, Le Breau sans Nappe, France, 1987.

[19] Leonard A., Computing incompressible flows with vortex elements, lecture notes from *Numerical methods in fluid mechanics*, Ae 232, Caltech, 1989, and *Particle methods in fluid mechanics*, Ecole d'été d'analyse numérique, Le Breau sans Nappe, France, 1987.; see also Saffman P.E., *Vortex dynamics*, Cambridge University Press, 1993.

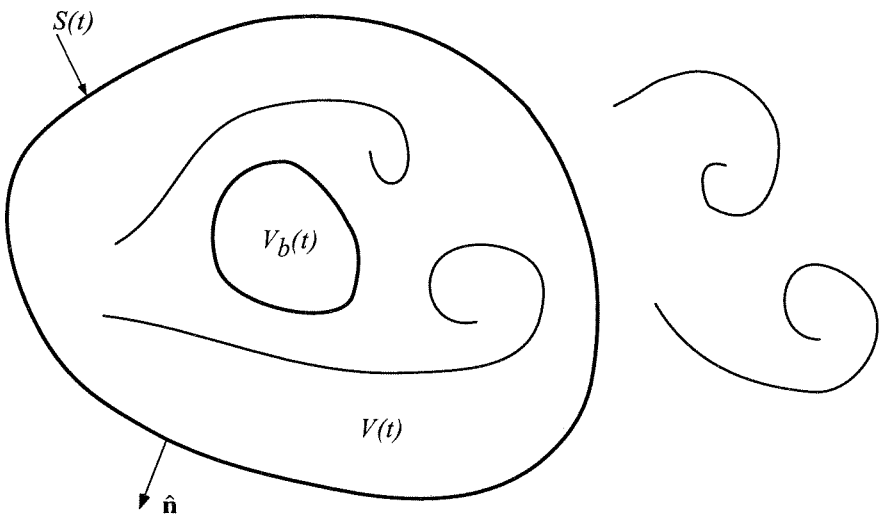


Figure 2.4: The fluid body.

(for the case of a rigid bluff-body for example), volume integrals over the body may be kept since the fluid velocity and vorticity within the fluid body are then just the translational velocity and (twice) the angular velocity of the rigid body.

Two remarks should be made at this point.

First, the kinematical body is a useful concept only in derivations which do not involve explicitly dynamical quantities (such as pressure). We will see that pressure terms are, in general, *arbitrarily* removed to avoid such complications.

Second, there exists an alternative derivation of the "impulse equation" for an infinite domain which does not involve integrals over the body explicitly. We will show that, in general, kinematical integrals can be evaluated without including the body volume in the integrations.

### 2.4.3 Boundary conditions at infinity

The topic of boundary conditions at infinity is not easy to tackle. In this section, only boundary conditions proper to vortex methods will be considered.

In vortex methods, all the vorticity is produced at the surface of the body and is generally confined in a finite region of space. As such, some deductions can be made regarding vorticity and velocity at infinity.

When the vorticity decays exponentially at large distances, then the velocity, in a material frame

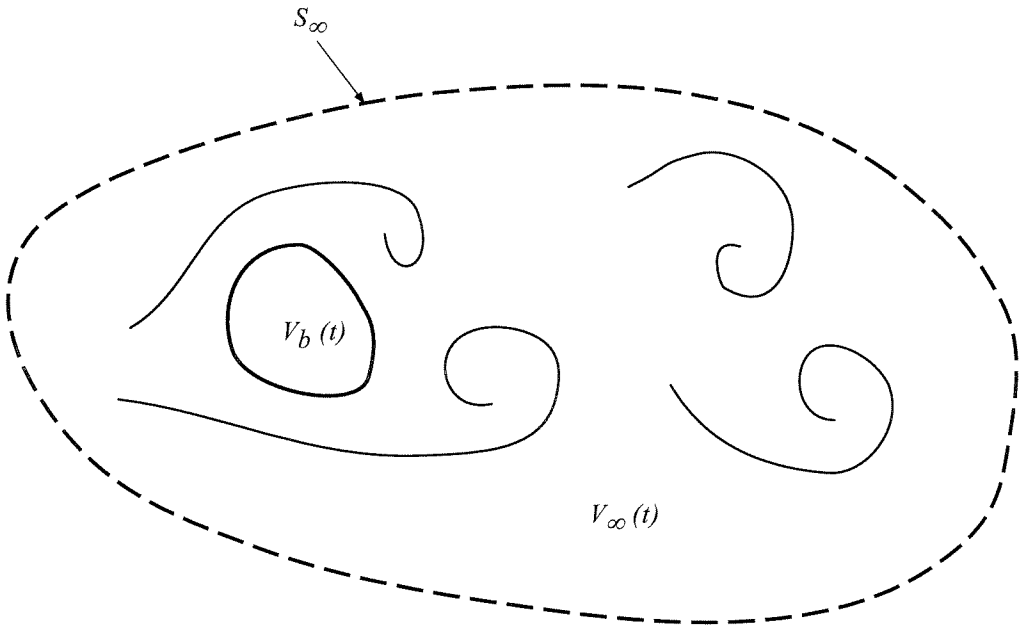


Figure 2.5: Control volume analysis for the derivation of the "impulse equation" using a fluid body.

at rest at infinity, obeys the following relations[20]:

$$r \to \infty, \quad |\boldsymbol{\omega}| \sim e^{-\alpha r}, \quad |\mathbf{u}| \sim \begin{cases} r^{-3} & \text{3D} \\ r^{-1} & \text{2D} \quad \text{with circulation} \\ r^{-2} & \text{2D} \quad \text{with no net circulation} \end{cases} \tag{2.55}$$

Note, however, that no condition can be imposed on the pressure at infinity.

### 2.4.4 Incorrect starting equation

The surface $S(t)$ bounding the control volume is now assumed to extend to infinity, as shown in Figure 2.5.

Assuming that there is no net circulation (in 2D), that the control volume surface is stationary ($\mathbf{u}_{S_\infty} = 0$), and that viscous effects are negligible at infinity, we then have:

$$\oint_{S_\infty} \hat{\mathbf{n}} \cdot (-(\mathbf{u} - \mathbf{u}_S)\,\mathbf{u} + \mathbf{T})\,dS \sim 0. \tag{2.56}$$

A priori, nothing can be said about the pressure integral. Often, it is tacitly (and wrongly!)

[20] Batchelor G. K., *An introduction to fluid dynamics*, Cambridge University Press, 1967; Ting L., *J. Fluid Mech.*, **127** (1983) 497.

assumed that this pressure integral is null[21]:

$$\oint_{S_\infty} p\hat{\mathbf{n}}\, dS \sim 0, \tag{2.57}$$

such that the (incorrect) starting equation turns out to be simply:

$$\mathbf{F} = -\frac{d}{dt}\int_{V_\infty(t)} \mathbf{u}\, dV - \oint_{S_b(t)} \hat{\mathbf{n}}\cdot(\mathbf{u}-\mathbf{u}_S)\,\mathbf{u}\, dS. \tag{2.58}$$

However, we will see in Chapter 3 that *the assumption of the pressure integral vanishing at infinity is not necessary, notwithstanding the fact that it is incorrect as well!* Equation 2.58 will nevertheless yield the right answer because of an additional wrong assumption in the derivation.

### 2.4.5 Derivation, using the fluid body

The following derivation is similar to the one given by Leonard[22]. The integral in Equation 2.58 is first extended into the body as follows (see Figure 2.5):

$$\begin{aligned}\mathbf{F} \;=\; & -\frac{d}{dt}\int_{V_\infty(t)+V_b(t)} \mathbf{u}\, dV + \frac{d}{dt}\int_{V_b(t)} \mathbf{u}\, dV \\ & - \oint_{S_b(t)} \hat{\mathbf{n}}\cdot(\mathbf{u}-\mathbf{u}_S)\,\mathbf{u}\, dS.\end{aligned} \tag{2.59}$$

This integral can be evaluated by integration by parts, or we could just set $\mathbf{u} = \mathbf{a}$ in the vector identity given by Equation 2.54. The volume $V$ is just the volume of "fluid" $V_\infty(t) + V_b(t)$ whereas the surface $S$ corresponds to the external bounding surface $S_\infty$. The result is:

$$\int_{V_\infty+V_b(t)} \mathbf{x}\wedge\boldsymbol{\nabla}\wedge\mathbf{u}\, dV = (\mathcal{N}-1)\int_{V_\infty+V_b(t)} \mathbf{u}\, dV + \oint_{S_\infty} \mathbf{x}\wedge(\hat{\mathbf{n}}\wedge\mathbf{u})\, dS. \tag{2.60}$$

The derivation then requires the erroneous assumption that:

$$\oint_{S_\infty} \mathbf{x}\wedge(\hat{\mathbf{n}}\wedge\mathbf{u})\, dS \sim 0. \tag{2.61}$$

With the $\mathbf{x}$-dependence of the velocity at infinity, this integral does not vanish, but is conditionally convergent to some non-zero value. We will see in Chapter 3 how the (time derivative of the) latter term cancels the contribution from the pressure integral.

Nevertheless, forcing the latter integral to vanish and introducing the vorticity $\boldsymbol{\omega} = \boldsymbol{\nabla}\wedge\mathbf{u}$, we

[21] Wu J. Z. & Wu J. M., Vorticity dynamics on boundaries, *Advances in Applied Mechanics*, **32** (1996) 119.

[22] Leonard A., Computing incompressible flows with vortex elements, lecture notes from *Numerical methods in fluid mechanics*, Ae 232, Caltech, 1989.

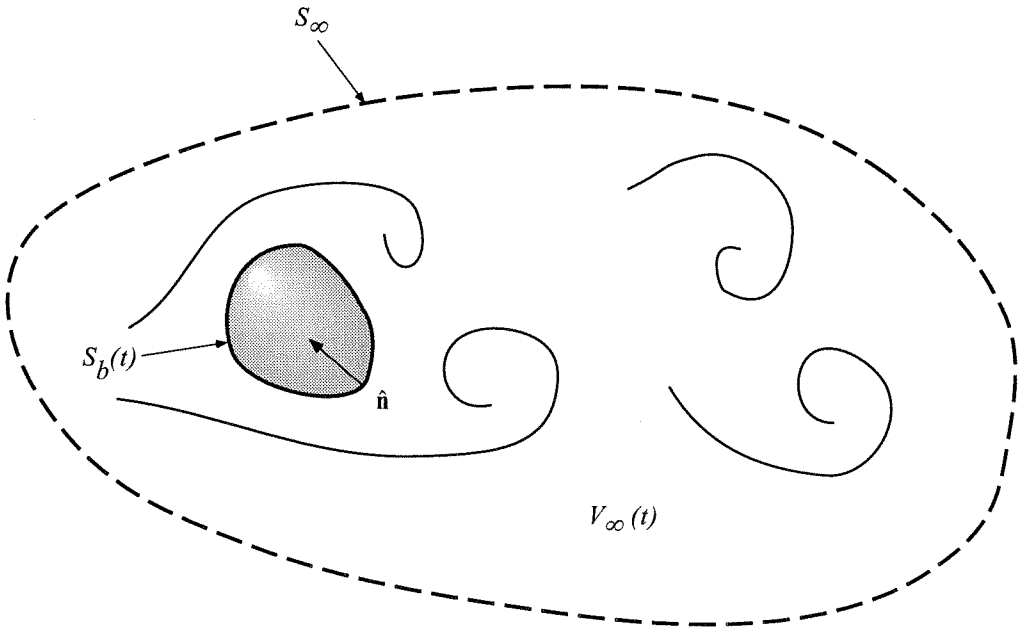


Figure 2.6: Control volume analysis for the derivation of the "impulse equation" *without* using the fluid body.

then obtain:

$$\int_{V_\infty+V_b(t)} \mathbf{u}\, dV = \frac{1}{\mathcal{N}-1} \int_{V_\infty+V_b(t)} \mathbf{x}\wedge\boldsymbol{\omega}\, dV. \tag{2.62}$$

The "impulse equation" for an infinite domain then takes the form:

$$\begin{aligned}\mathbf{F} \;=\; & -\frac{1}{\mathcal{N}-1}\frac{d}{dt}\int_{V_\infty} \mathbf{x}\wedge\boldsymbol{\omega}\, dV \\ & + \frac{d}{dt}\int_{V_b(t)} \mathbf{u}\, dV - \frac{1}{\mathcal{N}-1}\frac{d}{dt}\int_{V_b(t)} \mathbf{x}\wedge\boldsymbol{\omega}\, dV - \oint_{S_b(t)} \hat{\mathbf{n}}\cdot(\mathbf{u}-\mathbf{u}_S)\,\mathbf{u}\, dS.\end{aligned} \tag{2.63}$$

The integrals over the body can be readily evaluated for a solid body, and just represent the linear and angular acceleration of the body.

In the following paragraph, we will rederive the same equation without including the body into the integration.

### 2.4.6 Derivation, without fluid body

What follows is a derivation similar to one given by Wu & Wu[23]. We first set $\mathbf{u} = \mathbf{a}$ in the vector identity given by Equation 2.54. From Figure 2.6, the volume $V$ is just the volume of fluid $V_\infty(t)$ whereas the surface $S$ comprises the external surface $S_\infty$, the body surface $S_b(t)$, and the umbilicus surface $S_u(t)$ (over which the integral is made to vanish). The result is:

[23]Wu J. Z. & Wu J. M., Vorticity dynamics on boundaries, *Advances in Applied Mechanics*, **32** (1996) 119.

$$\int_{V_\infty(t)} \mathbf{x} \wedge \boldsymbol{\nabla} \wedge \mathbf{u}\, dV = (\mathcal{N}-1) \int_{V_\infty(t)} \mathbf{u}\, dV + \oint_{S_\infty} \mathbf{x} \wedge (\hat{\mathbf{n}} \wedge \mathbf{u})\, dS + \oint_{S_b(t)} \mathbf{x} \wedge (\hat{\mathbf{n}} \wedge \mathbf{u})\, dS. \quad (2.64)$$

Introducing the vorticity $\boldsymbol{\omega} = \boldsymbol{\nabla} \wedge \mathbf{u}$ and assuming (wrongly!) that:

$$\oint_{S_\infty} \mathbf{x} \wedge (\hat{\mathbf{n}} \wedge \mathbf{u})\, dS \sim 0, \quad (2.65)$$

then:

$$\int_{V_\infty(t)} \mathbf{u}\, dV = \frac{1}{\mathcal{N}-1} \int_{V_\infty(t)} \mathbf{x} \wedge \boldsymbol{\omega}\, dV - \frac{1}{\mathcal{N}-1} \oint_{S_b(t)} \mathbf{x} \wedge (\hat{\mathbf{n}} \wedge \mathbf{u})\, dS. \quad (2.66)$$

The "impulse equation" for an infinite domain then takes the form:

$$\begin{aligned} \mathbf{F} \;=\; & -\frac{1}{\mathcal{N}-1} \frac{d}{dt} \int_{V_\infty(t)} \mathbf{x} \wedge \boldsymbol{\omega}\, dV \\ & + \frac{1}{\mathcal{N}-1} \frac{d}{dt} \oint_{S_b(t)} \mathbf{x} \wedge (\hat{\mathbf{n}} \wedge \mathbf{u})\, dS - \oint_{S_b(t)} \hat{\mathbf{n}} \cdot (\mathbf{u} - \mathbf{u}_S)\, \mathbf{u}\, dS, \end{aligned} \quad (2.67)$$

where the unit vector $\hat{\mathbf{n}}$ points *into* the body.

When the no-slip boundary conditions applies, the second term just describes the unsteady motion of the body surface since the flow velocity is then equal to the surface velocity. The surface could move as a rigid body or could just be a flexible surface as in the case of a fish or a bird. Note that Equation 2.67 and Equation 2.63 are actually equivalent, since from the identity in Equation 2.54, we have:

$$\frac{1}{\mathcal{N}-1} \frac{d}{dt} \oint_{S_b(t)} \mathbf{x} \wedge (\hat{\mathbf{n}} \wedge \mathbf{u})\, dS = \frac{d}{dt} \int_{V_b(t)} \mathbf{u}\, dV - \frac{1}{n-1} \frac{d}{dt} \int_{V_b(t)} \mathbf{x} \wedge \boldsymbol{\omega}\, dV, \quad (2.68)$$

where $\hat{\mathbf{n}}$ points *into* the body[24]. Equation 2.67 has the correct form despite the fallacious derivation. In Chapter 3, we will rederive it in a rigorous way, without any *a priori* assumptions about the pressure terms which ultimately cancel.

In terms of the *fluid-dynamic impulse* $\mathbf{i}$:

$$\mathbf{i} = \frac{1}{\mathcal{N}-1} \int_{V_\infty(t)} \mathbf{x} \wedge \boldsymbol{\omega}\, dV, \quad (2.69)$$

the equation takes the form:

$$\begin{aligned} \mathbf{F} \;=\; & -\frac{d\mathbf{i}}{dt} \\ & + \frac{d}{dt} \int_{S_b(t)} \mathbf{x} \wedge (\hat{\mathbf{n}} \wedge \mathbf{u})\, dS - \oint_{S_b(t)} \hat{\mathbf{n}} \cdot (\mathbf{u} - \mathbf{u}_S)\, \mathbf{u}\, dS, \end{aligned} \quad (2.70)$$

[24]This vector identity has been originally written for a unit vector pointing *outward*. In the few cases where the unit vector points *inward*, as on the body surface, the signs have to be reversed. The reader will be notified each time such case occurs.

from which stems the name "*impulse equation*".

### 2.4.7 The infinite domain problem

As it stands, Equation 2.67 could indeed be used for the measurement of bluff body forces. It does not involve the pressure field, and can thus be used effectively in the laboratory with a technique like Digital Particle Image Velocimetry. Also, note that the equation is very convenient because it involves only a single quadrature, instead of two as seen Paragraph 2.3.

However, this equation suffers from a major handicap: it requires a knowledge of the *vorticity over the whole flowfield*! For starting flows, the equation would be appropriate, since the vorticity is then confined to a region close to the body. It would also be applicable for the case the body performing small amplitude motions in an otherwise quiescent fluid (such that the vorticity remains enclosed in a finite domain).

The "impulse equation" for an infinite domain has indeed been applied successfully in laboratory experiments by Lin & Rockwell[25], who measured the loading on an oscillating cylinder in quiescent water.

However, in most experimental situations, it is rare for the vorticity to be confined in a finite domain. Examples are cylinders in crossflow, for which wakes extend to infinity. The "impulse equation" would then not be applicable in these flow situations.

In the following paragraph (Paragraph 2.5), we will see that the problem can actually be circumvented by keeping the surface of the control volume from extending to infinity. The result will involve a single quadrature of the velocity field (and its derivatives) in an arbitrary, finite domain. However, the derivation will require the use of a *simply connected domain* and the fluid body concept. In Chapter 3, we will re-derive the equation for a doubly connected domain (thus keeping the body apart from the surrounding fluid).

## 2.5 "Impulse equation" for a finite, simply connected domain

In this section, it will be shown that the force on a body can actually be evaluated from information given in a finite domain, when the body itself is considered as a *dynamical fluid body*.

### 2.5.1 The dynamical fluid body

Contrary to workers in vortex methods, Saffman[26] prefers the view of using the fluid body as an actual part of the fluid. The fluid body is not merely a kinematical, but also a dynamical, entity. The domain is thus *simply connected* (see Figure 2.7). A body force density $\mathbf{f}_{\text{ext}}$ is applied within

[25]Lin J. C. & Rockwell D., Force identification by vorticity fields: techniques based on flow imaging, *Journal of*

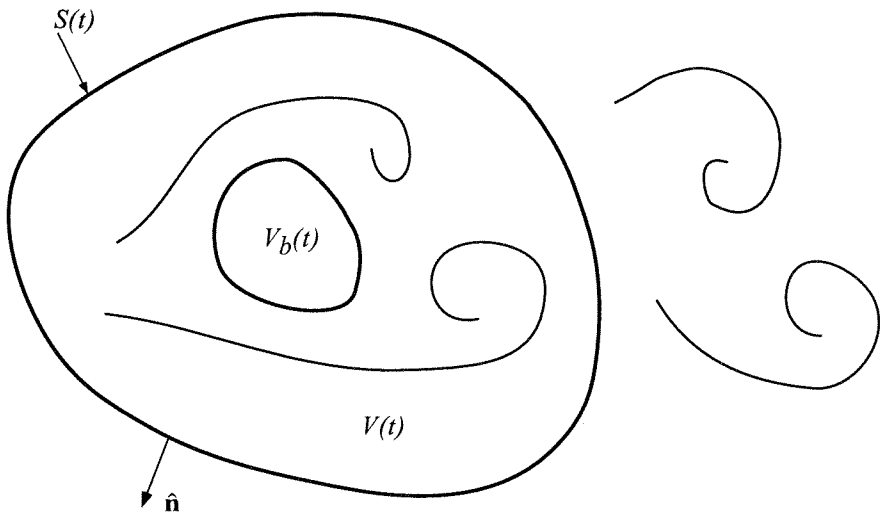


Figure 2.7: Control volume analysis for the derivation of the "impulse equation" in a finite, simply connected domain.

the body volume such that the external force required to maintain the fluid body in a given motion can be expressed as:

$$\mathbf{F}_{\text{ext}} = \int_{V_b(t)} \mathbf{f}_{\text{ext}}\, dV. \tag{2.71}$$

The force $\mathbf{F}$ of the fluid onto the body has to be inferred from $\mathbf{F}_{\text{ext}}$. Writing the sum of the forces as the rate of change of momentum $\mathbf{p}$, we obtain:

$$\mathbf{F} + \mathbf{F}_{\text{ext}} = \frac{d\mathbf{p}}{dt}. \tag{2.72}$$

The "rate of change of body momentum" may require some thought since the body is fluid. For bodies in steady motion, it vanishes, and we just have: $\mathbf{F} = -\mathbf{F}_{\text{ext}}$. Saffman[27] does offer an expression for it:

$$\mathbf{F} + \mathbf{F}_{\text{ext}} = \frac{d}{dt} \int_{V_b(t)} \mathbf{u}\, dV. \tag{2.73}$$

We will see that this result, besides being acceptable from a physical point of view, is also consistent with the equations obtained in Chapter 3.

---

*Fluids and Structures* **10** (1996) 663-668.

[26]Saffman P.E., *Vortex dynamics*, Cambridge University Press, 1993.

[27]Saffman P.E., *Vortex dynamics*, §4.2, Cambridge University Press, 1993.

### 2.5.2 Starting equations

The starting point for Saffman's derivation is the Navier-Stokes equations (actually the inviscid form of them, i.e. , the Euler equations):

$$\frac{\partial \mathbf{u}}{\partial t} + \boldsymbol{\nabla}(\frac{1}{2}u^2) - \mathbf{u} \wedge \boldsymbol{\omega} = -\boldsymbol{\nabla} p + \mathbf{f}_{\text{ext}}, \tag{2.74}$$

which are made valid both *inside* and *outside* the body, with the condition that the force density $\mathbf{f}_{\text{ext}}$ be null outside the body. For instance, if the fluid body is *rigid*, the force density has to be just large enough to keep each fluid particle within the body from moving. As a matter of fact, it should just be equal to:

$$\mathbf{f}_{\text{ext}} = \frac{\partial \mathbf{u}_b}{\partial t} + \boldsymbol{\nabla} p, \tag{2.75}$$

where $\mathbf{u}_b$ is the rigid body translational velocity and $p$, the pressure field within the fluid body.

As for the vorticity equation, we have:

$$\frac{\partial \boldsymbol{\omega}}{\partial t} - \boldsymbol{\nabla} \wedge (\mathbf{u} \wedge \boldsymbol{\omega}) = \boldsymbol{\nabla} \wedge \mathbf{f}_{\text{ext}}. \tag{2.76}$$

In Chapter 3, we will see that the representation of the body by a volume of (kinematical or dynamical) fluid is actually unnecessary (even though it is perfectly valid).

### 2.5.3 Derivation

What follows is a derivation along the lines of the one given in Saffman's monograph[28]. He starts by taking the time derivative of the impulse, as defined in Paragraph 2.4.6:

$$\begin{aligned} \frac{1}{\mathcal{N}-1} \frac{d}{dt} \int_{V(t)+V_b(t)} \mathbf{x} \wedge \boldsymbol{\omega}\, dV &= \frac{1}{\mathcal{N}-1} \int_{V(t)+V_b(t)} \mathbf{x} \wedge \frac{\partial \boldsymbol{\omega}}{\partial t}\, dV \\ &\quad + \frac{1}{\mathcal{N}-1} \oint_{S(t)} \hat{\mathbf{n}} \cdot \mathbf{u}_S\, \mathbf{x} \wedge \boldsymbol{\omega}\, dS. \end{aligned} \tag{2.77}$$

Use of the vorticity equation (Equation 2.76) yields:

$$\begin{aligned} \frac{1}{\mathcal{N}-1} \frac{d}{dt} \int_{V(t)+V_b(t)} \mathbf{x} \wedge \boldsymbol{\omega}\, dV &= \frac{1}{\mathcal{N}-1} \int_{V(t)+V_b(t)} \mathbf{x} \wedge [\boldsymbol{\nabla} \wedge (\mathbf{u} \wedge \boldsymbol{\omega}) + \boldsymbol{\nabla} \wedge \mathbf{f}_{\text{ext}}]\, dV \\ &\quad + \frac{1}{\mathcal{N}-1} \oint_{S(t)} \hat{\mathbf{n}} \cdot \mathbf{u}_S\, (\mathbf{x} \wedge \boldsymbol{\omega})\, dS. \end{aligned} \tag{2.78}$$

Application of the identity given in Equation 2.54 gives:

$$\frac{1}{\mathcal{N}-1} \int_{V(t)+V_b(t)} \mathbf{x} \wedge [\boldsymbol{\nabla} \wedge (\mathbf{u} \wedge \boldsymbol{\omega})]\, dV = \int_{V(t)+V_b(t)} \mathbf{u} \wedge \boldsymbol{\omega}\, dV$$

[28] Saffman P.E., *Vortex dynamics*, Chapters 3, 4, & 7, Cambridge University Press, 1993.

$$+\frac{1}{\mathcal{N}-1}\oint_{S(t)}\mathbf{x}\wedge[\hat{\mathbf{n}}\wedge(\mathbf{u}\wedge\boldsymbol{\omega})]\,dS, \qquad (2.79)$$

and:

$$\begin{aligned}\frac{1}{\mathcal{N}-1}\int_{V(t)+V_b(t)}\mathbf{x}\wedge\boldsymbol{\nabla}\wedge\mathbf{f}_{\text{ext}}\,dV &= \int_{V(t)+V_b(t)}\mathbf{f}_{\text{ext}}\,dV \\ &\quad+\frac{1}{\mathcal{N}-1}\oint_{S(t)}\mathbf{x}\wedge(\hat{\mathbf{n}}\wedge\mathbf{f}_{\text{ext}})\,dS. \qquad (2.80)\end{aligned}$$

If the force density vanishes outside the body, the surface integral in the latter equation vanishes as well. Also, with:

$$\int_{V(t)+V_b(t)}\mathbf{f}_{\text{ext}}\,dV=\int_{V_b(t)}\mathbf{f}_{\text{ext}}\,dV=\mathbf{F}_{\text{ext}}, \qquad (2.81)$$

we obtain:

$$\begin{aligned}\frac{1}{\mathcal{N}-1}\frac{d}{dt}\int_{V(t)+V_b(t)}\mathbf{x}\wedge\boldsymbol{\omega}\,dV &= \mathbf{F}_{\text{ext}}+\int_{V(t)+V_b(t)}\mathbf{u}\wedge\boldsymbol{\omega}\,dV \\ &\quad+\frac{1}{\mathcal{N}-1}\oint_{S(t)}\mathbf{x}\wedge[\hat{\mathbf{n}}\wedge(\mathbf{u}\wedge\boldsymbol{\omega})]\,dS+\frac{1}{\mathcal{N}-1}\oint_{S(t)}\hat{\mathbf{n}}\cdot\mathbf{u}_S\,\mathbf{x}\wedge\boldsymbol{\omega}\,dS. \qquad (2.82)\end{aligned}$$

Rearranging the equation, we finally reach the desired result:

$$\begin{aligned}-\mathbf{F}_{\text{ext}} &= -\frac{1}{\mathcal{N}-1}\frac{d}{dt}\int_{V(t)+V_b(t)}\mathbf{x}\wedge\boldsymbol{\omega}\,dV+\int_{V(t)+V_b(t)}\mathbf{u}\wedge\boldsymbol{\omega}\,dV \\ &\quad+\frac{1}{\mathcal{N}-1}\oint_{S(t)}\{\mathbf{x}\wedge[\hat{\mathbf{n}}\wedge(\mathbf{u}\wedge\boldsymbol{\omega})]+\hat{\mathbf{n}}\cdot\mathbf{u}_S\,\mathbf{x}\wedge\boldsymbol{\omega}\}\,dS. \qquad (2.83)\end{aligned}$$

This equation can be modified a bit further using a previously encountered identity:

$$\int_{V(t)+V_b(t)}\mathbf{u}\wedge\boldsymbol{\omega}\,dV=\oint_{S(t)}\hat{\mathbf{n}}\cdot(\frac{1}{2}u^2\mathbf{I}-\mathbf{u}\,\mathbf{u})\,dS. \qquad (2.84)$$

The final result is:

$$-\mathbf{F}_{\text{ext}}=-\frac{1}{\mathcal{N}-1}\frac{d}{dt}\int_{V(t)+V_b(t)}\mathbf{x}\wedge\boldsymbol{\omega}\,dV+\oint_{S(t)}\hat{\mathbf{n}}\cdot\boldsymbol{\Upsilon}_{\mathbf{i}}^{*}\,dS, \qquad (2.85)$$

where the tensor $\boldsymbol{\Upsilon}_{\mathbf{i}}^{*}$ is:

$$\boldsymbol{\Upsilon}_{\mathbf{i}}^{*} = \frac{1}{2}u^2\mathbf{I}-\mathbf{u}\mathbf{u}-\frac{1}{\mathcal{N}-1}(\mathbf{u}-\mathbf{u}_S)\,(\mathbf{x}\wedge\boldsymbol{\omega})+\frac{1}{\mathcal{N}-1}\,\boldsymbol{\omega}\,(\mathbf{x}\wedge\mathbf{u}). \qquad (2.86)$$

The tensor $\boldsymbol{\Upsilon}_{\mathbf{i}}^{*}$ has been written with the subscript $\mathbf{i}$, which stands for the *impulse*, since it appears in an equation in which the impulse appears explicitly[29]. As a matter of fact, we can write:

$$-\mathbf{F}_{\text{ext}} = -\frac{d\mathbf{i}_T}{dt} + \oint_{S(t)} \hat{\mathbf{n}} \cdot \boldsymbol{\Upsilon}_{\mathbf{i}}^{*}\, dS, \tag{2.87}$$

where $\mathbf{i}_T$ is the *total impulse in the whole region* $V(t) + V_b(t)$:

$$\mathbf{i}_T = \frac{1}{\mathcal{N}-1} \int_{V(t)+V_b(t)} \mathbf{x} \wedge \boldsymbol{\omega}\, dV. \tag{2.88}$$

This equation can be found in Saffman's monograph[30]. With a similar derivation, Moreau[31] obtained an equation which included the viscous terms.

Note that the "impulse equation" for an infinite domain can be recovered since at suitably large distances (with no net circulation in 2D), the surface integral vanishes:

$$\oint_{S_\infty} \hat{\mathbf{n}} \cdot \boldsymbol{\Upsilon}_{\mathbf{i}}^{*}\, dS \sim 0, \tag{2.89}$$

Using the result in Equation 2.73 which relates $\mathbf{F}_{\text{ext}}$ to $\mathbf{F}$, the actual fluid-dynamic force, we then see that Equation 2.85 does indeed transform into Equation 2.63. Incidentally, this result justifies *a posteriori* the relation between $\mathbf{F}_{\text{ext}}$ and $\mathbf{F}$ as given in Equation 2.73.

We will see in Chapter 3 that Equation 2.85 can be recovered with a derivation in a *doubly connected* domain in which the body is not used as a domain of integration. We will thus remove any ambiguity that may have arisen in the reader's mind from the use of a fluid body concept.

[29]The asterisk just characterizes the *inviscid* form of the expression. Moreau derived a viscous version of this equation, see Moreau J. J., *J. Math. Pures Appl.*, Equation 14.5, **32** (1953) 41.

[30]Saffman P.E., *Vortex dynamics*, Chapter 3, 4 & 7, Cambridge University Press, 1993.

[31]Moreau J. J., *J. Math. Pures Appl.*, Equation 14.5, **32** (1953) 41.

# Chapter 3 "Impulse equation" for a finite, doubly connected domain

In Chapter 2, it was first shown that the fluid-dynamic force on a bluff-body could be evaluated *exactly* from a knowledge of the velocity field (and its derivatives) in an *arbitrary, finite domain* surrounding the body. However, the formulation required a *double quadrature*, i.e. , two successive integrations.

It was also shown that the force on a bluff-body could be obtained from a *single quadrature* of the velocity field (and its derivatives) albeit at the expense that *the domain of integration be infinite.* Also, the derivation was strongly dependent on the pressure conditions at infinity.

Finally, we presented an expression for the force on a bluff-body which only depended on the velocity field (and its derivatives) in a finite domain, with the condition that the domain be *simply connected.* As such, the use of a fluid body concept was essential.

In this chapter, we will breed these formulations and derive an expression for forces in *doubly connected domains*, i.e. , without integrations within the body, which only requires a *single quadrature* of the velocity field (and its derivatives) in a *finite, arbitrary domain* surrounding the body.

In Paragraph 3.1, we will present some useful vector identities, including the Impulse-Momentum Identity, which was already briefly introduced in Chapter 2, and the Pressure Identity.

In Paragraph 3.2, we will re-derive the "impulse equation", as obtained in Chapter 2, using a doubly connected domain.

In Paragraph 3.3, we will show a numerical validation of the resulting "impulse" equation.

In Paragraph 3.4, we will present a brief discussion about the added mass concept.

Finally, in Paragraph 3.5, we will give a detailed description of each term in the "impulse" equation.

In Chapter 4, we will present a relation similar to the "impulse equation", but with the impulse replaced by the flow momentum. Chapter 5 will remove the impulse and momentum altogether, and express the force in terms of surface integrals only.

## 3.1 Some useful vector identities

### 3.1.1 The Impulse-Momentum Identity

Most of the transformations that will be used in this chapter rely on the following identity, which we have already introduced in Chapter 2:

$$\boxed{\int_V \mathbf{x} \wedge \boldsymbol{\nabla} \wedge \mathbf{a}\, dV = (\mathcal{N}-1) \int_V \mathbf{a}\, dV + \oint_S \mathbf{x} \wedge (\hat{\mathbf{n}} \wedge \mathbf{a})\, dS}\,, \tag{3.1}$$

where $\mathbf{a}$ is an arbitrary vector field in a volume $V$ bounded by a surface $S$ and $\mathcal{N}$ is the dimension of the space under consideration ($\mathcal{N} = 3$ in 3D and $\mathcal{N} = 2$ in 2D for example).

#### Historical prelude

Invariably, anyone trying to relate the vorticity to the velocity field will (unknowingly) "derive" this identity. As a matter of fact, setting $\mathbf{a} = \mathbf{u}$ in Equation 3.1 yields:

$$\int_V \mathbf{x} \wedge \boldsymbol{\nabla} \wedge \mathbf{u}\, dV = (\mathcal{N}-1) \int_V \mathbf{u}\, dV + \oint_S \mathbf{x} \wedge (\hat{\mathbf{n}} \wedge \mathbf{u})\, dS, \tag{3.2}$$

or:

$$\frac{1}{\mathcal{N}-1} \int_V \mathbf{x} \wedge \boldsymbol{\omega}\, dV = \int_V \mathbf{u}\, dV + \frac{1}{\mathcal{N}-1} \oint_S \mathbf{x} \wedge (\hat{\mathbf{n}} \wedge \mathbf{u})\, dS, \tag{3.3}$$

where $\mathbf{u}$ is the velocity field and $\boldsymbol{\omega} = \boldsymbol{\nabla} \wedge \mathbf{u}$ the vorticity. The term on the left-hand side is the *impulse* as already introduced in Chapter 2, whereas the volume integral on the right-hand side should remind us of the flow *momentum*. It is Equation 3.3 (or an equation similar to it) which appears in the works of Thomson[1], Lamb[2], and Batchelor[3], although it is generally obtained from *integration by parts* without invoking Equation 3.1 like it was done here. Saffman[4] is among the few authors who calls directly upon Equation 3.1 for his derivations.

In 1931, Burgatti[5] derived an identity, of which Equation 3.1 was a particular case. However, even though Burgatti recovered many already known fluid-dynamic identities from his generalized identity, he did not write down Equation 3.1 nor Equation 3.3 explicitly, probably because he was not aware of the latter at the time.

Thus, the identity given in Equation 3.1 cannot really be attributed to any single author. Also, as we shall see, its proof is quite trivial, and ought not be christened with any particular name. As a result, we will just refer to it as the *Impulse-Momentum Identity*.

[1] Thomson J. J., *On the motion of vortex rings*, Adams prize Essay, London, 1883.
[2] Lamb H., *Hydrodynamics*, §152, Cambridge University Press, 1924.
[3] Batchelor G. K., *An introduction to fluid dynamics*, §7.2, Cambridge University Press, 1967.
[4] Saffman P.E., *Vortex dynamics*, Cambridge University Press, 1993.
[5] Burgatti P., *Bolletino della Unione Matematica Italiana*, **10** (1931) 1-5; see also Truesdell C., *Kinematics of vorticity*, Equation 7.4, Indiana University Press, 1954.

**Proof**

Note that the form of the Impulse-Momentum Identity depends strongly on the dimension of the space, $\mathcal{N}$. It is instructive to see how the space dimension arises in this identity. As in other identities involving the position vector (see the Appendix), the space dimension $\mathcal{N}$ appears quite often because of the identity:

$$\boldsymbol{\nabla} \cdot \mathbf{x} = \mathcal{N}, \tag{3.4}$$

where $\mathbf{x}$ is the position vector. The proof of this result is straightforward and is left to the reader.

With the help of indicial notation, it is possible to derive a myriad of new identities involving the position vector $\mathbf{x}$ and any arbitrary vector $\mathbf{a}$. The reader is encouraged to refer to the Appendix for a partial listing of them.

One such identity is:

$$\mathbf{x} \wedge (\boldsymbol{\nabla} \wedge \mathbf{a}) = (\mathcal{N} - 1)\mathbf{a} + \boldsymbol{\nabla}(\mathbf{x} \cdot \mathbf{a}) - \boldsymbol{\nabla} \cdot (\mathbf{x}\mathbf{a}), \tag{3.5}$$

which can be readily proven using indicial notation. Volume integration of this vector identity yields:

$$\int_V \mathbf{x} \wedge (\boldsymbol{\nabla} \wedge \mathbf{a})\, dV = (\mathcal{N} - 1) \int_V \mathbf{a}\, dV + \int_V [\boldsymbol{\nabla}(\mathbf{x} \cdot \mathbf{a}) - \boldsymbol{\nabla} \cdot (\mathbf{x}\mathbf{a})]\, dV. \tag{3.6}$$

The second integral on the right-hand side can be transformed into a surface integral through Green's theorem, thus yielding:

$$\int_V \mathbf{x} \wedge (\boldsymbol{\nabla} \wedge \mathbf{a})\, dV = (\mathcal{N} - 1) \int_V \mathbf{a}\, dV + \oint_S \hat{\mathbf{n}} \cdot [(\mathbf{x} \cdot \mathbf{a})\mathbf{I} - (\mathbf{x}\mathbf{a})]\, dS. \tag{3.7}$$

We have basically arrived at the desired result. The surface integrand may be put into a more elegant form:

$$\begin{aligned} \hat{\mathbf{n}} \cdot [(\mathbf{x} \cdot \mathbf{a})\mathbf{I} - (\mathbf{x}\mathbf{a})] &= (\mathbf{x} \cdot \mathbf{a})\hat{\mathbf{n}} - (\hat{\mathbf{n}} \cdot \mathbf{x})\mathbf{a}, \\ &= \mathbf{x} \wedge (\hat{\mathbf{n}} \wedge \mathbf{a}), \end{aligned} \tag{3.8}$$

from which we obtain the desired Impulse-Momentum Identity:

$$\int_V \mathbf{x} \wedge (\boldsymbol{\nabla} \wedge \mathbf{a})\, dV = (\mathcal{N} - 1) \int_V \mathbf{a}\, dV + \oint_S \mathbf{x} \wedge (\hat{\mathbf{n}} \wedge \mathbf{a})\, dS. \tag{3.9}$$

As mentioned in the historical prelude, this result can also be obtained from the generalized

Burgatti identity[6]:

$$\int_V [(\boldsymbol{\nabla} \wedge \mathbf{a}) \wedge \mathbf{b} + (\boldsymbol{\nabla} \wedge \mathbf{b}) \wedge \mathbf{a} + \mathbf{a}(\boldsymbol{\nabla} \cdot \mathbf{b}) + \mathbf{b}(\boldsymbol{\nabla} \cdot \mathbf{a})]\, dV = \oint_S [\hat{\mathbf{n}} \cdot (\mathbf{ab} + \mathbf{ba}) - (\mathbf{a} \cdot \mathbf{b})\hat{\mathbf{n}}]\, dS, \tag{3.10}$$

where $\mathbf{a}$ and $\mathbf{b}$ are any two arbitrary vectors. Now let $\mathbf{b} = \mathbf{x}$, and rewrite the above equation, keeping in mind that:

$$\boldsymbol{\nabla} \wedge \mathbf{x} = 0, \tag{3.11}$$

and

$$\boldsymbol{\nabla} \cdot \mathbf{x} = \mathcal{N}, \tag{3.12}$$

which yields:

$$\int_V [(\boldsymbol{\nabla} \wedge \mathbf{a}) \wedge \mathbf{x} + \mathcal{N}\mathbf{a} + \mathbf{x}(\boldsymbol{\nabla} \cdot \mathbf{a})]\, dV = \oint_S [\hat{\mathbf{n}} \cdot (\mathbf{ax} + \mathbf{xa}) - (\mathbf{a} \cdot \mathbf{x})\hat{\mathbf{n}}]\, dS. \tag{3.13}$$

Also, using the vector identities:

$$\mathbf{x} \wedge (\hat{\mathbf{n}} \wedge \mathbf{a}) = (\mathbf{a} \cdot \mathbf{x})\hat{\mathbf{n}} - \hat{\mathbf{n}} \cdot (\mathbf{xa}), \tag{3.14}$$

and

$$\boldsymbol{\nabla} \cdot (\mathbf{ax}) = \mathbf{x}(\boldsymbol{\nabla} \cdot \mathbf{a}) + \mathbf{a}, \tag{3.15}$$

one obtains:

$$\begin{aligned} \int_V \mathbf{x} \wedge (\boldsymbol{\nabla} \wedge \mathbf{a})\, dV = \\ (\mathcal{N} - 1) \int_V \mathbf{a}\, dV + \oint_S \mathbf{x} \wedge (\hat{\mathbf{n}} \wedge \mathbf{a})\, dS \\ + \int_V \boldsymbol{\nabla} \cdot (\mathbf{ax})\, dV - \oint_S \hat{\mathbf{n}} \cdot (\mathbf{ax})\, dS. \end{aligned} \tag{3.16}$$

By Green's theorem, the last two integrals cancel, and one finally recovers the Impulse-Momentum Identity as given in Equation 3.1.

In Chapter 5, we will derive additional identities which will allow us to transform every volume integral into a surface integral (under incompressible conditions).

As a final note, the space dimension $\mathcal{N}$ will be kept in the formulae throughout the derivations. However, most of the equations involve the vorticity vector which can be defined rigorously only in three dimensions, that is $\mathcal{N} = 3$. Nevertheless, a vorticity vector for planar flows can be defined by

[6]Burgatti P., *Bolletino della Unione Matematica Italiana*, **10** (1931) 1-5.

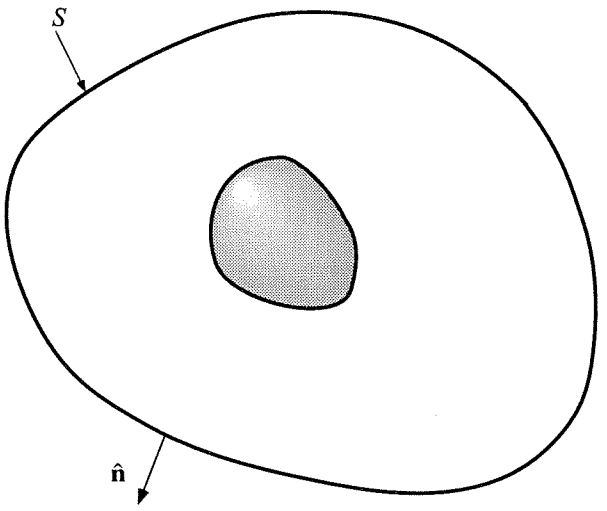


Figure 3.1: Doubly connected domain showing the surface of integration for the Pressure Identity.

extending the vortex lines to infinity in a direction normal to the plane of the flow. In this case, the flow is effectively two-dimensional, and we can set $\mathcal{N} = 2$.

### 3.1.2 The Pressure Identity

An essential identity which will allow us to bypass completely the fluid body concept is:

$$\boxed{(\mathcal{N}-1)\oint_S \phi\hat{\mathbf{n}}\,dS = -\oint_S \mathbf{x}\wedge(\hat{\mathbf{n}}\wedge\boldsymbol{\nabla}\phi)\,dS}\,, \tag{3.17}$$

where $\phi$ is a *single-valued* scalar on the surface $S$. Note that the domain enclosed by the surface can be *multiply connected* and need not to be simply connected (see Figure 3.1).

#### Prelude

The reader may point out that the identity in Equation 3.17 is just a particular case of the Impulse-Momentum identity in Equation 3.1 in which we set:

$$\mathbf{a} = \boldsymbol{\nabla}\phi. \tag{3.18}$$

This is true if the domain is simply connected, in which case the volume integrals over the volume $V$ enclosed by $S$ are well defined. As a matter of fact, we would have:

$$\int_V \mathbf{x}\wedge\boldsymbol{\nabla}\wedge(\boldsymbol{\nabla}\phi)\,dV = 0, \tag{3.19}$$

and, from Green's theorem:

$$\int_V \nabla\phi \, dV = \int_S \phi\hat{\mathbf{n}} \, dS, \tag{3.20}$$

and inserting these results into Equation 3.1 would, in fact, yield Equation 3.17. The above proof is actually the one given by Saffman[7].

However, for a *multiply-connected* domain, this derivation fails since the integrations are ill-defined in parts of the volume $V$.

We will now see that the identity given by Equation 3.17 is actually correct for a multiply-connected domain.

This identity will often arise when transforming integrals involving the pressure field $p$, in which case we will set $\phi = p$. We will thus refer to it as the *Pressure Identity*. Some authors know it only as a particular case of the Impulse-Momentum Identity, but this is true only for simply connected domains.

**Proof**

The proof of the Pressure Identity starts from the following vector identity:

$$\nabla \wedge (\mathbf{x} \wedge \phi\mathbf{I}) = -\mathbf{I}(\mathcal{N}-1)\phi - \mathbf{I}(\mathbf{x}\cdot\nabla\phi) + \mathbf{x}\nabla\phi, \tag{3.21}$$

where $\mathbf{I}$ is the unit tensor, $\phi$ a scalar, and $\mathbf{x}$ the position vector. Again, the reader is encouraged to prove this identity with simple indicial notation.

Multiplying this vector identity with the unit vector $\hat{\mathbf{n}}$ from the left, and performing a surface integration over $S$ yields:

$$\oint_S \hat{\mathbf{n}}\cdot\nabla\wedge(\mathbf{x}\wedge\phi\mathbf{I})\,dS = -(\mathcal{N}-1)\oint_S \phi\hat{\mathbf{n}}\,dS - \oint_S [\hat{\mathbf{n}}\cdot(\mathbf{x}\cdot\nabla\phi) - (\hat{\mathbf{n}}\cdot\mathbf{x})\nabla\phi]\,dS. \tag{3.22}$$

The last integral on the right-hand side can be modified further from the identity:

$$\hat{\mathbf{n}}\cdot(\mathbf{x}\cdot\nabla\phi) - (\hat{\mathbf{n}}\cdot\mathbf{x})\nabla\phi = \mathbf{x}\wedge(\hat{\mathbf{n}}\wedge\nabla\phi). \tag{3.23}$$

From Stokes' Theorem, the surface integral on the left-hand side vanishes exactly if the scalar $\phi$ is *single-valued* on the surface $S$:

$$\oint_S \hat{\mathbf{n}}\cdot\nabla\wedge(\mathbf{x}\wedge\phi\mathbf{I})\,dS \equiv 0. \tag{3.24}$$

We thus arrive at the desired result:

$$(\mathcal{N}-1)\oint_S \phi\hat{\mathbf{n}}\,dS = -\oint_S \mathbf{x}\wedge(\hat{\mathbf{n}}\wedge\nabla\phi)\,dS. \tag{3.25}$$

[7]Saffman P. G., *Vortex dynamics*, §4.2, Cambridge University Press, 1993.

The reader must appreciate that this derivation never required integrations anywhere else other than on the surface itself.

Also, note that this identity requires the scalar $\phi$ to be single valued. In the derivations, the scalar $\varphi$ will just represent the pressure field, which will be assumed single-valued from a physical point of view.

## 3.2 The "impulse equation"

In this paragraph, we will re-derive the "impulse equation" without using the fluid body concept. The starting equation will be Equation 2.22 as given in Chapter 2, which we reproduce here:

$$\begin{aligned}\mathbf{F} &= -\frac{d}{dt}\int_{V(t)} \mathbf{u}\, dV \\ &\quad + \oint_{S(t)} \hat{\mathbf{n}} \cdot [-p\mathbf{I} - (\mathbf{u} - \mathbf{u}_S)\,\mathbf{u} + \mathbf{T}]\, dS \\ &\quad - \oint_{S_b(t)} \hat{\mathbf{n}} \cdot (\mathbf{u} - \mathbf{u}_S)\,\mathbf{u}\, dS,\end{aligned} \tag{3.26}$$

where the last term just expresses a through flow condition at the body surface, as in the case of a jet engine.

### 3.2.1 Infinite domain

As in Chapter 2, we will assume that there is no net circulation, that $\mathbf{u}_{S_\infty} = 0$, and that the viscous terms are negligible at infinity (see Figure 3.2), so that:

$$\oint_{S_\infty} \hat{\mathbf{n}} \cdot (-(\mathbf{u} - \mathbf{u}_S)\,\mathbf{u} + \mathbf{T})\, dS \sim 0. \tag{3.27}$$

However, we will not make any assumptions regarding the pressure integral:

$$\oint_{S_\infty} p\hat{\mathbf{n}}\, dS, \tag{3.28}$$

which we are leaving as arbitrary[8]. We will actually see that it cancels another term often erroneously neglected. The starting equation will then be:

$$\begin{aligned}\mathbf{F} &= -\frac{d}{dt}\int_{V_\infty(t)} \mathbf{u}\, dV - \oint_{S_\infty} p\hat{\mathbf{n}}\, dS \\ &\quad - \oint_{S_b(t)} \hat{\mathbf{n}} \cdot (\mathbf{u} - \mathbf{u}_S)\,\mathbf{u}\, dS.\end{aligned} \tag{3.29}$$

[8]We will see in Chapter 4 that this term is indeed not equal to zero.

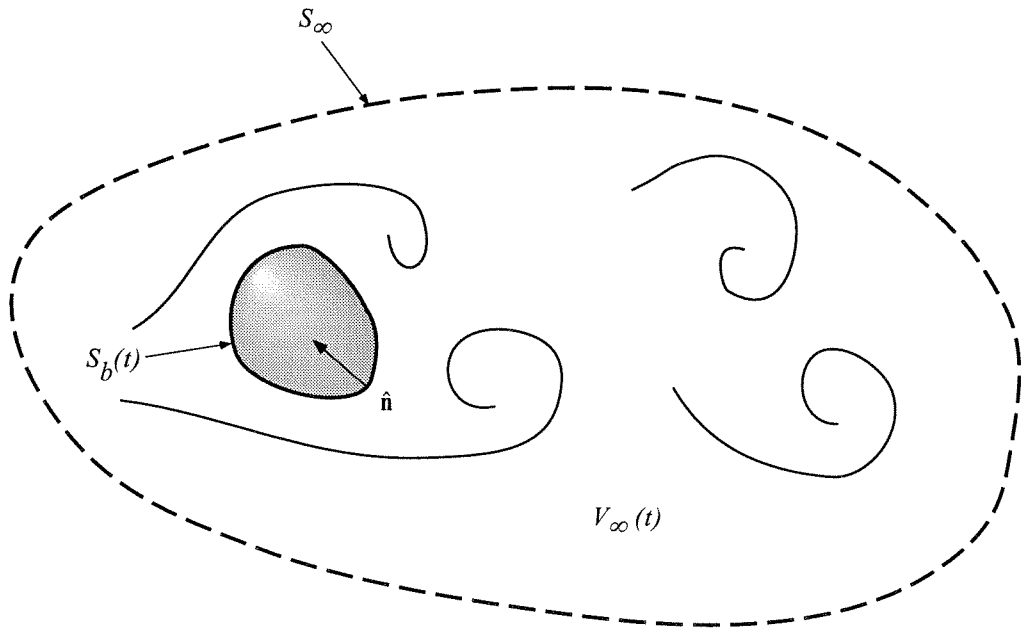


Figure 3.2: Control volume analysis for the derivation of the "impulse equation" in an infinite, doubly connected domain.

Using the Impulse-Momentum Identity with $\mathbf{a} = \mathbf{u}$ on the first integral, and an umbilicus over which the integral vanishes, we obtain:

$$\begin{aligned}
\mathbf{F} \;=\; & -\frac{1}{\mathcal{N}-1}\frac{d}{dt}\int_{V_\infty(t)} \mathbf{x}\wedge\boldsymbol{\omega}\,dV \\
& +\frac{1}{\mathcal{N}-1}\frac{d}{dt}\oint_{S_\infty} \mathbf{x}\wedge(\hat{\mathbf{n}}\wedge\mathbf{u})\,dS - \oint_{S_\infty} p\hat{\mathbf{n}}\,dS \\
& +\frac{1}{\mathcal{N}-1}\frac{d}{dt}\oint_{S_b(t)} \mathbf{x}\wedge(\hat{\mathbf{n}}\wedge\mathbf{u})\,dS - \oint_{S_b(t)} \hat{\mathbf{n}}\cdot(\mathbf{u}-\mathbf{u}_S)\,\mathbf{u}\,dS,
\end{aligned} \tag{3.30}$$

where $\hat{\mathbf{n}}$ on $S_b(t)$ points *into* the surface. Let us look at the time derivative of the surface integral over $S_\infty$. The time derivative can be taken inside the integral:

$$\frac{1}{\mathcal{N}-1}\frac{d}{dt}\oint_{S_\infty} \mathbf{x}\wedge(\hat{\mathbf{n}}\wedge\mathbf{u})\,dS = \frac{1}{\mathcal{N}-1}\oint_{S_\infty} \mathbf{x}\wedge(\hat{\mathbf{n}}\wedge\frac{\partial\mathbf{u}}{\partial t})\,dS. \tag{3.31}$$

The integrand can be evaluated through the use of the Navier-Stokes equations:

$$\frac{\partial\mathbf{u}}{\partial t} = -\boldsymbol{\nabla}p - \boldsymbol{\nabla}\cdot(\mathbf{u}\mathbf{u}) + \boldsymbol{\nabla}\cdot\mathbf{T}. \tag{3.32}$$

With the proper behavior of the velocity at infinity (as indicated above), the integral of the inertia and viscous terms over $S_\infty$ vanishes:

$$\oint_{S_\infty} \mathbf{x} \wedge [\hat{\mathbf{n}} \wedge (-\boldsymbol{\nabla} \cdot (\mathbf{uu}) + \boldsymbol{\nabla} \cdot \mathbf{T})]\, dS \sim 0. \tag{3.33}$$

The pressure term can be given a different form by using the Pressure Identity:

$$-\frac{1}{\mathcal{N}-1} \oint_{S_\infty} \mathbf{x} \wedge (\hat{\mathbf{n}} \wedge \boldsymbol{\nabla} p)\, dS = \oint_{S_\infty} p\hat{\mathbf{n}}\, dS. \tag{3.34}$$

We now see that this integral cancels the one in Equation 3.30, and the resulting equation becomes:

$$\begin{aligned} \mathbf{F} \;=\; & -\frac{1}{\mathcal{N}-1}\frac{d}{dt}\int_{V_\infty(t)} \mathbf{x} \wedge \boldsymbol{\omega}\, dV \\ & + \frac{1}{\mathcal{N}-1}\frac{d}{dt}\oint_{S_b(t)} \mathbf{x} \wedge (\hat{\mathbf{n}} \wedge \mathbf{u})\, dS - \oint_{S_b(t)} \hat{\mathbf{n}} \cdot (\mathbf{u} - \mathbf{u}_S)\, \mathbf{u}\, dS. \end{aligned} \tag{3.35}$$

This is the most general equation for the instantaneous force on a body with the following assumptions:

- The flow is incompressible,
- The volume $V_\infty(t)$ extends to infinity and encloses *all* the vorticity,
- The surface integrals of the viscous and convective terms vanish at infinity.

Note that no assumption was made about the nature of the body and about the pressure at infinity.

### 3.2.2 Finite domain

We are now ready to derive a general equation for the force on a bluff body in cross flow, in terms of the vorticity field in its vicinity (see Figure 3.3).

The derivation is identical to the one for the infinite domain, except that we do not neglect the surface integrals of the viscous and convective terms. The starting equation is then Equation 3.26 which we reproduce:

$$\begin{aligned} \mathbf{F} \;=\; & -\frac{d}{dt}\int_{V(t)} \mathbf{u}\, dV \\ & + \oint_{S(t)} \hat{\mathbf{n}} \cdot [-p\mathbf{I} - (\mathbf{u} - \mathbf{u}_S)\, \mathbf{u} + \mathbf{T}]\, dS \\ & - \oint_{S_b(t)} \hat{\mathbf{n}} \cdot (\mathbf{u} - \mathbf{u}_S)\, \mathbf{u}\, dS. \end{aligned} \tag{3.36}$$

Using the Impulse-Momentum Identity with $\mathbf{a} = \mathbf{u}$ on the first integral, and an umbilicus over which

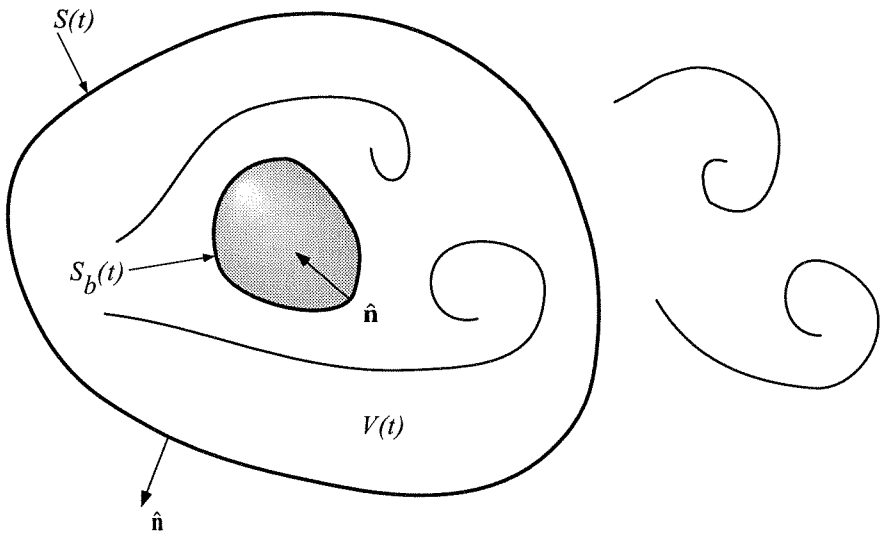


Figure 3.3: Control volume analysis for the derivation of the "impulse equation" in a finite, doubly connected domain.

the integral vanishes, we obtain:

$$\begin{aligned}\mathbf{F} \;=\; & -\frac{1}{\mathcal{N}-1}\frac{d}{dt}\int_{V(t)} \mathbf{x}\wedge\boldsymbol{\omega}\,dV \\ & +\frac{1}{\mathcal{N}-1}\frac{d}{dt}\oint_{S(t)} \mathbf{x}\wedge(\hat{\mathbf{n}}\wedge\mathbf{u})\,dS+\oint_{S(t)}\hat{\mathbf{n}}\cdot[-p\mathbf{I}-(\mathbf{u}-\mathbf{u}_S)\,\mathbf{u}+\mathbf{T}]\,dS \\ & +\frac{1}{\mathcal{N}-1}\frac{d}{dt}\oint_{S_b(t)} \mathbf{x}\wedge(\hat{\mathbf{n}}\wedge\mathbf{u})\,dS-\oint_{S_b(t)}\hat{\mathbf{n}}\cdot(\mathbf{u}-\mathbf{u}_S)\,\mathbf{u}\,dS,\end{aligned} \tag{3.37}$$

where it is to be remembered that $\hat{\mathbf{n}}$ on $S_b(t)$ points *into* the body. Let us look at the time derivative of the surface integral over $S(t)$. The time derivative of the surface integral can be manipulated through the use of a kinematic identity[9]:

$$\frac{d}{dt}\oint_{S(t)}\hat{\mathbf{n}}\cdot\Phi\,dS=\oint_{S(t)}\hat{\mathbf{n}}\cdot\left[\frac{\partial\Phi}{\partial t}+\mathbf{u}_S(\boldsymbol{\nabla}\cdot\Phi)\right]dS. \tag{3.38}$$

We can write the integrand of interest as follows:

$$\mathbf{x}\wedge(\hat{\mathbf{n}}\wedge\mathbf{u})=\hat{\mathbf{n}}\cdot[(\mathbf{x}\cdot\mathbf{u})\mathbf{I}-\mathbf{x}\mathbf{u}], \tag{3.39}$$

so that the Aris identity in Equation 3.38 can be used with:

$$\Phi=(\mathbf{x}\cdot\mathbf{u})\mathbf{I}-\mathbf{x}\mathbf{u}, \tag{3.40}$$

[9]Aris R., *Vectors, tensors, and the basic equations of fluid mechanics*, Dover, 1962; Aris only gives the relation for a vector, but it is easy to generalize it to a tensor.

which yields:

$$\frac{d}{dt}\oint_{S(t)} \hat{\mathbf{n}} \cdot [(\mathbf{x}\cdot\mathbf{u})\mathbf{I} - \mathbf{x}\mathbf{u}]\, dS = \tag{3.41}$$

$$\oint_{S(t)} \hat{\mathbf{n}} \cdot \left\{ \frac{\partial}{\partial t}[(\mathbf{x}\cdot\mathbf{u})\mathbf{I} - \mathbf{x}\mathbf{u}] + \mathbf{u}_S \boldsymbol{\nabla} \cdot [(\mathbf{x}\cdot\mathbf{u})\mathbf{I} - \mathbf{x}\mathbf{u}] \right\} dS. \tag{3.42}$$

The time derivative can be transformed back to:

$$\frac{\partial}{\partial t}[(\mathbf{x}\cdot\mathbf{u})\mathbf{I} - \mathbf{x}\mathbf{u}] = \mathbf{x} \wedge (\hat{\mathbf{n}} \wedge \frac{\partial \mathbf{u}}{\partial t}), \tag{3.43}$$

where the $\mathbf{u}$ time derivative can be obtained from the Navier Stokes equations:

$$\frac{\partial \mathbf{u}}{\partial t} = -\boldsymbol{\nabla}(p + \frac{1}{2}u^2) + \mathbf{u} \wedge \boldsymbol{\omega} + \boldsymbol{\nabla} \cdot \mathbf{T}. \tag{3.44}$$

The divergence term becomes:

$$\boldsymbol{\nabla} \cdot [(\mathbf{x}\cdot\mathbf{u})\mathbf{I} - \mathbf{x}\mathbf{u}] = \boldsymbol{\nabla}(\mathbf{x}\cdot\mathbf{u}) - \boldsymbol{\nabla}\cdot(\mathbf{x}\mathbf{u}). \tag{3.45}$$

Each term can be evaluated separately:

$$\boldsymbol{\nabla}(\mathbf{x}\cdot\mathbf{u}) = (\mathbf{x}\cdot\boldsymbol{\nabla})\mathbf{u} + \mathbf{u} + \mathbf{x}\wedge\boldsymbol{\omega}, \tag{3.46}$$

and:

$$\boldsymbol{\nabla}\cdot(\mathbf{x}\mathbf{u}) = \mathcal{N}\mathbf{u} + (\mathbf{x}\cdot\boldsymbol{\nabla})\mathbf{u}, \tag{3.47}$$

therefore:

$$\boldsymbol{\nabla} \cdot [(\mathbf{x}\cdot\mathbf{u})\mathbf{I} - \mathbf{x}\mathbf{u}] = -(\mathcal{N}-1)\mathbf{u} + \mathbf{x}\wedge\boldsymbol{\omega}. \tag{3.48}$$

Finally, we obtain:

$$\frac{d}{dt}\oint_{S(t)} \mathbf{x}\wedge(\hat{\mathbf{n}}\wedge\mathbf{u})\, dS =$$

$$\oint_{S(t)} \mathbf{x} \wedge \left\{ \hat{\mathbf{n}} \wedge [-\boldsymbol{\nabla}(p + \frac{1}{2}u^2) + \mathbf{u}\wedge\boldsymbol{\omega} + \boldsymbol{\nabla}\cdot\mathbf{T})] \right\} dS \tag{3.49}$$

$$+ \oint_{S(t)} \hat{\mathbf{n}} \cdot \mathbf{u}_S\, [-(\mathcal{N}-1)\mathbf{u} + \mathbf{x}\wedge\boldsymbol{\omega}]\, dS.$$

Now, the integral involving the pressure tensor can be transformed using the Pressure Identity:

$$\oint_{S(t)} \mathbf{x} \wedge \left\{ \hat{\mathbf{n}} \wedge [-\boldsymbol{\nabla}(p + \frac{1}{2}u^2)] \right\} dS = (\mathcal{N}-1) \oint_{S(t)} (p + \frac{1}{2}u^2)\hat{\mathbf{n}}\, dS. \tag{3.50}$$

Finally:

$$\begin{aligned}\frac{d}{dt}\oint_{S(t)} \mathbf{x}\wedge(\hat{\mathbf{n}}\wedge\mathbf{u})\,dS = \\ \oint_{S(t)} \mathbf{x}\wedge[\hat{\mathbf{n}}\wedge(\mathbf{u}\wedge\boldsymbol{\omega})]\,dS \\ +\oint_{S(t)} \hat{\mathbf{n}}\cdot\mathbf{u}_S\,[-(\mathcal{N}-1)\mathbf{u}+\mathbf{x}\wedge\boldsymbol{\omega}]\;dS \\ +(\mathcal{N}-1)\oint_{S(t)}(p+\frac{1}{2}u^2)\hat{\mathbf{n}}\,dS+\oint_{S(t)}\mathbf{x}\wedge[\hat{\mathbf{n}}\wedge(\boldsymbol{\nabla}\cdot\mathbf{T})]\,dS.\end{aligned} \tag{3.51}$$

The first integral on the right-hand side can be modified further:

$$\oint_{S(t)} \mathbf{x}\wedge[\hat{\mathbf{n}}\wedge(\mathbf{u}\wedge\boldsymbol{\omega})]\,dS = \oint_{S(t)}[\hat{\mathbf{n}}\cdot\boldsymbol{\omega}\,(\mathbf{x}\wedge\mathbf{u})-\hat{\mathbf{n}}\cdot\mathbf{u}\,(\mathbf{x}\wedge\boldsymbol{\omega})]\;dS. \tag{3.52}$$

Similarly, the last integral on the right-hand side becomes:

$$\oint_{S(t)} \mathbf{x}\wedge[\hat{\mathbf{n}}\wedge(\boldsymbol{\nabla}\cdot\mathbf{T})]\,dS = \oint_{S(t)}[(\mathbf{x}\cdot\boldsymbol{\nabla}\cdot\mathbf{T})\hat{\mathbf{n}}-(\mathbf{x}\cdot\hat{\mathbf{n}})\boldsymbol{\nabla}\cdot\mathbf{T}]\;dS. \tag{3.53}$$

Then, Equation 3.51 becomes:

$$\begin{aligned}\frac{d}{dt}\oint_{S(t)} \mathbf{x}\wedge(\hat{\mathbf{n}}\wedge\mathbf{u})\,dS = \\ -\oint_{S(t)} \hat{\mathbf{n}}\cdot(\mathbf{u}-\mathbf{u}_S)\,(\mathbf{x}\wedge\boldsymbol{\omega})\,dS \\ -(\mathcal{N}-1)\oint_{S(t)}\hat{\mathbf{n}}\cdot\mathbf{u}_S\,\mathbf{u}\,dS+\oint_{S(t)}\hat{\mathbf{n}}\cdot\boldsymbol{\omega}\,(\mathbf{x}\wedge\mathbf{u})\,dS \\ +(\mathcal{N}-1)\oint_{S(t)}(p+\frac{1}{2}u^2)\hat{\mathbf{n}}\,dS+\oint_{S(t)}[(\mathbf{x}\cdot\boldsymbol{\nabla}\cdot\mathbf{T})\hat{\mathbf{n}}-(\mathbf{x}\cdot\hat{\mathbf{n}})\boldsymbol{\nabla}\cdot\mathbf{T}]\;dS.\end{aligned} \tag{3.54}$$

Inserting Equation 3.54 back into Equation 3.37, one finally obtains the desired equation:

$$\begin{aligned}\mathbf{F} &= -\frac{1}{\mathcal{N}-1}\frac{d}{dt}\int_{V(t)}\mathbf{x}\wedge\boldsymbol{\omega}\,dV \\ &\quad+\oint_{S(t)}\hat{\mathbf{n}}\cdot\boldsymbol{\Upsilon}_{\mathbf{i}}\,dS \\ &\quad+\frac{1}{\mathcal{N}-1}\frac{d}{dt}\oint_{S_b(t)}\mathbf{x}\wedge(\hat{\mathbf{n}}\wedge\mathbf{u})\,dS-\oint_{S_b(t)}\hat{\mathbf{n}}\cdot(\mathbf{u}-\mathbf{u}_S)\,\mathbf{u}\,dS,\end{aligned} \tag{3.55}$$

where the tensor $\boldsymbol{\Upsilon}_{\mathbf{i}}$ is:

$$\begin{aligned}\boldsymbol{\Upsilon}_{\mathbf{i}} &= \frac{1}{2}u^2\mathbf{I}-\mathbf{u}\mathbf{u}-\frac{1}{\mathcal{N}-1}(\mathbf{u}-\mathbf{u}_S)\,(\mathbf{x}\wedge\boldsymbol{\omega})+\frac{1}{\mathcal{N}-1}\boldsymbol{\omega}\,(\mathbf{x}\wedge\mathbf{u}) \\ &\quad+\frac{1}{\mathcal{N}-1}[\mathbf{x}\cdot(\boldsymbol{\nabla}\cdot\mathbf{T})\mathbf{I}-\mathbf{x}(\boldsymbol{\nabla}\cdot\mathbf{T})]+\mathbf{T}.\end{aligned} \tag{3.56}$$

The subscript $\mathbf{i}$ in $\boldsymbol{\Upsilon}_\mathbf{i}$ stands for the $\mathbf{i}$-mpulse as given by the volume integral[10].

This is the most general equation for the force on a body. The body is not required to be neither rigid nor solid. It is valid for rotational and viscous flows. The control volume which encloses the body is arbitrary, and can be chosen at will. The surface of the control volume can lie anywhere in the flow as long as it englobes the body.

### Alternative forms

This expression can take many alternative forms. In Chapter 2, we introduced the identity:

$$\oint_{S(t)} \hat{\mathbf{n}} \cdot (\frac{1}{2}u^2\mathbf{I} - \mathbf{u}\,\mathbf{u})\,dS = \int_{V(t)} \mathbf{u} \wedge \boldsymbol{\omega}\,dV - \oint_{S_b(t)} \hat{\mathbf{n}} \cdot (\frac{1}{2}u^2\mathbf{I} - \mathbf{u}\,\mathbf{u})\,dS, \tag{3.57}$$

where the volume term is recognized as being the Kutta-Zhukovsky force (with the difference that the present volume integral does not include the body). Introducing this identity into Equation 3.55 gives:

$$\begin{aligned} \mathbf{F} \;=\; & -\frac{1}{\mathcal{N}-1}\frac{d}{dt}\int_{V(t)} \mathbf{x} \wedge \boldsymbol{\omega}\,dV + \int_{V(t)} \mathbf{u} \wedge \boldsymbol{\omega}\,dV \\ & + \oint_{S(t)} \hat{\mathbf{n}} \cdot \boldsymbol{\Upsilon}'_\mathbf{i}\,dS \\ & + \frac{1}{\mathcal{N}-1}\frac{d}{dt}\oint_{S_b(t)} \mathbf{x} \wedge (\hat{\mathbf{n}} \wedge \mathbf{u})\,dS - \oint_{S_b(t)} (\frac{1}{2}u^2\hat{\mathbf{n}} - \hat{\mathbf{n}} \cdot \mathbf{u}_S\,\mathbf{u})\,dS, \end{aligned} \tag{3.58}$$

where the tensor $\boldsymbol{\Upsilon}'_\mathbf{i}$ is:

$$\begin{aligned} \boldsymbol{\Upsilon}'_\mathbf{i} \;=\; & -\frac{1}{\mathcal{N}-1}(\mathbf{u} - \mathbf{u}_S)\,(\mathbf{x} \wedge \boldsymbol{\omega}) + \frac{1}{\mathcal{N}-1}\boldsymbol{\omega}\,(\mathbf{x} \wedge \mathbf{u}) \\ & + \frac{1}{\mathcal{N}-1}[\mathbf{x} \cdot (\boldsymbol{\nabla} \cdot \mathbf{T})\mathbf{I} - \mathbf{x}(\boldsymbol{\nabla} \cdot \mathbf{T})] + \mathbf{T}. \end{aligned} \tag{3.59}$$

Yet another form can be obtained by considering the volume $V(t)$ to be material such that on $S(t)$ and $S_b(t)$, $\mathbf{u}_S = \mathbf{u}$. Then:

$$\begin{aligned} \mathbf{F} \;=\; & -\frac{1}{\mathcal{N}-1}\frac{d}{dt}\int_{V_m(t)} \mathbf{x} \wedge \boldsymbol{\omega}\,dV \\ & + \oint_{S_m(t)} \hat{\mathbf{n}} \cdot \boldsymbol{\Upsilon}_{\mathbf{i}_m}\,dS \\ & + \frac{1}{\mathcal{N}-1}\frac{d}{dt}\oint_{S_b(t)} \mathbf{x} \wedge (\hat{\mathbf{n}} \wedge \mathbf{u})\,dS, \end{aligned} \tag{3.60}$$

[10] We will derive in Chapter 4 an equation with a volume integral representing the momentum, for which we will use the subscript $\mathbf{p}$. We will also present an expression devoid of volume integrals, in which case the subscript will be absent all together.

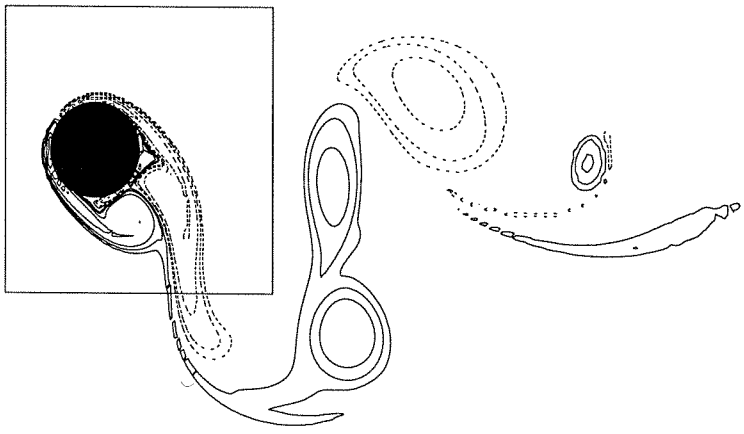

Figure 3.4: Vorticity field from computations with bounding box for force calculations. (Courtesy Doug Shiels.)

where the tensor $\boldsymbol{\Upsilon}_{\mathbf{i}_m}$ is:

$$\begin{aligned}\boldsymbol{\Upsilon}_{\mathbf{i}_m} &= \frac{1}{2}u^2\mathbf{I} - \mathbf{uu} + \frac{1}{\mathcal{N}-1}\boldsymbol{\omega}\,(\mathbf{x}\wedge\mathbf{u}) \\ &\quad + \frac{1}{\mathcal{N}-1}[\mathbf{x}\cdot(\boldsymbol{\nabla}\cdot\mathbf{T})\mathbf{I} - \mathbf{x}(\boldsymbol{\nabla}\cdot\mathbf{T})] + \mathbf{T}. \end{aligned} \tag{3.61}$$

We have thus arrived at some expressions (as given in Equation 3.55, Equation 3.58, or Equation 3.60) which could be used experimentally for the determination of forces. In the next paragraph, we will show some numerical validations of these equations. In Paragraph 3.5, we will dissect these equations, in order to develop a feel for each term and raise possible issues associated with these formulations. Chapter 4 and Chapter 5 will be dedicated to the solution of these issues.

## 3.3 Numerical validation

The computational work was performed by Doug Shiels, to whom I am strongly indebted. The details of the computation are given in a recent paper[11], and we will only mention the gross features. A high resolution vortex-method code[12] was used on the flow past a cylinder performing a normal oscillation normal to the flow direction with velocity $\sin(4\pi t/13)$. The cylinder traveled 12 diameters

[11]Noca F., Shiels D., & Jeon D., Measuring instantaneous fluid dynamic forces on bodies, using only velocity fields and their derivatives, *Journal of Fluids and Structures*, in press, 1997.

[12]Koumoutsakos P. & Leonard A., High-resolution simulations of the flow around an impulsively started cylinder using vortex methods, *Journal of Fluid Mechanics* **296** (1995) 1-38.

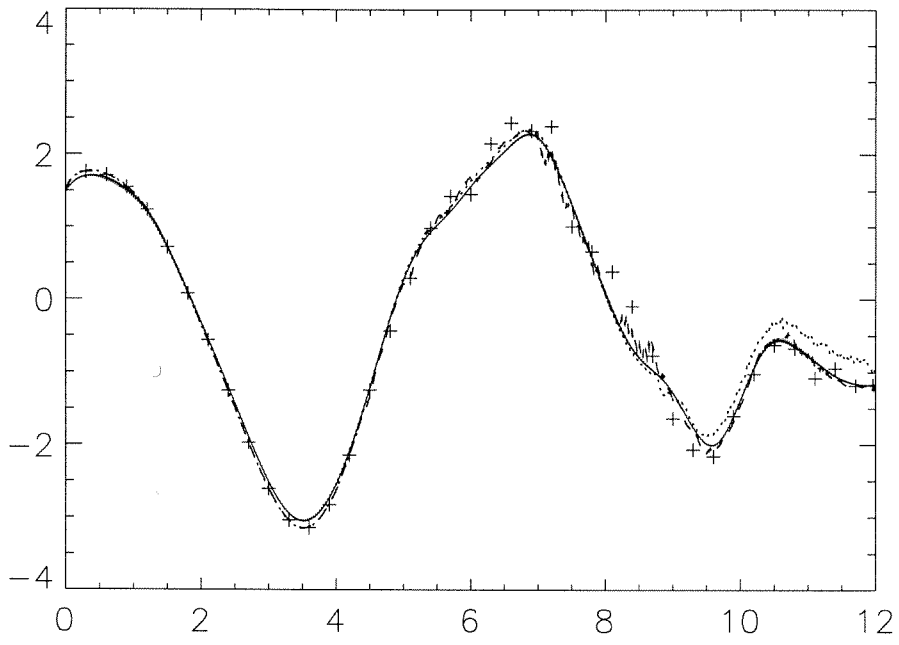


Figure 3.5: Comparison of lift coefficients $C_L$ obtained by several methods: $\cdots$, "impulse equation" in an infinite domain (particle-based data); ——, pressure and shear stress on the body; $- - -$, "impulse equation" in a finite domain (particle-based data); $+ + +$, "impulse equation" in a finite domain (gridded data). (Courtesy Doug Shiels.)

downstream from an impulsive start, resulting in the vorticity field in Figure 3.4.

The lift coefficient on the cylinder was computed with different methods:

- pressure and shear stress on the body surface, Equation 2.10;
- "impulse equation" for an infinite domain, Equation 3.35;
- "impulse equation" for an finite domain, Equation 3.55, where the domain of integration is shown by the box surrounding the cylinder in Figure 3.4;
- "impulse equation" for an finite domain, Equation 3.55, with data placed on a grid of mesh size $\sim 0.004$ diameters.

The results are shown in Figure 3.5. The agreement is obviously very satisfactory. The reader is strongly encouraged to refer to Doug Shiels' report[13] for a thorough discussion of the numerical results.

[13]Shiels D., *Ae 200 Report*, California institute of Technology, Spring 1996.

## 3.4 Added mass

Much confusion exists in the fluid mechanics community regarding the *added mass* concept. Saffman[14] gives a clear account of it. We will try to expand on Saffman discussion in order to provide a clearer view of the concept.

If:

- the flow is inviscid,
- the flow is vorticity-free,
- there exists no net circulation around the body (in two dimensions),
- the no-through flow condition applies at the body surface,

then the fluid-dynamic force given by Equation 3.55 takes the form:

$$\mathbf{F} = \frac{1}{\mathcal{N}-1}\frac{d}{dt}\oint_{S_b(t)} \mathbf{x} \wedge (\hat{\mathbf{n}} \wedge \mathbf{u})\, dS, \tag{3.62}$$

which Saffman[15] proves to be the force due to added mass. In particular, he shows that the term:

$$\mathbf{i}_b = \frac{1}{\mathcal{N}-1}\oint_{S_b(t)} \mathbf{x} \wedge (\hat{\mathbf{n}} \wedge \mathbf{u})\, dS, \tag{3.63}$$

is the *virtual momentum* of the body.

We would like to investigate the case where any of the conditions stated above fails to apply.

We will look at the case of a body which is started from rest with an impulsive acceleration in a (initially vorticity-free) quiescent, viscous fluid. We assume that:

- the flow is viscous,
- the no-slip boundary condition applies at the body surface,
- the no-through flow condition applies at the body surface.

For early times (when the vorticity is limited to a vortex-sheet on the body surface), the fluid-dynamic force on the body is given by:

$$\mathbf{F}(t=0^+) = -\frac{1}{\mathcal{N}-1}\frac{d}{dt}\int_{V(t)} \mathbf{x} \wedge \boldsymbol{\omega}\, dV + \frac{1}{\mathcal{N}-1}\frac{d}{dt}\oint_{S_b(t)} \mathbf{x} \wedge (\hat{\mathbf{n}} \wedge \mathbf{u}_b)\, dS, \tag{3.64}$$

where $\mathbf{u}_b$ is the body velocity.

[14] Saffman, P. G., *Vortex dynamics*, §4, Cambridge University Press, 1993.
[15] Saffman, P. G., *Vortex dynamics*, §4, Cambridge University Press, 1993.

For early times, the vortex sheet on the body surface is given by:

$$\boldsymbol{\omega} = [\hat{\mathbf{n}} \wedge (\mathbf{u} - \mathbf{u}_b)]\, \delta(\mathbf{x} - \mathbf{x}_b), \tag{3.65}$$

where $\mathbf{u}$ is the potential flow velocity outside the vortex sheet and $\mathbf{u}_b$ is the body velocity. Then, we can write:

$$\begin{aligned} \int_{V(t)} \mathbf{x} \wedge \boldsymbol{\omega}\, dV &= \int_{V(t)} \mathbf{x} \wedge [\hat{\mathbf{n}} \wedge (\mathbf{u} - \mathbf{u}_b)]\, \delta(\mathbf{x} - \mathbf{x}_b)\, dV \\ &= \oint_{S_b(t)} \mathbf{x} \wedge [\hat{\mathbf{n}} \wedge (\mathbf{u} - \mathbf{u}_b)]\, dS, \end{aligned} \tag{3.66}$$

where $\hat{\mathbf{n}}$ points outward from the body. Inserting this result in Equation 3.64 and choosing the unit vector $\hat{\mathbf{n}}$ to point *into* the body, we obtain:

$$\begin{aligned} \mathbf{F}(t = 0^+) &= \frac{1}{\mathcal{N} - 1} \frac{d}{dt} \oint_{S_b(t)} \mathbf{x} \wedge [\hat{\mathbf{n}} \wedge (\mathbf{u} - \mathbf{u}_b)]\, dS + \frac{1}{\mathcal{N} - 1} \frac{d}{dt} \oint_{S_b(t)} \mathbf{x} \wedge (\hat{\mathbf{n}} \wedge \mathbf{u}_b)\, dS, \\ &= \frac{1}{\mathcal{N} - 1} \frac{d}{dt} \oint_{S_b(t)} \mathbf{x} \wedge (\hat{\mathbf{n}} \wedge \mathbf{u})\, dS, \end{aligned} \tag{3.67}$$

which is exactly the same result as obtained previously with $\mathbf{u}$ representing not the body surface velocity but the potential flow velocity right outside the body vortex sheet.

## 3.5 Discussion

Obviously, all the expressions in Equation 3.55, Equation 3.58, or Equation 3.60, are independent of pressure. As a result, they can be evaluated as long as velocity field data is known. Experimentally, a technique such as Digital Particle Image Velocimetry (DPIV) does yield velocity data, and thus forces can actually be measured from a knowledge of the flowfield only.

A closer look at Equation 3.55 reveals three main terms, a volume term,

$$\frac{1}{\mathcal{N} - 1} \frac{d}{dt} \int_{V(t)} \mathbf{x} \wedge \boldsymbol{\omega}\, dV, \tag{3.68}$$

a control surface term,

$$\oint_{S(t)} \hat{\mathbf{n}} \cdot \boldsymbol{\Upsilon}_{\mathbf{i}}\, dS, \tag{3.69}$$

and a body surface term,

$$\frac{1}{\mathcal{N} - 1} \frac{d}{dt} \oint_{S_b(t)} \mathbf{x} \wedge (\hat{\mathbf{n}} \wedge \mathbf{u})\, dS - \oint_{S_b(t)} \hat{\mathbf{n}} \cdot (\mathbf{u} - \mathbf{u}_S)\, \mathbf{u}\, dS. \tag{3.70}$$

We will now examine practical problems involved in the evaluation of these terms.

- The volume integral:

$$\frac{1}{\mathcal{N}-1}\frac{d}{dt}\int_{V(t)}\mathbf{x}\wedge\boldsymbol{\omega}\,dV, \tag{3.71}$$

requires the evaluation of vorticity within the *whole* control volume. The DPIV technique does allow such a measurement with good accuracy, except in the boundary layer region next to the body, which may be under resolved. Note, though, that only the time derivative of this quantity is needed. If the flow happens to be steady in the boundary layers, this term can be reasonably neglected. However, in the case of unsteady boundary layers as for the flow past an oscillating cylinder (or even for the flow past a stationary cylinder with an unsteady wake), this assumption is completely invalid.

Note that a straight application of this volume integral to a quasi-steady boundary layer does generate extremely noisy signal levels, well above the sought force signal. To begin with, the vorticity levels in the boundary layer are extremely high, and any small *virtual* fluctuation generated by under resolution yields a very large time derivative. Thus, for practical purposes, this volume term has to be intentionally omitted in boundary layer regions, even in the case of quasi-steady boundary layers.

Also, note that since DPIV is a two-dimensional technique, only the vorticity component normal to the measurement plane can effectively be evaluated. Thus, this technique is only suitable for nominally two-dimensional flows[16].

- The surface term:

$$\oint_{S(t)}\hat{\mathbf{n}}\cdot\boldsymbol{\Upsilon}_{\mathbf{i}}\,dS, \tag{3.72}$$

is quite benign, since it involves no time derivatives and only integration over a surface at some distance from the body. We therefore expect the flow scales to be larger than in a boundary layer (at least for nominally two-dimensional flows) and to be accurately resolved. We will now look at each term under the surface integral separately.

1. The control surface term,

$$\oint_{S(t)}[\frac{1}{2}u^2\hat{\mathbf{n}}-(\hat{\mathbf{n}}\cdot\mathbf{u})\,\mathbf{u}]\,dS, \tag{3.73}$$

was shown to be equivalent to the Kutta-Zhukovsky or vortex force:

$$\int_{V(t)}\mathbf{u}\wedge\boldsymbol{\omega}\,dV-\oint_{S_b(t)}\hat{\mathbf{n}}\cdot(\frac{1}{2}u^2\mathbf{I}-\mathbf{u}\,\mathbf{u})\,dS, \tag{3.74}$$

where the second term can be evaluated readily when the no-slip condition applies and the body surface motion is known (see the discussion below about the body surface terms). DPIV can evaluate both the surface and volume integrals independently, and

[16] An upcoming three-dimensional version of DPIV may render the formulation applicable to 3D flows.

thus offers two equivalent ways of evaluating the same term. From various experiments applied to different flowfields, it was noticed that the results are essentially identical, even if boundary layers are under resolved. This particularity probably results from the presence of the velocity vector $\mathbf{u}$ inside the volume integral. Since in a boundary layer velocity is small, it may remove the contribution from the boundary layers all together. Nonetheless, if boundary layers may be a source of worry, the surface integral may just be used instead.

Experiments show that this term (whether taken as a surface or as a volume integral) yields a very "clean" signal, and it seems to be a dominant term for the force on bodies in *steady* motion. The numerical and experimental results in Chapter 5 will illustrate this point.

2. The term,

$$-\frac{1}{\mathcal{N}-1}\oint_{S(t)}\hat{\mathbf{n}}\cdot(\mathbf{u}-\mathbf{u}_S)\,(\mathbf{x}\wedge\boldsymbol{\omega})\,dS, \tag{3.75}$$

requires the evaluation of vorticity along the surface of the control volume. This term is in general smooth in an inertial frame. However, in the case of body-fixed frames for non-inertial motions, it was noticed[17] that this term is quite substantial in magnitude and appears to be closely anticorrelated with the volume integral term. That is, whenever one term is very large, the other one will be of the same order of magnitude, and opposite. When added up, they tend to cancel for the most part except for a small remainder. In experimental situations, it is always very problematic to have two large terms cancel each other, and yield an accurate (small) remainder. This result probably suggests that either the two terms ought to be combined or that the forces be measured in an inertial frame (not body-fixed). Actually, the two terms are indeed connected through the relation:

$$\begin{aligned}\frac{1}{\mathcal{N}-1}\frac{d}{dt}\int_{V_m(t)}\mathbf{x}\wedge\boldsymbol{\omega}\,dV = \\ \frac{1}{\mathcal{N}-1}\frac{d}{dt}\int_{V(t)}\mathbf{x}\wedge\boldsymbol{\omega}\,dV+\frac{1}{\mathcal{N}-1}\oint_{S(t)}\hat{\mathbf{n}}\cdot(\mathbf{u}-\mathbf{u}_S)\,(\mathbf{x}\wedge\boldsymbol{\omega})\,dS,\end{aligned} \tag{3.76}$$

where $V_m(t)$ is the *material* control volume coinciding at time $t$ with the arbitrary control volume $V(t)$. However, in practice, material volumes are not easy to deal with experimentally, and one often prefers to work with fixed volumes.

3. The term,

$$\frac{1}{\mathcal{N}-1}\oint_{S(t)}\hat{\mathbf{n}}\cdot\boldsymbol{\omega}\,(\mathbf{x}\wedge\mathbf{u})\,dS, \tag{3.77}$$

is a three-dimensional term. Since DPIV is intrinsically a 2D technique, this term can-

[17] D. Jeon, personal communication.

not effectively be evaluated, and the technique for measuring forces is thus limited to nominally two-dimensional flows. DPIV makes measurements over a plane, and only the components of vorticity normal to this plane can be evaluated. Thus, by construction, the measured vorticity field is perpendicular to the unit normal of the control volume surface.

4. The term,

$$\oint_{S(t)} \hat{\mathbf{n}} \cdot \left\{ \frac{1}{\mathcal{N}-1} [\mathbf{x} \cdot (\boldsymbol{\nabla} \cdot \mathbf{T})\mathbf{I} - \mathbf{x}(\boldsymbol{\nabla} \cdot \mathbf{T})] + \mathbf{T} \right\} dS, \tag{3.78}$$

involves only a knowledge of the viscous tensor over the surface of the control volume. For flows at moderate to high Reynolds numbers and for control surfaces sufficiently distant from the body (by one body diameter or more), this term is essentially negligible. Nonetheless, it can be evaluated by DPIV, at least for nominally two-dimensional flows.

- The body surface term:

$$\frac{1}{\mathcal{N}-1} \frac{d}{dt} \oint_{S_b(t)} \mathbf{x} \wedge (\hat{\mathbf{n}} \wedge \mathbf{u})\, dS - \oint_{S_b(t)} \hat{\mathbf{n}} \cdot (\mathbf{u} - \mathbf{u}_S)\, \mathbf{u}\, dS, \tag{3.79}$$

may be evaluated in a straightforward manner from a knowledge of the body motion and the body surface velocity.

1. The term,

$$\frac{1}{\mathcal{N}-1} \frac{d}{dt} \oint_{S_b(t)} \mathbf{x} \wedge (\hat{\mathbf{n}} \wedge \mathbf{u})\, dS, \tag{3.80}$$

can be easily evaluated from the unsteady flow velocity at the body surface $S_b(t)$.

For a *no-slip condition* at the wall, this term just requires the velocity component of the wall. For instance, in the case of a fish, one would need to know the motion of the body surface of the fish. If a body is suited with a sliding belt, as in the case of airfoils which try to delay separation, then the velocity of the belt would have to be known.

2. The term,

$$-\oint_{S_b(t)} \hat{\mathbf{n}} \cdot (\mathbf{u} - \mathbf{u}_S)\, \mathbf{u}\, dS, \tag{3.81}$$

represents the net mass flux through the body surface. It is particularly important for self-propelling bodies with a jet flow such as jet engines, or animals such as salps or squids[18]. Again, this term has to be known. In particular, for a *no-through flow* condition, this integral vanishes.

3. The term,

$$-\oint_{S_b(t)} (\frac{1}{2} u^2 \hat{\mathbf{n}} - \hat{\mathbf{n}} \cdot \mathbf{u}_S\, \mathbf{u})\, dS, \tag{3.82}$$

[18] Gharib M., lecture notes from *Fluid mechanics in Nature*, Ae 240, Caltech, 1997.

which arises in Equation 3.58 in connection with the Kutta-Zhukovsky or vortex force, can similarly be evaluated. The reader is referred to the preceding discussion regarding the other body terms.

In summary, the only term that requires particular attention is the volume integral in Equation 3.71, i.e. , the time derivative of the impulse. In the following Chapter, we will see that this volume integral (which involves the vorticity $\boldsymbol{\omega}$) can be transformed into a volume integral involving the velocity field $\mathbf{u}$ only, i.e. , the time derivative of the momentum. In Chapter 5, we will also show that the volume terms can actually be removed altogether in incompressible flows, and be replaced with surface integrals only.

# Chapter 4 "Momentum equation" for a finite, doubly connected domain

In Chapter 3, we derived an "impulse equation" for a doubly connected domain which allowed the evaluation of the force on a bluff body only from a knowledge of the velocity field (and its derivatives) in an arbitrary, finite region surrounding the body. The expression required a single quadrature, and was given by:

$$\begin{aligned}\mathbf{F} &= -\frac{1}{\mathcal{N}-1}\frac{d}{dt}\int_{V(t)}\mathbf{x}\wedge\boldsymbol{\omega}\,dV \\ &\quad+\oint_{S(t)}\hat{\mathbf{n}}\cdot\boldsymbol{\Upsilon}_{\mathbf{i}}\,dS \\ &\quad+\frac{1}{\mathcal{N}-1}\frac{d}{dt}\oint_{S_b(t)}\mathbf{x}\wedge(\hat{\mathbf{n}}\wedge\mathbf{u})\,dS-\oint_{S_b(t)}\hat{\mathbf{n}}\cdot(\mathbf{u}-\mathbf{u}_S)\,\mathbf{u}\,dS,\end{aligned} \tag{4.1}$$

where the tensor $\boldsymbol{\Upsilon}_{\mathbf{i}}$ is:

$$\begin{aligned}\boldsymbol{\Upsilon}_{\mathbf{i}} &= \frac{1}{2}u^2\mathbf{I}-\mathbf{uu}-\frac{1}{\mathcal{N}-1}(\mathbf{u}-\mathbf{u}_S)\,(\mathbf{x}\wedge\boldsymbol{\omega})+\frac{1}{\mathcal{N}-1}\boldsymbol{\omega}\,(\mathbf{x}\wedge\mathbf{u}) \\ &\quad+\frac{1}{\mathcal{N}-1}[\mathbf{x}\cdot(\boldsymbol{\nabla}\cdot\mathbf{T})\mathbf{I}-\mathbf{x}(\boldsymbol{\nabla}\cdot\mathbf{T})]+\mathbf{T}.\end{aligned} \tag{4.2}$$

We pointed out that the volume integral, i.e. , the time derivative of the impulse, was problematic in experimental work, since it required the evaluation of the vorticity in the body boundary layer.

In Paragraph 4.1 of this Chapter, we will replace the time derivative of the impulse by the time derivative of the momentum with some algebraic manipulations. The resulting "momentum" equation will thus involve volume integrations of the *velocity field* only, which presumably is easier to resolve than the vorticity field, especially in the boundary layers.

In Paragraph 4.2, we will present a numerical validation of the "momentum" equation.

In Paragraph 4.3, we will compare the resulting equation with previous versions derived in Chapter 2 which involve the flow momentum. In particular, we will see how the equations written in terms of double quadrature can actually be transformed into single quadratures. We will then discover how the pressure integral can be written as a surface integral of the velocity field and its derivatives.

In Chapter 5, we will present an alternative expression which will be completely devoid of volume integrals, and which will involve only surface integrals. This transformation will be made possible by the incompressiblity condition.

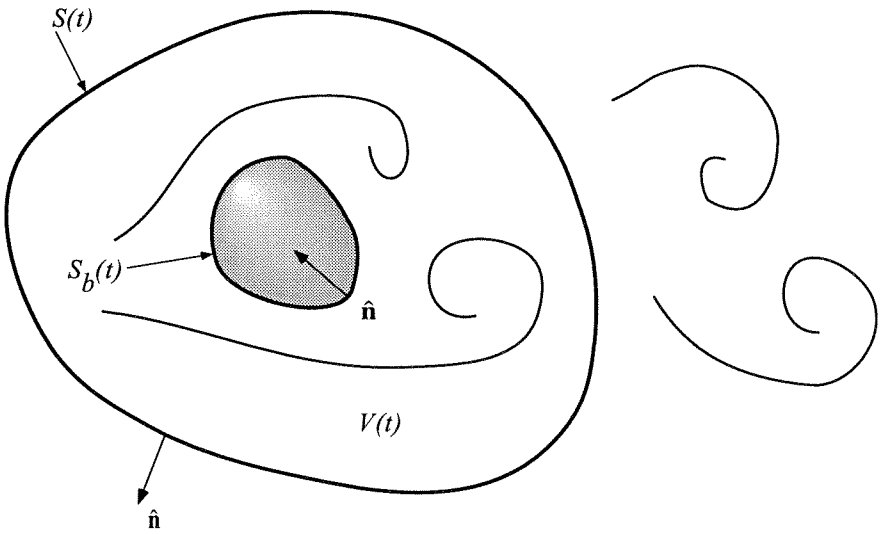


Figure 4.1: Control volume analysis for the "momentum equation".

## 4.1 The "momentum equation"

### 4.1.1 Derivation

The starting point is the use of the Impulse-Momentum Identity on the volume integral in Equation 4.1 (see Figure 4.1):

$$\begin{aligned} -\frac{1}{\mathcal{N}-1}\frac{d}{dt}\int_{V(t)} \mathbf{x}\wedge\boldsymbol{\omega}\,dV = \\ -\frac{d}{dt}\int_{V(t)} \mathbf{u}\,dV - \frac{1}{\mathcal{N}-1}\frac{d}{dt}\int_{S(t)} \mathbf{x}\wedge(\hat{\mathbf{n}}\wedge\mathbf{u})\,dS \\ -\frac{1}{\mathcal{N}-1}\frac{d}{dt}\int_{S_b(t)} \mathbf{x}\wedge(\hat{\mathbf{n}}\wedge\mathbf{u})\,dS. \end{aligned} \tag{4.3}$$

The force in Equation 4.1 then takes the form:

$$\begin{aligned} \mathbf{F} \;=\; & -\frac{d}{dt}\int_{V(t)} \mathbf{u}\,dV \\ & -\frac{1}{\mathcal{N}-1}\frac{d}{dt}\int_{S(t)} \mathbf{x}\wedge(\hat{\mathbf{n}}\wedge\mathbf{u})\,dS + \oint_{S(t)} \hat{\mathbf{n}}\cdot\boldsymbol{\Upsilon}'_{\mathbf{p}}\,dS \\ & -\oint_{S_b(t)} \hat{\mathbf{n}}\cdot(\mathbf{u}-\mathbf{u}_S)\,\mathbf{u}\,dS, \end{aligned} \tag{4.4}$$

where the tensor $\boldsymbol{\Upsilon}'_{\mathbf{p}}$ is just equal to $\boldsymbol{\Upsilon}_{\mathbf{i}}$ given in Equation 4.2. The tensor $\boldsymbol{\Upsilon}'_{\mathbf{p}}$ has been written with the subscript $\mathbf{p}$, which stands for the momentum, since the equation involves the flow momentum.

In Equation 4.4, the volume integral is now taken over the velocity field $\mathbf{u}$ which presumably

is smoother than the vorticity field $\boldsymbol{\omega}$ (or more exactly the moment of vorticity field $\mathbf{x} \wedge \boldsymbol{\omega}$). This is true in particular within the boundary layers next to the body. The penalty to be paid is the evaluation of an additional integral over the surface of the bounding box and a time derivative of it.

The time derivative of the surface integral can be transformed further following the procedure given in Chapter 3:

$$\begin{aligned} -\frac{1}{\mathcal{N}-1}\frac{d}{dt}\int_{S(t)} \mathbf{x} \wedge (\hat{\mathbf{n}} \wedge \mathbf{u})\, dS = \\ -\frac{1}{\mathcal{N}-1}\int_{S(t)} \hat{\mathbf{n}} \cdot \left[ (\mathbf{x} \cdot \frac{\partial \mathbf{u}}{\partial t})\mathbf{I} - \mathbf{x}\frac{\partial \mathbf{u}}{\partial t} \right] dS \\ -\frac{1}{\mathcal{N}-1}\int_{S(t)} \hat{\mathbf{n}} \cdot \mathbf{u}_S \left[ -(\mathcal{N}-1)\mathbf{u} + \mathbf{x} \wedge \boldsymbol{\omega} \right] dS, \end{aligned} \tag{4.5}$$

thus yielding:

$$\begin{aligned} \mathbf{F} &= -\frac{d}{dt}\int_{V(t)} \mathbf{u}\, dV \\ &\quad + \oint_{S(t)} \hat{\mathbf{n}} \cdot \boldsymbol{\Upsilon}_{\mathbf{p}}\, dS \\ &\quad - \oint_{S_b(t)} \hat{\mathbf{n}} \cdot (\mathbf{u} - \mathbf{u}_S)\, \mathbf{u}\, dS, \end{aligned} \tag{4.6}$$

where the tensor $\boldsymbol{\Upsilon}_{\mathbf{p}}$ is equal to:

$$\begin{aligned} \boldsymbol{\Upsilon}_{\mathbf{p}} &= \frac{1}{2}u^2\mathbf{I} + (\mathbf{u}_S - \mathbf{u})\mathbf{u} - \frac{1}{\mathcal{N}-1}\mathbf{u}\,(\mathbf{x} \wedge \boldsymbol{\omega}) + \frac{1}{\mathcal{N}-1}\,\boldsymbol{\omega}\,(\mathbf{x} \wedge \mathbf{u}) \\ &\quad -\frac{1}{\mathcal{N}-1}\left[ (\mathbf{x} \cdot \frac{\partial \mathbf{u}}{\partial t})\mathbf{I} - \mathbf{x}\frac{\partial \mathbf{u}}{\partial t} \right] \\ &\quad +\frac{1}{\mathcal{N}-1}[\mathbf{x} \cdot (\boldsymbol{\nabla} \cdot \mathbf{T})\mathbf{I} - \mathbf{x}(\boldsymbol{\nabla} \cdot \mathbf{T})] + \mathbf{T}. \end{aligned} \tag{4.7}$$

This last version (Equation 4.6) may or may not be preferable to Equation 4.4, depending on whether the time derivative of a surface integral is smoother than the integral of a time derivative.

We are leaving to the reader the task of deriving alternate expressions in terms of material volumes or in terms of the Kutta-Zhukovsky force, as in Chapter 3.

## 4.2 Numerical validation

The procedure used was identical to the one given in Paragraph 3.3. The only difference regards the mesh size of the grid onto which the data was placed. Instead of a fine grid size of $\sim 0.004$ diameters, a coarser grid size of $\sim 0.05$ diameters was now used. A snapshot of the vorticity field at $t \sim 13$ is shown in Figure 4.2.

The size of Figure 4.2 also represents the box size used for the domain of integration. The result

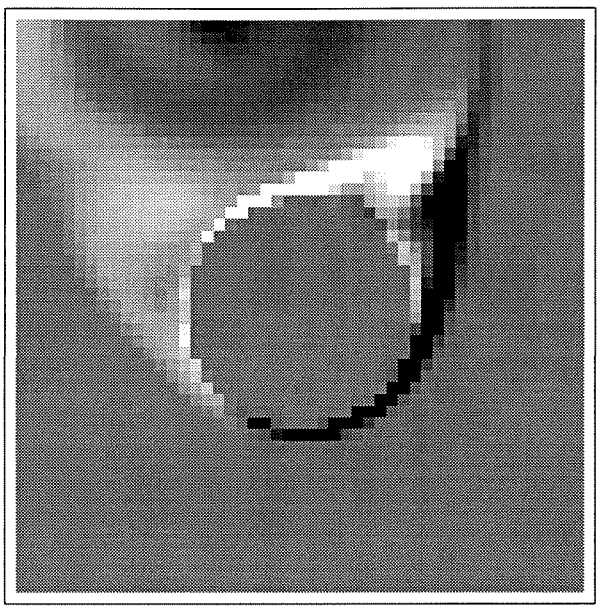

Figure 4.2: Vorticity field from computations with data placed on a coarse grid.

for the lift coefficient is shown in Figure 4.3 and compared to the "exact" result as obtained from the "impulse equation" with highly resolved data (see Paragraph 3.3). Again, the results are very satisfactory. As a comparison, the "impulse equation" was tested on this coarse data, and Figure 4.3 certainly shows that the latter equation does not fare as well as the "momentum equation". This suggests that volume integration of velocity data is preferable to volume integration of vorticity data (or more exactly, moment of vorticity data $\mathbf{x} \wedge \boldsymbol{\omega}$). We will return to this point when discussing our experimental results.

## 4.3 Comparison with other equations

In Chapter 2, we derived some expressions based on momentum. It would be interesting at this point to see how they relate to Equation 4.6.

### 4.3.1 The original "momentum equation"

The original "momentum equation" is given in Equation 2.22 which we reproduce here:

$$\begin{aligned} \mathbf{F} \;=\; & -\frac{d}{dt}\int_{V(t)} \mathbf{u}\, dV \\ & + \oint_{S(t)} \hat{\mathbf{n}} \cdot [-p\mathbf{l} - (\mathbf{u} - \mathbf{u}_S)\,\mathbf{u} + \mathbf{T}]\, dS \\ & - \oint_{S_b(t)} \hat{\mathbf{n}} \cdot (\mathbf{u} - \mathbf{u}_S)\,\mathbf{u}\, dS. \end{aligned} \tag{4.8}$$

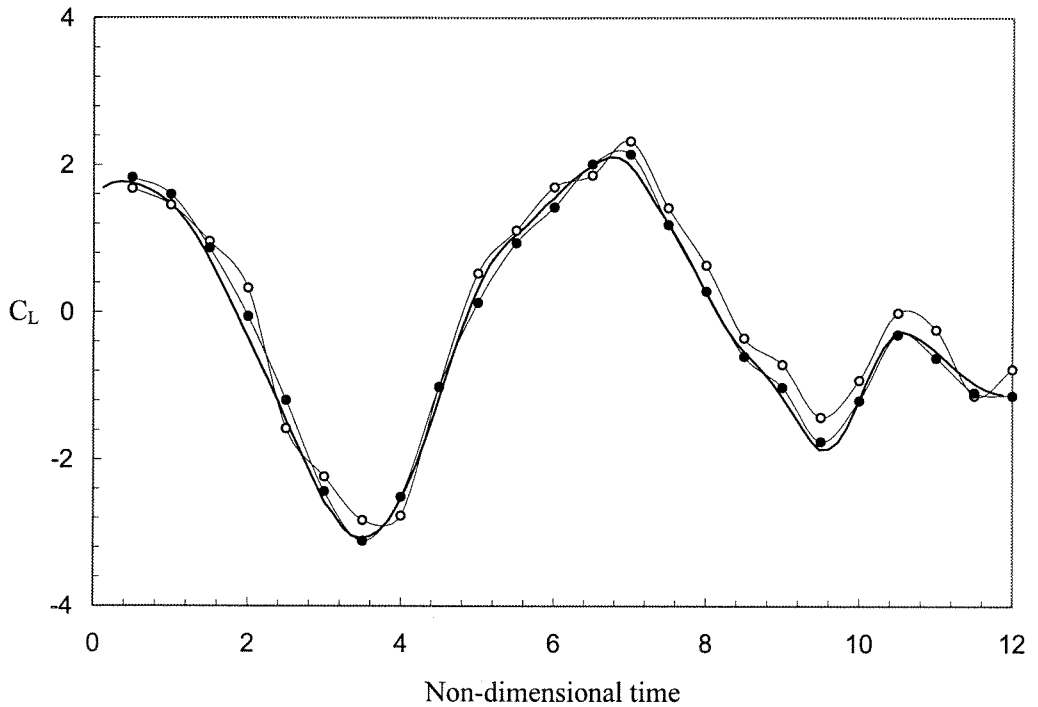


Figure 4.3: Comparison of lift coefficients $C_L$ obtained by several methods: ——, "exact" data; – – ∘ – –, impulse equation; —●—, "momentum equation".

Comparison with equation 4.6 shows that the pressure integral is equal to:

$$-\oint_{S(t)} p\hat{\mathbf{n}}\, dS = \oint_{S(t)} \boldsymbol{\Upsilon}'_p\, dS, \tag{4.9}$$

where:

$$\begin{aligned} \boldsymbol{\Upsilon}'_p \;=\; & \frac{1}{2}u^2\mathbf{I} - \frac{1}{\mathcal{N}-1}\mathbf{u}\,(\mathbf{x}\wedge\boldsymbol{\omega}) + \frac{1}{\mathcal{N}-1}\boldsymbol{\omega}\,(\mathbf{x}\wedge\mathbf{u}) \\ & -\frac{1}{\mathcal{N}-1}\left[(\mathbf{x}\cdot\frac{\partial\mathbf{u}}{\partial t})\mathbf{I} - \mathbf{x}\frac{\partial\mathbf{u}}{\partial t}\right] \\ & +\frac{1}{\mathcal{N}-1}[\mathbf{x}\cdot(\boldsymbol{\nabla}\cdot\mathbf{T})\mathbf{I} - \mathbf{x}(\boldsymbol{\nabla}\cdot\mathbf{T})]. \end{aligned} \tag{4.10}$$

This relation can be rearranged into the following more elegant form:

$$\oint_{S(t)} (p+\frac{1}{2}u^2)\hat{\mathbf{n}}\, dS = \frac{1}{\mathcal{N}-1}\oint_{S(t)} \mathbf{x}\wedge(\hat{\mathbf{n}}\wedge\boldsymbol{v}_p)\, dS, \tag{4.11}$$

where the vector $\boldsymbol{v}_p$ is given by:

$$\boldsymbol{v}_p = \frac{\partial\mathbf{u}}{\partial t} - \mathbf{u}\wedge\boldsymbol{\omega} - \boldsymbol{\nabla}\cdot\mathbf{T}. \tag{4.12}$$

Equation 4.11 should not surprise us. It is just the Pressure Identity itself, since from the Navier-Stokes equations, we have:

$$\boldsymbol{v}_p = -\boldsymbol{\nabla}(p + \frac{1}{2}u^2). \tag{4.13}$$

Basically, Equation 4.6 could have been arrived at by applying the Pressure Identity to Equation 2.22.

Equation 4.9 reveals that as the surface $S(t)$ is taken to infinity, the surface integral of the pressure does not vanish because of the terms containing time-derivatives:

$$\frac{1}{\mathcal{N}-1}\left[(\mathbf{x}\cdot\frac{\partial \mathbf{u}}{\partial t})\mathbf{I} - \mathbf{x}\frac{\partial \mathbf{u}}{\partial t}\right]. \tag{4.14}$$

Actually, for *2D flows with net circulation*, the integral diverges. Saffman[1] shows that in the 3D case, the integral is conditionally convergent and can be expressed in terms of the time derivative of the impulse for a *spherical* control surface $S_\infty$:

$$-\oint_{S_\infty} p\hat{\mathbf{n}}\, dS = -\frac{1}{6}\frac{d}{dt}\int_{V(t)+V_b(t)} \mathbf{x}\wedge\boldsymbol{\omega}\, dV. \tag{4.15}$$

### 4.3.2 The double-quadrature equation

It is interesting to compare Equation 4.6 to Equation 2.48 which we reproduce here:

$$\begin{aligned}\mathbf{F} \;=\; & -\frac{d}{dt}\int_{V(t)} \mathbf{u}\, dV \\ & + \oint_{S(t)} \hat{\mathbf{n}}\cdot\tilde{\boldsymbol{\Upsilon}}_{\mathbf{p}}\, dS \\ & - \oint_{S_b(t)} \hat{\mathbf{n}}\cdot(\mathbf{u}-\mathbf{u}_S)\,\mathbf{u}\, dS,\end{aligned} \tag{4.16}$$

where the tensor $\tilde{\boldsymbol{\Upsilon}}_{\mathbf{p}}$ is given by:

$$\tilde{\boldsymbol{\Upsilon}}_{\mathbf{p}} = \left[\int_{\mathbf{x}_0}^{\mathbf{x}} \hat{\mathbf{l}}\cdot(\frac{\partial \mathbf{u}}{\partial t} + \mathbf{u}\cdot\boldsymbol{\nabla}\mathbf{u} - \boldsymbol{\nabla}\cdot\mathbf{T})\, dl\right]\mathbf{I} - (\mathbf{u}-\mathbf{u}_S)\,\mathbf{u} + \mathbf{T}. \tag{4.17}$$

The result of the comparison is (after some algebra):

$$\begin{aligned}&\oint_{S(t)} \hat{\mathbf{n}}\left[\int_{\mathbf{x}_0}^{\mathbf{x}} \hat{\mathbf{l}}\cdot(\frac{\partial \mathbf{u}}{\partial t} + \mathbf{u}\cdot\boldsymbol{\nabla}\mathbf{u} - \boldsymbol{\nabla}\cdot\mathbf{T})\, dl\right] dS = \\ &\qquad \oint_{S(t)} \frac{1}{2}u^2\hat{\mathbf{n}}\, dS - \frac{1}{\mathcal{N}-1}\oint_{S(t)} \mathbf{x}\wedge\hat{\mathbf{n}}\left(\frac{\partial \mathbf{u}}{\partial t} - \mathbf{u}\wedge\boldsymbol{\omega} - \boldsymbol{\nabla}\cdot\mathbf{T}\right) dS.\end{aligned} \tag{4.18}$$

We, therefore, see that the double-quadrature in Equation 2.48 can be turned into a simple quadrature. In experimental work, we will thus completely omit the double-quadrature equation, and

[1] Saffman P.E., *Vortex dynamics*, §3.3, Cambridge University Press, 1993; Batchelor presents a similar discussion, see Batchelor G. K., *An introduction to fluid dynamics*, §7.2, Cambridge University Press, 1967.

instead make use of Equation 4.6.

# Chapter 5 "Flux equation" for a finite, doubly connected domain

It was mentioned in Chapter 3 that the volume integral is troublesome because it requires the boundary layers on the body surface to be resolved - an experimentally prohibitive task most of the time. Even though the volume integral can be taken over the velocity field instead of the vorticity field, as shown in Chapter 4, the procedure may still raise problems.

In this chapter, it will be shown that *the volume integral can be substituted with a surface integral* in the case of an *incompressible flow.*

In Paragraph 5.1, we will first derive a useful vector identity which will allow us to carry on the algebra.

In Paragraph 5.2, the force will then be obtained in terms of surface integrals over the control surface. The expression, valid for incompressible flows only, will be derived in a doubly connected domain. It will be termed the "flux" equation.

In Paragraph 5.3, we will show a numerical validation of the "flux" equation.

In Paragraph 5.4, we will discuss the possibility of implementing a time-dependent wake survey technique.

## 5.1 A useful vector identity

The algebraic procedure relies on the following vector identity:

$$\mathbf{a} = \boldsymbol{\nabla} \cdot (\mathbf{a}\mathbf{x}) - (\boldsymbol{\nabla} \cdot \mathbf{a})\mathbf{x}, \tag{5.1}$$

where $\mathbf{x}$ is the position vector and $\mathbf{a}$ any vector. Inserting this identity into the local form of the Impulse-Momentum Identity (see Equation 3.5 in Chapter 3):

$$\mathbf{x} \wedge (\boldsymbol{\nabla} \wedge \mathbf{a}) = (\mathcal{N} - 1)\mathbf{a} + \boldsymbol{\nabla}(\mathbf{x} \cdot \mathbf{a}) - \boldsymbol{\nabla} \cdot (\mathbf{x}\mathbf{a}), \tag{5.2}$$

we obtain:

$$\mathbf{x} \wedge (\boldsymbol{\nabla} \wedge \mathbf{a}) = (\mathcal{N} - 1)\boldsymbol{\nabla} \cdot (\mathbf{a}\mathbf{x}) + \boldsymbol{\nabla}(\mathbf{x} \cdot \mathbf{a}) - \boldsymbol{\nabla} \cdot (\mathbf{x}\mathbf{a}) - (\mathcal{N} - 1)(\boldsymbol{\nabla} \cdot \mathbf{a})\mathbf{x}. \tag{5.3}$$

Equation 5.1 and Equation 5.3 are not particularly well known. The reader is referred to the Appendix for a listing of many such relations involving the position vector. Note in particular that for a divergence free vector $\mathbf{a}$ (that is $\boldsymbol{\nabla} \cdot \mathbf{a} = 0$), these identities take the form:

$$\mathbf{a} = \boldsymbol{\nabla} \cdot (\mathbf{a}\mathbf{x}), \tag{5.4}$$

$$\mathbf{x} \wedge (\boldsymbol{\nabla} \wedge \mathbf{a}) = (\mathcal{N} - 1)\boldsymbol{\nabla} \cdot (\mathbf{a}\mathbf{x}) + \boldsymbol{\nabla}(\mathbf{x} \cdot \mathbf{a}) - \boldsymbol{\nabla} \cdot (\mathbf{x}\mathbf{a}). \tag{5.5}$$

In a two-dimesional space ($\mathcal{N} = 2$), the latter expression takes the form:

$$\mathbf{x} \wedge (\boldsymbol{\nabla} \wedge \mathbf{a}) = \boldsymbol{\nabla}(\mathbf{x} \cdot \mathbf{a}) + \boldsymbol{\nabla} \wedge (\mathbf{x} \wedge \mathbf{a}), \tag{5.6}$$

where use was made of the general identity:

$$\boldsymbol{\nabla} \wedge (\mathbf{x} \wedge \mathbf{a}) = \boldsymbol{\nabla} \cdot (\mathbf{a}\mathbf{x} - \mathbf{x}\mathbf{a}). \tag{5.7}$$

The usefulness of the identities in Equation 5.1 and Equation 5.3 will now be demonstrated. Equation 5.1 and Equation 5.3 can be put in volume integral form. Some of the volume terms can be transformed into surface terms through the use of Green's theorem. The result is:

$$\int_V \mathbf{a}\, dV = -\int_V (\boldsymbol{\nabla} \cdot \mathbf{a})\mathbf{x}\, dV + \oint_S \hat{\mathbf{n}} \cdot (\mathbf{a}\mathbf{x})\, dS, \tag{5.8}$$

$$\begin{aligned} \int_V \mathbf{x} \wedge (\boldsymbol{\nabla} \wedge \mathbf{a})\, dV &= -(\mathcal{N} - 1)\int_V (\boldsymbol{\nabla} \cdot \mathbf{a})\mathbf{x}\, dV \\ &\quad + \oint_S \hat{\mathbf{n}} \cdot [(\mathbf{x} \cdot \mathbf{a})\mathbf{I} - \mathbf{x}\mathbf{a} + (\mathcal{N} - 1)\mathbf{a}\mathbf{x}]\, dS. \end{aligned} \tag{5.9}$$

In particular, if the vector $\mathbf{a}$ happens to be divergence-free ($\boldsymbol{\nabla} \cdot \mathbf{a} = 0$), then all volume integrals on the right-hand side of these expressions drop out, and we are left with:

$$\boxed{\int_V \mathbf{a}\, dV = \oint_S \hat{\mathbf{n}} \cdot (\mathbf{a}\mathbf{x})\, dS}\ , \quad \boldsymbol{\nabla} \cdot \mathbf{a} = 0, \tag{5.10}$$

$$\boxed{\int_V \mathbf{x} \wedge (\boldsymbol{\nabla} \wedge \mathbf{a})\, dV = \oint_S \hat{\mathbf{n}} \cdot [(\mathbf{x} \cdot \mathbf{a})\mathbf{I} - \mathbf{x}\mathbf{a} + (\mathcal{N} - 1)\mathbf{a}\mathbf{x}]\, dS}\ , \quad \boldsymbol{\nabla} \cdot \mathbf{a} = 0. \tag{5.11}$$

Equation5.10 does appear in Saffman's monograph[1].

[1]Saffman P. G., *Vortex dynamics*, §3.2, Cambridge University press, 1993.

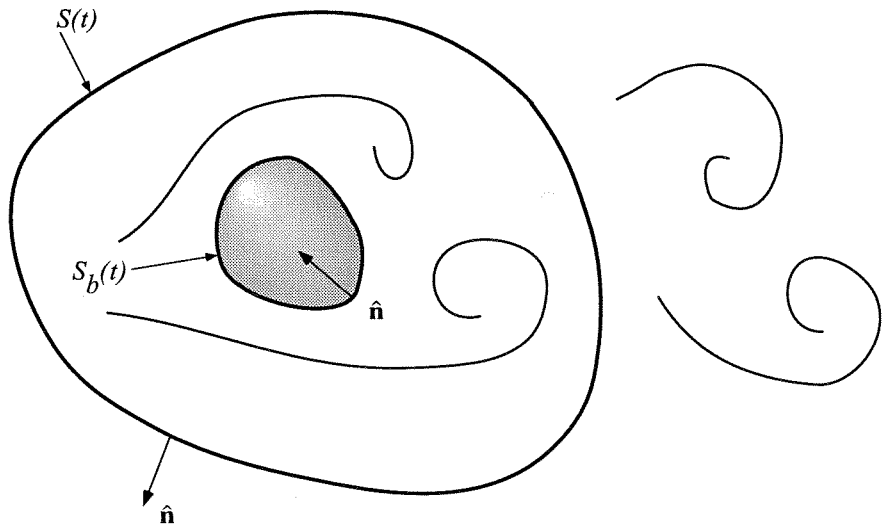


Figure 5.1: Control volume analysis for the "flux equation".

## 5.2 The "flux equation"

In Equation 5.10 and Equation 5.11, we can now set **a** equal to the flow velocity **u** and impose the flow to be incompressible ($\boldsymbol{\nabla} \cdot \mathbf{u} = 0$):

$$\int_V \mathbf{u}\, dV = \oint_S \hat{\mathbf{n}} \cdot (\mathbf{ux})\, dS \ , \ \boldsymbol{\nabla} \cdot \mathbf{u} = 0, \tag{5.12}$$

$$\int_V \mathbf{x} \wedge \boldsymbol{\omega}\, dV = \oint_S \hat{\mathbf{n}} \cdot [(\mathbf{x} \cdot \mathbf{u})\mathbf{l} - \mathbf{xu} + (\mathcal{N} - 1)\mathbf{ux}]\, dS \ , \ \boldsymbol{\nabla} \cdot \mathbf{u} = 0. \tag{5.13}$$

We thus have the possibility of converting all volume integrals encountered thus far into surface integrals.

Thus, Equation 3.55 or Equation 4.4 become (see Figure 5.1):

$$\begin{aligned} \mathbf{F} \ = \ & -\frac{1}{\mathcal{N}-1} \frac{d}{dt} \oint_S \hat{\mathbf{n}} \cdot [(\mathbf{x} \cdot \mathbf{u})\mathbf{l} - \mathbf{xu} + (\mathcal{N} - 1)\mathbf{ux}]\, dS \\ & + \oint_{S(t)} \hat{\mathbf{n}} \cdot \boldsymbol{\Upsilon}'\, dS \\ & - \oint_{S_b(t)} \hat{\mathbf{n}} \cdot (\mathbf{u} - \mathbf{u}_S)\, \mathbf{u}\, dS - \frac{d}{dt} \oint_{S_b(t)} \hat{\mathbf{n}} \cdot (\mathbf{ux})\, dS, \end{aligned} \tag{5.14}$$

where the tensor $\boldsymbol{\Upsilon}'$ is equal to $\boldsymbol{\Upsilon}_\mathbf{i}$ in Equation 4.2. This equation can be transformed further by inserting the time derivative inside the integral. The result is:

$$\begin{aligned} \mathbf{F} \ = \ & \oint_{S(t)} \hat{\mathbf{n}} \cdot \boldsymbol{\Upsilon}\, dS \\ & - \oint_{S_b(t)} \hat{\mathbf{n}} \cdot (\mathbf{u} - \mathbf{u}_S)\, \mathbf{u}\, dS - \frac{d}{dt} \oint_{S_b(t)} \hat{\mathbf{n}} \cdot (\mathbf{ux})\, dS, \end{aligned} \tag{5.15}$$

where:

$$\begin{aligned}\boldsymbol{\Upsilon} &= \frac{1}{2}u^2\mathbf{I} - \mathbf{uu} - \frac{1}{\mathcal{N}-1}\mathbf{u}\,(\mathbf{x}\wedge\boldsymbol{\omega}) + \frac{1}{\mathcal{N}-1}\boldsymbol{\omega}\,(\mathbf{x}\wedge\mathbf{u}) \\ &\quad -\frac{1}{\mathcal{N}-1}\left[(\mathbf{x}\cdot\frac{\partial\mathbf{u}}{\partial t})\mathbf{I} - \mathbf{x}\frac{\partial\mathbf{u}}{\partial t} + (\mathcal{N}-1)\frac{\partial\mathbf{u}}{\partial t}\mathbf{x}\right] \\ &\quad +\frac{1}{\mathcal{N}-1}[\mathbf{x}\cdot(\boldsymbol{\nabla}\cdot\mathbf{T})\mathbf{I} - \mathbf{x}(\boldsymbol{\nabla}\cdot\mathbf{T})] + \mathbf{T}.\end{aligned} \tag{5.16}$$

Note that the latter expression is also valid for a material surface $S(t) = S_m(t)$. Also, for a *rigid body*, the second body term can be shown to be equal to:

$$-\frac{d}{dt}\oint_{S_b(t)}\hat{\mathbf{n}}\cdot(\mathbf{ux})\,dS = V_b\frac{d\mathbf{u}_b}{dt}, \tag{5.17}$$

where $V_b$ is the body volume and $\mathbf{u}_b$ its velocity.

## 5.3 Numerical validation

Following the procedure of Paragraph 3.3 and Paragraph 4.2, Equation 5.15 was tested on coarse gridded data as shown in Figure 4.2. The results are given in Figure 5.2, and again reveal a good agreement with the "exact data". As a comparison, the results from the momentum formulation are plotted as well.

## 5.4 Application to wake surveys

In this paragraph, we will discuss whether Equation 5.15 is well suited for possible *time-dependent wake surveys*. We will first concentrate on time-averaged wakes (similarly to the procedure followed in Paragraph 2.2.2), and then try to extend the technique to instantaneous wakes.

### 5.4.1 Time-averaged wake surveys

In this picture, the flow is assumed stochastically periodic (as defined in Paragraph 2.2.2) such that a time average of the equations over any number of periods removes effectively the time derivatives. As a result, the "impulse equation", the "momentum equation", and the "flux equation" become identical and equal to:

$$\begin{aligned}\langle\mathbf{F}\rangle &= \oint_S \hat{\mathbf{n}}\cdot\langle\boldsymbol{\Upsilon}\rangle\,dS \\ &\quad -\langle\oint_{S_b(t)}\hat{\mathbf{n}}\cdot(\mathbf{u}-\mathbf{u}_S)\,\mathbf{u}\,dS\rangle,\end{aligned} \tag{5.18}$$

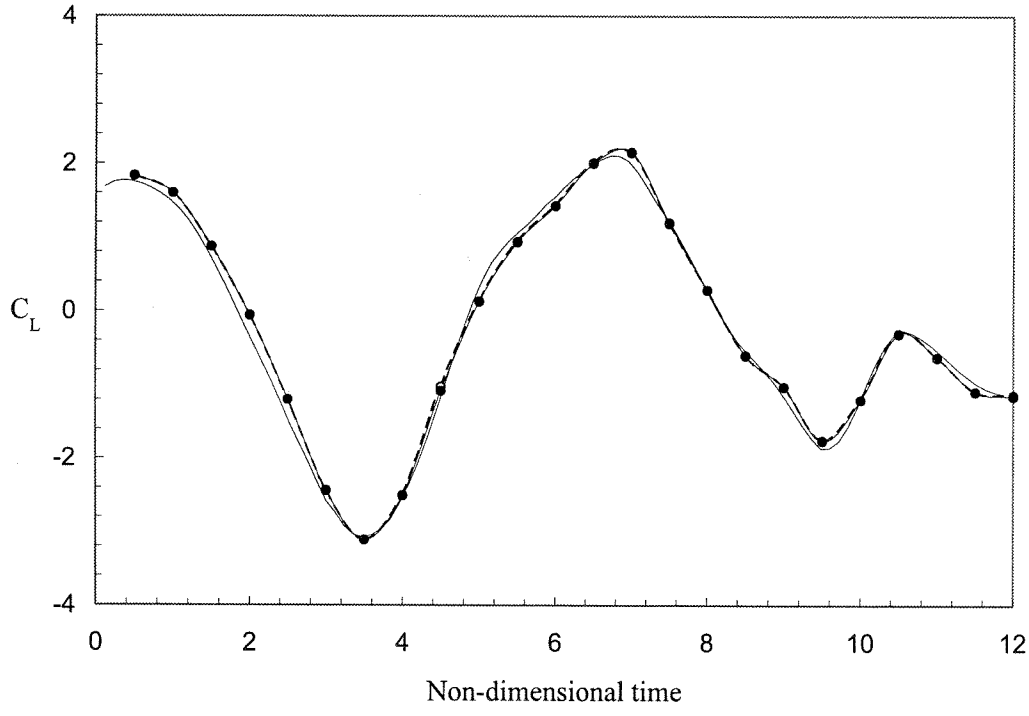


Figure 5.2: Comparison of lift coefficients $C_L$ obtained by several methods: ——, "exact" data; – – o – –, "momentum equation"; —●—, "flux equation". (The open circle symbols may not be apparent on the graph because they lie almost exactly underneath the solid circle symbols.)

where:

$$\begin{aligned}\langle \boldsymbol{\Upsilon} \rangle &= \frac{1}{2}\langle u^2 \rangle \mathbf{I} - \langle \mathbf{u}\mathbf{u} \rangle - \frac{1}{\mathcal{N}-1}\langle \mathbf{u}\,(\mathbf{x} \wedge \boldsymbol{\omega}) \rangle + \frac{1}{\mathcal{N}-1}\,\langle \boldsymbol{\omega}\,(\mathbf{x} \wedge \mathbf{u}) \rangle \\ &\quad + \frac{1}{\mathcal{N}-1}[\mathbf{x} \cdot \langle \boldsymbol{\nabla} \cdot \mathbf{T} \rangle)\mathbf{I} - \mathbf{x}\langle \boldsymbol{\nabla} \cdot \mathbf{T} \rangle] + \langle \mathbf{T} \rangle, \end{aligned} \tag{5.19}$$

and where the surface $S$ is assumed to be independent of time. If the no-through flow condition applies at the body surface, the integration over the body surface vanishes, and we are just left with:

$$\langle \mathbf{F} \rangle = \oint_S \hat{\mathbf{n}} \cdot \langle \boldsymbol{\Upsilon} \rangle \, dS. \tag{5.20}$$

The velocity $\mathbf{u}$ can be set equal to the sum of a freestream velocity $\mathbf{u}_\infty$ and a "disturbance" velocity $\mathbf{u}'$:

$$\mathbf{u}(\mathbf{x}, t) = \mathbf{u}_\infty + \mathbf{u}'(\mathbf{x}, t), \tag{5.21}$$

such that:

$$\langle \mathbf{u}'(\mathbf{x}, t) \rangle = 0. \tag{5.22}$$

After some simple algebra, the time-averaged force takes the form:

$$\langle \mathbf{F} \rangle = \oint_S \hat{\mathbf{n}} \cdot \langle \boldsymbol{\Upsilon}' \rangle \, dS, \tag{5.23}$$

with:

$$\begin{aligned}\langle \boldsymbol{\Upsilon}' \rangle &= \frac{1}{2}\langle u'^2 \rangle \mathbf{I} - \langle \mathbf{u}'\mathbf{u}' \rangle - \frac{1}{\mathcal{N}-1}\langle \mathbf{u}'\,(\mathbf{x} \wedge \boldsymbol{\omega}') \rangle + \frac{1}{\mathcal{N}-1}\,\langle \boldsymbol{\omega}'\,(\mathbf{x} \wedge \mathbf{u}') \rangle \\ &\quad + \frac{1}{\mathcal{N}-1}[\mathbf{x} \cdot \langle \boldsymbol{\nabla} \cdot \mathbf{T}' \rangle)\mathbf{I} - \mathbf{x}\langle \boldsymbol{\nabla} \cdot \mathbf{T}' \rangle] + \langle \mathbf{T}' \rangle. \end{aligned} \tag{5.24}$$

We could have arrived at this equation in an alternate way, by using the expression for the surface integral of the pressure field derived in Chapter 4.

In many flow cases, the disturbance velocity $\mathbf{u}'$ is non-zero only in the wake portion of the flow. Thus, measurements can be limited to the wake only.

For flows with net circulation, the disturbance velocity would be present over the whole surface $S$. The Kutta-Zhukovsky term, which requires integration over the whole surface, would actually contribute to yield a net lift force on the body.

### 5.4.2 Time-dependent wake surveys

Instead of taking the time average of the "flux" equation, we now have to preserve its original form. Setting like before:

$$\mathbf{u}(\mathbf{x},t) = \mathbf{u}_\infty + \mathbf{u}'(\mathbf{x},t), \tag{5.25}$$

we arrive at the equation:

$$\begin{aligned}\mathbf{F} &= \oint_S \hat{\mathbf{n}}\cdot\boldsymbol{\Upsilon}_t\, dS \\ &\quad - \oint_{S_b(t)} \hat{\mathbf{n}}\cdot(\mathbf{u}-\mathbf{u}_S)\,\mathbf{u}\, dS - \frac{d}{dt}\oint_{S_b(t)} \hat{\mathbf{n}}\cdot(\mathbf{ux})\, dS,\end{aligned} \tag{5.26}$$

where

$$\begin{aligned}\boldsymbol{\Upsilon}_t &= \frac{1}{2}u'^2\mathbf{I} + \mathbf{u}_\infty\cdot\mathbf{u}'\mathbf{I} - \mathbf{u}'\mathbf{u}_\infty - \mathbf{u}_\infty\mathbf{u}' - \mathbf{u}'\mathbf{u}' \\ &\quad + \frac{1}{\mathcal{N}-1}(\mathbf{u}'+\mathbf{u}_\infty)\,(\mathbf{x}\wedge\boldsymbol{\omega}') + \frac{1}{\mathcal{N}-1}\boldsymbol{\omega}'\,[\mathbf{x}\wedge(\mathbf{u}'+\mathbf{u}_\infty)] \qquad (5.27) \\ &\quad - \frac{1}{\mathcal{N}-1}\left[(\mathbf{x}\cdot\frac{\partial\mathbf{u}'}{\partial t})\mathbf{I} - \mathbf{x}\frac{\partial\mathbf{u}'}{\partial t} + (\mathcal{N}-1)\frac{\partial\mathbf{u}'}{\partial t}\mathbf{x}\right] \qquad (5.28) \\ &\quad + \frac{1}{\mathcal{N}-1}[\mathbf{x}\cdot(\boldsymbol{\nabla}\cdot\mathbf{T}')\mathbf{I} - \mathbf{x}(\boldsymbol{\nabla}\cdot\mathbf{T}')] + \mathbf{T}'.\end{aligned}$$

One may conjecture that $\mathbf{u}'$ is non-zero in the wake only, and evaluate time-dependent forces using the latter equation and data from a wake survey only.

Anatol Roshko[2] suggested placing the CCD camera downstream of the cylinder, and concentrating on the structure of the far wake in order to gather the velocity field (and its derivatives) with great accuracy in this region. The cylinder would then be completely omitted from the field of view. If indeed all the information lies on the patch of surface cutting the wake (a Trefftz plane, as it is usually called when the plane lies far downstream), then the forces could be evaluated by applying the "flux" equation on this surface as well as on an imaginary surface lying at infinity on which the velocity is presumably known and assumed to be steady. This technique would effectively be identical to a classical wake survey technique, with the only difference that on the *wake plane*, not only the velocity but also its derivatives (temporal and spatial) would have to be measured.

However, we believe that such a procedure may be too ambitious because the surface integral of the terms:

$$\frac{1}{\mathcal{N}-1}\left[(\mathbf{x}\cdot\frac{\partial\mathbf{u}'}{\partial t})\mathbf{I} - \mathbf{x}\frac{\partial\mathbf{u}'}{\partial t} + (\mathcal{N}-1)\frac{\partial\mathbf{u}'}{\partial t}\mathbf{x}\right], \tag{5.29}$$

may not vanish on a distant surface (even if it does not intersect the wake). This feature was already encountered in the previous chapters where it was argued that the surface integral of the pressure at infinity could not be neglected because the surface integral of similar terms did not vanish at

[2]Personal communication.

infinity.

# Chapter 6 Experimental procedure

The formulations developed in the preceding chapters for the evaluation of fluid-dynamic force acting on a body will now be applied to laboratory situations.

Since the technique used in this work for measuring flow velocities (Digital Particle Image Velocimetry) yields the projection of the velocity fields onto a plane only, our focus will be mostly on *nominally* two-dimensional flows. In other words, the bodies used will be cylinders placed normal to a cross-flow, and the measuring plane will be normal to the cylinder axis. As a result, we expect that the velocity vectors will have components mostly on that plane (*two-dimensional flow*) such that a measurement of the flow velocity on that plane will yield a complete description of the velocity field. At low Reynolds numbers, the flow is indeed two-dimensional, and a plane measurement does provide all the necessary information about the flowfield. However, we do know that this is not the case for flows at intermediate or high Reynolds numbers since the flow becomes *intrinsically* three-dimensional despite the cylinder geometry being two-dimensional. As a result, a plane measurement will be in general incomplete since the out-of-plane velocity component will not be captured.

In Paragraph 6.1, we will describe the experimental setup in a tow tank for the low Reynolds number, two-dimensional studies.

In Paragraph 6.2, the methodology for the evaluation of forces will be presented.

In Chapter 7, we will apply the force formulations to a circular cylinder flow at low Reynolds number ($Re \sim 100$) which we can compare with numerical data.

In Chapter 8, we will apply the formulation to a circular cylinder in a jerking motion, i.e. , a sinusoidal motion along the direction of travel.

Finally, in Chapter 9, we will discuss the results and try to see how present day techniques are viable for the intrinsic measurement of fluid-dynamic forces.

## 6.1 Low Reynolds number experimental setup

### 6.1.1 The tow tank facility

The experiments were conducted in the GALCIT Towing Tank. The facility was built by Charles Williamson in 1986, and was extensively used by him and Derek Lisoski, a former graduate student of Anatol Roshko. A complete account of the laboratory set-up can be found Lisoski's Ph.D. thesis[1], and only a quick overview will be given here.

[1]Lisoski, D. L. A., *Nominally two-dimensional flow about a normal flat plate*, Ph.D. Thesis, California Institute of Technology, 1993.

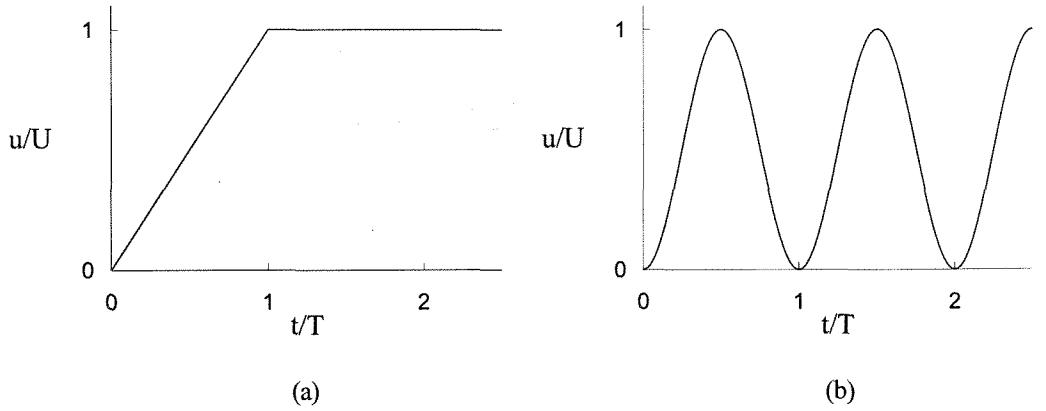


Figure 6.1: Carriage velocity profiles $u/U$ vs. time $t/T$: (a) Start-up motion with constant acceleration followed by a constant velocity motion; (b) Jerking motion, i.e. , a time-dependent sinusoidal motion.

The tank is 450 cm long, 96 cm wide and 78 cm deep. The wetted depth is typically 75 cm. On top of the tank, a carriage rides along two cylindrical Lintech rails which run parallel to the length of the tank. Lisoski originally supported the carriage with Teflon blocks in order to minimize vibrations. Since our work did not include the use of a force balance (which is most sensitive to vibrations especially at low force levels), and since we wanted to avoid problems associated with the stickiness of Teflon blocks especially at start-up[2], we decided to opt for stainless steel wheels.

The carriage is driven by a pulley and cable drive from a DC servo motor and gear box mounted at one end of the tank. The DC servo motor is attached to a PMI optical encoder with a resolution of 1024 counts per revolution, which corresponds to about 1500 counts per cm of travel (with the gearing used). The encoder is attached to a Galil DMC 400b position controller in a PC AT computer. A computer program, written by Lisoski, allows a variety of carriage motions, of which two were selected:

- Start-up motion with constant acceleration during a time $T$, followed by a constant velocity motion with velocity $U$ (Figure 6.1(a));
- Jerking motion, i.e. , a time-dependent sinusoidal motion, with period $T$ and with the velocity bound between 0 and $U$ (Figure 6.1(b)).

### 6.1.2 Model

The model was a thin-wall, glass cylinder of 1 cm in diameter. When immersed, its aspect ratio was about 75. The cylinder was held vertically and was adjusted to graze the bottom of the tank

[2]Lisoski was very meticulous at lifting the carriage by a couple of millimeters before each run, greasing the underpart of the Teflon blocks, and lowering the carriage back onto the rails right before start-up.

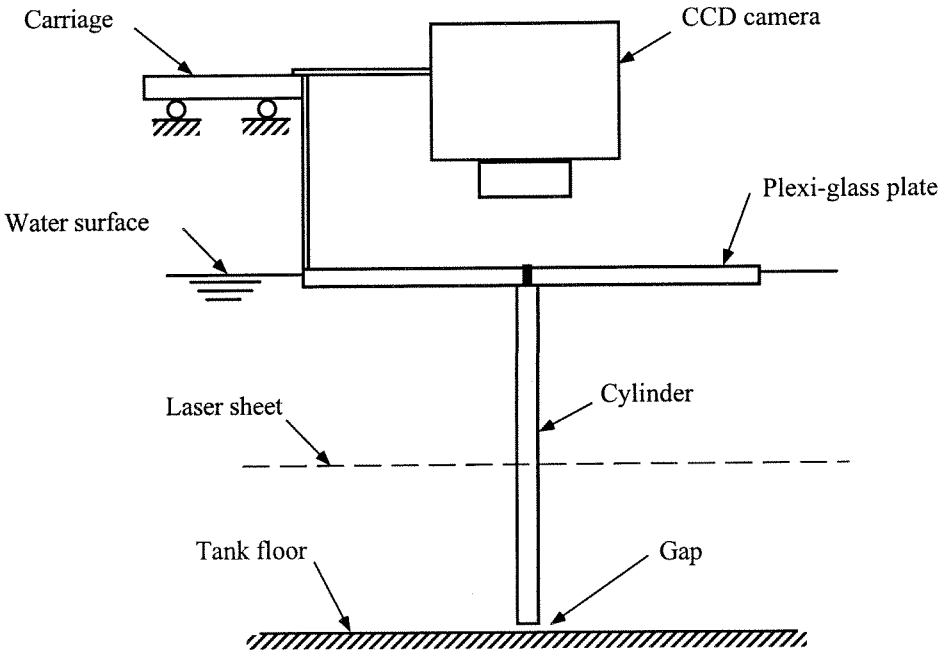


Figure 6.2: Sketch of experimental setup.

(about 2 mm off the bottom). No endplate was used at the lower end, and from the work of Slaouti & Gerrard[3], it was concluded that a small gap between the cylinder end and the tank bottom was a satisfactory boundary condition for preserving parallel shedding.

The boundary condition at the upper end of the cylinder was dictated by the supporting mechanism for the cylinder. A 30 cm x 30 cm, 1/2 inch thick, plexiglas plate was attached to the carriage and placed flat on top of the water surface. The purpose of the plate was to hold the cylinder vertically and at the same time allow optical access from the top over the whole circumference of the cylinder, as shown in Figure 6.2 (thereby the need for a transparent plate).

The plate actually served an additional purpose. With the plexiglas plate not touching the water, a lensing effect, due to a meniscus at the cylinder and water surface junction, prevented the flowfield from being resolved very near the cylinder. Following an idea by Mory Gharib on one of his student's project, we removed the problem by lowering the plexiglas plate by a couple of millimeters into the water. However, we realized that, as demonstrated by Slaouti & Gerrard[4], the plate is not an ideal boundary condition for promoting parallel shedding along the whole span of the cylinder. As observed by these authors, a clean water surface is clearly a better alternative to a plate. The authors suggest that if a plate is used at the free-surface, then a better boundary condition at the lower end of the cylinder is just a free-end. Under such conditions, the flow does assume parallel shedding over the central portion of the cylinder span, as shown in their Figure 3.

[3]Slaouti A. & Gerrard J. H., An experimental investigation of the end effects on the wake of a circular cylinder towed through water at low Reynolds number, *Journal of Fluid Mechanics*, **112** (1981) 297-314.

[4]*idem.*

In our experiments, we decided to keep the lower end of the cylinder close to the tank bottom. As a result, the shedding was oblique, as shown in Figure 6.3 which compares very well with their Figure 7. Even though the shedding was not parallel, it was very *uniform* along a large portion of the span. The flow visualization was performed by introducing some dye (with a syringe) around the cylinder just before the start of the motion. As a result, the background turbulence was probably higher than in typical DPIV measurements where care was taken not to disturb the flow (see later sections).

Our motivation for preferring flow uniformity over a parallel-shedding condition was based on the results of Williamson & Roshko[5] and Hammache & Gharib[6]. These authors first showed that oblique shedding affects the base pressure coefficient by only a few percent. Thus, forces don't seem to be greatly affected by slanted shedding. Also, both groups noted that near the cylinder ends (within 30 or 40 diameters from the ends) the flow is non-uniform because of the control mechanisms (end-plates or end-cylinders), and the base pressure coefficient can be affected by as much as thirty percent (see Figure 5 of Williamson & Roshko, and Figure 9 of Hammache & Gharib). Since our aspect ratio was only 75, we argued that any control mechanism at the ends to promote parallel shedding would have introduced substantial non-uniformities along the span of the cylinder.

For these reasons, uniform but oblique shedding was preferred to parallel shedding with manipulated end conditions.

The readers may object to an oblique shedding condition since it destroys the two-dimensionality of the flow which was sought in the first place. However, we noted the following phenomenon with our DPIV particle images. Particles were observed to enter and leave the field of view of the camera without ever leaving the laser sheet which was placed normal to the cylinder axis at midspan. It was thus concluded that the flow was at least very close to being *planar* if not *two-dimensional.* This feature was judged as sufficient for the implementation of a two-dimensional force formulation.

### 6.1.3 Velocity measurement technique

The technique used was Digital Particle Image Velocimetry as described in Willert & Gharib[7]. A laser sheet was generated by sending a beam from a continuous 8-Watt argon-ion laser through a cylindrical lens. The sheet was projected horizontally at about the cylinder midspan, from the downstream side of the cylinder. In order to provide seamless illumination over the whole circumference of the cylinder, including the upstream side, we followed an idea of Mory Gharib and used a thin-wall, glass cylinder filled with water. A slight lensing effect was observed because of the finite thickness of the cylinder walls. As a result, two thin regions of shade appeared on the upstream side,

[5]Williamson C. H. K. & Roshko A., Measurements of base pressure in the wake of a cylinder at low Reynolds numbers, *Z. Flugwiss. Weltraumforsch* **14** (1990) 38-46.

[6]Hammache M. & Gharib M., An experimental study of the parallel and oblique vortex shedding from circular cylinders, **232** (1991) 567-590.

[7]Willert C. & Gharib M., Digital Particle Image Velocimetry, *Experiments in Fluids* **10** (1991) 181-193.

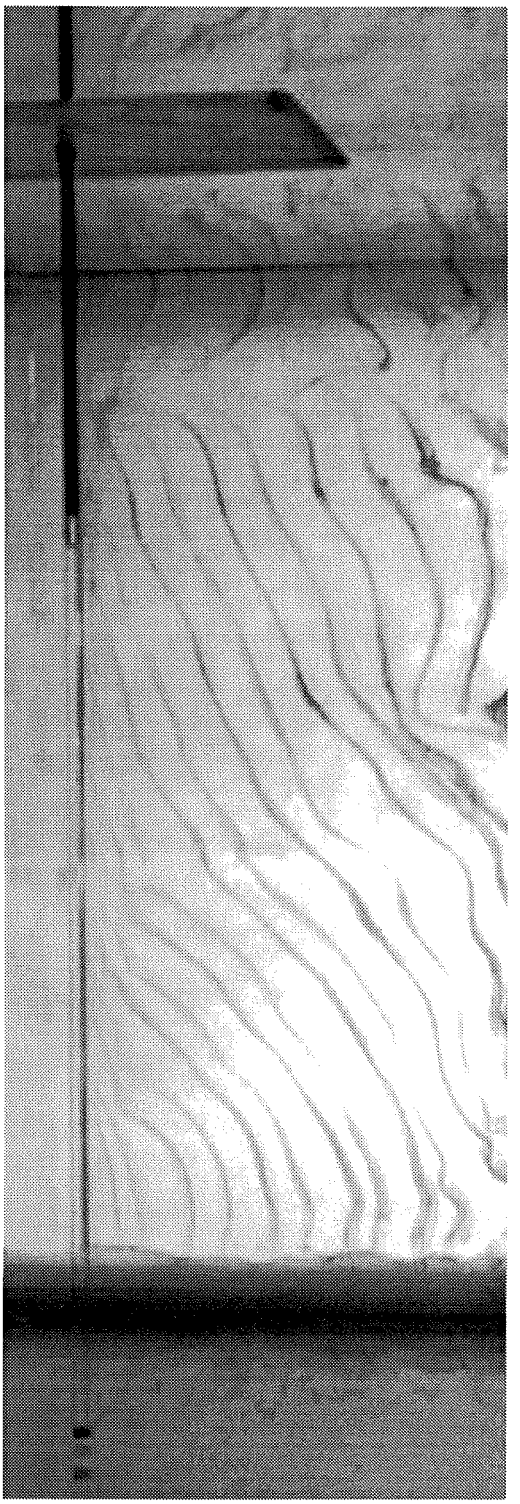

Figure 6.3: Spanwise view of cylinder flow at $Re \sim 100$ obtained with dye visualization.

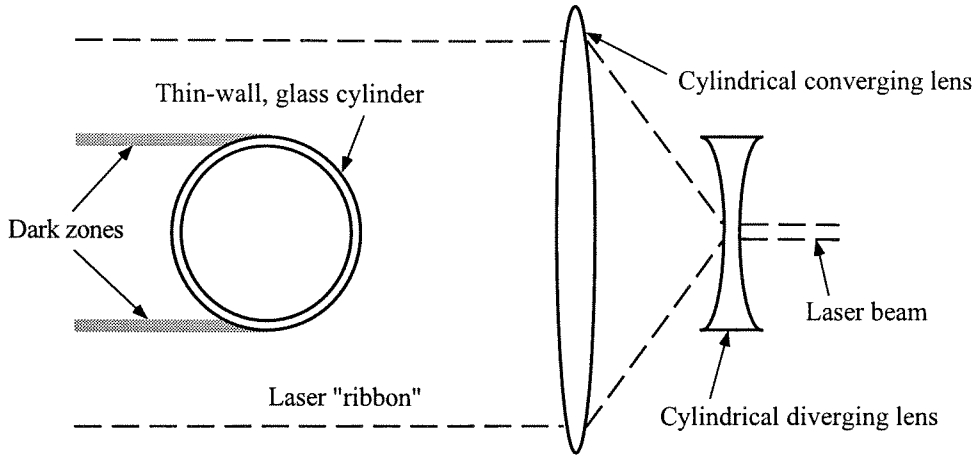


Figure 6.4: Optical setup for DPIV.

as shown in Figure 6.4. These regions often led to spurious velocity vectors, which were anyway automatically removed as outliers during the processing procedure.

Since the cylinder traveled several diameters away from the laser source, the light intensity diminished because of the spreading of the sheet. To remove this problem, we introduced a second cylindrical lens of large breadth (about 5 cm) in order to focus the diverging sheet into a ribbon of parallel rays. The size of the resulting ribbon was basically equal to the breadth of the second cylindrical lens. Since the cylinder diameter was only 1 cm, we were able to visualize the flow over about two diameters on each side of the cylinder.

In another experiment where a bigger field of view was required, we settled for the diverging sheet, and tried to optimize the sheet intensity between the beginning of the run and the end of the run by regulating the divergence angle.

The flow was seeded with 14-micron, silver-coated particles. The particles were not neutrally buoyant and had a tendency of settling to the bottom of the tank quite rapidly (within a couple of hours). Since the tank needed to be stirred in order to eliminate large scale convection currents, the particles were thus automatically re-distributed throughout the tank. For best results, it was observed by Lisoski that a waiting time of about one hour was sufficient for the small scale turbulence generated by the stirring process to dissipate, and still not too long for the particles to settle or for the convection currents to set in. No effort was made to control convection currents, as in Williamson[8] or Slaouti & Gerrard[9].

An image of the particle-seeded sheet was captured with a 768-pixel × 480-pixel CCD camera which was placed above the plexiglas plate and was towed along on the carriage. The CCD camera was thus always at rest with respect to the cylinder. Depending on the field of view needed, we

[8]Williamson C. H. K., Oblique and parallel modes of vortex shedding in the wake of a circular cylinder at low Reynolds numbers, *Journal of Fluid mechanics*, **206** (1989) 579-627.

[9]Slaouti A. & Gerrard J. H., An experimental investigation of the end effects on the wake of a circular cylinder towed through water at low Reynolds number, *Journal of Fluid Mechanics*, **112** (1981) 297-314.

used lenses of different focal length. Since the effective diameter of the lens was larger than the dimension of the cylinder, we were able to capture the whole field around the cylinder including the near wall region of the cylinder. However, this near-wall region was dimmer than the outer region because of the extent of the cylinder. Also, some of the particles near the wall had a slight crescent, instead of spherical, shape. Yet, satisfactory velocity fields were obtained despite the poor quality of the images near the wall of the cylinder. Nevertheless, it is highly improbable that we were able to resolve the boundary layer structure near the body. We will return to this point when discussing the results.

Since the flow was very slow (1 cm/s over a field of view of 5cm x 5cm), no shutting of the laser sheet was necessary. Thus, images were acquired at video rate (30 Hz). In order to avoid streaking, the internal camera shutter was set at 1/125 s.

Time sequences of images from the CCD camera were fed into videodisks which can store up to 86,000 images. The images were subsequently retrieved for further processing.

Each image captures a field of particles, and from two such images separated by a time interval $\delta t$, it is possible to reconstruct the velocity field by cross-correlating the two images and obtaining the displacement field. Depending on the flow velocity and field of view, we correlated either every image with the next one (image 1 and image 2, image 2 and image 3, etc, ...) or the second to next (image 1 and image 3, image 2 and image 4, etc, ...). The analysis was performed with 32-pixel $\times$ 32-pixel windows (the quality of the images did not allow for a smaller window).

From the velocity data, we computed the vorticity field, after having removed beforehand any velocity vector from inside the cylinder region (which are present because of particle reflections on the cylinder wall).

An example of processed velocity and vorticity fields is shown in Figure 6.5.

### 6.1.4 On the impossibility of using a force balance

A preliminary idea was to use a force balance in order to produce independent force measurements to compare with. However, it was soon realized that this project was not realizable, for the reasons listed below.

The force balance that we wanted to use was designed by Derek Lisoski and is fully described in his Ph.D. Thesis[10]. It is a three-component force balance which can resolve two normal loads and one side load, from which it is possible to infer lift, drag, and moment. The balance can support a maximum load of about 180 g. Since the accuracy of the force balance is 0.1 g (in the best conditions), the flow has to be such that the fluid dynamic force is of the order of at least 1 g.

[10]Lisoski, D. L. A., *Nominally two-dimensional flow about a normal flat plate*, Ph.D. Thesis, California Institute of Technology, 1993.

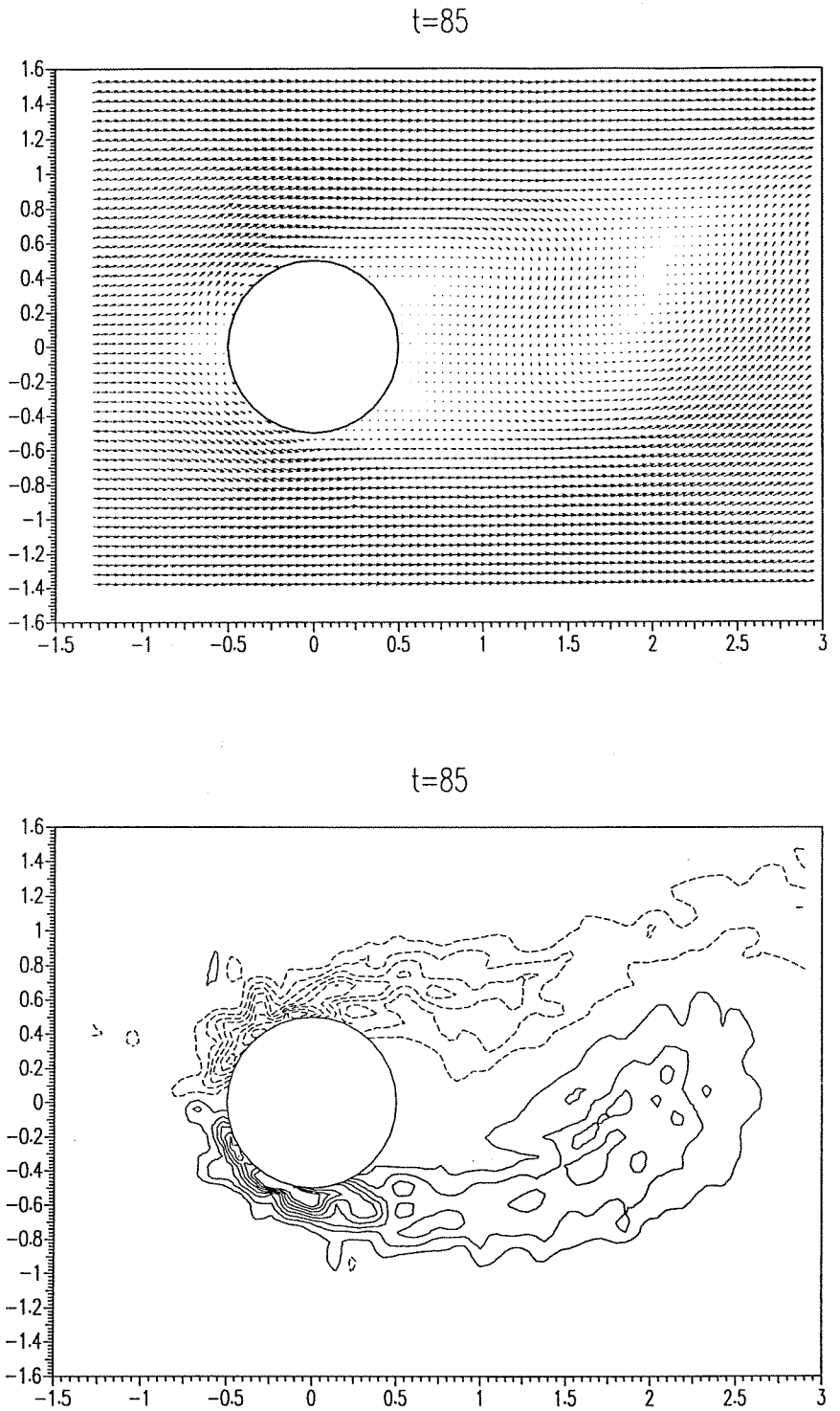


Figure 6.5: Example of velocity field (top) and vorticity field (bottom) for a circular cylinder flow at $Re \sim 100$ in the tow tank.

An estimate of the order of magnitude of the force on the cylinder is given by:

$$F = \frac{1}{2} C_d \rho U^2 d L, \tag{6.1}$$

where $U$ is a characteristic flow velocity, $d$ a characteristic body dimension (cylinder diameter), $L$ the cylinder length (equal to the wetted depth of the tank, i.e. , about 75 cm), $C_d$ the drag coefficient of the body (close to unity for a circular cylinder in cross flow), and $\rho$ the density of water (around 1000 kg/m$^3$). The quantities which can be chosen at will in this equation are $U$ and $d$.

A constraint on $U$ and $d$ is given by the Reynolds number which we fixed at 100 to ensure that the flow was two-dimensional:

$$Re = \frac{Ud}{\nu} \sim 100, \tag{6.2}$$

where $\nu$ is the kinematic viscosity of water.

Another condition on $U$ and $d$ can be derived based on the flow time scales. Since our formulations require a time derivative between pairs of *velocity fields* (not images) for which the minimum time separation is $\tau \sim 1/30$ s, we do not want the flow variations to be too large during this timelength.

A characteristic timescale of the flow is given by the shedding frequency:

$$f = St \frac{U}{d}, \tag{6.3}$$

where $St$ is the Strouhal number (close to 0.2 for a circular cylinder at $Re \sim 100$). If we would like to capture about $N$ velocity fields per shedding cycle, then the flow time scale, $1/f$, would have to be:

$$\frac{1}{f} \sim N\tau, \tag{6.4}$$

i.e. :

$$\frac{1}{St} \frac{d}{U\tau} \sim N. \tag{6.5}$$

If $N$ has been set (at 200 images/cycle say), the only flexible quantities in this relation are $U$ and $d$.

Combining Equation 6.2 and Equation 6.5, one can solve for the flow velocity $U$ and the diameter $d$:

$$U \sim \left( \frac{\nu Re}{N\tau St} \right)^{\frac{1}{2}}, \tag{6.6}$$

$$d \sim (\nu Re St N \tau)^{\frac{1}{2}}. \tag{6.7}$$

Application to our flowcase yields $U \sim 1.0$ cm/s and $d \sim 1$ cm. If these values are inserted into Equation 6.1, the force on the cylinder can be evaluated to be:

$$F \sim 0.05 \text{ g}, \tag{6.8}$$

which is well below the resolution of our force balance. For such reasons, the idea of using a force balance was abandoned.

## 6.2 Force evaluation

### 6.2.1 Compendium

We give here a compendium of all the formulae that can be used for evaluating forces. All the equations are written for an arbitrary control volume (CV) in the following way:

$$\begin{aligned} \mathbf{F} \;=\; & \text{integral over the volume of fluid enclosed by the CV} \\ & + \text{integral over the outer surface of the CV} \\ & + \text{integral over the body surface (body motion).} \end{aligned} \tag{6.9}$$

The body surface integral generally describes the body surface motion when the no-slip condition applies. The equations involve only single integrations of the velocity field and its (temporal and spatial) derivatives.

The equations include the "impulse equation", the "momentum equation" and the "flux equation". Some use the Kutta-Zhukovsky term as either a surface integral or volume integral. Some are expressed with either time derivatives of integrals or integrals of time derivatives. In parentheses, we have labeled the equations with a code ("mom1" or "flux3") which will be useful for future reference.

**"Impulse equation" ("imp")**

- "imp1",

$$\begin{aligned} \mathbf{F} \;=\; & -\frac{1}{\mathcal{N}-1}\frac{d}{dt}\int_{V(t)} \mathbf{x}\wedge\boldsymbol{\omega}\,dV + \int_{V(t)} \mathbf{u}\wedge\boldsymbol{\omega}\,dV \\ & + \oint_{S(t)} \hat{\mathbf{n}}\cdot\boldsymbol{\Upsilon}'_{\mathbf{i}}\,dS \\ & + \frac{1}{\mathcal{N}-1}\frac{d}{dt}\oint_{S_b(t)} \mathbf{x}\wedge(\hat{\mathbf{n}}\wedge\mathbf{u})\,dS - \oint_{S_b(t)} (\frac{1}{2}u^2\hat{\mathbf{n}} - \hat{\mathbf{n}}\cdot\mathbf{u}_S\,\mathbf{u})\,dS, \end{aligned} \tag{6.10}$$

$$\begin{aligned} \boldsymbol{\Upsilon}'_{\mathbf{i}} \;=\; & -\frac{1}{\mathcal{N}-1}(\mathbf{u}-\mathbf{u}_S)\,(\mathbf{x}\wedge\boldsymbol{\omega}) + \frac{1}{\mathcal{N}-1}\boldsymbol{\omega}\,(\mathbf{x}\wedge\mathbf{u}) \\ & + \frac{1}{\mathcal{N}-1}[\mathbf{x}\cdot(\boldsymbol{\nabla}\cdot\mathbf{T})\mathbf{I} - \mathbf{x}(\boldsymbol{\nabla}\cdot\mathbf{T})] + \mathbf{T}. \end{aligned} \tag{6.11}$$

- "imp2",

$$\begin{aligned}\mathbf{F} &= -\frac{1}{\mathcal{N}-1}\frac{d}{dt}\int_{V(t)}\mathbf{x}\wedge\boldsymbol{\omega}\,dV \\ &+\oint_{S(t)}\hat{\mathbf{n}}\cdot\boldsymbol{\Upsilon}_{\mathbf{i}}\,dS \\ &+\frac{1}{\mathcal{N}-1}\frac{d}{dt}\oint_{S_b(t)}\mathbf{x}\wedge(\hat{\mathbf{n}}\wedge\mathbf{u})\,dS-\oint_{S_b(t)}\hat{\mathbf{n}}\cdot(\mathbf{u}-\mathbf{u}_S)\,\mathbf{u}\,dS,\end{aligned} \tag{6.12}$$

$$\begin{aligned}\boldsymbol{\Upsilon}_{\mathbf{i}} &= \frac{1}{2}u^2\mathbf{I}-\mathbf{u}\mathbf{u}-\frac{1}{\mathcal{N}-1}(\mathbf{u}-\mathbf{u}_S)\,(\mathbf{x}\wedge\boldsymbol{\omega})+\frac{1}{\mathcal{N}-1}\boldsymbol{\omega}\,(\mathbf{x}\wedge\mathbf{u}) \\ &+\frac{1}{\mathcal{N}-1}[\mathbf{x}\cdot(\boldsymbol{\nabla}\cdot\mathbf{T})\mathbf{I}-\mathbf{x}(\boldsymbol{\nabla}\cdot\mathbf{T})]+\mathbf{T}.\end{aligned} \tag{6.13}$$

**"Momentum equation" ("mom")**

- "mom1",

$$\begin{aligned}\mathbf{F} &= -\frac{d}{dt}\int_{V(t)}\mathbf{u}\,dV+\int_{V(t)}\mathbf{u}\wedge\boldsymbol{\omega}\,dV \\ &+\oint_{S(t)}\hat{\mathbf{n}}\cdot\boldsymbol{\Upsilon}'_{\mathbf{p}}\,dS \\ &-\oint_{S_b(t)}(\frac{1}{2}u^2\hat{\mathbf{n}}-\hat{\mathbf{n}}\cdot\mathbf{u}_S\,\mathbf{u})\,dS,\end{aligned} \tag{6.14}$$

$$\begin{aligned}\boldsymbol{\Upsilon}'_{\mathbf{p}} &= \mathbf{u}_S\mathbf{u}-\frac{1}{\mathcal{N}-1}\mathbf{u}\,(\mathbf{x}\wedge\boldsymbol{\omega})+\frac{1}{\mathcal{N}-1}\boldsymbol{\omega}\,(\mathbf{x}\wedge\mathbf{u}) \\ &-\frac{1}{\mathcal{N}-1}\left[(\mathbf{x}\cdot\frac{\partial\mathbf{u}}{\partial t})\mathbf{I}-\mathbf{x}\frac{\partial\mathbf{u}}{\partial t}\right] \\ &+\frac{1}{\mathcal{N}-1}[\mathbf{x}\cdot(\boldsymbol{\nabla}\cdot\mathbf{T})\mathbf{I}-\mathbf{x}(\boldsymbol{\nabla}\cdot\mathbf{T})]+\mathbf{T}.\end{aligned} \tag{6.15}$$

- "mom2",

$$\begin{aligned}\mathbf{F} &= -\frac{d}{dt}\int_{V(t)}\mathbf{u}\,dV \\ &+\oint_{S(t)}\hat{\mathbf{n}}\cdot\boldsymbol{\Upsilon}_{\mathbf{p}}\,dS \\ &-\oint_{S_b(t)}\hat{\mathbf{n}}\cdot(\mathbf{u}-\mathbf{u}_S)\,\mathbf{u}\,dS,\end{aligned} \tag{6.16}$$

$$\begin{aligned}\boldsymbol{\Upsilon}_{\mathbf{p}} &= \frac{1}{2}u^2\mathbf{I} + (\mathbf{u}_S - \mathbf{u})\mathbf{u} - \frac{1}{\mathcal{N}-1}\mathbf{u}\,(\mathbf{x}\wedge\boldsymbol{\omega}) + \frac{1}{\mathcal{N}-1}\boldsymbol{\omega}\,(\mathbf{x}\wedge\mathbf{u}) \\ &\quad -\frac{1}{\mathcal{N}-1}\left[(\mathbf{x}\cdot\frac{\partial\mathbf{u}}{\partial t})\mathbf{I} - \mathbf{x}\frac{\partial\mathbf{u}}{\partial t}\right] \\ &\quad +\frac{1}{\mathcal{N}-1}[\mathbf{x}\cdot(\boldsymbol{\nabla}\cdot\mathbf{T})\mathbf{I} - \mathbf{x}(\boldsymbol{\nabla}\cdot\mathbf{T})] + \mathbf{T}.\end{aligned} \tag{6.17}$$

- "mom3",

$$\begin{aligned}\mathbf{F} &= -\frac{d}{dt}\int_{V(t)}\mathbf{u}\,dV + \int_{V(t)}\mathbf{u}\wedge\boldsymbol{\omega}\,dV \\ &\quad -\frac{1}{\mathcal{N}-1}\frac{d}{dt}\int_{S(t)}\mathbf{x}\wedge(\hat{\mathbf{n}}\wedge\mathbf{u})\,dS + \oint_{S(t)}\hat{\mathbf{n}}\cdot\boldsymbol{\Upsilon}'_{\mathbf{i}}\,dS \\ &\quad -\oint_{S_b(t)}(\frac{1}{2}u^2\hat{\mathbf{n}} - \hat{\mathbf{n}}\cdot\mathbf{u}_S\,\mathbf{u})\,dS,\end{aligned} \tag{6.18}$$

- "mom4",

$$\begin{aligned}\mathbf{F} &= -\frac{d}{dt}\int_{V(t)}\mathbf{u}\,dV \\ &\quad -\frac{1}{\mathcal{N}-1}\frac{d}{dt}\int_{S(t)}\mathbf{x}\wedge(\hat{\mathbf{n}}\wedge\mathbf{u})\,dS + \oint_{S(t)}\hat{\mathbf{n}}\cdot\boldsymbol{\Upsilon}_{\mathbf{i}}\,dS \\ &\quad -\oint_{S_b(t)}\hat{\mathbf{n}}\cdot(\mathbf{u}-\mathbf{u}_S)\,\mathbf{u}\,dS,\end{aligned} \tag{6.19}$$

**"Flux equation" ("flux")**

- "flux1",

$$\begin{aligned}\mathbf{F} &= \int_{V(t)}\mathbf{u}\wedge\boldsymbol{\omega}\,dV \\ &\quad +\oint_{S(t)}\hat{\mathbf{n}}\cdot\boldsymbol{\Upsilon}'\,dS \\ &\quad -\oint_{S_b(t)}(\frac{1}{2}u^2\hat{\mathbf{n}} - \hat{\mathbf{n}}\cdot\mathbf{u}_S\,\mathbf{u})\,dS - \frac{d}{dt}\oint_{S_b(t)}\hat{\mathbf{n}}\cdot(\mathbf{ux})\,dS,\end{aligned} \tag{6.20}$$

$$\begin{aligned}\boldsymbol{\Upsilon}' &= -\frac{1}{\mathcal{N}-1}\mathbf{u}\,(\mathbf{x}\wedge\boldsymbol{\omega}) + \frac{1}{\mathcal{N}-1}\boldsymbol{\omega}\,(\mathbf{x}\wedge\mathbf{u}) \\ &\quad -\frac{1}{\mathcal{N}-1}\left[(\mathbf{x}\cdot\frac{\partial\mathbf{u}}{\partial t})\mathbf{I} - \mathbf{x}\frac{\partial\mathbf{u}}{\partial t} + (\mathcal{N}-1)\frac{\partial\mathbf{u}}{\partial t}\mathbf{x}\right] \\ &\quad +\frac{1}{\mathcal{N}-1}[\mathbf{x}\cdot(\boldsymbol{\nabla}\cdot\mathbf{T})\mathbf{I} - \mathbf{x}(\boldsymbol{\nabla}\cdot\mathbf{T})] + \mathbf{T}.\end{aligned} \tag{6.21}$$

- "flux2",

$$\begin{aligned}\mathbf{F} &= \oint_{S(t)} \hat{\mathbf{n}} \cdot \boldsymbol{\Upsilon}\, dS \\ &\quad - \oint_{S_b(t)} \hat{\mathbf{n}} \cdot (\mathbf{u} - \mathbf{u}_S)\, \mathbf{u}\, dS - \frac{d}{dt} \oint_{S_b(t)} \hat{\mathbf{n}} \cdot (\mathbf{ux})\, dS,\end{aligned} \tag{6.22}$$

$$\begin{aligned}\boldsymbol{\Upsilon} &= \frac{1}{2}u^2\mathbf{I} - \mathbf{uu} - \frac{1}{\mathcal{N}-1}\mathbf{u}\,(\mathbf{x} \wedge \boldsymbol{\omega}) + \frac{1}{\mathcal{N}-1}\boldsymbol{\omega}\,(\mathbf{x} \wedge \mathbf{u}) \\ &\quad - \frac{1}{\mathcal{N}-1}\left[(\mathbf{x} \cdot \frac{\partial \mathbf{u}}{\partial t})\mathbf{I} - \mathbf{x}\frac{\partial \mathbf{u}}{\partial t} + (\mathcal{N}-1)\frac{\partial \mathbf{u}}{\partial t}\mathbf{x}\right] \\ &\quad + \frac{1}{\mathcal{N}-1}[\mathbf{x} \cdot (\boldsymbol{\nabla} \cdot \mathbf{T})\mathbf{I} - \mathbf{x}(\boldsymbol{\nabla} \cdot \mathbf{T})] + \mathbf{T}.\end{aligned} \tag{6.23}$$

- "flux3",

$$\begin{aligned}\mathbf{F} &= \int_{V(t)} \mathbf{u} \wedge \boldsymbol{\omega}\, dV \\ &\quad - \frac{1}{\mathcal{N}-1}\frac{d}{dt}\oint_S \hat{\mathbf{n}} \cdot [(\mathbf{x} \cdot \mathbf{u})\mathbf{I} - \mathbf{xu} + (\mathcal{N}-1)\mathbf{ux}]\, dS + \oint_{S(t)} \hat{\mathbf{n}} \cdot \boldsymbol{\Upsilon}'_{\mathbf{i}}\, dS \\ &\quad - \oint_{S_b(t)} (\frac{1}{2}u^2\hat{\mathbf{n}} - \hat{\mathbf{n}} \cdot \mathbf{u}_S\, \mathbf{u})\, dS - \frac{d}{dt}\oint_{S_b(t)} \hat{\mathbf{n}} \cdot (\mathbf{ux})\, dS,\end{aligned} \tag{6.24}$$

- "flux4",

$$\begin{aligned}\mathbf{F} &= -\frac{1}{\mathcal{N}-1}\frac{d}{dt}\oint_S \hat{\mathbf{n}} \cdot [(\mathbf{x} \cdot \mathbf{u})\mathbf{I} - \mathbf{xu} + (\mathcal{N}-1)\mathbf{ux}]\, dS + \oint_{S(t)} \hat{\mathbf{n}} \cdot \boldsymbol{\Upsilon}_{\mathbf{i}}\, dS \\ &\quad - \oint_{S_b(t)} \hat{\mathbf{n}} \cdot (\mathbf{u} - \mathbf{u}_S)\, \mathbf{u}\, dS - \frac{d}{dt}\oint_{S_b(t)} \hat{\mathbf{n}} \cdot (\mathbf{ux})\, dS,\end{aligned} \tag{6.25}$$

### 6.2.2 Space dimension

Since DPIV is intrinsically a two-dimensional technique, it can yield only the projection of a velocity field onto a plane. To be able to apply the above formulae with accuracy, the flow ought to be two-dimensional. For this reason, most of the work in this monograph will concentrate on flows which are two-dimensional (low Reynolds number) or at least nominally two-dimensional.

As a result, only the two-dimensional version of the equations given above is used. The space is thus two-dimensional, i.e. :

$$\mathcal{N} = 2. \tag{6.26}$$

The effets of three-dimensionality in the flow will not be considered in this monograph.

### 6.2.3 Spatial differentiation and integration

Spatial differentiation of velocity fields was performed with first-order differencing schemes. The vorticity fields were obtained directly from the DPIV post-processing software which also uses first-order differencing schemes. For spatial integration, a simple trapezoidal scheme was used.

### 6.2.4 Time sequences

The formulations presented in the previous chapters require not only the spatial description of the velocity field at a particular instant of time, but also the variation in time of this velocity field. A single snapshot of the velocity field (and its spatial derivatives) is insufficient for evaluating the fluid-dynamic forces on a bluff body.

This statement raises the following interesting remark: if we run two different experiments, and at a particular instant of time, the velocity field in one experiment happens to be identical to a velocity field in the other experiment, the fluid-dynamical forces on the body may not be the same because the time variation of these velocity fields may be different!

Thus, it is necessary that a time sequence of the velocity fields be acquired. With DPIV, the rate at which subsequent velocity fields may be captured is limited by video rate (30 Hz). For the low Reynolds number experiments, it was possible to achieve this rate for the velocity fields (see Paragraph 6.1.3).

### 6.2.5 Forward time differencing

The first step was a simple implementation of the code written by Doug Shiels for the validation of the formulations. The code was written for numerical data which is highly accurate. Thus, a simple *forward time differencing* was implemented. In such case, the code needs the velocity field (and its spatial derivatives) at time $t$ and the velocity field (and its spatial derivatives) at time $t + \delta t$.

In the experiments, the smallest $\delta t$ was $\delta t_{\min} \sim 0.033$ s. Just as a test, we processed the images by varying the time interval $\delta t$ to integer values of $\delta t_{\min}$, i.e. :

$$\delta t = (n + 1) \times \delta t_{\min}, \tag{6.27}$$

where $n$ is a positive integer, $n \geq 0$, corresponding to the number of images skipped in a time sequence. For example, if $n = 0$, then no images are skipped, and the time derivative is applied to two successive images.

The time derivative of a quantity $A$ is then taken as:

$$\frac{dA}{dt} \sim \frac{A(t+\delta t) - A(t)}{\delta t}. \tag{6.28}$$

### 6.2.6 Central time differencing

In a second step, it was decided to improve on the time differencing algorithm by going from forward time differencing to central time differencing. In this case, the code needs velocity fields at time $t - \delta t$, time $t$, and time $t + \delta t$. The quantities which were not subject to time differencing were evaluated at time $t$ whereas the time derivative of a quantity $A$ was performed as follows:

$$\frac{dA}{dt} \sim \frac{A(t+\delta t) - A(t-\delta t)}{2\delta t}. \tag{6.29}$$

### 6.2.7 Time differencing and spatial integration

As seen in Paragraph 6.2.1, the equations can be written either in terms of time derivatives of spatial integrals or in terms of spatial integrals of time derivatives. We noticed that both versions yielded identical results. This was to be expected since the time differencing procedure and the spatial integration procedure are both linear, and can be freely interchanged. We will return to this point in the next Chapter.

### 6.2.8 Filtering

The evaluation of forces following the above procedure generally produced very noisy signals. In the next Chapter, we will investigate the origin of this noise and show how it can be effectively removed through a filtering procedure, which we describe here.

The filter that was used is a IIR lowpass, 5th order Butterworth filter. The filter is monotonic throughout the spectrum, with ripples in neither the passband nor the stopband (see Figure 6.6). Because the filter is of IIR type (instead Of FIR), it introduces non-linear phase distortions. To eliminate these phase delays, the filter is run twice, first for increasing time and then for decreasing time. The result is a zero-phase distortion output. The drawback is a reduction in amplitude by the square of the original amplitude reduction of the single filter. In our experiments, the amplitude reduction was less than a few percent.

All the filtering functions were obtained from Matlab. No particular care was taken to ensure the reliability of the filter. This is because our analysis focused more on the self-consistency of the results than on their absolute magnitude.

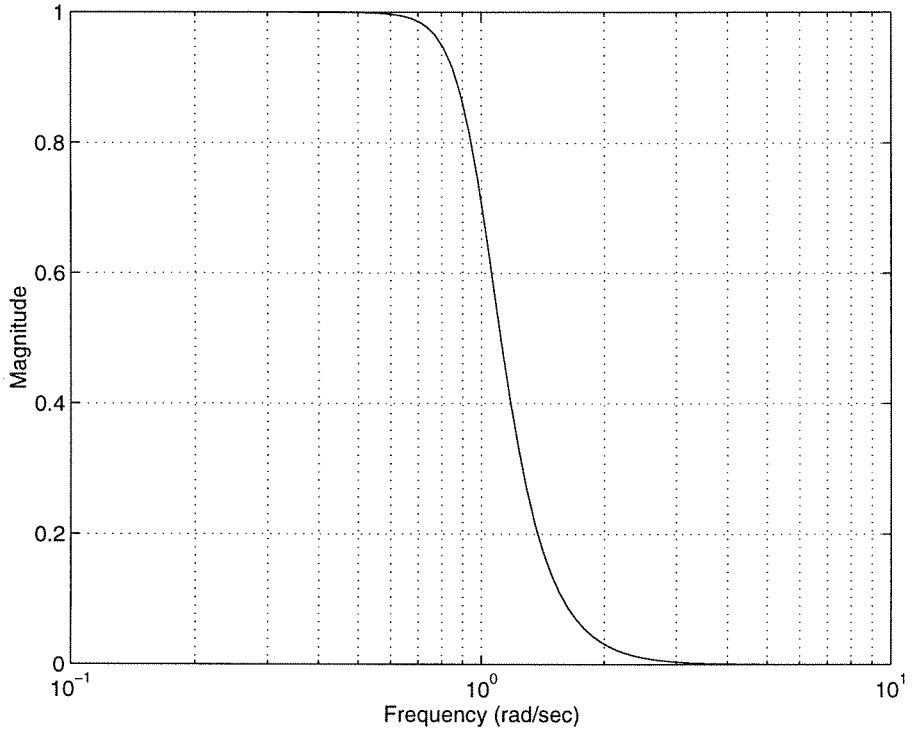


Figure 6.6: Magnitude squared for a Butterworth lowpass filter (5th order) with cutoff frequency at 1 rad/sec.

# Chapter 7 Low Reynolds number experiments: steady motions

In this Chapter, the force formulation will be applied to a circular cylinder in steady motion at $Re \sim 100$. For the reader's convenience, most of the figures have been placed at the end of the Chapter.

## 7.1 Experimental results

### 7.1.1 Motion parameters

As explained in Chapter 6, the experiments were conducted in a tow tank. The motion imposed on the cylinder is shown in Figure 7.1. It consists of a start-up motion with constant acceleration during a time $T = 1$ s, followed by a constant velocity motion with velocity $U = 1$ cm/s. Since the cylinder had a diameter of $d = 1$ cm and since the experiment was run in water, the Reynolds number based on the diameter of the cylinder was:

$$Re = \frac{Ud}{\nu} \sim 100, \tag{7.1}$$

where $\nu$ is the kinematic viscosity of water, which, for the water conditions in the tank (temperature $\Theta \sim 18°$ C) was equal to $\nu \sim 1.0 \times 10^{-6}$ m$^2$/s.

The units were normalized as follows. The length unit was normalized with the cylinder diameter.

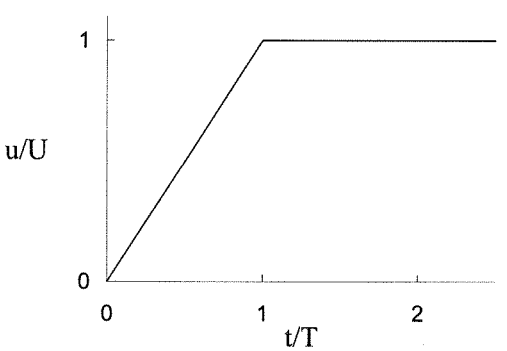


Figure 7.1: Carriage velocity profiles $u/U$ vs. time $t/T$ for a cylinder 1 cm in diameter at $Re \sim 100$ in water: start-up motion with constant acceleration during a time $T = 1$ s, followed by a constant velocity motion with velocity $U = 1$ cm/s.

The time unit was taken as the number of diameters that the cylinder would have travelled if it had moved with velocity $U = 1$ cm/s from $t = 0$. Note that $t$ does not represent the actual distance travelled by the cylinder since the cylinder is accelerated during the first second of motion. Frequency is just the inverse of this time unit. The sampling of the images, which was at 30 Hz, was thus 30 in these non-dimensional units. Similarly, the shedding frequency of the cylinder, which was around 0.16 Hz, was 0.16.

### 7.1.2 Flowfields

A 100-diameter time sequence of the flow was captured with DPIV (i.e. , $0 < t < 100$). Figure 7.2 and Figure 7.3 show a short time sequence of the velocity and vorticity fields obtained for approximately one shedding cycle (6 time units) between times $t = 85$ and $t = 90$.

The fields were obtained by cross-correlating particle images (captured at 30 Hz) in the following way: image 1 and image 2, image 2 and image 3, etc.... The sampling frequency for the velocity and vorticity fields was thus 30 (in non-dimensional units).

Note that in the velocity field, some spurious velocity vectors are present. These vectors are the result of poor correlations in the thin regions of shade cast by the cylinder (upstream) or in the regions of laser reflections (on the port and starboard sides of the cylinder). The wake seems to be free of these kind of vectors.

As for the vorticity field, it is just the result of numerical differentiation of the velocity field. We will, therefore, not discuss the resolution of the vorticity field, since it is a derived, not a measured, quantity. This point will become clearer as we we apply the force formulations.

## 7.2 Force evaluation

As mentioned in the previous Chapter, only the two-dimensional version of the equations (with $\mathcal{N} = 2$) has been used. When comparing the equations with each other, we will raise the problems involved by using the two-dimensional version instead of the three-dimensional version of the equations.

### 7.2.1 Forward time differencing scheme

As a first step, we applied the force formulations like they were written for the numerical code, i.e. , with simple forward time differencing. This procedure was later improved with a central differencing scheme, as we shall see in a later section.

For the analysis given in this and subsequent sections, we chose Equation "mom1" from the compendium in the previous Chapter. It is one of the "momentum" equations with the Kutta-Zhukovsky term as a volume integral. We will later see how the different equations fare with respect to each other.

Choosing a time step $\delta t$ equal to the sampling period, $\delta t \sim 0.033$ s, we performed the computations with the velocity fields given at time $t$ and time $t + \delta t$ and the vorticity fields given at time $t$, for the full range of motion $0 < t < 100$. The results for the lift coefficient are shown in Figure 7.4. Obviously, the signal is *very* noisy. A RMS lift coefficient of 0.2 is expected at $Re \sim 100$, whereas we seemed to obtain values larger by two orders of magnitudes.

We then decided to look at the power spectral density (PSD) of the signal in order to locate the source of noise. The PSD is shown in Figure 7.5 on a semi-log scale for which the frequency axis extends up to the Nyquist frequency at 15 (or about 1.2 in log coordinates). The PSD was computed for the time interval $50 < t < 100$ where presumably the cylinder had reached a steady shedding state.

The figure reveals some interesting features. First, the shedding frequency is very well apparent at a normalized frequency around $10^{-0.75 \pm .05} \sim 0.18 \pm 0.02$. This frequency is a bit higher than what it should be (0.165 from numerical computations), but it is also very coarse since there are only ten shedding cycles in the signal. We will later improve on this value by counting zero-value crossings.

Also, most of the power in the noise seems to arise at much higher frequencies, around and above the Nyquist frequency. We, therefore, decided to apply a lowpass filter to remove the high frequency components (the filter is described in the previous Chapter). With a cutoff frequency at 1, the resulting filtered signal is shown in Figure 7.6 with a PSD as given in Figure 7.7. The periodic lift coefficient signal associated with vortex shedding is now strongly apparent. The RMS for $50 < t < 100$ has been evaluated to be about 0.28. From the PSD, it may be noticed that the filtering process has only slightly reduced the power of the shedding peak.

Further filtering at a cutoff frequency of 0.3 yields the lift signal as given in Figure 7.8 with a PSD as given in Figure 7.9. The shedding peak has been reduced further by the filtering process, and the RMS value at 0.23 should probably not be trusted. However, this signal will be used for comparison with other time differencing schemes.

### 7.2.2 Forward time differencing scheme with large time step

In the previous paragraph, the time step for time differencing was taken as the sampling period of $\delta t = \delta t_{\min} \sim 0.033$. In this paragraph, we examine the effect of this time step on the results. Figure 7.10 and Figure 7.11 show the unfiltered lift coefficient for $\delta t = 5\,\delta t_{\min}$ and $\delta t = 10\,\delta t_{\min}$ respectively. The noise level is remarkably reduced with an increasing time step.

However, a major drawback of the increase in time step is the alteration of the (filtered) lift signal: as the time step is increased, the amplitude of the signal increases, as shown in Figure 7.12 and Figure 7.13. We attributed this effect to the forward time differencing scheme, and we, therefore, decided to turn to a central differencing scheme, which will be the topic of the following paragraph.

### 7.2.3 Central time differencing scheme

As in the previous paragraphs, the "momentum" equation "mom1" was used to test the central differencing scheme. With a time step equal to the sampling period, i.e. , $\delta t = \delta t_{\min}$, the lift coefficient was computed, and the unfiltered result is shown in Figure 7.14, which seems to be less noisy than the equivalent signal obtained from forward time differencing (Figure 7.4). A look at the PSD in Figure 7.15 definitely reveals the reduction in noise around the Nyquist frequency. Applying a filter with a cutoff frequency of .3 yields the signal shown in Figure 7.16, where we have included the similar filtered signal obtained with forward differencing. The RMS of the signal for the time interval $50 < t < 100$ is around 0.27, which is higher than the value of 0.23 obtained with forward time differencing.

### 7.2.4 Central time differencing with large time step

As for the forward time differencing scheme, we investigated the effect of time step on the convergence of the scheme. Figure 7.17 and Figure 7.18 show the unfiltered result for $\delta t = 5\,\delta t_{\min}$ and $\delta t = 10\,\delta t_{\min}$ respectively. For the latter case, the periodic signal associated with shedding is indeed apparent.

After filtering at a cutoff frequency of 0.3, we see that a large time step scheme does not affect the signal amplitude, as exemplified in Figure 7.19. This is in contrast with the forward differencing scheme for which the amplitude of the signal increased dramatically by increasing the time step. From a single-time step scheme to a ten-time step scheme, the RMS is only slightly reduced (from 0.27 to 0.26).

In summary, we felt that the central time differencing scheme was a better alternative to the forward time differencing scheme.

### 7.2.5 Temporal differentiation and spatial integration

Thus far, we have only investigated the time differentiation scheme. In the previous Chapter, the equations were written with either time derivatives of integrals (equations "mom3", "mom4", "flux3", and "flux4") or with integrals of time derivatives (equations "mom1", "mom2", "flux1", and "flux2"). We have argued already that for differencing schemes, the two alternatives should be identical within precision error. In Figure 7.20, we compare the results for the lift signal as obtained from Equation "mom1" and Equation "mom2" which are different only in the order of the temporal differentiation and the spatial integration. Obviously, the results are identical. The same procedure has been tested on the pairs of equations, "mom3"-"mom4", "flux1"-"flux2", and "flux3"-"flux4", which only differ in the order of the operators, and good agreement was obtained.

### 7.2.6 Kutta-Zhukovsky term

The Kutta-Zhukovsky term can be evaluated as either a surface integral (involving only the velocity) or a volume integral (involving the velocity and the vorticity) thanks to the following identity:

$$\oint_S \hat{\mathbf{n}} \cdot (\frac{1}{2}u^2\mathbf{I} - \mathbf{u}\,\mathbf{u})\,dS = \int_V \mathbf{u} \wedge \boldsymbol{\omega}\,dV - \oint_{S_b} \hat{\mathbf{n}} \cdot (\frac{1}{2}u^2\mathbf{I} - \mathbf{u}\,\mathbf{u})\,dS. \tag{7.2}$$

For a non-rotating, rigid body with a no-slip condition at the body surface, the body surface integration can be shown to vanish, and we are left with:

$$\oint_S \hat{\mathbf{n}} \cdot (\frac{1}{2}u^2\mathbf{I} - \mathbf{u}\,\mathbf{u})\,dS = \int_V \mathbf{u} \wedge \boldsymbol{\omega}\,dV. \tag{7.3}$$

Thus, some of the equations differ only by the Kutta-Zhukovsky force being a surface integration or a volume integration, such as the pairs of equations "impl"-"imp2", "moml"-"mom2", "mom3"-"mom4", "flux1"-"flux2", and "flux3"-"flux4".

A comparison was made of our original Equation "moml" with its counterpart Equation "mom2". The result is shown in Figure 7.21. Again, the agreement between the two equations is remarkable, even though it is not perfect.

Note that the identity is valid in two dimensions if the flow is two-dimensional and in three dimensions if the flow is three-dimensional, but it cannot be valid on a two-dimensional plane (like a DPIV image) if the flow is three-dimensional. If our nominally two-dimensional flow suffers from some *intrinsic* three-dimensionality, then it cannot be said which version, the surface or the volume integration, yields a better result.

The problems related to three-dimensionality will not be tackled in this monograph.

### 7.2.7 The "impulse", "momentum", and "flux" equations

Forces can be evaluated with three different versions of the equations, as presented in Chapter 3, Chapter 4, and Chapter 5.

#### The "impulse" and "momentum" equation

The "impulse equation" requires an integration of the moment of vorticity $\mathbf{x} \wedge \boldsymbol{\omega}$ over the volume of fluid surrounding the body. The use of such an equation may be objectionable on the ground that the vorticity field cannot be resolved in the boundary layers next to the body. Note though that only the time derivative of this integral is needed. Thus, steady boundary layers would not contribute to the force.

Nevertheless, the objection may be overruled by using an "improved" version of the equation, the "momentum equation", which requires only the integration of the velocity over the volume of

fluid surrounding the body. One may argue that the velocity field being smoother may yield better results.

However, this statement is not correct in the present experimental situation. The only *measured* quantity is the velocity field. The vorticity field is a *computed* quantity. Since the "impulse" and the "momentum" equation are related by a vector identity, they must yield the same answer (within precision error) just because they are both based on the same original data - the *velocity field.* Note that the argument holds if the flow were wholly three-dimensional because we are using the two-dimensional version of the vector identity with a vector field based on a plane. The vector field on the plane is completely arbitrary and is not even required to be divergence free!

This can be demonstrated by comparing the results of equation "impl" and "moml" in Figure 7.22 for the filtered (cutoff frequency of 1) lift coefficient. Obviously, the two signals are very similar.

If an experiment were setup to generate vorticity and velocity *independently*, then the two equations would probably produce different answers, depending on the accuracy of the experimental technique for measuring either fields.

The reader may be left perplexed by the numerical results shown in Chapter 4, which revealed a difference between the results of the "impulse" and "momentum" equation. There, the derived quantity was the velocity field which was computed from the original vorticity field based on the particles, and not from the vorticity field placed on the grid. The vorticity field was only later placed on a grid (by interpolation) for processing purposes. Thus, because of interpolation, the vorticity field (on the grid) lacked the accuracy of the velocity field. If the forces had been computed from the original vorticity field, the results would have been identical to the ones obtained with the velocity field.

### The "momentum" and "flux" equation

The "flux" equation is related to the other equations through a vector identity which holds only when the velocity field is divergence free, i.e. :

$$\nabla \cdot \mathbf{u} = 0, \tag{7.4}$$

or:

$$\frac{\partial u}{\partial x} + \frac{\partial v}{\partial y} + \frac{\partial w}{\partial z} = 0, \tag{7.5}$$

where $u$, $v$, and $w$ are respectively the $x$-component, $y$-component, and $z$-component of the velocity field. It may be thought that this condition should be trivially satisfied if the experiments are conducted in water at low speeds, in which case the flow is almost truly incompressible.

However, it should be remembered that the two-dimensional version of the equations was used,

for which the divergence-free condition takes the form:

$$\frac{\partial u}{\partial x} + \frac{\partial v}{\partial y} = 0. \tag{7.6}$$

Even though Equation 7.5 is always satisfied under incompressible conditions, it is not so for Equation 7.6. The solenoidal nature of the velocity field may be respected in the whole three-dimensional flow, and yet, the projection of the same velocity field onto a plane may not be divergence free! If the flow is purely two-dimensional and if the plane of measurement (say the $x$-$y$ plane) is coplanar with the flow, then indeed the velocity field will be solenoidal on the plane of measurement, i.e. :

$$\frac{\partial u}{\partial x} + \frac{\partial v}{\partial y} = 0, \tag{7.7}$$

since $w = 0$ from the experimental conditions. However, if there happens to be some intrinsic three-dimensionality such that $w \neq 0$, or more precisely, $\partial w/\partial z \neq 0$, then on the plane of the measurement we will still have:

$$\frac{\partial u}{\partial x} + \frac{\partial v}{\partial y} + \frac{\partial w}{\partial z} = 0, \tag{7.8}$$

but:

$$\frac{\partial u}{\partial x} + \frac{\partial v}{\partial y} \neq 0. \tag{7.9}$$

Thus, if we use the two-dimensional version of the identity (which we must since DPIV is a two-dimensional technique), it may not be satisfied because of intrinsic three-dimensionality in the flow.

This point is confirmed in Figure 7.23 where we have plotted the lift coefficient as obtained from the "momentum" equation and the "flux" equation. There are indeed some slight differences between the two signals, whereas the "impulse" equation yielded almost identical results as the "momentum" equation. The difference is even more substantial in the drag signal, shown in Figure 7.24. In order to locate the origin of the slight discrepancy, the divergence field was evaluated, and is shown in Figure 7.25. We immediately see that the velocity field is non-solenoidal near the body. We do not believe that the divergence arises because of actual intrinsic three-dimensionality. We think that it is an artifact of the measurement, which was quite delicate especially near the body surface as explained in Chapter 6. Also, since the regions near the body are regions of high strain, it may be difficult experimentally to force a large quantity such as $\partial u/\partial x$ to cancel a similar large quantity of opposite sign $\partial v/\partial y$.

The question that arises naturally is which of the formulae, the "momentum" (or equivalently, the "impulse") or the "flux" equation, gives the most reliable result[1]. The answer is as follows.

If the flow is actually *three-dimensional*, we do not believe that either gives an accurate result.

[1] We obviously mean the *two-dimensional* versions of these equations. The three-dimensional versions are identically equivalent if the three-dimensional velocity field is given.

It is beyond the scope of the present monograph to include the effects of three-dimensionality, but we do realize that it is a relevant consideration that ought to be studied in future work.

If the flow is *two-dimensional*, but the measurement generates spurious divergence in the velocity field, then the "flux" equation will give the most accurate answer because it does not rely on any (spurious) information contained within the control volume. The flux equation is thus strongly preferred in situations where parallax or lensing effects (see Chapter 6) prevent the flow from being resolved accurately near the body surface.

### 7.2.8 Domain size

Since the equations depend on an integration over a volume and/or a surface, it is natural to investigate the effect of domain size or shape on the results.

#### Identical data with different domains of integration

In Figure 7.26, we show the three different domains that were considered. These domains are obtained by cropping the original data set to some desired dimension. The "intermediate" domain is thus only a subset of the "large" domain, and the "small" domain is a subset of the two larger ones.

Figure 7.27 shows a comparison of the lift coefficient evaluated with the "large" and the "intermediate" domain. The trend is very similar in both signals, but there exists a slight discrepancy of the order of 0.1 for the peak values. The RMS value calculated for the "intermediate" domain is around 0.20, which is very close to the value obtained from numerical computations. This value is definitely smaller than the value for the "large" domain (about 0.28).

When comparing the "intermediate" domain to the "small" domain, a similar discrepancy is present, as shown in Figure 7.28. Here, the RMS value for the lift coefficient evaluated with the "small" domain is about 0.23, which is intermediary between the values obtained from the "large" and the "intermediate" domain.

Before discussing these results, we will look at another case where the domain of integration was chosen to be much larger.

#### Different data on a very large domain of integration

The field of view that was used in this study is shown in Figure 7.29. Note that since the cylinder was off-axis with respect to the optical axis of the CCD camera, a small region (half cylinder diameter in size) near the "leading edge" of the cylinder was obscured by the cylinder itself ("parallax" effect). The computed vorticity thus seems to extend upstream of the cylinder. The "flux" equation which is oblivious to the measurement inaccuracies within the volume will give us an estimate of the errors

introduced by these parallax effects. Note also that the resolution is much lower than in the domains studied thus far. We will now investigate the effects of a lower resolution and a bigger domain on the evaluation of forces.

Figure 7.30 and Figure 7.31 show the unfiltered signal along with the power spectral density. Note that compared to Figure 7.15, the power in the shedding signal as well as in the high frequency noise seems to be higher in this very large domain. This high power is illustrated vividly in the next figure which shows the filtered lift signal (Figure 7.32). The peak values for the lift coefficient are an order of magnitude higher, 1.5 instead of 0.2 for the smaller domains! These large values are not due to the spurious vorticity fields near the body, since the "flux" equation yields similar high signals. The drag coefficient is also slightly altered in the mean (Figure 7.33). For times greater than 20, the mean was evaluated at 2.0, which is higher than the value of 1.4 as obtained with smaller domains (see Figure 7.24).

In Chapter 9, we will present a brief analysis of the discrepancies created by the domain size.

## 7.3 Discussion of physical results

### 7.3.1 Lift coefficient

The lift coefficient was evaluated with a central time differencing scheme, and the filtered signal (cutoff frequency at 0.3) is shown in Figure 7.34, along with the period-based mean lift signal (obtained with a filtering procedure with a cutoff frequency at 0.05) obtained form the "large" domain.

As stated in the previous paragraphs, the RMS of the lift signal was around 0.27, which is slightly larger than the value obtained from numerical computations[2] (around 0.21). We can attribute this higher experimental value to several factors.

From a physical point of view, the background turbulence level is larger in the tow tank than it is in numerical computations (where "background turbulence" arises only from truncation errors in general). These turbulent structures occur on a large scale (several cylinder diameters) and thus affect the wake as a whole. Instead of being rectilinear, the wake assumes an irregular, serpentine shape which could raise the RMS lift signal.

The irregularity of the wake structure is strongly suggested by the wandering of the period-based mean lift signal in Figure 7.34 which, instead of lying at zero, varies as a function of time. This feature was also observed visually. The shedding of vortices did not seem to be spatially symmetric from one half-period to the next: the cylinder would preferentially shed vortices towards one side, and would then revert towards the other side after a few cycles. As we mentioned it before, we

[2]Henderson R., personal communication.

believe that this phenomenon is a result of the large scale convection currents which were present in the tank and which probably distorted the whole wake.

We think, however, that the discrepancy between the measured and computed value is purely a result of experimental precision. We will see in Chapter 9, that the force formulations are very sensitive to the position vector which introduces a "moment arm" effect and amplifies the error. We already saw in this Chapter that the domain size does indeed affect the absolute measured values (RMS lift coefficients of 0.27 and 0.20 for the "large" and "intermediate" domains respectively). One may argue that since the flow is not purely two-dimensional, the information contained in a given integration volume may not be preserved in a larger or smaller volume, thereby altering the value of evaluated forces. Even though the latter argument may be satisfactory, it does not completely explain why for the *very large* domain, the lift coefficient is an order of magnitude larger! In Chapter 9, we will elucidate this mystery.

Returning to Figure 7.34, we can use the filtered signal to measure the shedding frequency from a count of the zero-crossing points. This procedure yields an estimate of the shedding frequency at $0.16 \pm 0.01$, which is in good agreement with published results[3]. This number lacks accuracy because of the oblique shedding regime in our experiments, and precision because of the little number of sampled shedding cycles.

### 7.3.2 Drag coefficient

The drag signal filtered with a cutoff frequency of 1 is shown in Figure 7.35. The signal reveals a low drag portion for the time interval $0 < t < 70$, with $C_D \sim 1.27$, and a high drag portion for the time interval $70 < t < 100$, with $C_D \sim 1.48$. This feature correlates well with the lift coefficient signal which tends to reach maximum amplitude only after about 50 diameters of travel. This phenomenon is characteristic of low (small-scale) turbulence tanks in which the shedding pattern behind a bluff body requires many diameters of travel to reach its final, periodic state.

Using a force balance, Lisoski[4] measured the drag on a flat plate towed in the same facility, and his Figure 3.5 strongly resembles the drag curve obtained here for the cylinder. He also observed a "drag plateau" before the inception of "steady-state" shedding.

The drag coefficient obtained in our experiments ($C_D \sim 1.48$ in the shedding regime) is, like the RMS lift coefficient, higher than what it should be. Numerical computations[5] yield a value only slightly above 1.3. We attribute our higher value to the wake structure being more irregular in our experiments.

[3]Hammache M. & Gharib M., An experimental study of the parallel and oblique vortex shedding from circular cylinders, **232** (1991) 567-590.

[4]Lisoski, D. L. A., *Nominally two-dimensional flow about a normal flat plate*, Ph.D. Thesis, California Institute of Technology, 1993.

[5]Henderson R. D., Details of the drag curve near the onset of vortex shedding, *Physics of fluids* (1995).

Figure 7.35 also reveals an interesting peak at the start of the motion. Since the camera was towed with the cylinder, it was not in an inertial frame during the accelerated part of the motion. The forces obtained from the formulations should have been corrected for the acceleration of the frame during this initial stage of motion. We decided not to worry with this correction (which can be readily done) for the following reasons.

A ramp acceleration has two singularities, one at the start of the motion and one at the end of the acceleration. At these two points, the time derivative of the velocity is discontinuous. Experimentally, such discontinuities cannot be captured reliably. Since the acceleration signal is a hat profile, it must be broadband and contain an infinite number of frequencies. Because our signal had to be filtered, and because it was limited by the sampling frequency at 30, we believe that we could not resolve the initial peak accurately. As a matter of fact, by varying the cutoff frequency of the filtered signal, we did observe that the peak amplitude varied, as shown in Figure 7.36 and Figure 7.37.

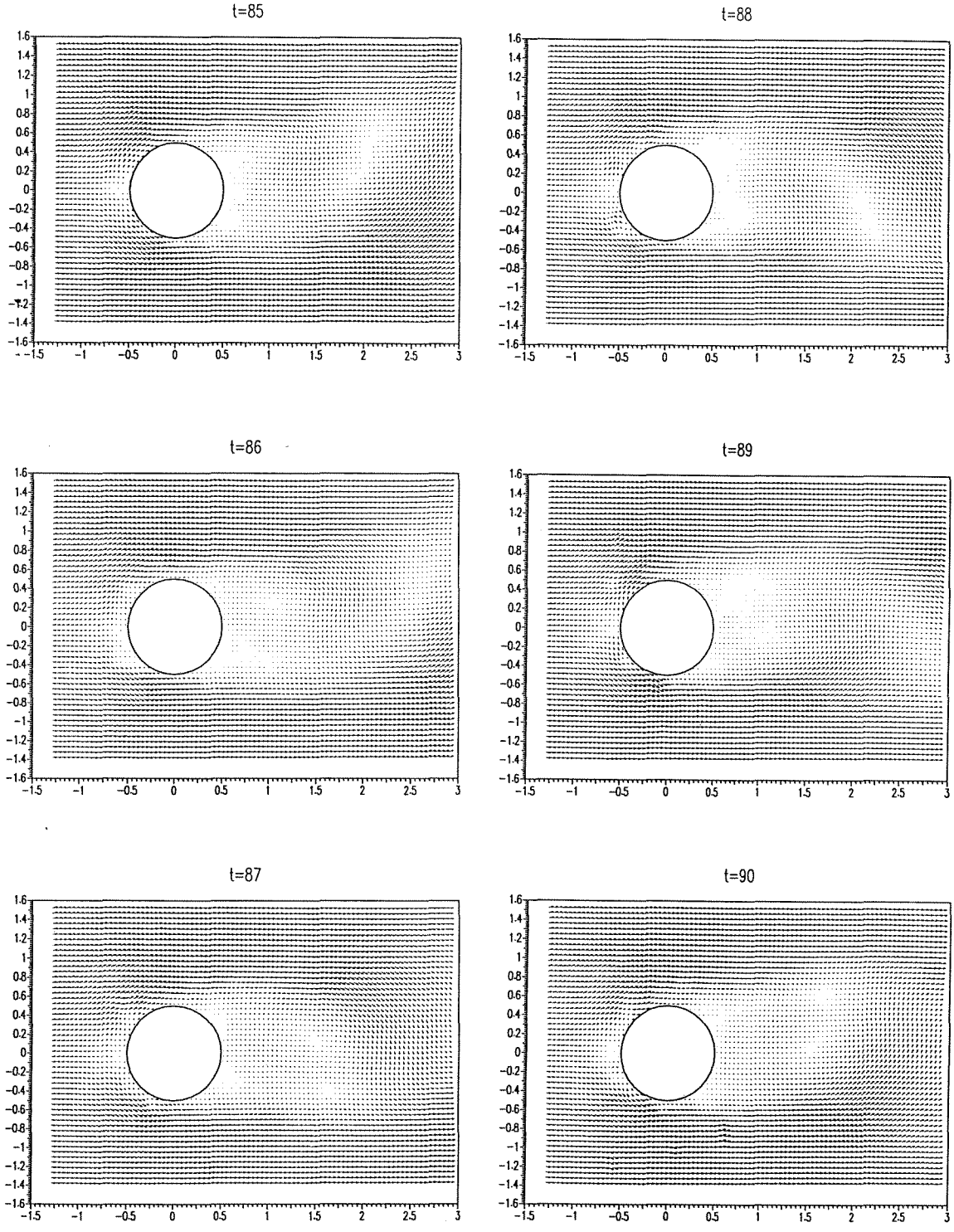


Figure 7.2: Time sequence of velocity fields for a circular cylinder at $Re \sim 100$ during one shedding cycle.

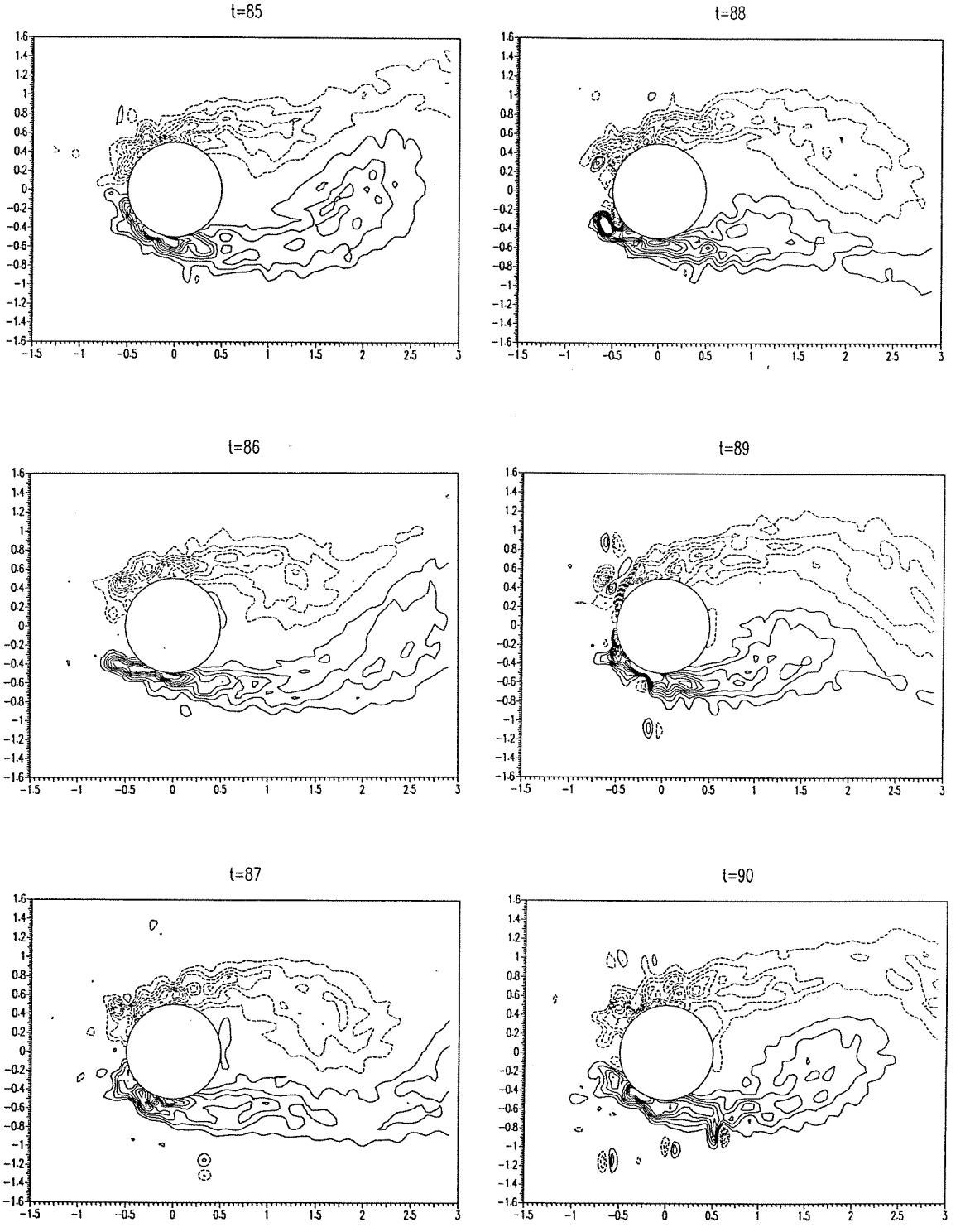


Figure 7.3: Time sequence of vorticity fields for a circular cylinder at $Re \sim 100$ during one shedding cycle (contours are incremented by 1; dashed lines represent negative values, solid lines positive values).

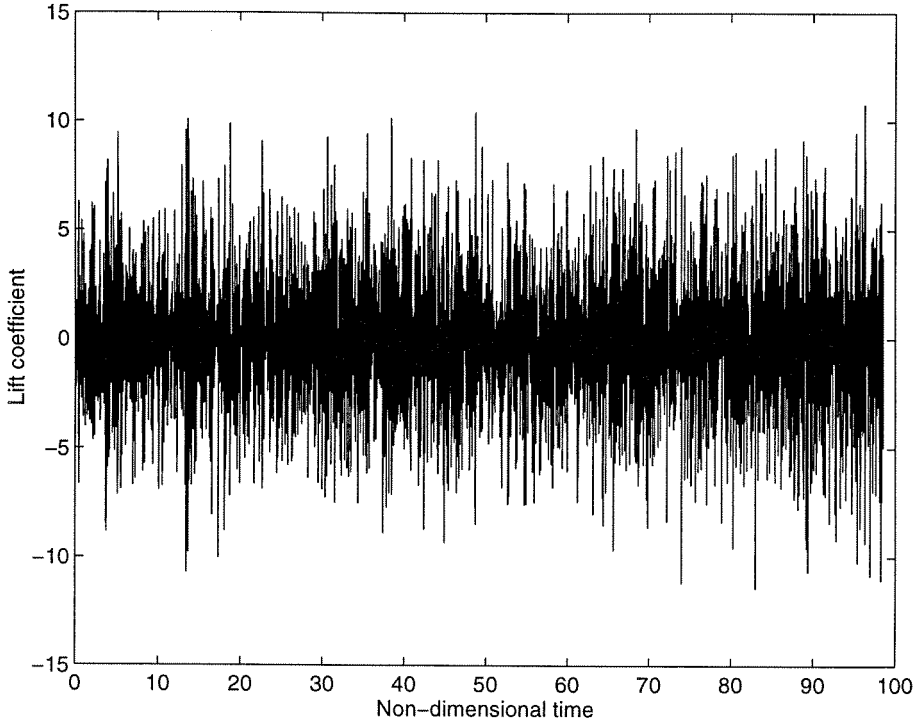


Figure 7.4: Unfiltered lift coefficient vs. time, obtained with forward time differencing (time step equal to sampling period).

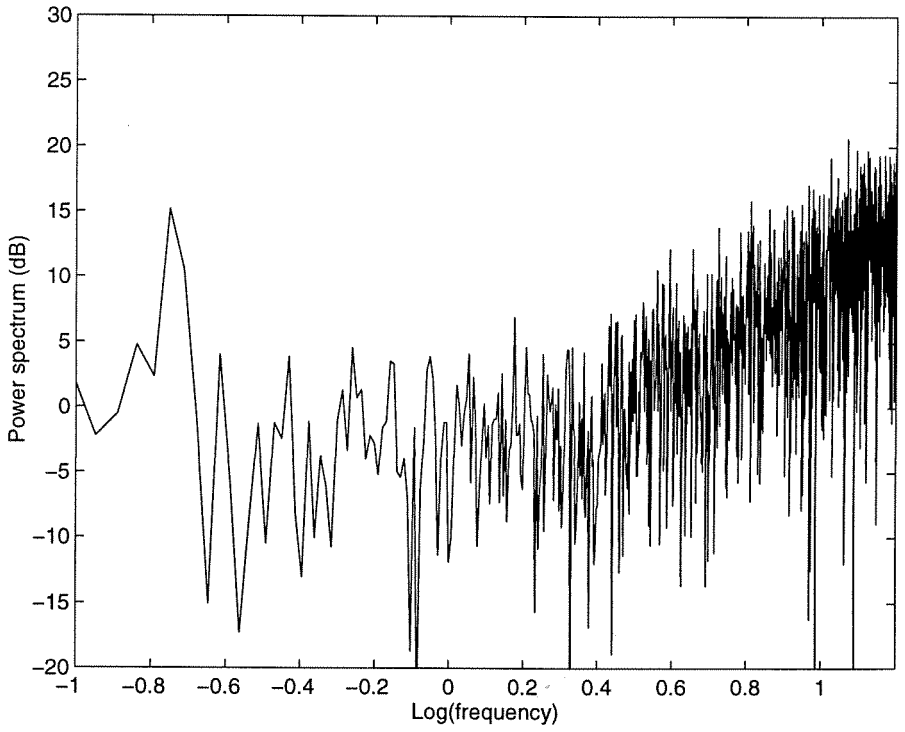


Figure 7.5: Power spectral density of lift coefficient, obtained with forward time differencing (time step equal to sampling period).

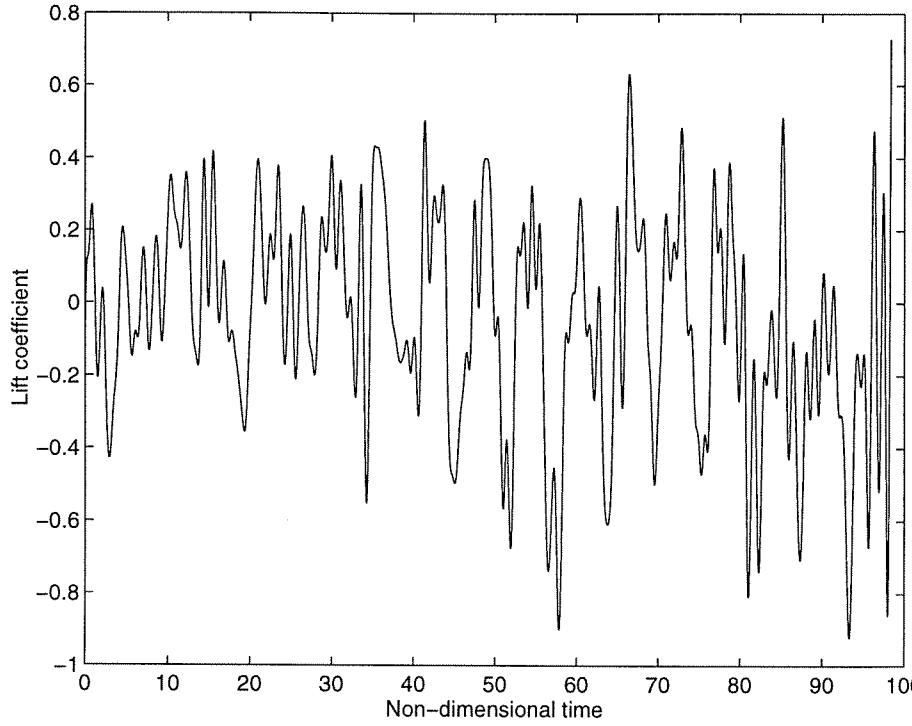


Figure 7.6: Lift coefficient vs. time, obtained with forward time differencing (time step equal to sampling period) and low-pass cutoff at a frequency of 1.

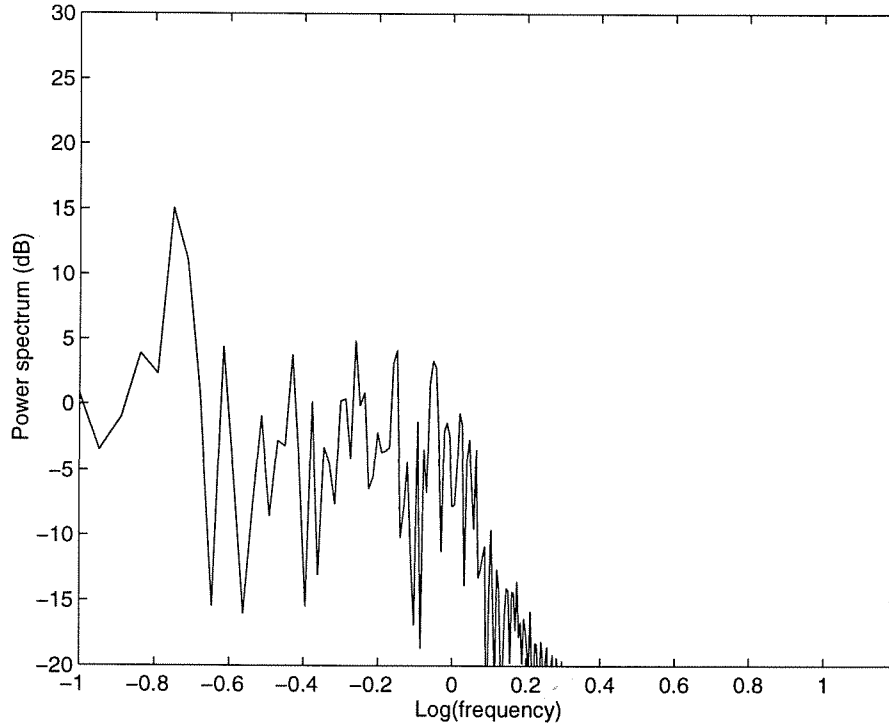


Figure 7.7: Power spectral density of lift coefficient, obtained with forward time differencing (time step equal to sampling period) and low-pass cutoff at a frequency of 1.

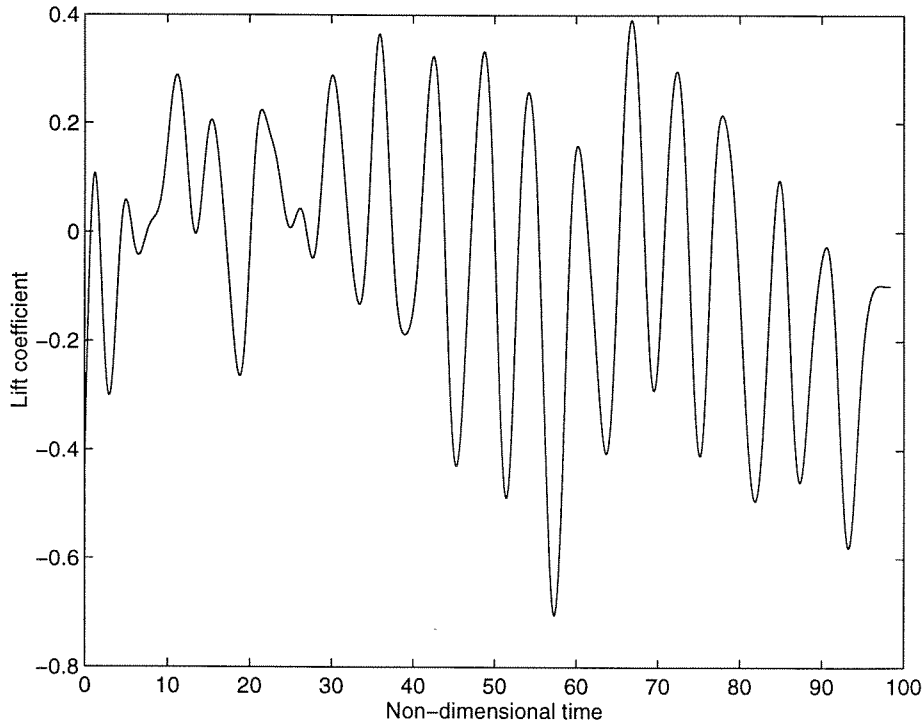


Figure 7.8: Lift coefficient vs. time, obtained with forward time differencing (time step equal to sampling period) and low-pass cutoff at a frequency of 0.3.

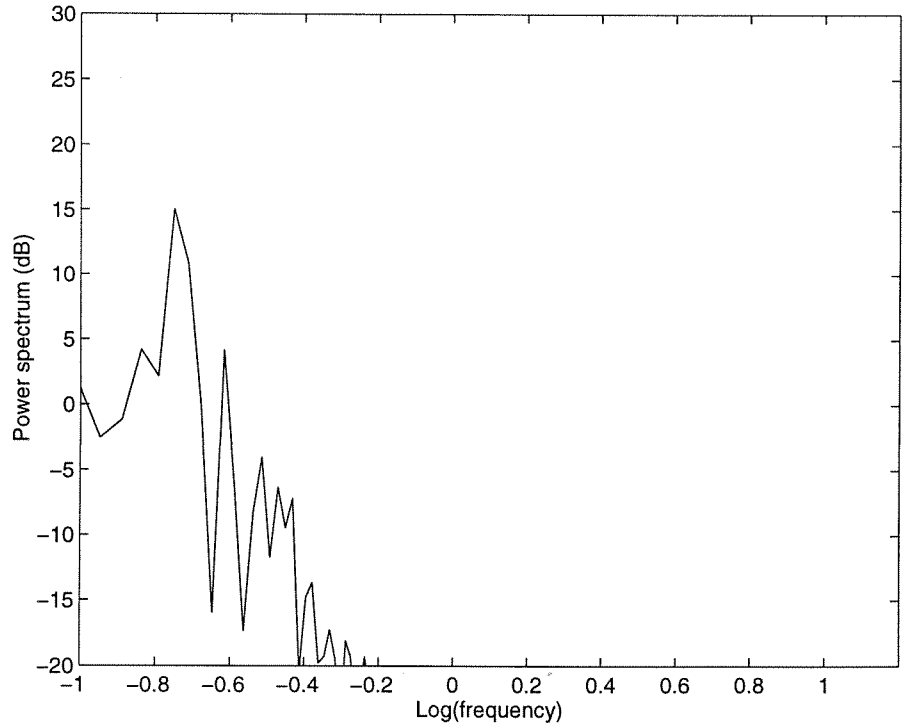


Figure 7.9: Power spectral density of lift coefficient, obtained with forward time differencing (time step equal to sampling period) and low-pass cutoff at a frequency of 0.3.

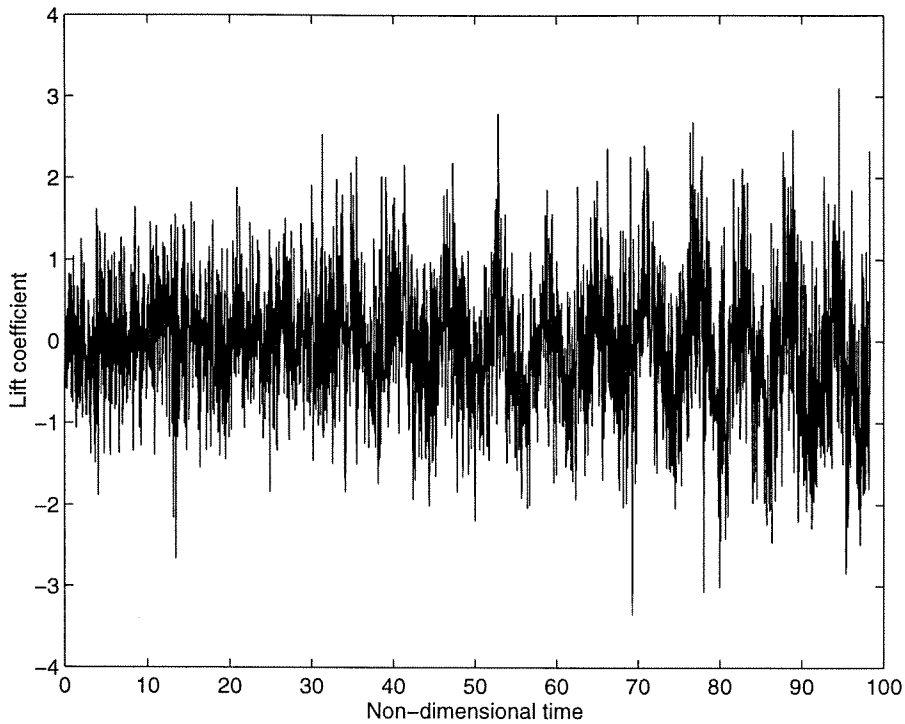


Figure 7.10: Unfiltered lift coefficient vs. time, obtained with forward time differencing (time step equal to 5 times sampling period).

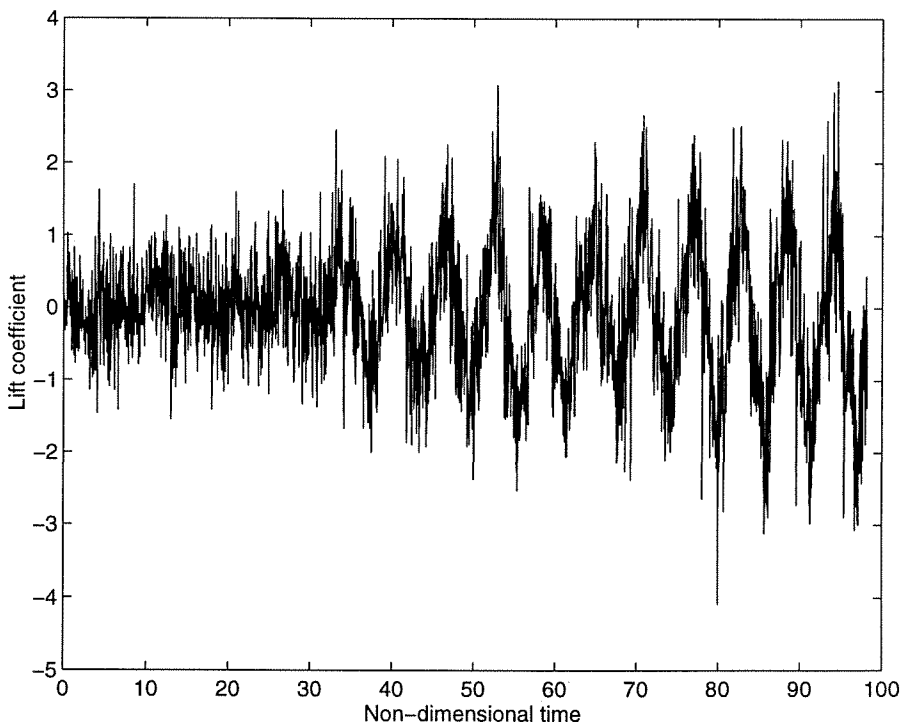


Figure 7.11: Unfiltered lift coefficient vs. time, obtained with forward time differencing (time step equal to 10 times sampling period).

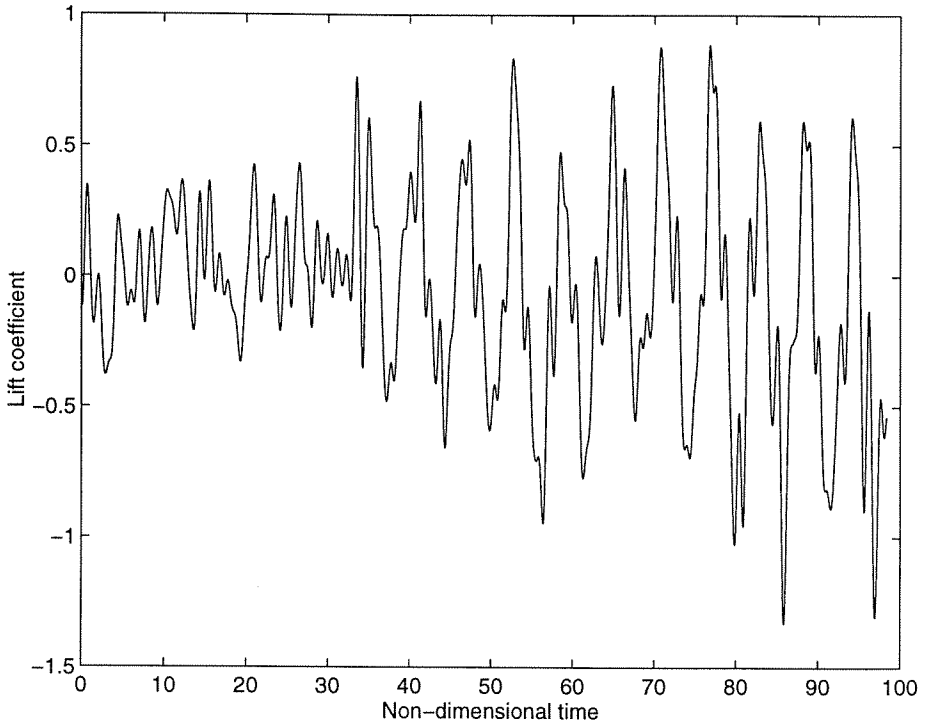


Figure 7.12: Lift coefficient vs. time, obtained with forward time differencing (time step equal to 5 times sampling period) and low-pass cutoff at a frequency of 1.

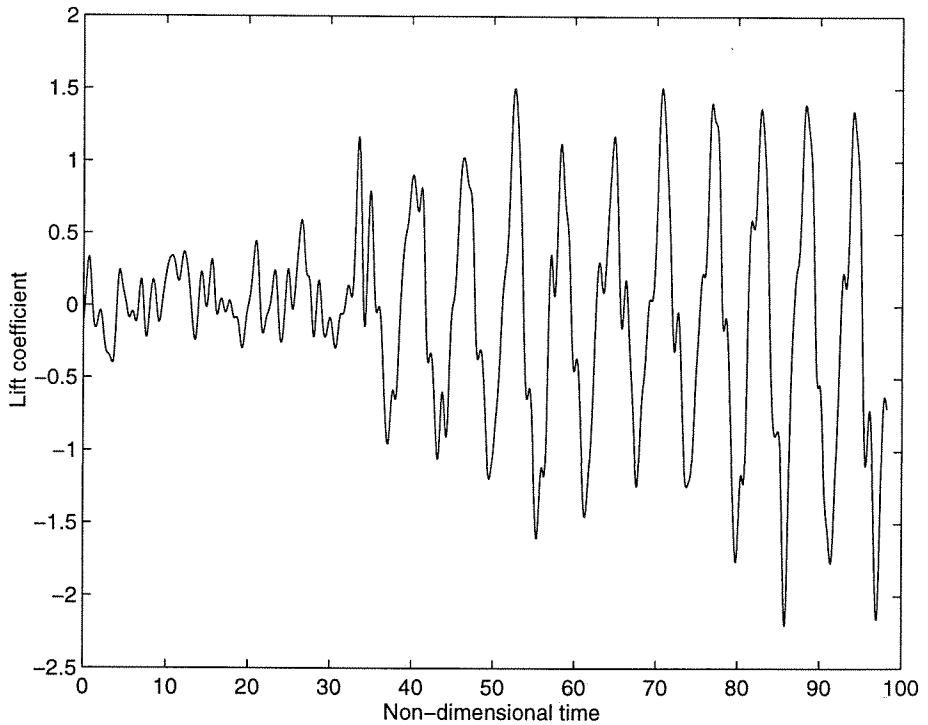


Figure 7.13: Lift coefficient vs. time, obtained with forward time differencing (time step equal to 10 times sampling period) and low-pass cutoff at a frequency of 1.

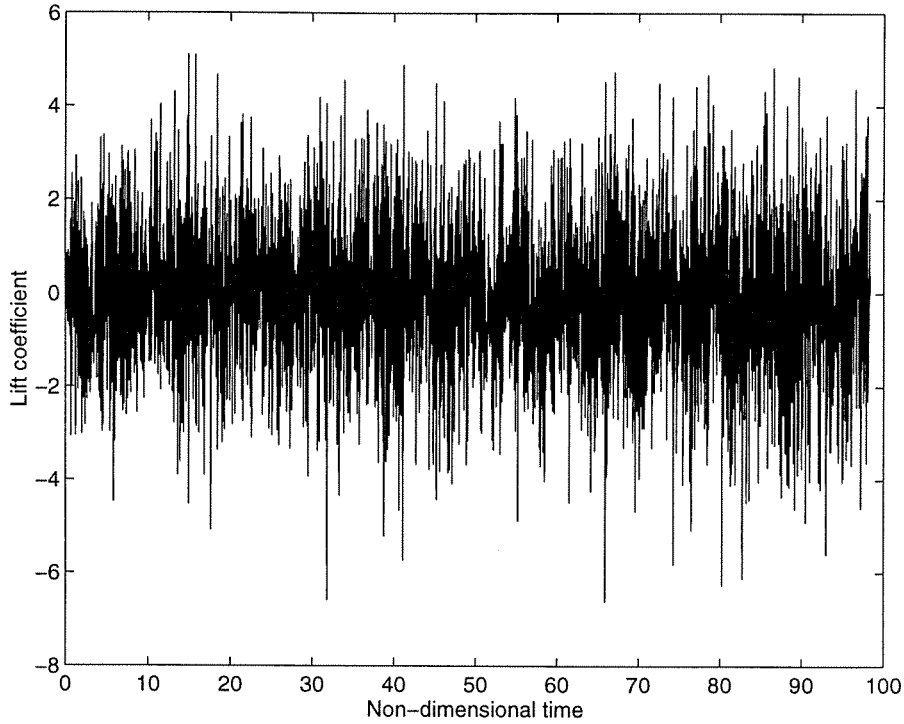


Figure 7.14: Unfiltered lift coefficient vs. time, obtained with central time differencing (time step equal to sampling period).

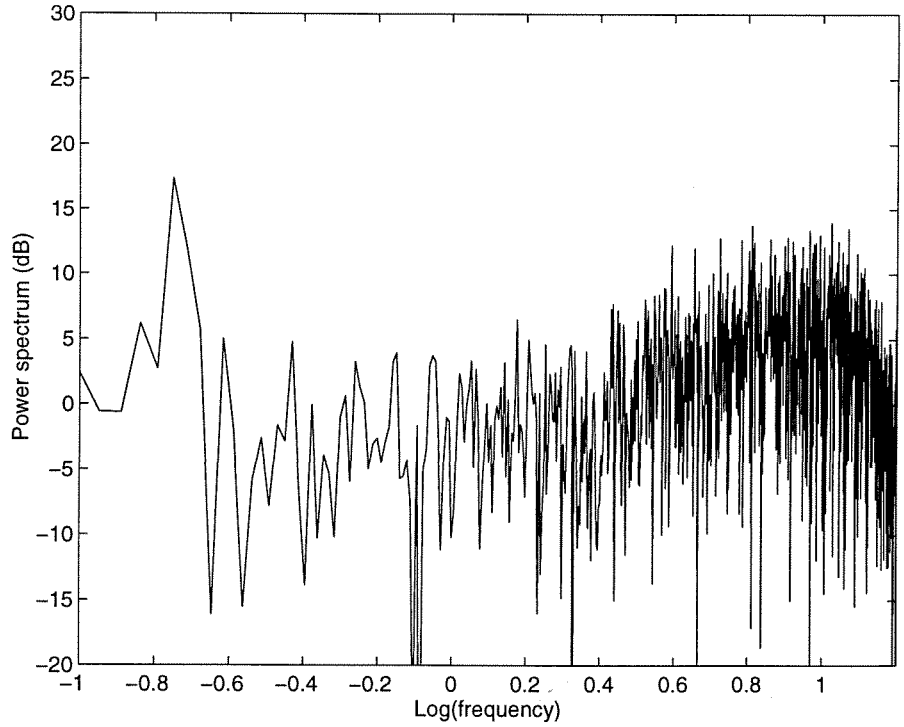


Figure 7.15: Power spectral density of lift coefficient, obtained with central time differencing (time step equal to sampling period).

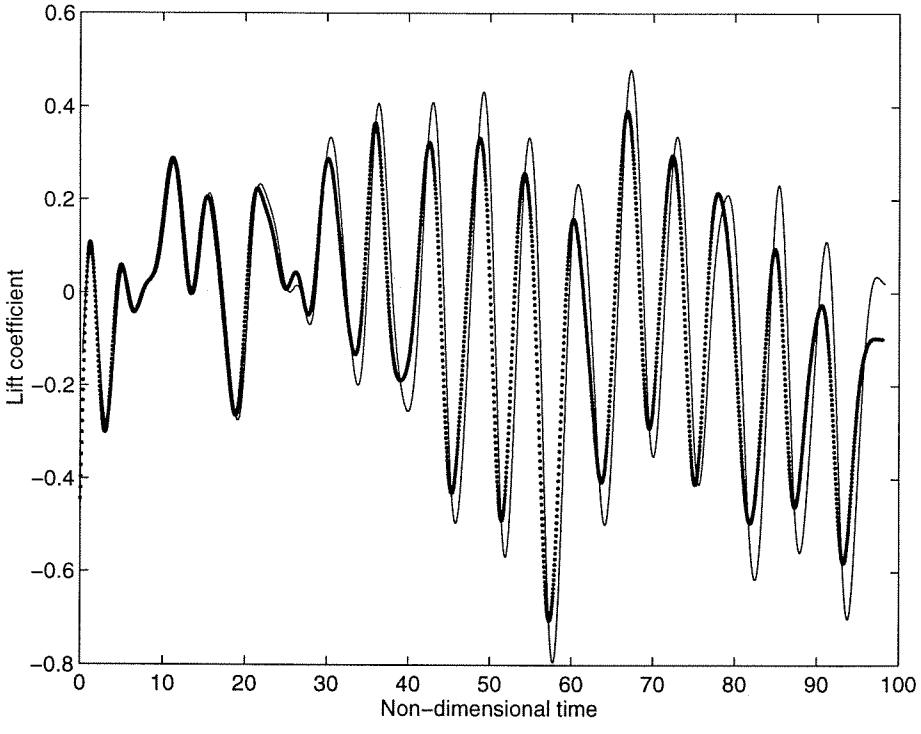


Figure 7.16: Lift coefficient vs. time, obtained with low-pass cutoff at a frequency of 0.3: ——, central time differencing (time step equal to sampling period); • • •, forward time differencing (time step equal to sampling period).

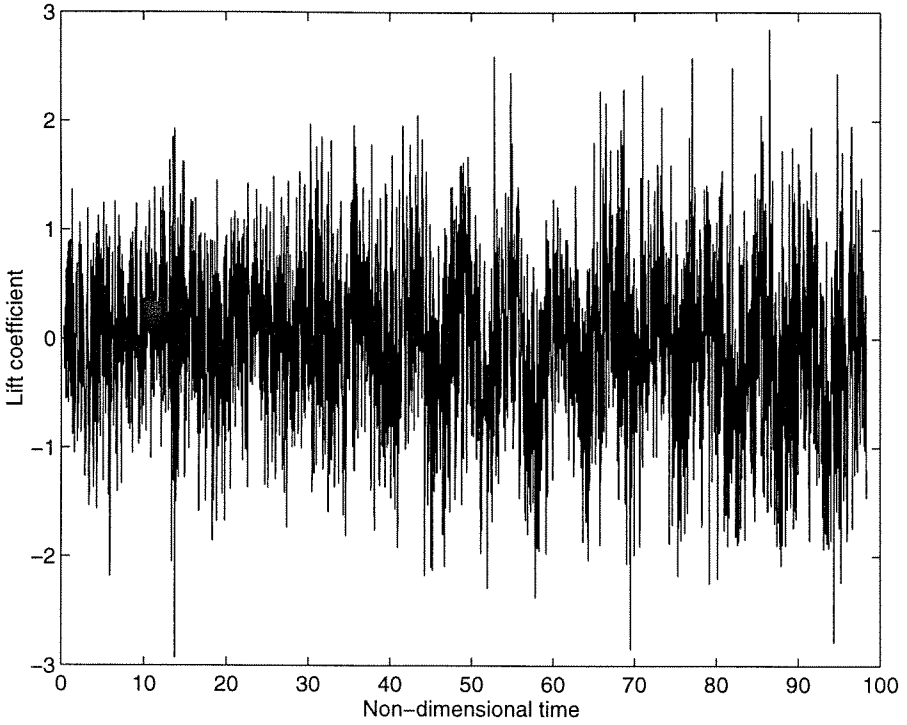


Figure 7.17: Unfiltered lift coefficient vs. time, obtained with central time differencing (time step equal to 5 times sampling period).

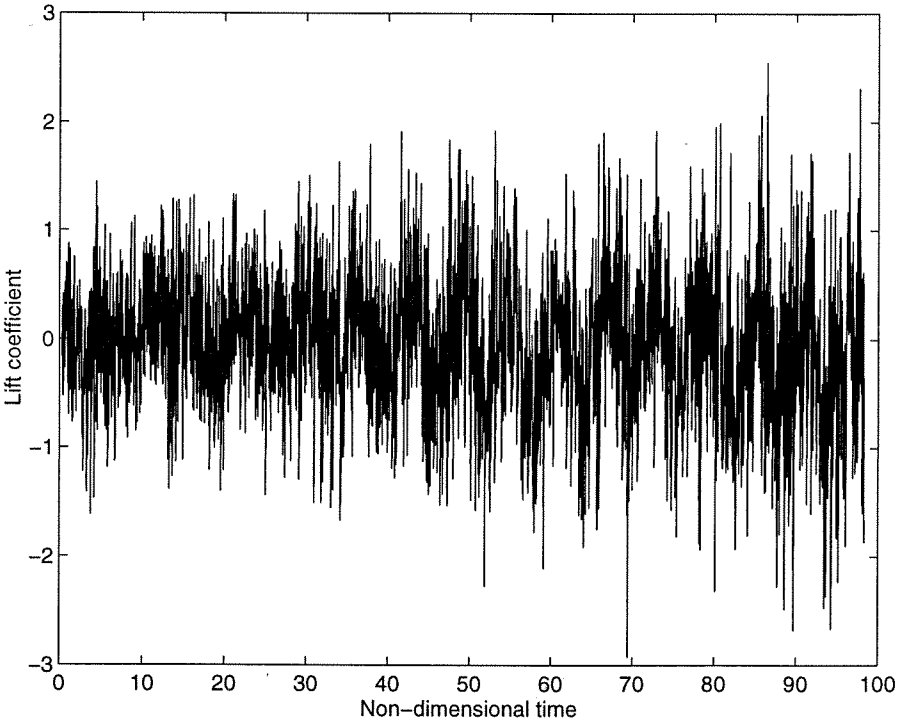


Figure 7.18: Unfiltered lift coefficient vs. time, obtained with central time differencing (time step equal to 10 times sampling period).

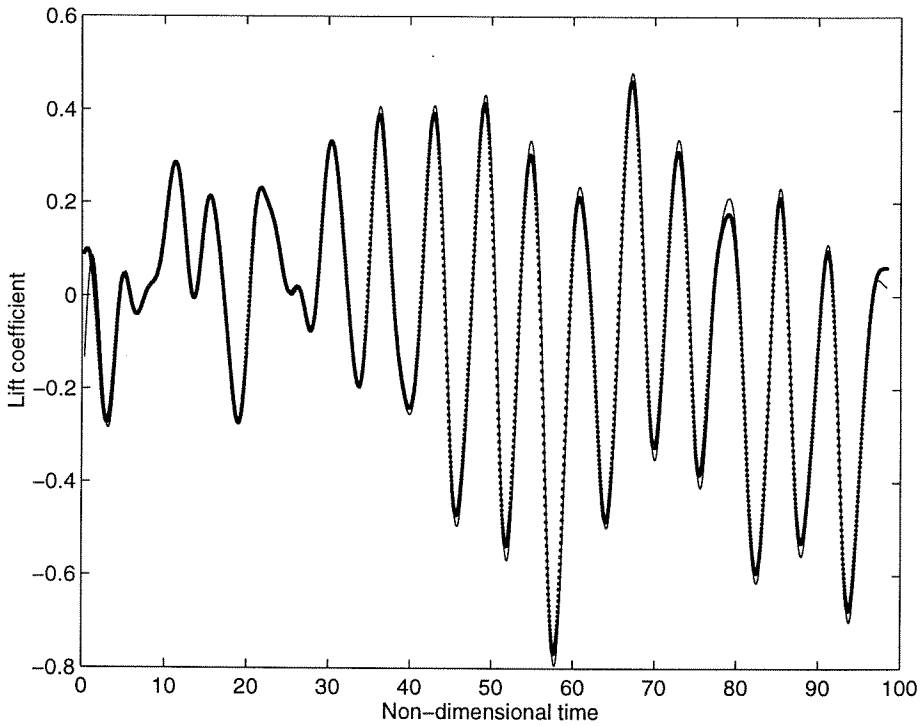


Figure 7.19: Lift coefficient vs. time, obtained with low-pass cutoff at a frequency of 0.3: ——, central time differencing (time step equal to 10 times sampling period); · · ·, central time differencing (time step equal to sampling period).

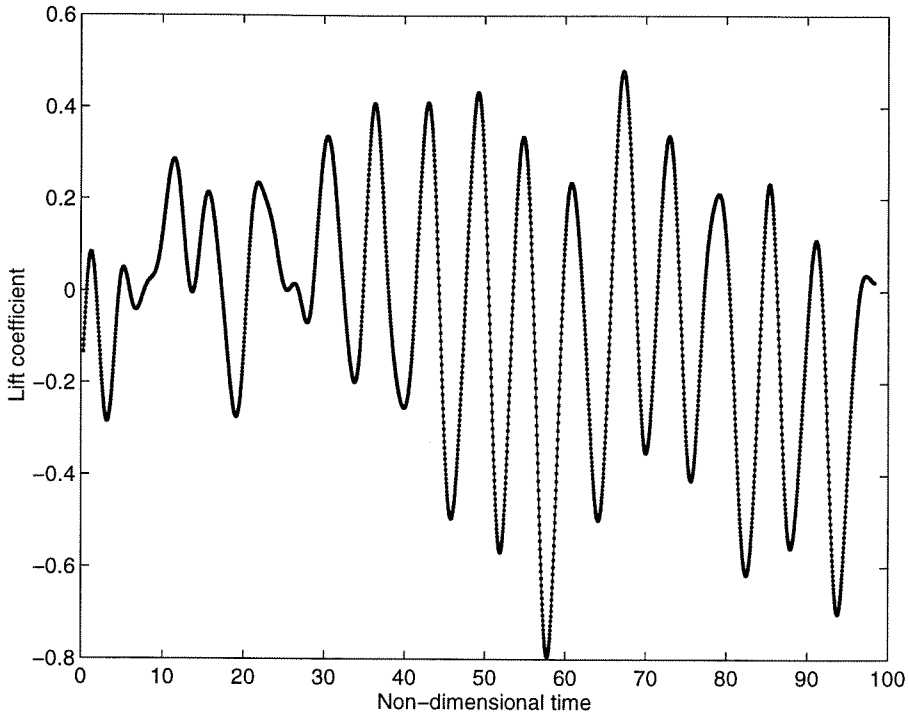


Figure 7.20: Lift coefficient vs. time, obtained with low-pass cutoff at a frequency of 0.3: ——, equation "mom3" (time derivative of spatial integral); • • •, equation "mom1" (spatial integral of time derivative).

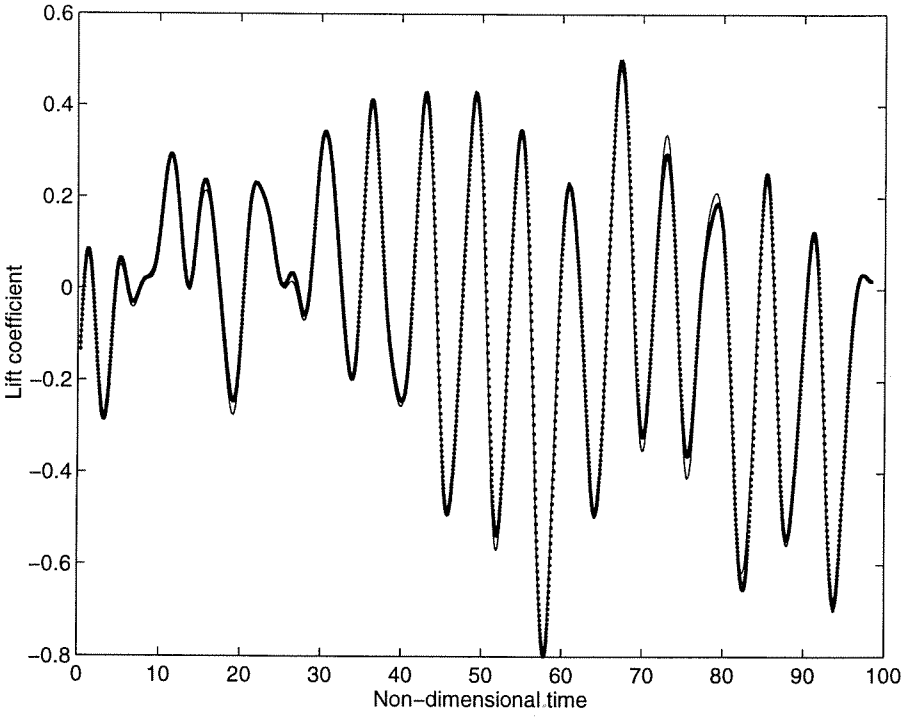


Figure 7.21: Lift coefficient vs. time, obtained with low-pass cutoff at a frequency of 0.3: —— , equation "mom1" (Kutta-Zhukovsky term as volume integral); • • •, equation "mom2" (Kutta-Zhukovsky term as surface integral).

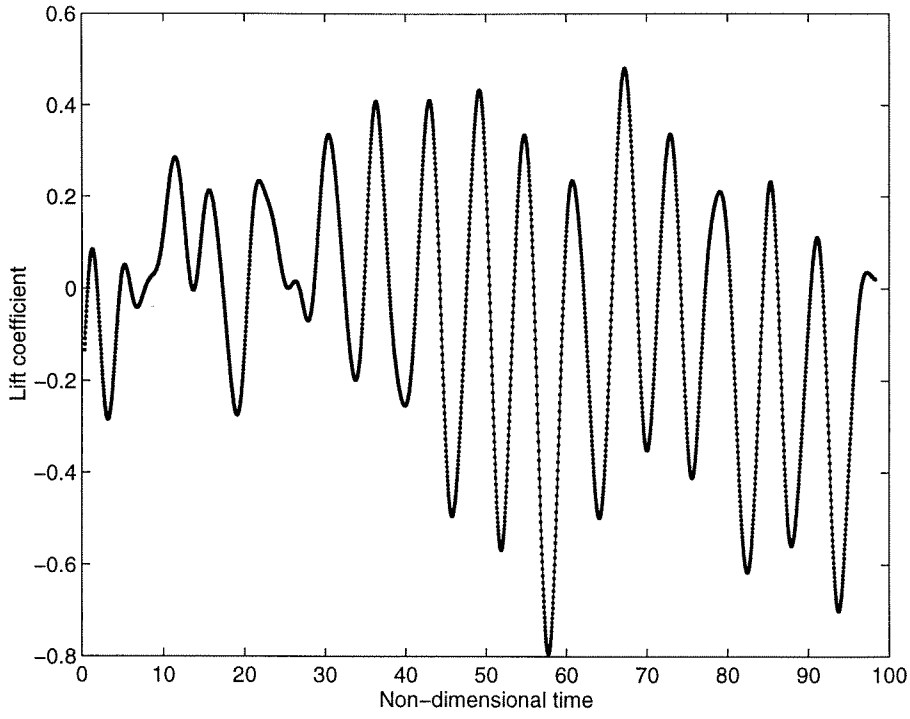


Figure 7.22: Lift coefficient vs. time, obtained with low-pass cutoff at a frequency of 0.3: ——, "impulse equation"; · · ·, "momentum equation".

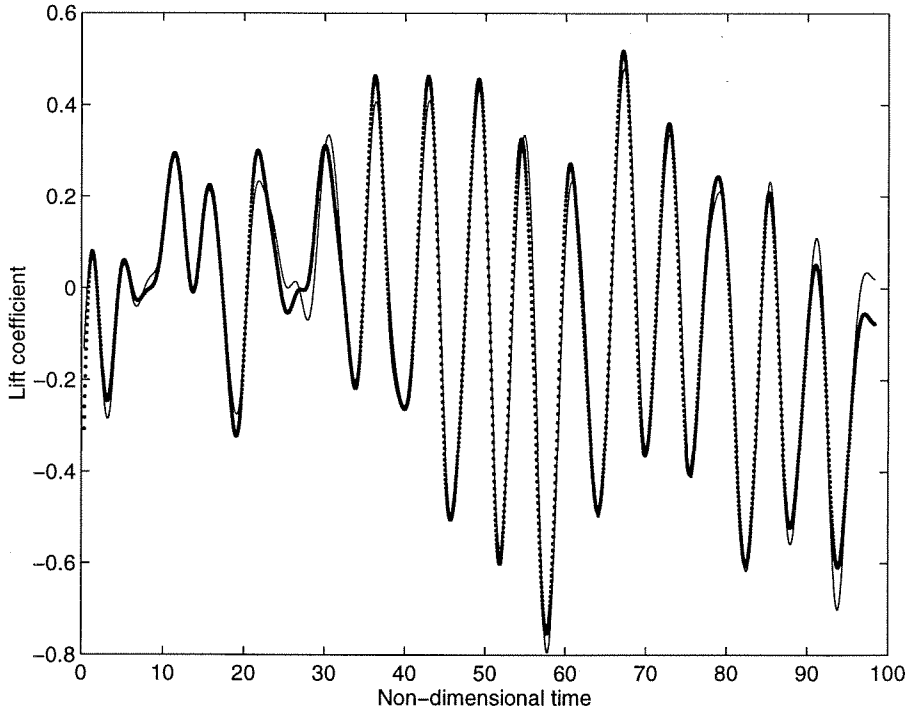


Figure 7.23: Lift coefficient vs. time, obtained with low-pass cutoff at a frequency of 0.3: ——, "momentum" equation; · · ·, "flux" equation.

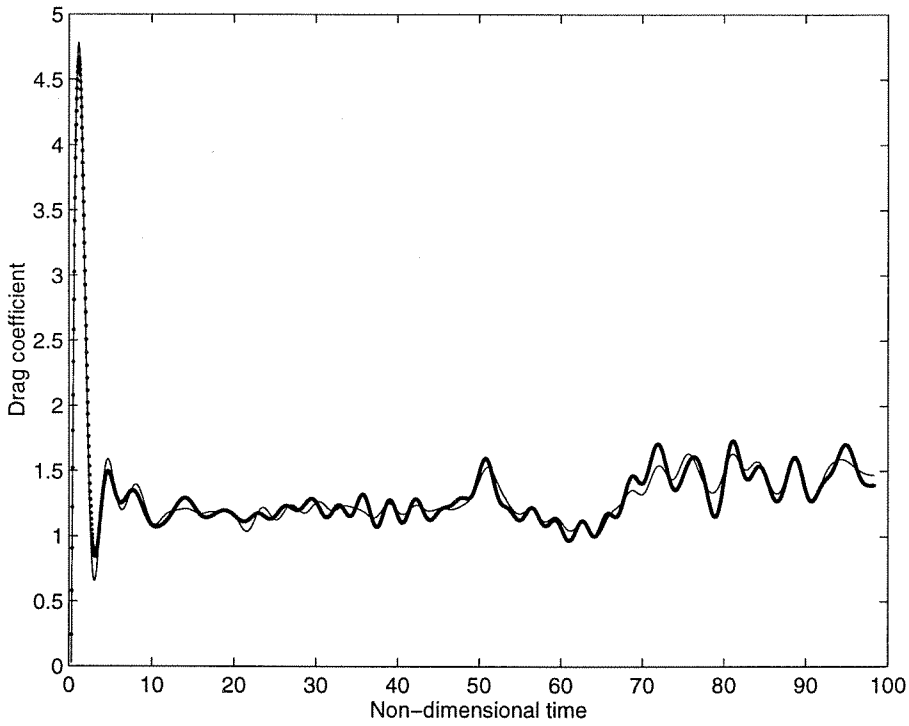


Figure 7.24: Drag coefficient vs. time, obtained with low-pass cutoff at a frequency of 0.3: ——, "momentum" equation; • • •, "flux" equation.

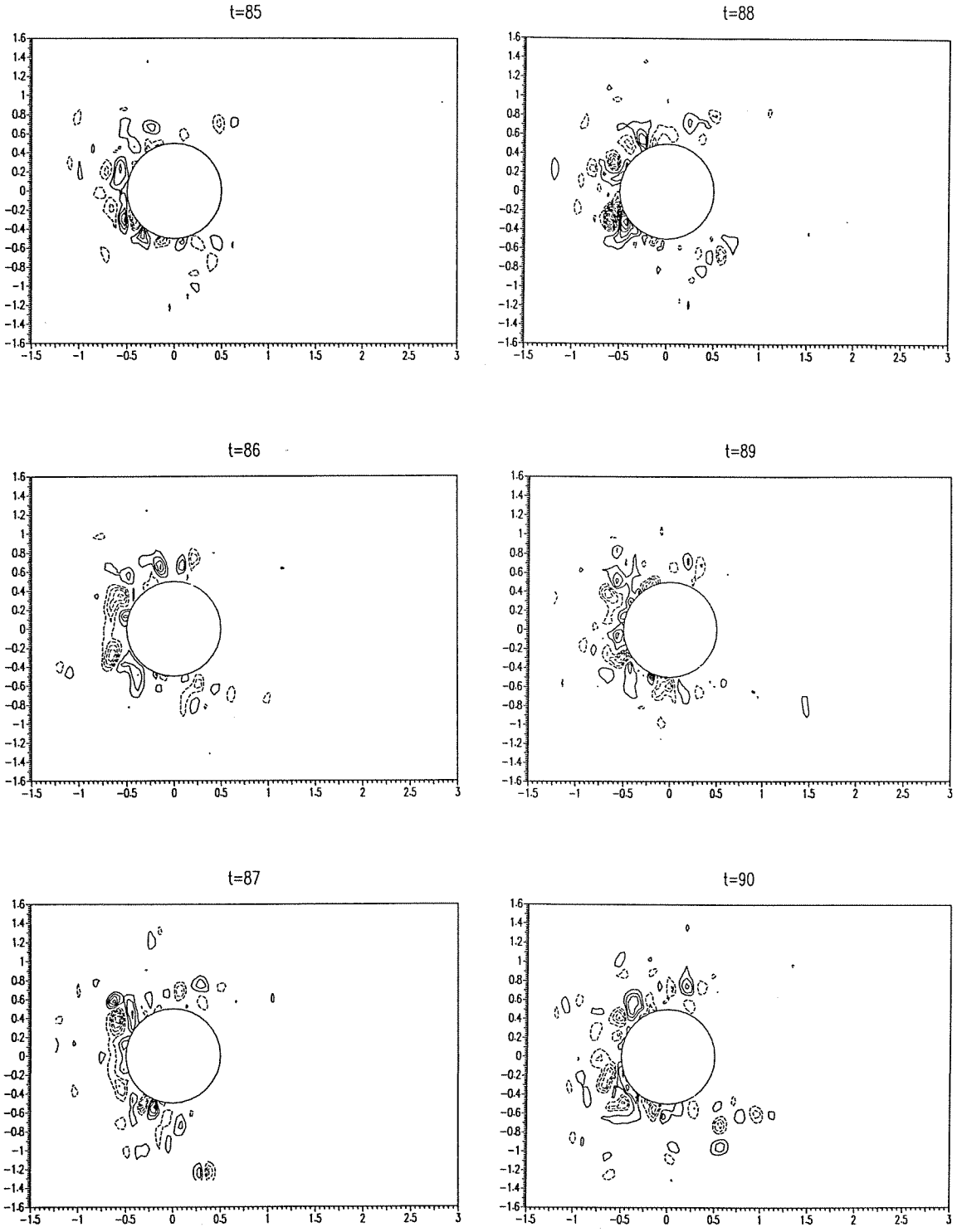


Figure 7.25: Time sequence of normalized velocity divergence fields for a circular cylinder at $Re \sim 100$ during one shedding cycle (contours are incremented by 1; dashed lines represent negative values, solid lines positive values).

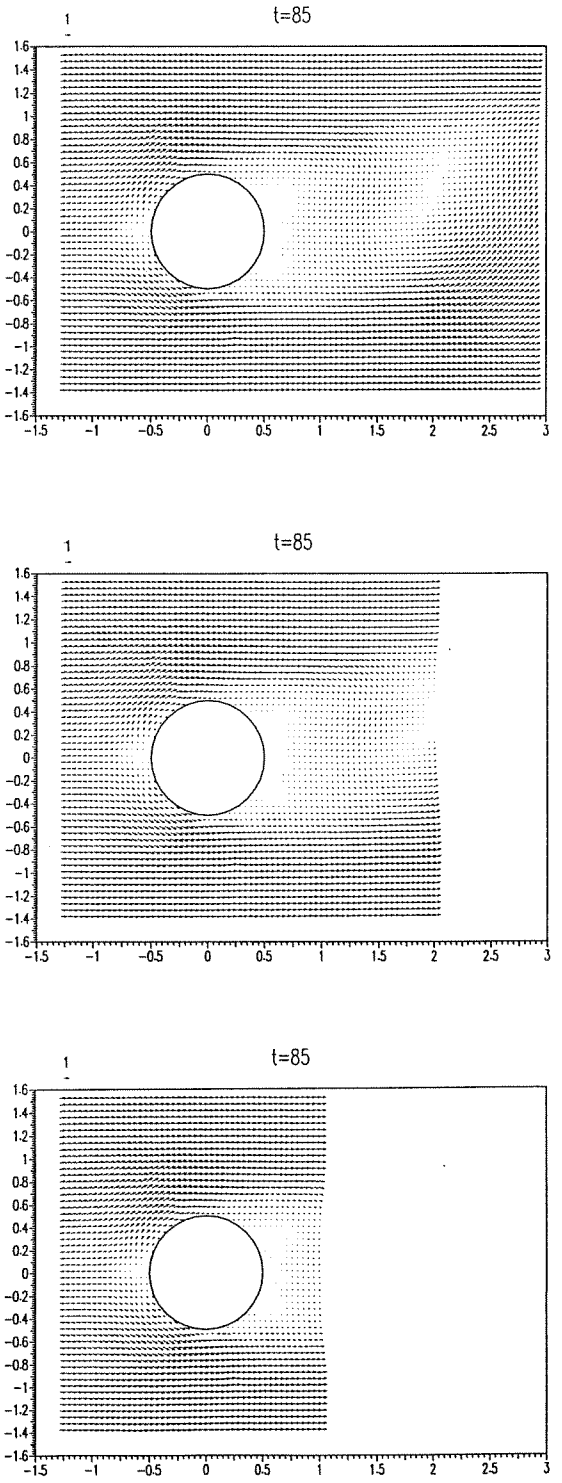


Figure 7.26: Domain sizes used for integration, from top to bottom: large domain, intermediate domain, small domain.

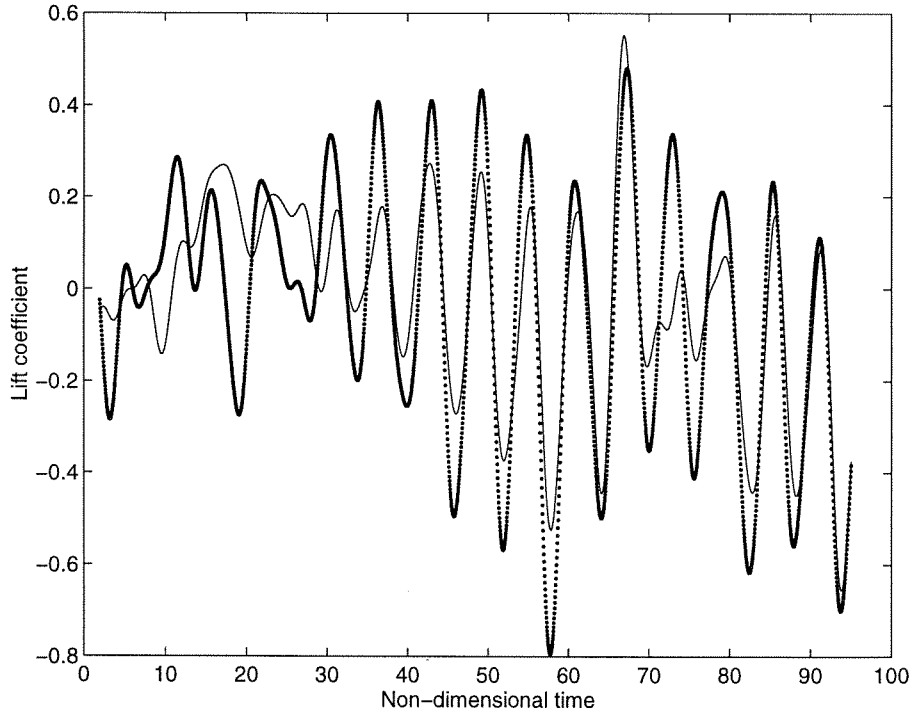


Figure 7.27: Lift coefficient vs. time, obtained with low-pass cutoff at a frequency of 0.3: ——, intermediate domain; • • •, large domain.

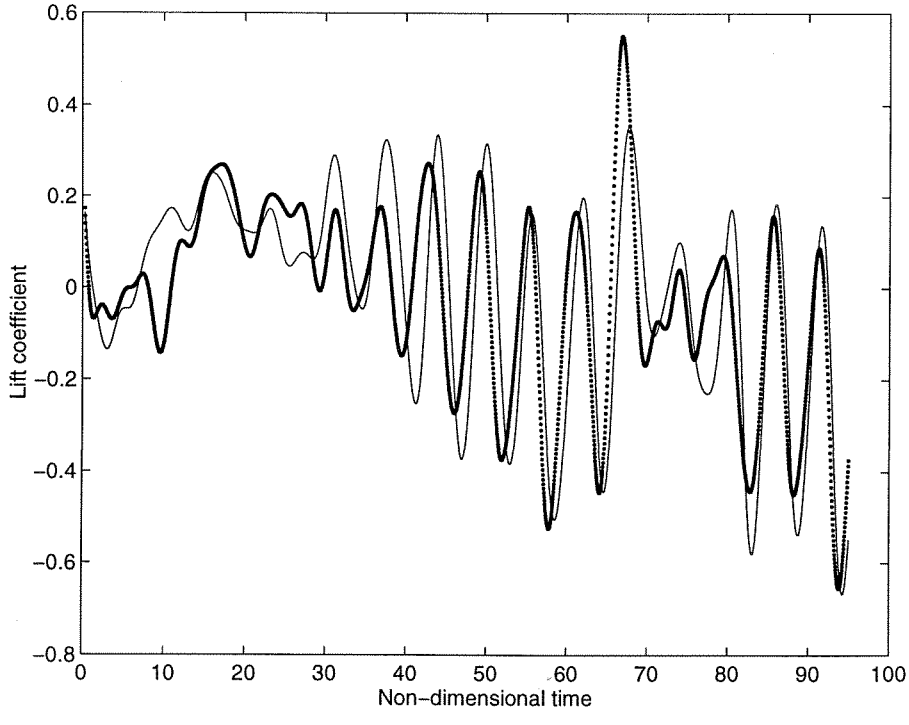


Figure 7.28: Lift coefficient vs. time, obtained with low-pass cutoff at a frequency of 0.3: ——, small domain; • • •, intermediate domain.

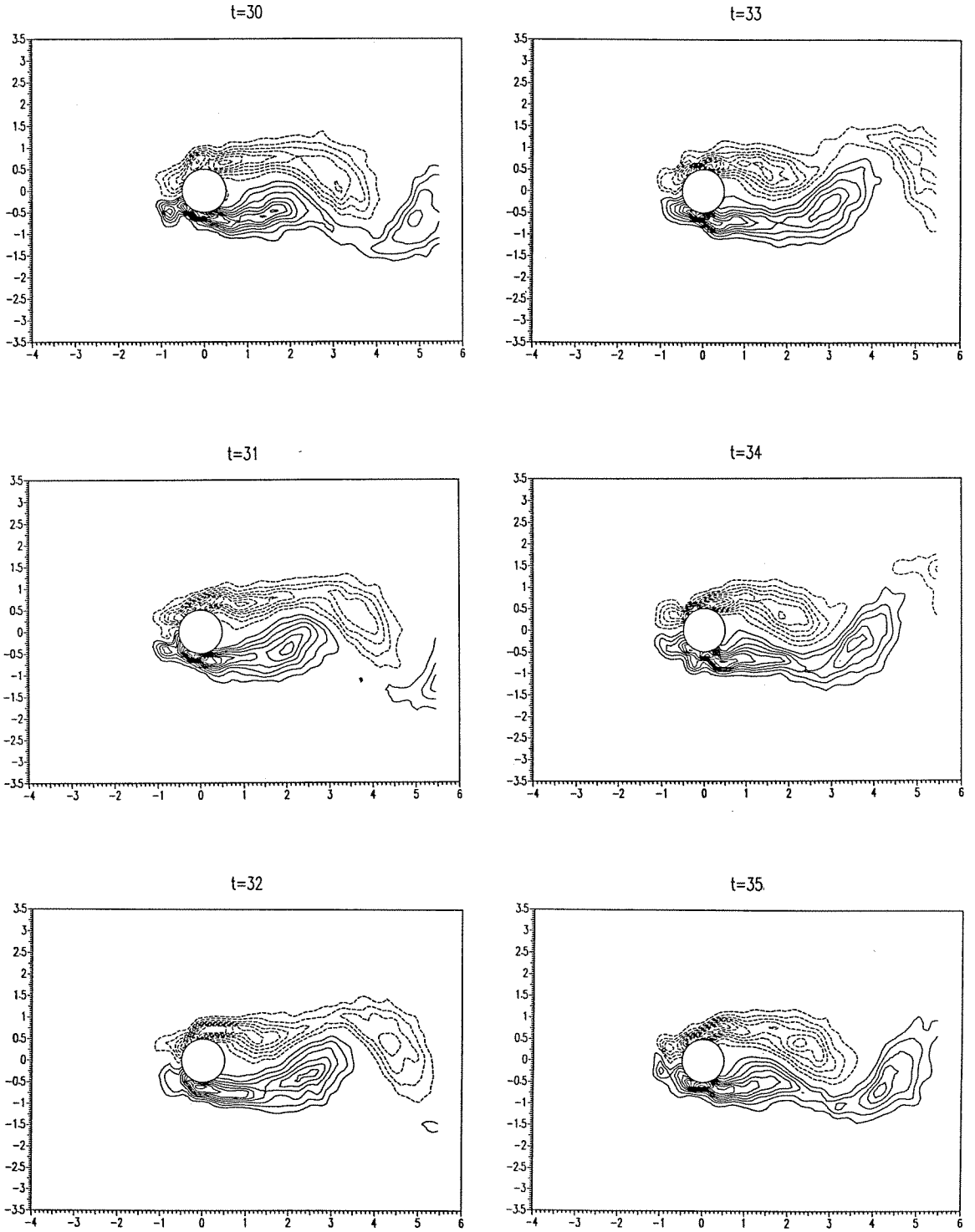


Figure 7.29: Time sequence of vorticity fields for a circular cylinder at $Re \sim 100$ during one shedding cycle for the very large domain (contours are incremented by 0.4; dashed lines represent negative values, solid lines positive values).

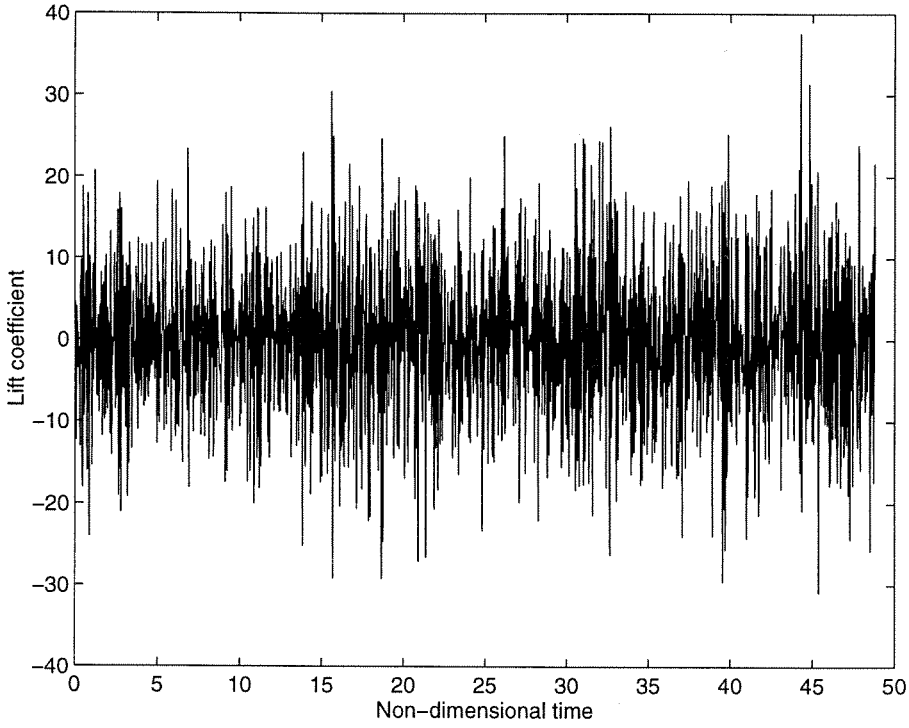


Figure 7.30: Unfiltered lift coefficient vs. time for the very large domain.

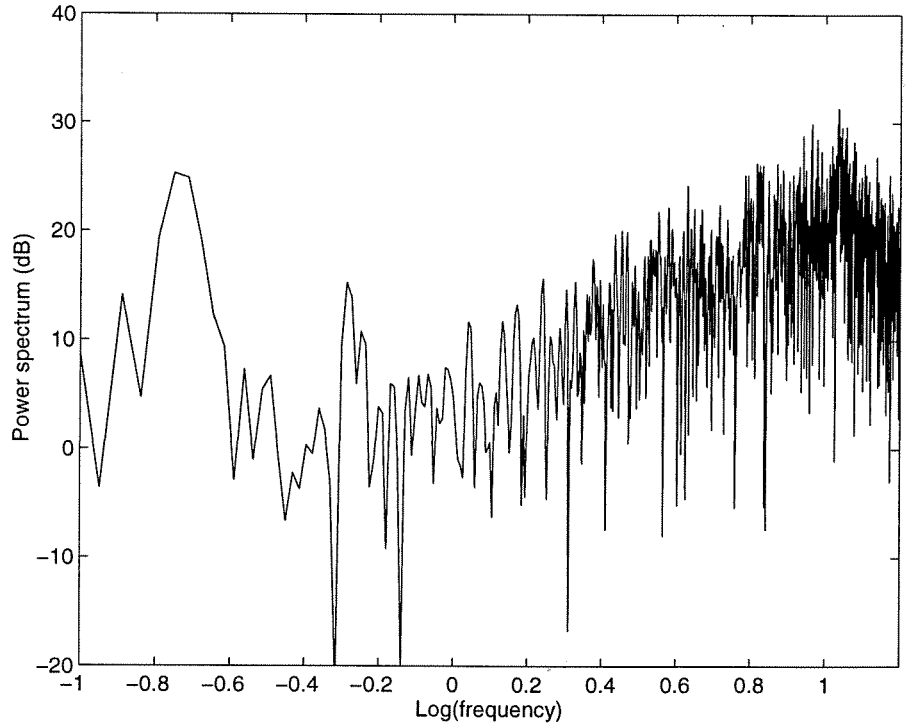


Figure 7.31: Power spectral density of lift coefficient for the very large domain.

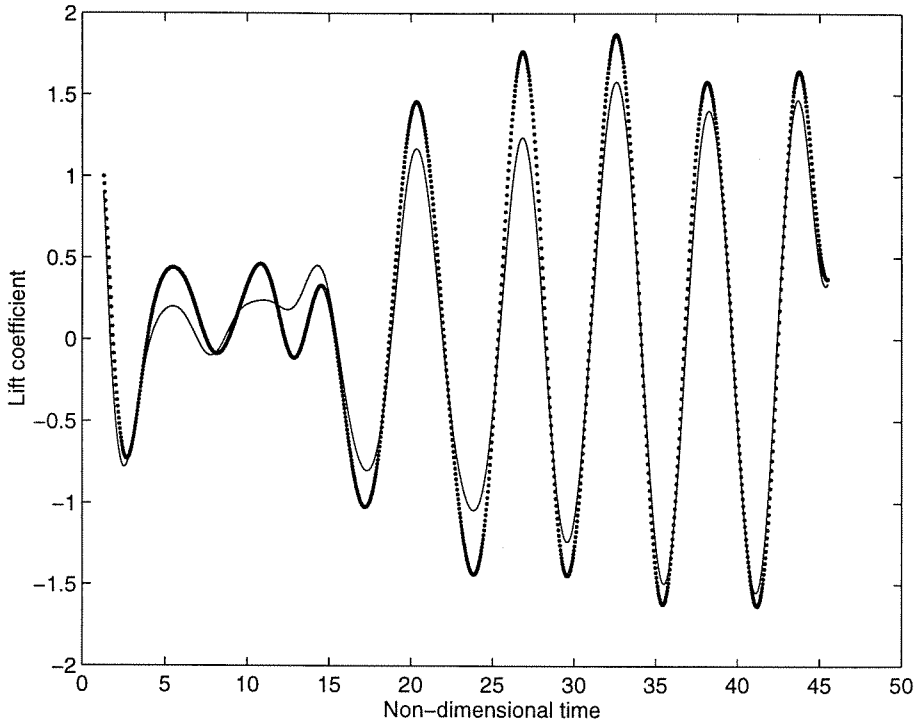


Figure 7.32: Lift coefficient vs. time for the very large domain, obtained with low-pass cutoff at a frequency of 0.3: ——, "momentum" equation; • • •, "flux" equation.

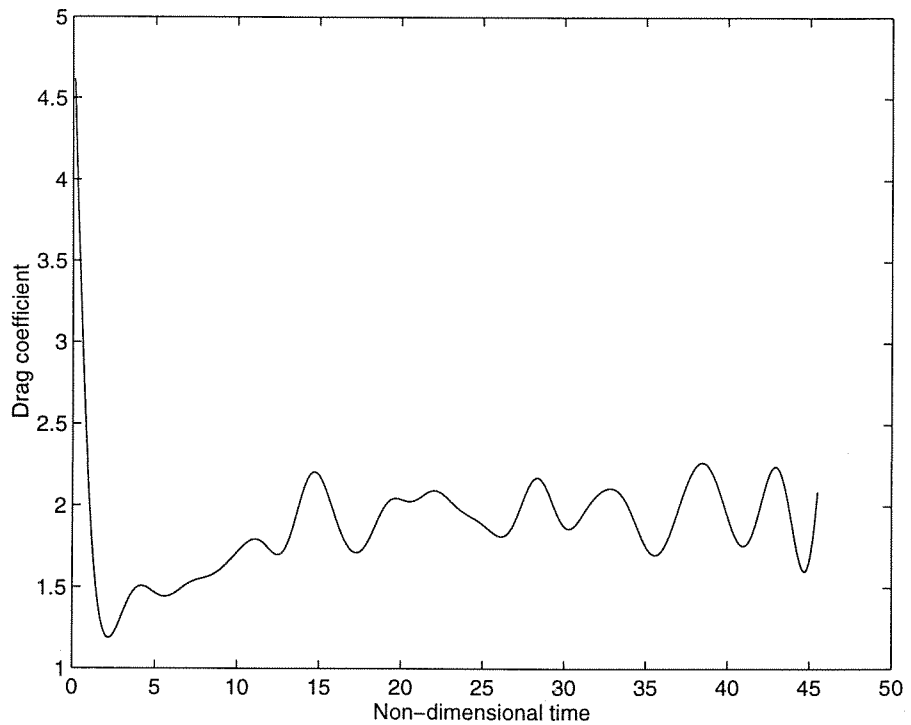


Figure 7.33: Drag coefficient vs. time for the very large domain, obtained with low-pass cutoff at a frequency of 0.3.

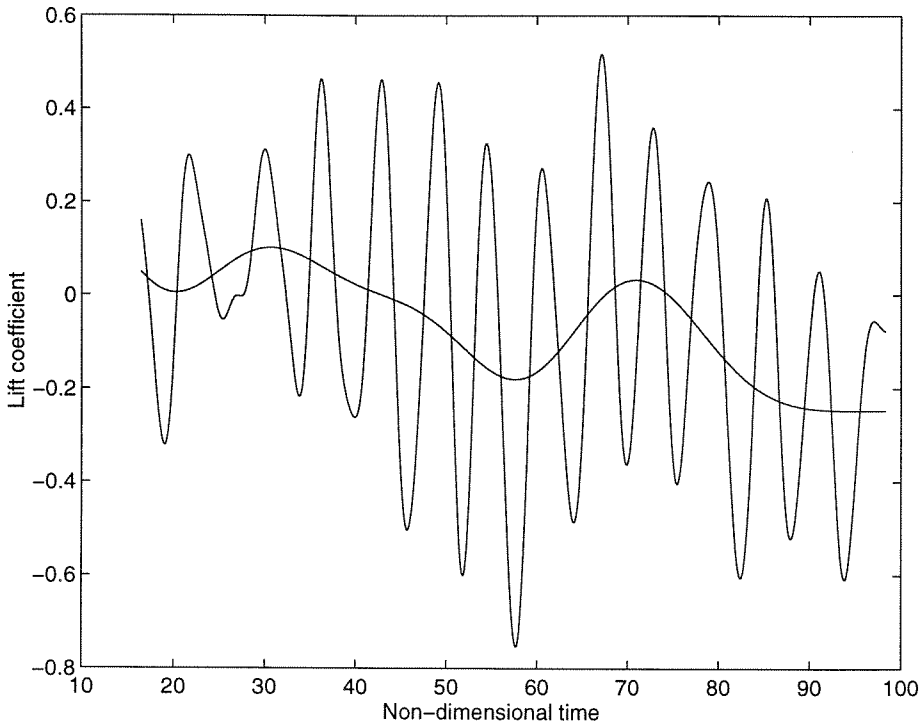


Figure 7.34: Lift coefficient vs. time, obtained with low-pass cutoff at a frequency of 0.3; also shown, low frequency oscillation with low-pass cutoff at a frequency of 0.05.

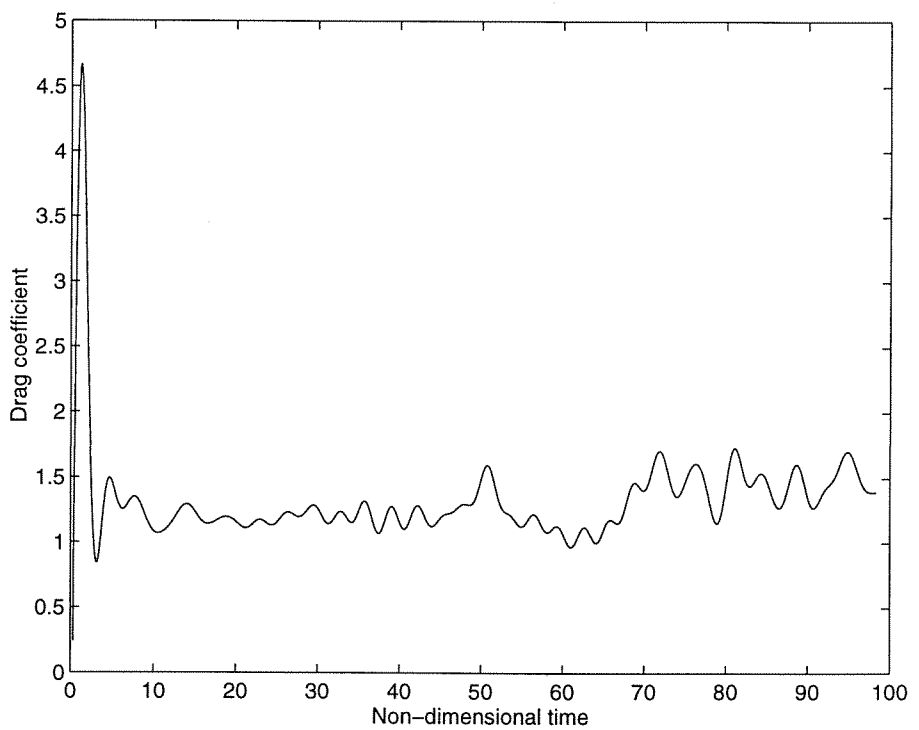


Figure 7.35: Drag coefficient vs. time, obtained with low-pass cutoff at a frequency of 0.3.

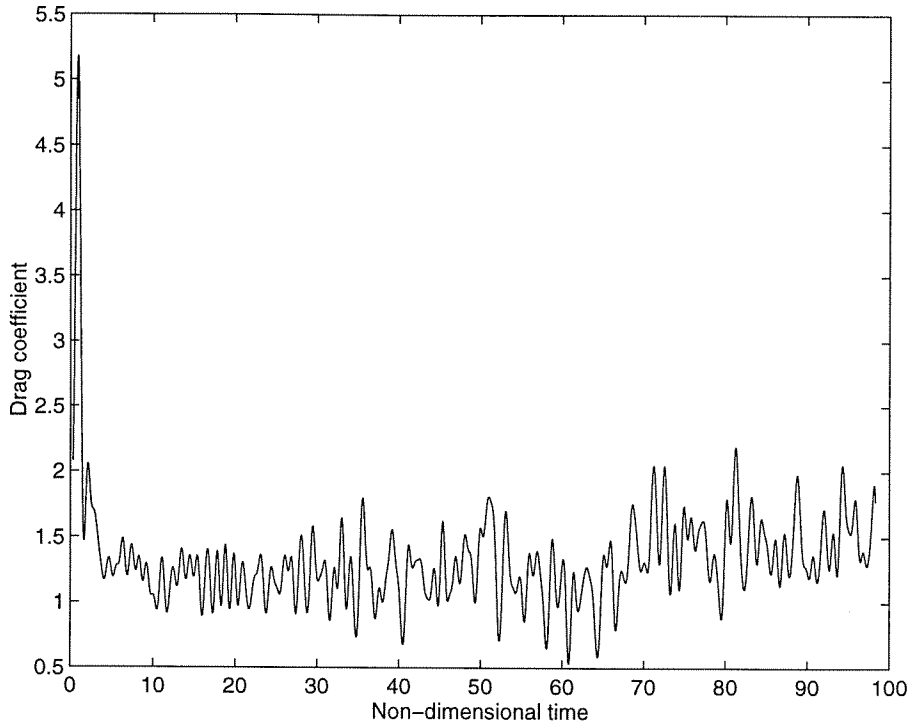


Figure 7.36: Drag coefficient vs. time, obtained with low-pass cutoff at a frequency of 1.

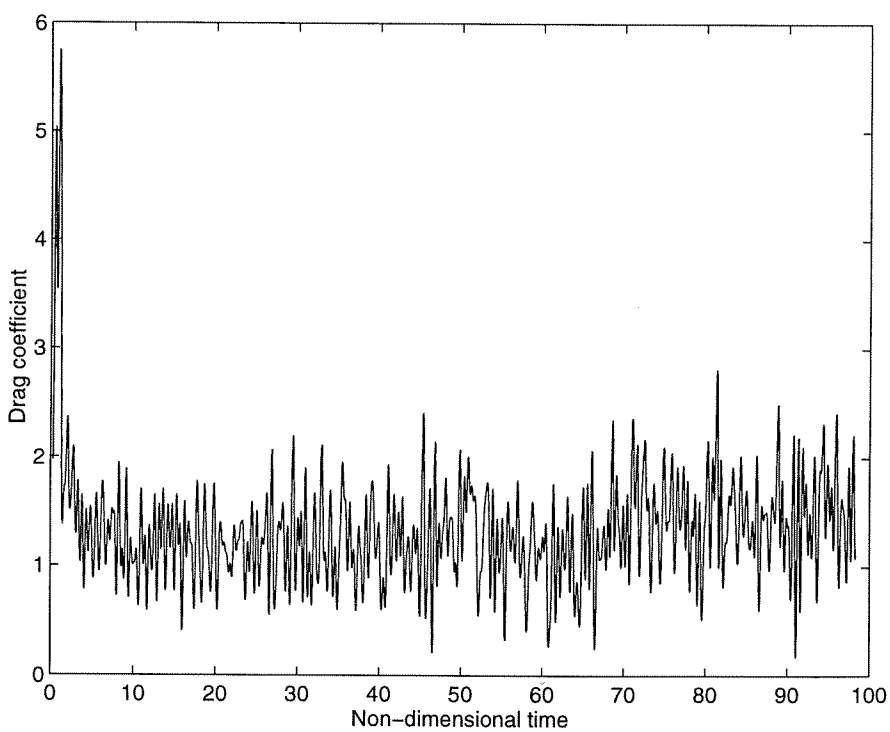


Figure 7.37: Drag coefficient vs. time, obtained with low-pass cutoff at a frequency of 2.

# Chapter 8 Low Reynolds number experiments: unsteady motions

In this Chapter, the force formulation will be applied to a circular cylinder performing a jerking motion at $Re \sim 100$. For the reader's convenience, most of the figures have been placed at the end of the Chapter. Most of the analysis performed in the previous Chapter will be applied to the present case as well.

## 8.1 Experimental results

### 8.1.1 Motion parameters

As explained in Chapter 6, the experiments were conducted in a tow tank. The motion imposed on the cylinder is shown in Figure 8.1. The streamwise velocity is sinusoidal in time, reaching a peak velocity $U = 1$ cm/s. The period of oscillation was chosen such that it matched the natural shedding period of steady cylinder flow at $Re \sim 100$, i.e. , $T = 1/0.164 \sim 6.10$ s.

The units were normalized as for the steady cylinder flow case (see Chapter 7). Thus, the jerking frequency was 0.164.

### 8.1.2 Non-inertial frame

All of the results were acquired in a frame fixed with the cylinder. The frame was thus non-inertial. The forces evaluated from the flowfields are, therefore, not the actual fluid-dynamic forces, and have

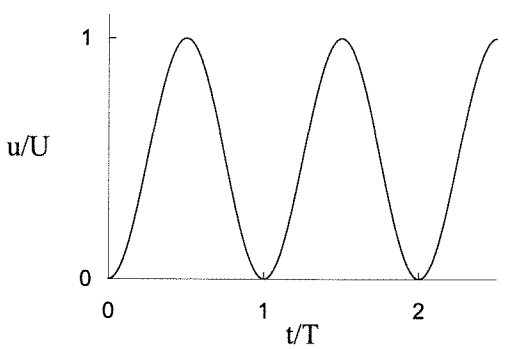


Figure 8.1: Carriage velocity profiles $u/U$ vs. time $t/T$ for a cylinder 1 cm in diameter: sinusoidal velocity profile of frequency $1/T = 0.164$ Hz with minimum velocity $U = 0$ and peak velocity $U = 1$ cm/s.

to be corrected by adding a (time-dependent) term which describes the acceleration of the frame.

In the analysis portion of the section, the signals were left uncorrected, and the graphs were labeled accordingly.

### 8.1.3 Flowfields

A 50-diameter time sequence of the flow was captured with DPIV (i.e. , $0 < t < 50$). Figure 8.2 and Figure 8.3 show a short time sequence of the velocity and vorticity fields obtained for approximately one shedding cycle (6 time units) between times $t = 20$ and $t = 25$.

The fields were obtained by cross-correlating particle images (captured at 30 Hz) in the following way: image 1 and image 2, image 2 and image 3, etc.... The sampling fequency for the velocity and vorticity fields was thus 30 (in non-dimensional units).

## 8.2 Force evaluation

### 8.2.1 Forward time differencing scheme

As in the previous Chapter, we chose Equation "mom1" as a benchmark equation.

Choosing a time step $\delta t$ equal to the sampling period, $\delta t \sim 0.033$ s, we performed the computations with the velocity fields given at time $t$ and time $t + \delta t$ and the vorticity fields given at time $t$, for the full range of motion $0 < t < 50$. The results for the drag coefficient are shown in Figure 8.4. The signal is noisy, but still the periodic trend is easily noticeable contrary to the lift signal in the steady motion case.

Applying a low-pass filter with a cutoff frequency at 1, we obtained the drag signal as shown in Figure 8.5. Contrary to the steady motion case, not much effort is needed to extract a very "clean" force signal. It is to be noted that the peak-to-peak amplitude is around 5 in this case, instead of only 0.5 for the lift coefficient in the steady case.

### 8.2.2 Forward time differencing scheme with large time step

In the previous Chapter, it was noted that increasing the time step in a forward time differencing scheme would alter the amplitude of the signal. Figure 8.6 shows the unfiltered drag coefficient for a time step $\delta t = 10\,\delta t_{\min}$ in the present case. The noise level is remarkably reduced with an increasing time step. Also, contrary to the steady motion case, the large time step scheme seems to yield the same answer as the small time step scheme. This feature can be seen in the filtered signal in Figure 8.7.

### 8.2.3 Central time differencing scheme

With a time step equal to the sampling period, i.e. , $\delta t = \delta t_{\min}$, the drag coefficient was computed, and the unfiltered result is shown in Figure 8.8, along with the power spectral density which reveals noise mostly near the Nyquist frequency (Figure 8.9). Applying a filter with a cutoff frequency of 1 yields the signal shown in Figure 8.10, where we have included the similar filtered signal obtained with forward differencing. The two signals are practically identical.

### 8.2.4 Central time differencing with large time step

As for the forward time differencing scheme, we investigated the effect of time step on the convergence of the scheme. Figure 8.11 shows the unfiltered result for $\delta t = 10\,\delta t_{\min}$. After filtering at a cutoff frequency of 1, the signals do not lose or gain amplitude, as exemplified in Figure 8.12.

In summary, for strong signals, the central time differencing scheme is very much equivalent to the forward time differencing scheme.

### 8.2.5 The "impulse", "momentum", and "flux" equations

We saw in the previous Chapter that the "impulse" and "momentum" equation are practically equivalent. Figure 8.13 reveals again the similitude for this flow case. As for the "flux" equation, it is compared to the "momentum" equation in Figure 8.14. Again, a slight discrepancy arises between the two equations, probably because of a spurious divergence field near the body surface as seen in Figure 8.15.

### 8.2.6 Domain size

We used two different domain sizes in the analysis, as shown in Figure 8.16. In Figure 8.17, the drag was computed with the "momentum" equation for both domains. The peak values seem to differ by about 0.1, which incidentally is close to the discrepancy in lift amplitude obtained in the steady case for similar domains. However, since the signal is very much stronger in the unsteady case, the discrepancy is not as noticeable. The "flux" equation shows a similar discrepancy (Figure 8.18).

We also tried a different smaller domain by squeezing the lateral boundaries instead of the downstream boundary, as shown in Figure 8.19. The results again seem to be almost unaffected by the change in domain size, as exemplified in Figure 8.20. The discrepancy is again of the order of 0.1.

The reader is referred to Chapter 9 for a dicussion of the influence of the domain size on the accuracy of the results.

## 8.3 Discussion of results

### 8.3.1 Repeatability

The experiment was repeated under the same conditions in order to check for the repeatability of the experiment and/or the technique. The results are shown in Figure 8.21. The agreement between the two drag signals is quite remarkable.

### 8.3.2 Lift coefficient

For perfect flow conditions, the lift signal should be identically zero throughout the motion. However, because of asymmetries in the flow conditions, the vortices were observed not to shed symmetrically on either side of the cylinder trajectory. Thus, from the start, we expected to measure a substantial lift signal. Figure 8.22 shows such a signal obtained from the "momentum" and the "flux" equation. Note that the two equations do not seem to yield the same result. From the analysis above, it is probable that the "flux" equation yields a better estimate than the "momentum" equation does.

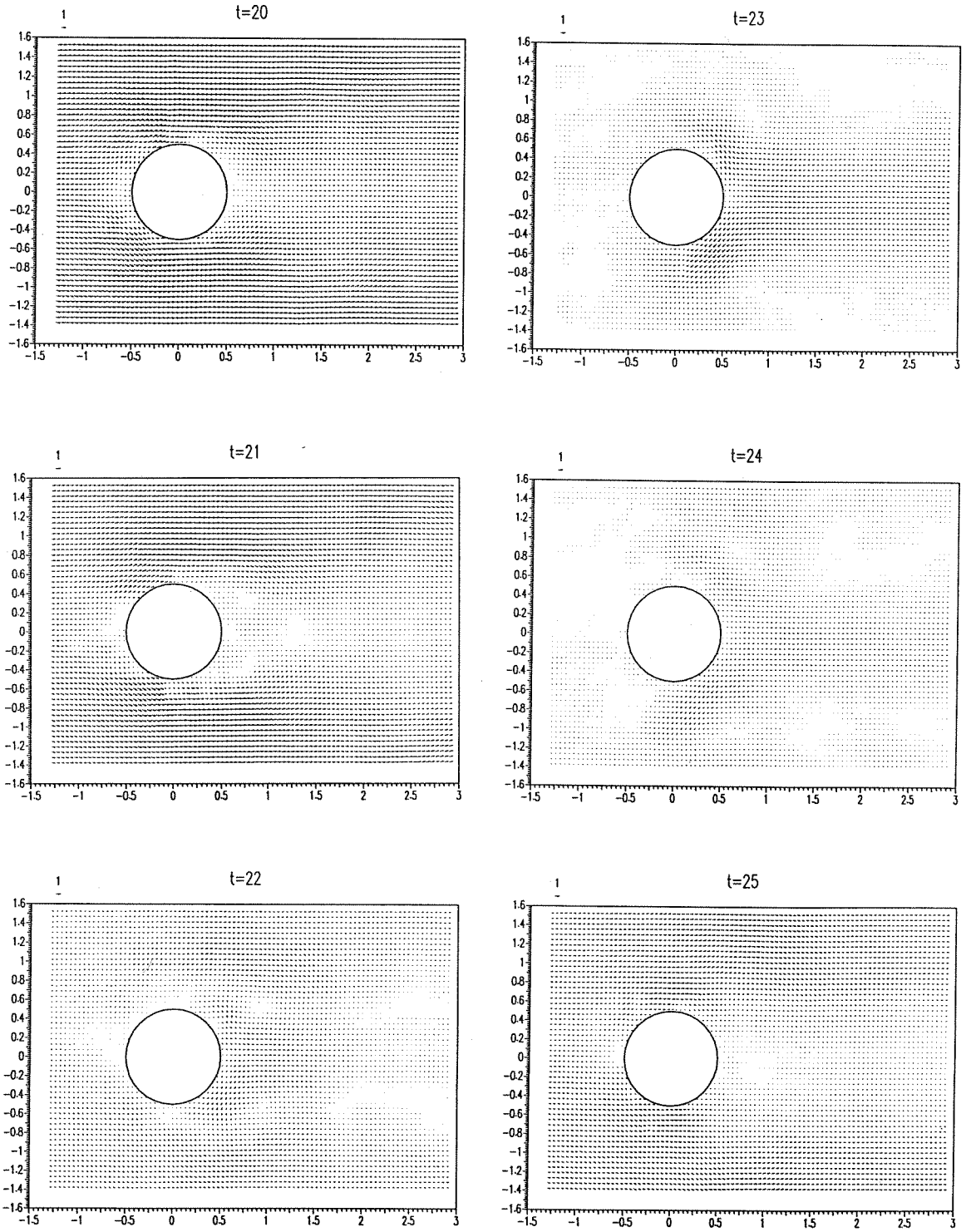


Figure 8.2: Time sequence of velocity fields for a jerking circular cylinder at $Re \sim 100$ during one shedding cycle.

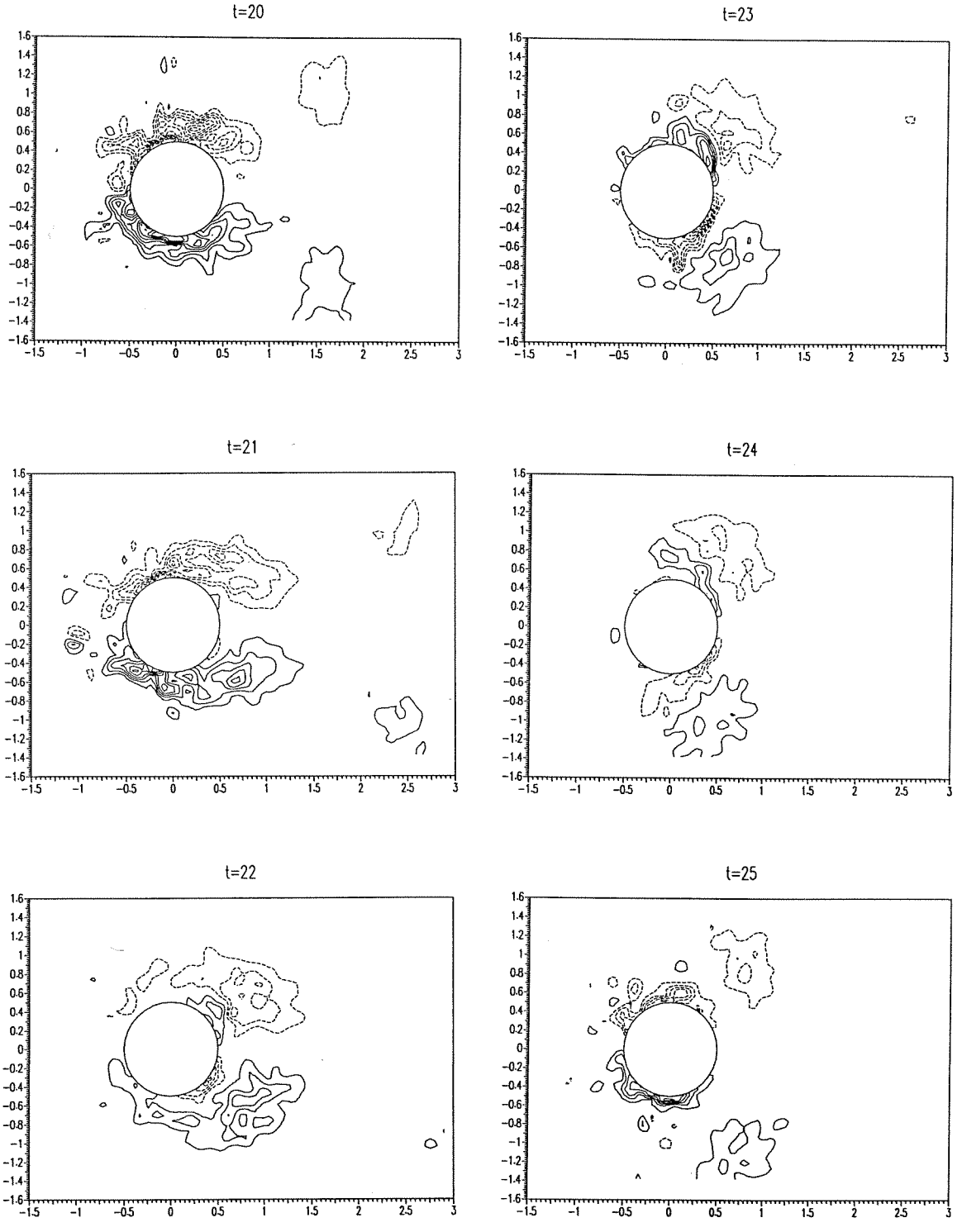


Figure 8.3: Time sequence of vorticity fields for a jerking circular cylinder at $Re \sim 100$ during one shedding cycle (contours are incremented by 1; dashed lines represent negative values, solid lines positive values).

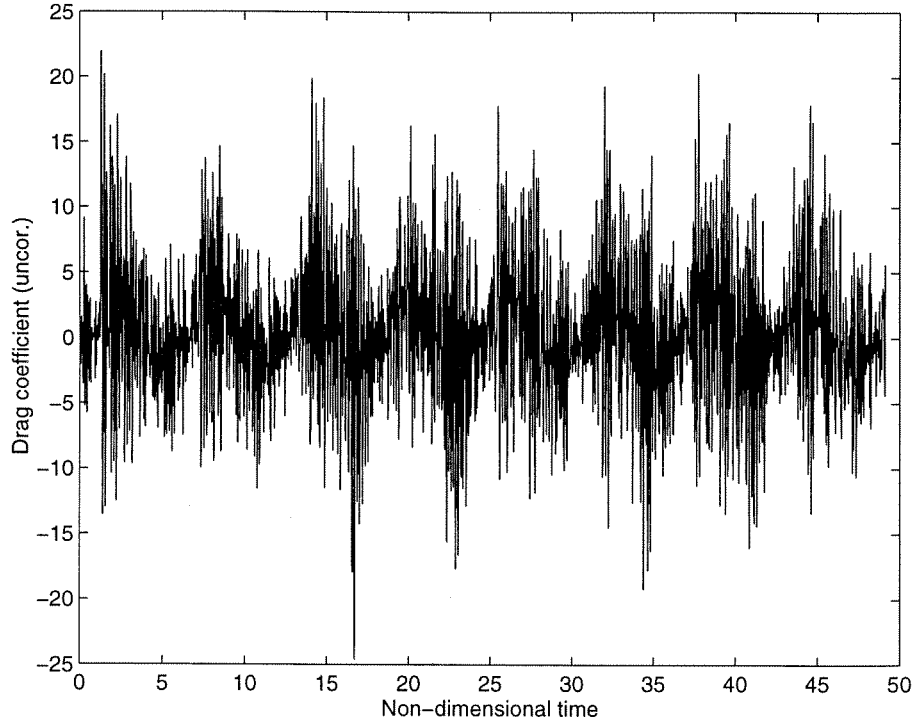


Figure 8.4: Unfiltered drag coefficient vs. time, obtained with forward time differencing (time step equal to sampling period).

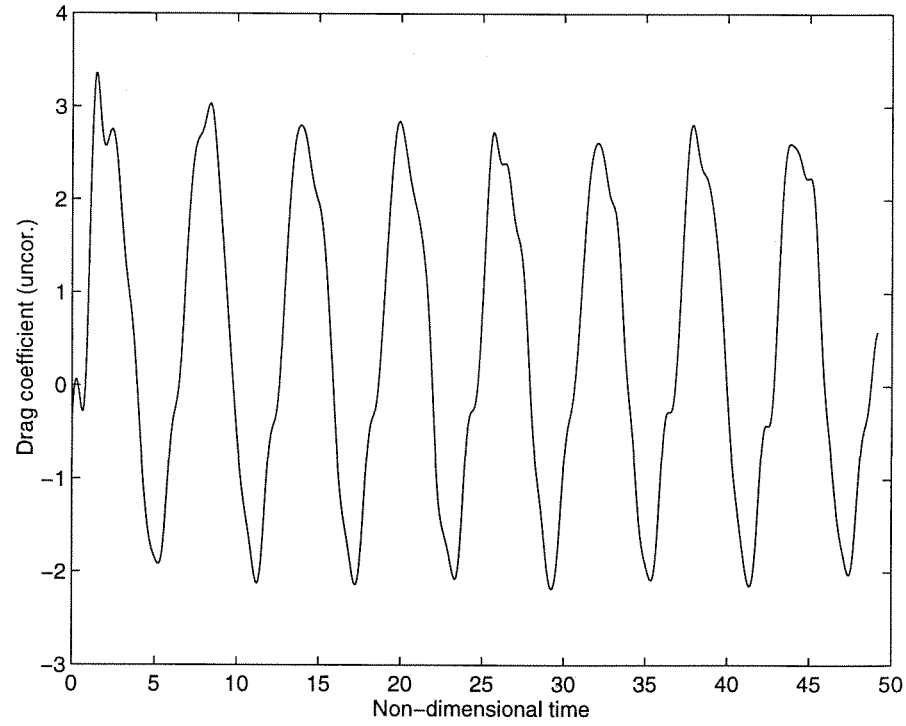


Figure 8.5: Drag coefficient vs. time, obtained with forward time differencing (time step equal to sampling period) and low-pass cutoff at a frequency of 1.

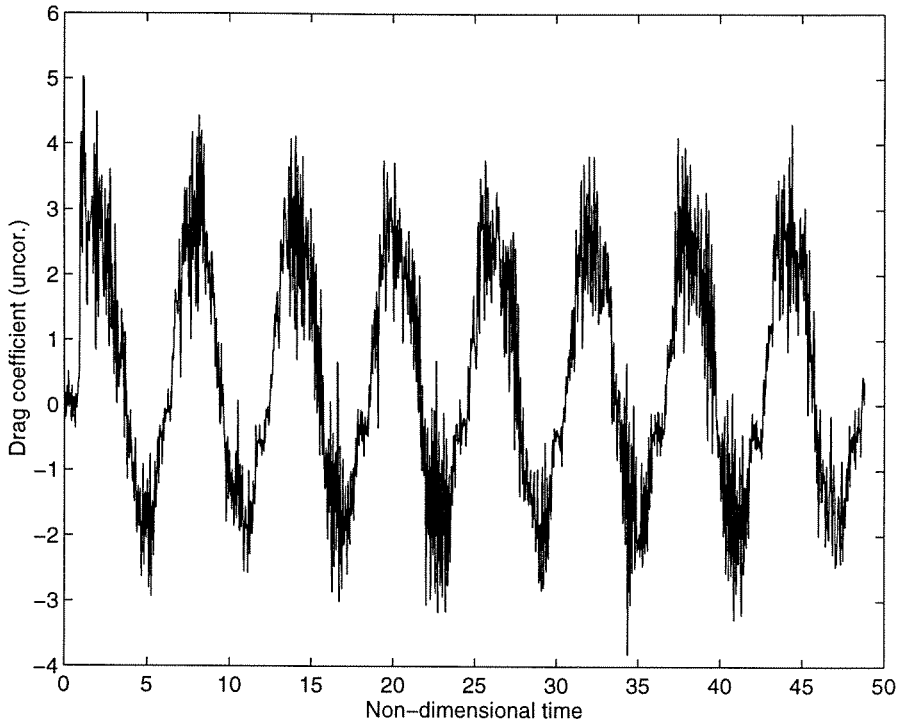


Figure 8.6: Unfiltered drag coefficient vs. time, obtained with forward time differencing (time step equal to 10 times sampling period).

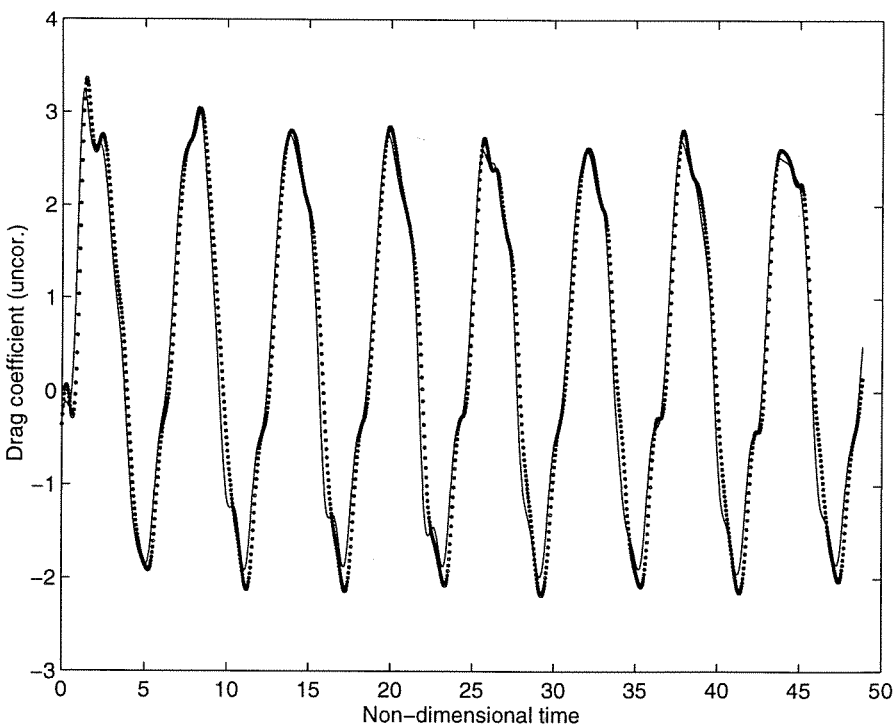


Figure 8.7: Drag coefficient, obtained with forward time differencing and low-pass cutoff at a frequency of 1: ——, time step equal to 10 times sampling period; · · ·, time step equal to sampling period.

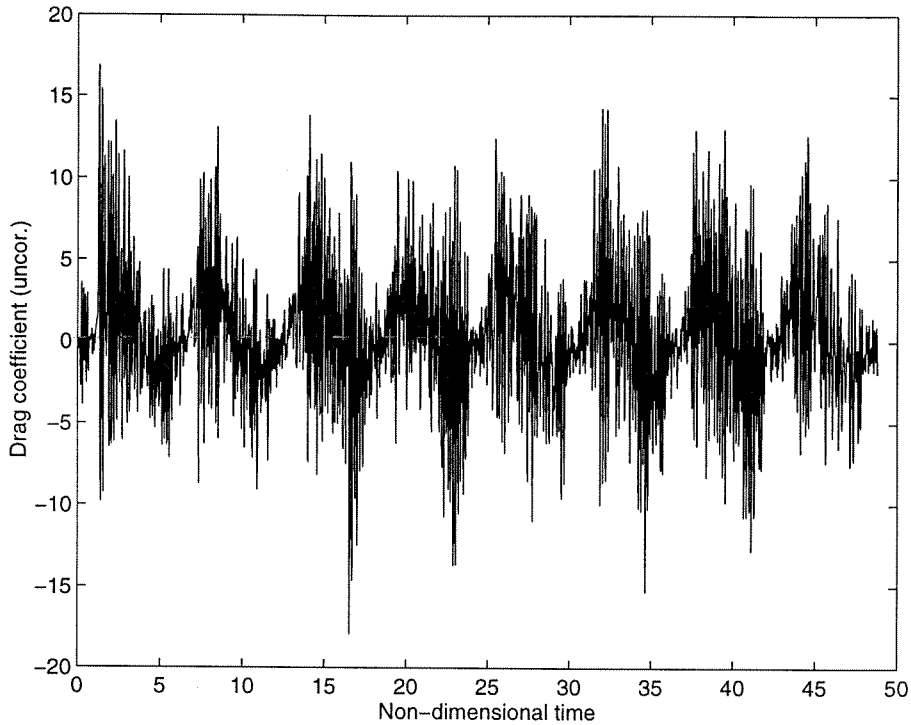


Figure 8.8: Unfiltered drag coefficient vs. time, obtained with central time differencing (time step equal to sampling period).

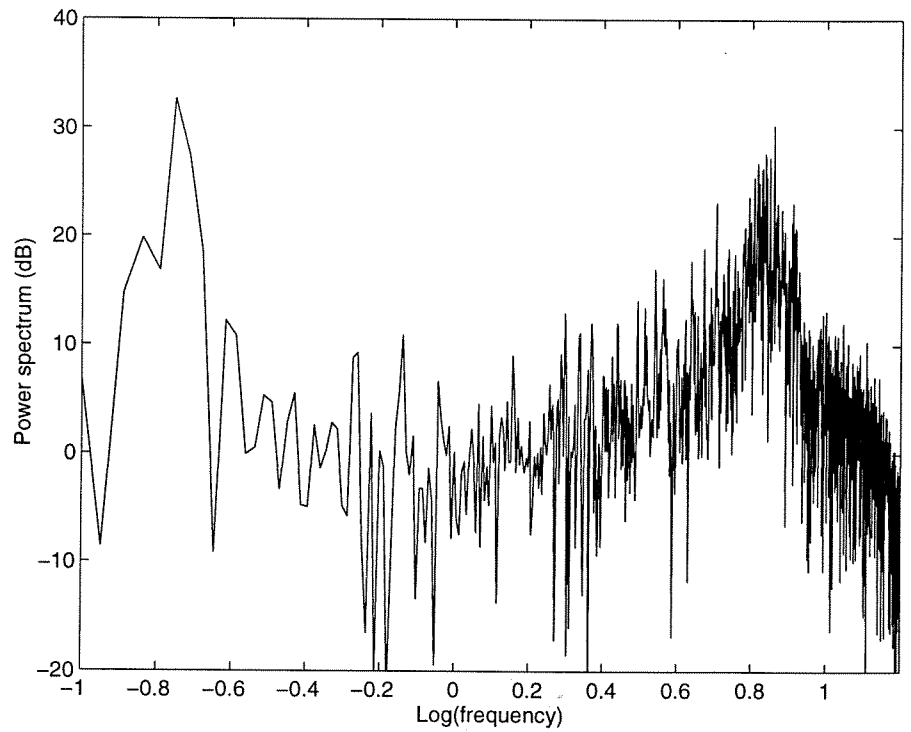


Figure 8.9: Power spectral density of drag coefficient, obtained with central time differencing (time step equal to sampling period).

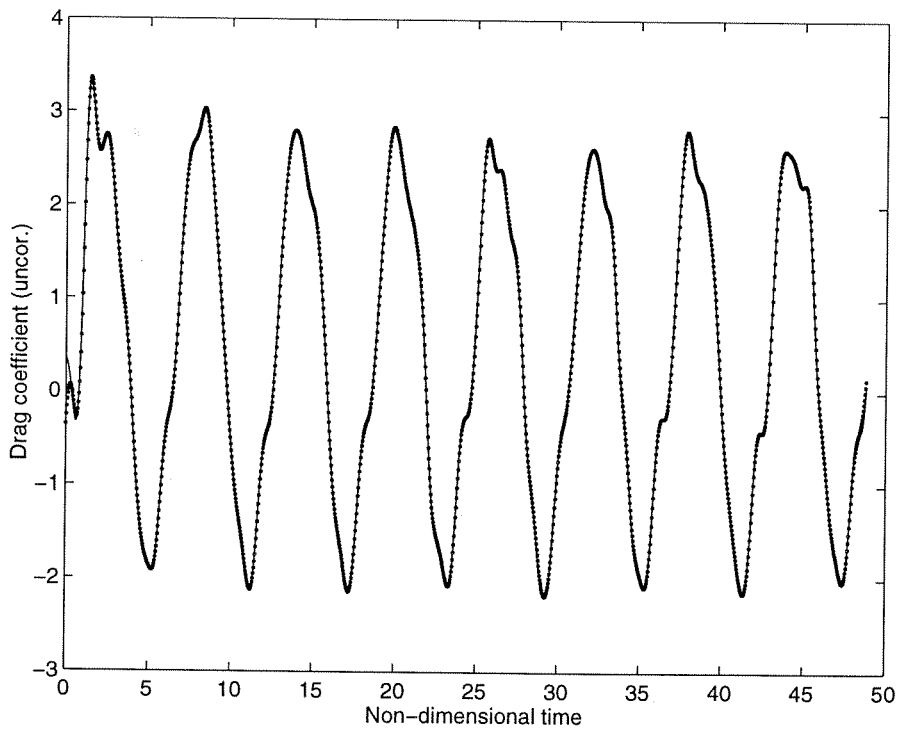


Figure 8.10: Drag coefficient vs. time, obtained with low-pass cutoff at a frequency of 1: ——, central time differencing (time step equal to sampling period); • • •, forward time differencing (time step equal to sampling period).

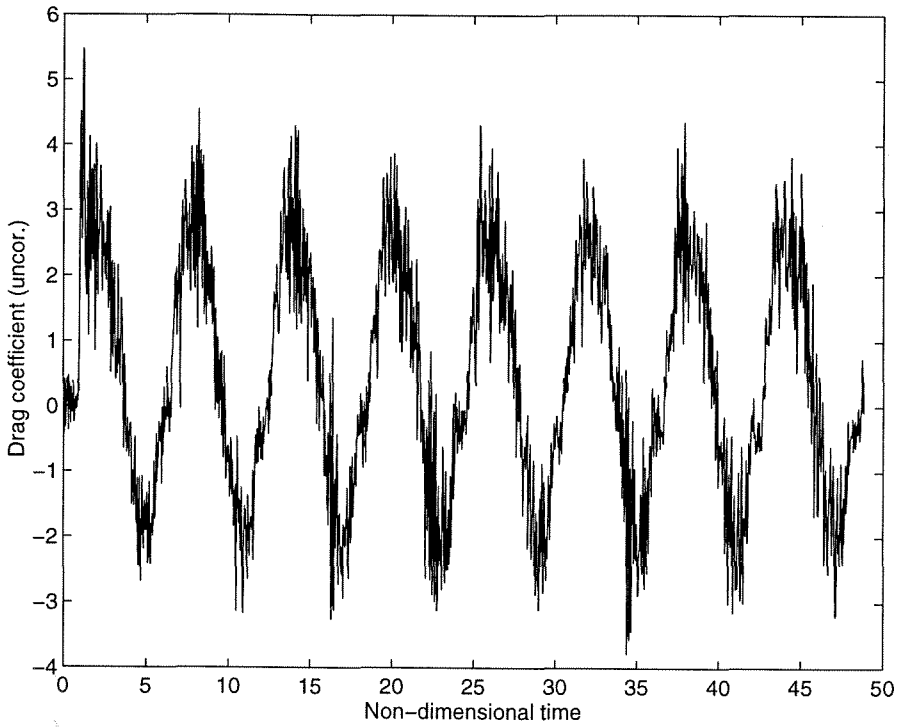


Figure 8.11: Unfiltered drag coefficient vs. time, obtained with central time differencing (time step equal to 10 times sampling period).

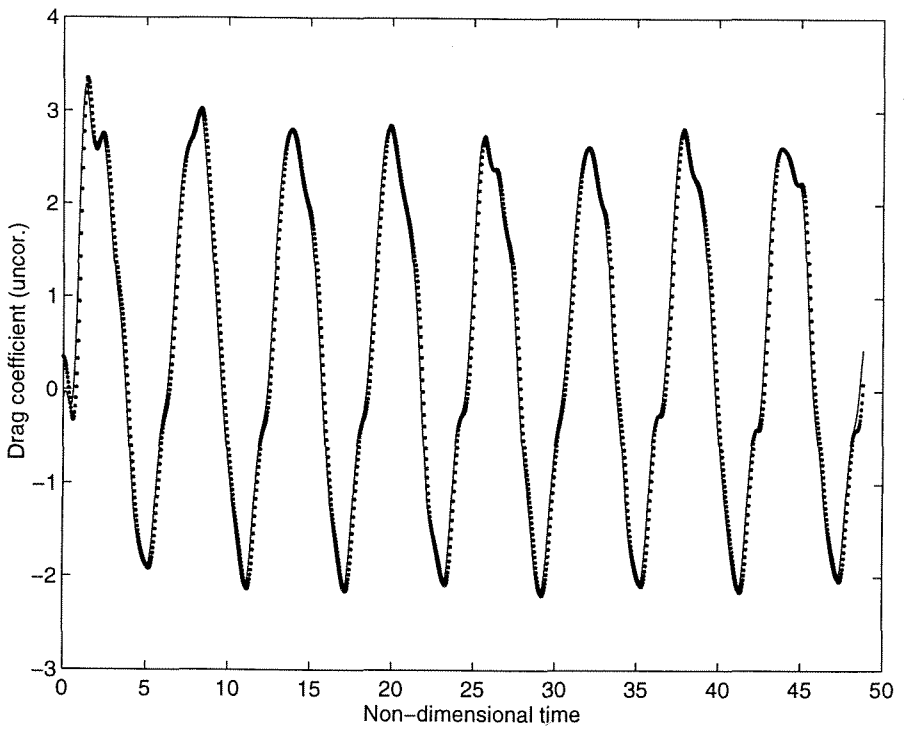


Figure 8.12: Drag coefficient vs. time, obtained with low-pass cutoff at a frequency of 1: ——, central time differencing (time step equal to 10 times sampling period); • • •, central time differencing (time step equal to sampling period).

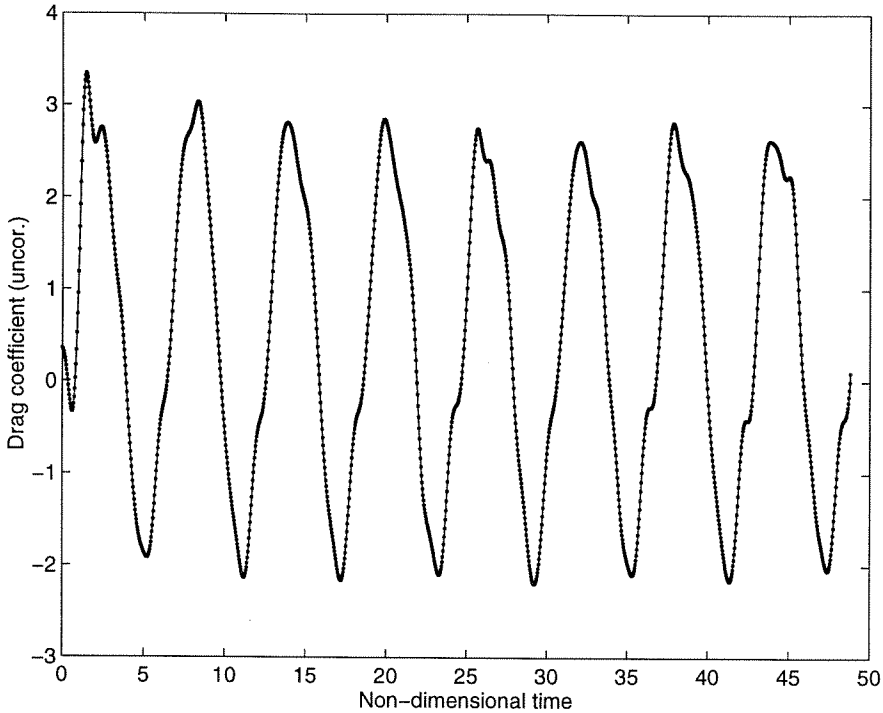


Figure 8.13: Drag coefficient vs. time, obtained with low-pass cutoff at a frequency of 1: ——, "impulse equation"; • • •, "momentum equation".

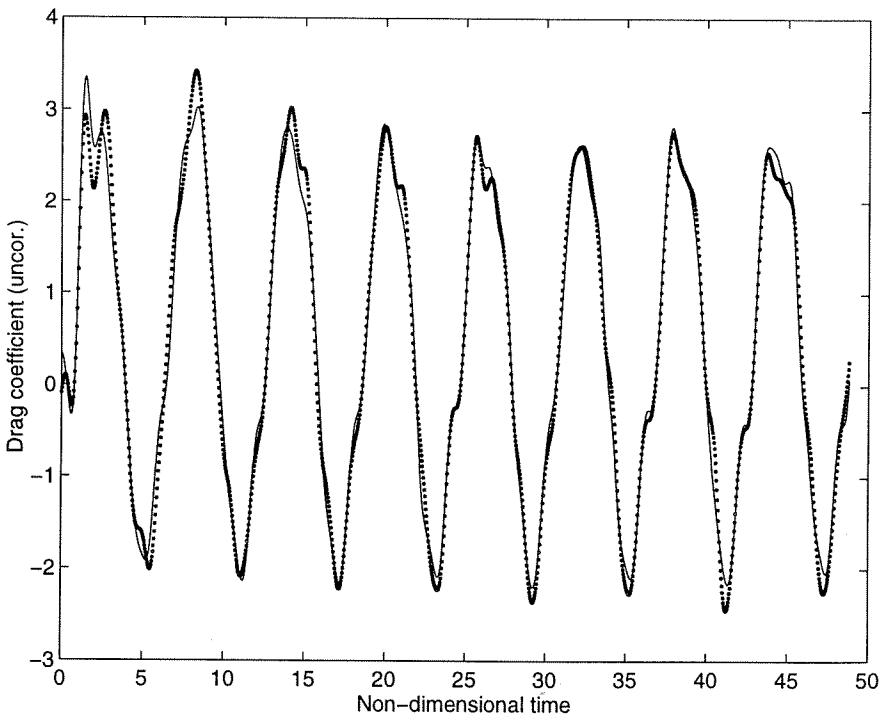


Figure 8.14: Drag coefficient vs. time, obtained with low-pass cutoff at a frequency of 1: ——, "momentum" equation; • • •, "flux" equation.

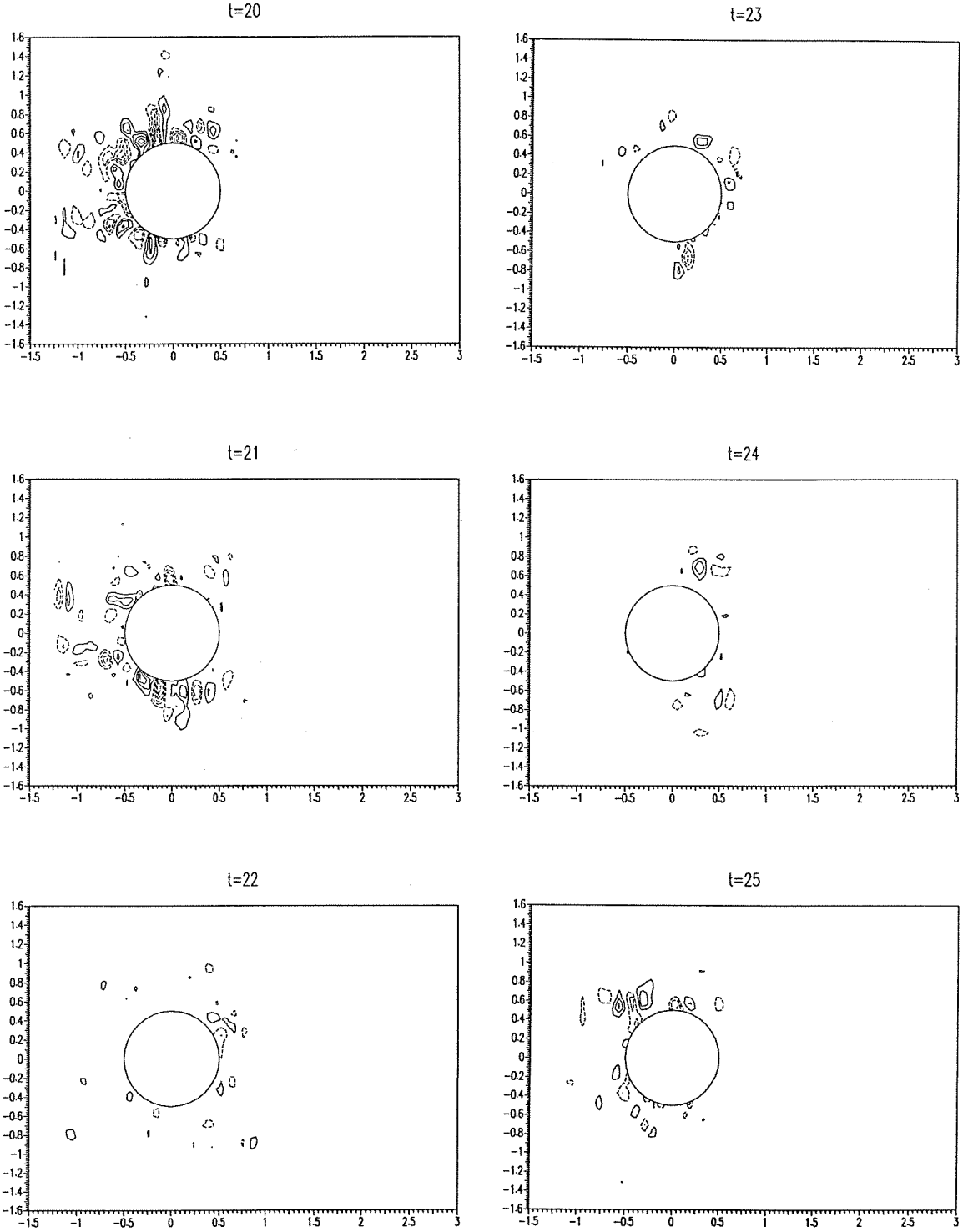


Figure 8.15: Time sequence of normalized velocity divergence fields for a jerking circular cylinder at $Re \sim 100$ during one shedding cycle (contours are incremented by 1; dashed lines represent negative values, solid lines positive values).

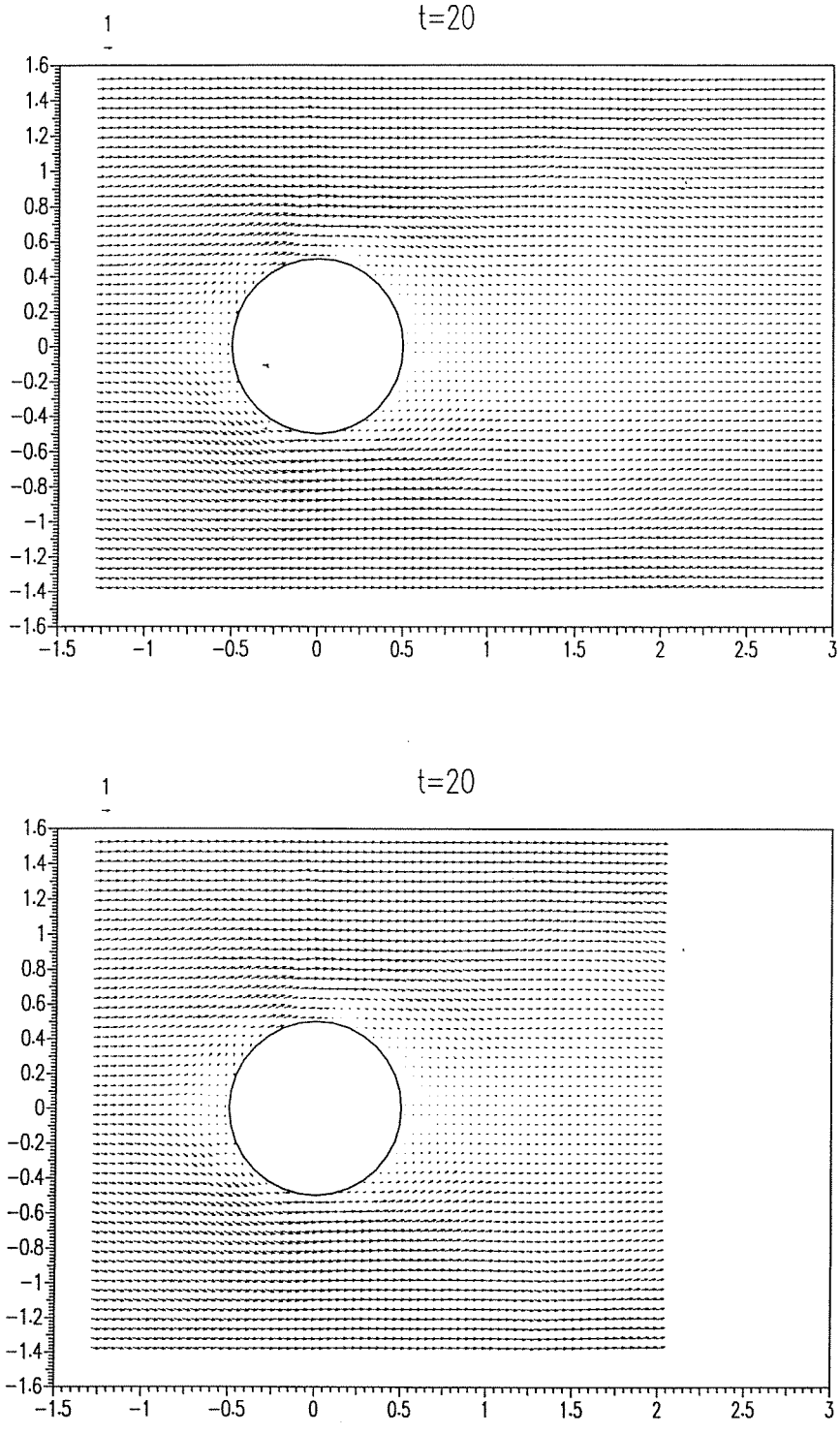


Figure 8.16: Domain sizes used for integration, from top to bottom: large domain, small domain.

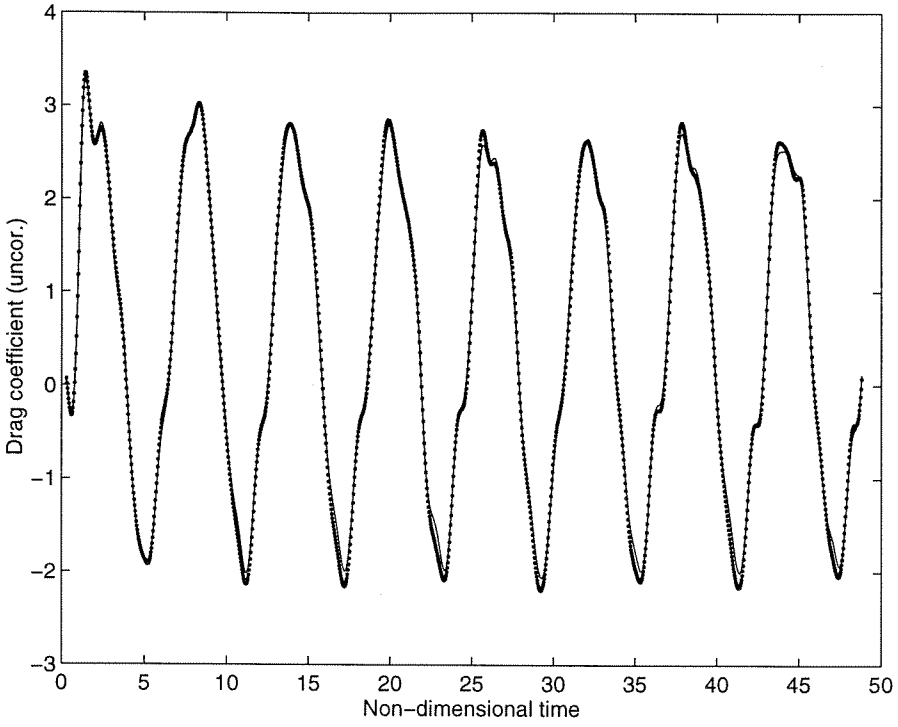


Figure 8.17: Drag coefficient vs. time, obtained with low-pass cutoff at a frequency of 1 and the "momentum" equation: ——, small domain; • • •, large domain.

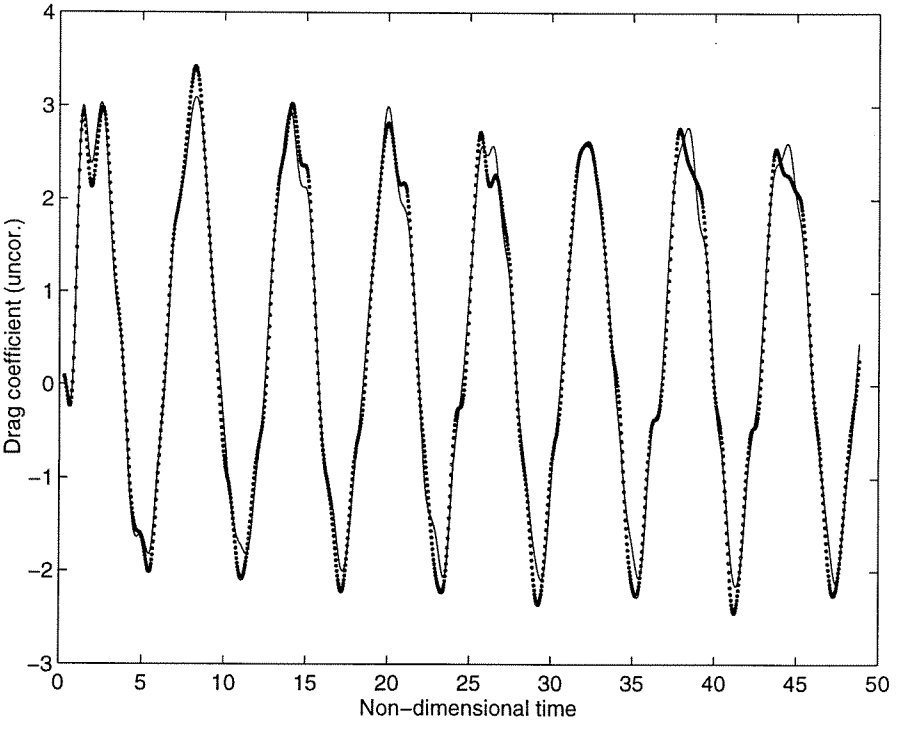


Figure 8.18: Drag coefficient vs. time, obtained with low-pass cutoff at a frequency of 1 and the "flux" equation: ——, small domain; • • •, large domain.

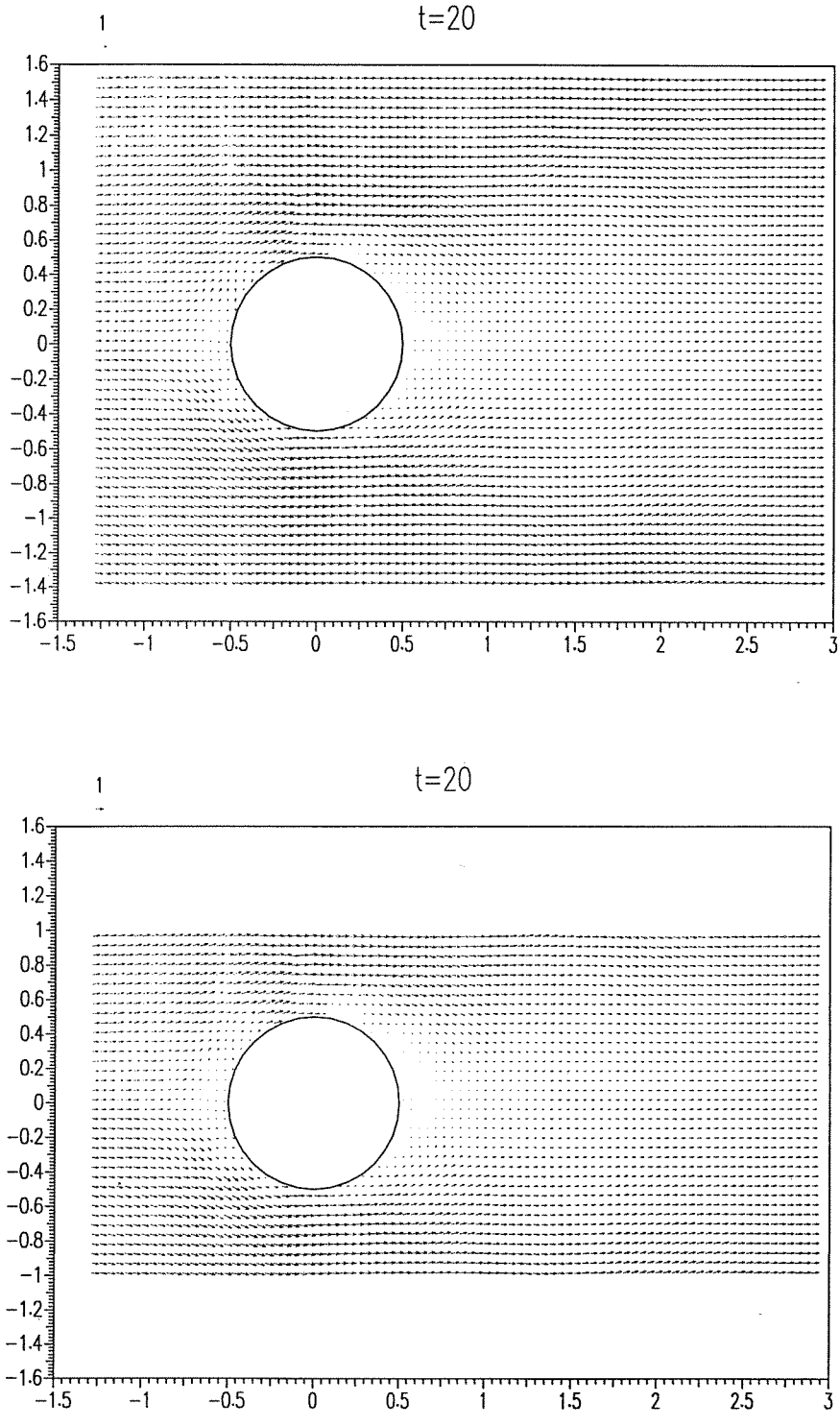


Figure 8.19: Domain sizes used for integration, from top to bottom: large domain, small domain.

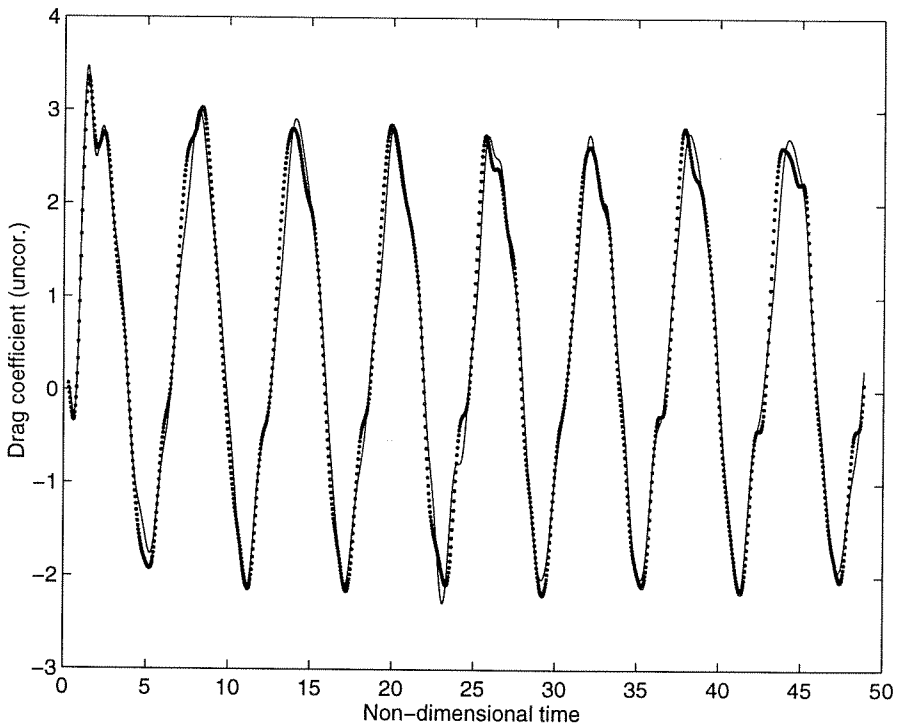


Figure 8.20: Drag coefficient vs. time, obtained with low-pass cutoff at a frequency of 1 and the "momentum" equation: ——, small domain; • • •, large domain.

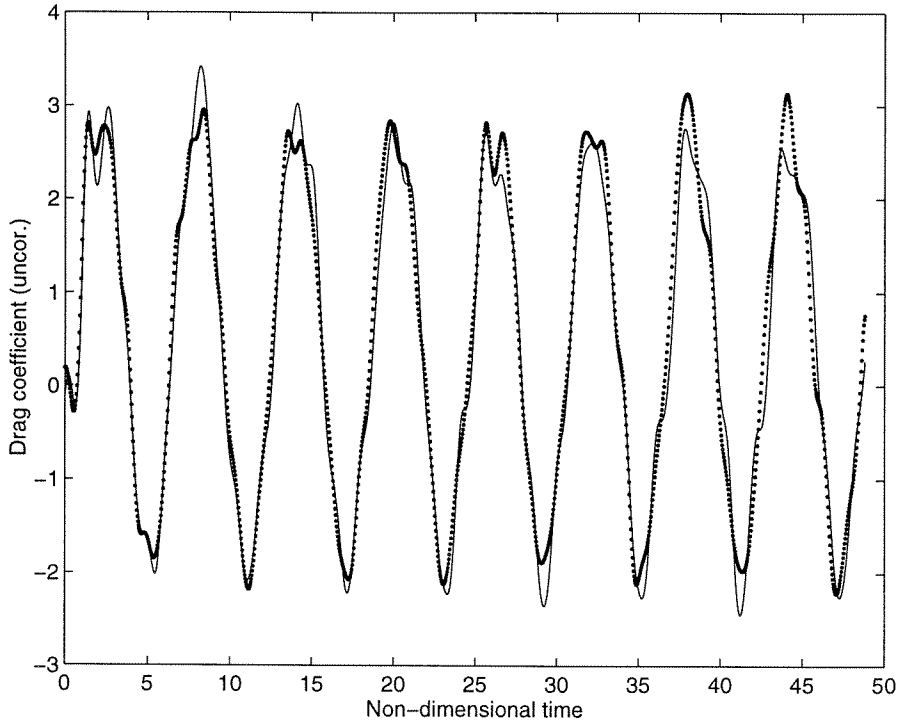


Figure 8.21: Drag coefficient obtained from two different runs: ——, run 1; • • •, run 2.

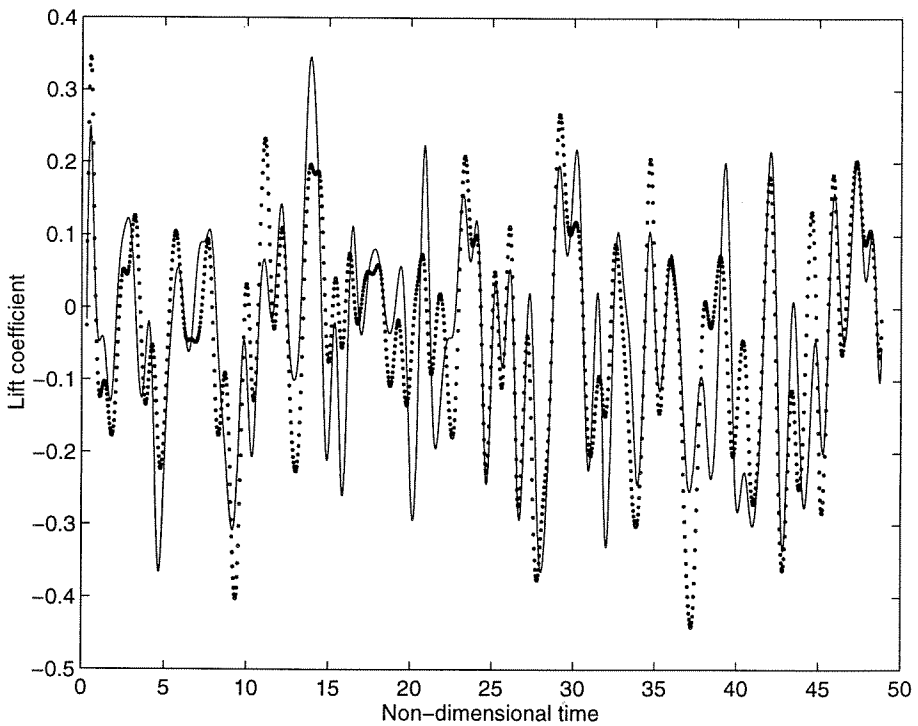


Figure 8.22: Lift coefficient vs. time obtained with a low-pass cutoff at a frequency of 1: ——, "momentum" equation; • • •, "flux" equation.

# Chapter 9 Discussion and conclusions

In this work, no independent force measurement (with a force balance for instance) was performed, and thus the precision of the method could not be determined. Nevertheless, the method was tested for self-consistency by using different equations and modifying the domains of integrations. In this Chapter, the discussion will thus bear only on self-consistency.

In the two previous chapters, we observed that the method was indeed self-consistent when the force levels were high (as in the case of the cylinder in jerking motion). However, for small force levels (around 0.2), we noticed some inconsistency when the domain size was varied.

From a theoretical point of view, as demonstrated by the formulations, time-dependent forces on a body can be evaluated with measurements of the velocity field at arbitrarily large distances from the body (using the "flux" equation). Looking at the flow some 100 diameters away from the cylinder, an observer can theoretically affirm: "Haha, I know exactly the instantaneous force acting right now on a body which I can't even see since it lies so far away from me!" Philosophically, this is a disturbing fact, and experimentally, we did see (in Chapter 7) that a very large domain does not yield the right answer. Somehow, Nature seems to prevent the observer from performing such a measurement with accuracy.

In Paragraph 9.1, we will show how errors, introduced from the velocity measurement technique, actually amplify when the domain size increases.

In Paragraph 9.2, we will discover that it is indeed possible to trick Nature, and obtain a reasonable force measurement, even in a very big domain.

Finally, in Paragraph 9.3, we will present some conclusive remarks and lay out the work that is needed in the future to pin down the accuracy and precision of the method and to possibly develop a time-dependent wake-survey technique.

## 9.1 The "moment arm" dilemma

All equations contain the position vector $\mathbf{x}$ which enters predominantly as a factor in a velocity time derivative (for surface integrals) or a vorticity time derivative (for volume integrals). For the "flux" equation, the time dependence of the force roughly depends on the surface integral of terms of the form:

$$\mathbf{x} \cdot \frac{\delta \mathbf{u}}{\delta t}, \tag{9.1}$$

where $\mathbf{u}$ is the velocity and $\mathbf{x}$ the position vector, which had the cylinder center as origin in our experiments. We will assume that the time derivative can be evaluated with infinite precision. We saw in our experiments that the noise in the time derivative actually occurred at much higher frequencies that the actual flow frequency (shedding frequency) if the sampling time was small enough. With a filtering process, the noise could then be effectively removed.

With proper normalization, the term can be put in the following non-dimensional form:

$$\frac{x}{d} \times St \frac{u}{U}, \tag{9.2}$$

where $d$ is the cylinder diameter, $U$, the flow velocity, and $St$, the Strouhal frequency which takes the role of the time derivative.

In a two-dimensional wake, the $x$-component of the velocity field at large distances from the body assumes a self-similar profile given by[1]:

$$\frac{u}{U} \propto \left(\frac{x}{d}\right)^{-\frac{1}{2}} \left[1 - \left(\frac{y}{b}\right)^{\frac{3}{2}}\right]^2, \tag{9.3}$$

where $u$ is the velocity defect in the wake, $U$ is the external flow velocity, $x$ is a coordinate along the flow direction (roughly equal to the downstream distance from the cylinder), $y$ is the coordinate normal to the flow direction with origin at the wake centerline, $d$ is the cylinder characteristic dimension, and $b$ is the wake width. The term,

$$\left[1 - \left(\frac{y}{b}\right)^{\frac{3}{2}}\right], \tag{9.4}$$

has always a value between 0 and 1 from the definition of the wake width, and thus does not affect the order of magnitude variation of the velocity defect with downstream distance:

$$\frac{u(x)}{U} \propto \left(\frac{x}{d}\right)^{-\frac{1}{2}}. \tag{9.5}$$

We will assume that the fluctuating components of the velocity scale in a similar way. If we now take the moment of the time derivative of the velocity, we obtain the following $x$-dependence:

$$\frac{x}{d} \times St \frac{u}{U} \propto \left(\frac{x}{d}\right)^{\frac{1}{2}}, \tag{9.6}$$

where we have omitted the Strouhal number since it is of order unity. A surface integration of this term across the wake (i.e. , along $y$) does not change its $x$-dependence. We arrive at the (annoying) result that as $x$ increases, i.e. , as the domain of integration increases, this term increases as the square root of the distance. Obviously, this term cannot be the only one in the equation, otherwise

[1] Schlichting H., *Boundary-layer theory*, §XXXIV-c-3, McGraw-Hill, 1979.

it would lead to an infinite force if the domain were infinite. There must be (and there are!) other terms in the "flux" equation (the reader is invited to browse through Chapter 5 to remind himself of the form of the "flux" equation) with the same $x$ dependence which ought to cancel these infinities. In practical situation as in experimental work, it is always delicate to force two very large terms to cancel!

We believe that this (un)balance between large terms may be responsible for the much larger force amplitudes in larger domains. In smaller domains, the effect may not be as pronounced, but it may arise (and it did!), especially if the force levels are very low (as in the case of a cylinder in steady motion).

One may think that this problem arises only in two-dimensional flows. This is inexact. For a turbulent circular wake, the $x$ dependence of the velocity along the centerline scales as $x^{-2/3}$, and therefore, the moment grows also as $x^{1/3}$, which also diverges for large $x$.

## 9.2 A solution to the "moment arm" dilemma

A possible solution to the "moment arm" problem was suggested by Anthony Leonard[2] to whom I am strongly indebted.

Since all the information about the fluid-dynamic force on the body *seems* to lie in the wake, it would be interesting to evaluate the force by taking the origin of coordinates where the wake crosses the domain of integration. If, indeed, the only relevant information is in the wake, then this procedure should decrease the moment arm expecially for the "flux" equation.

However, this procedure may not be intuitively right for the "impulse" equation which requires a "moment arm" throughout the volume. If the origin of coordinates is downstream in the wake, the moment arm of the vorticity near the body may become very large!

This idea was nonetheless tested on the circular cylinder flow for the very large domain, as investigated in Chapter 7. There, we evaluated lift forces which seemed to be an order of magnitude larger than what they ought to be (see Figure 7.32). We do understand now why this was so.

The graphs were rescaled such as to place the origin of coordinates near the downstream edge of the integration box, as shown in Figure 9.1. The lift coefficient evaluated with this rescaling is shown in Figure 9.2 and Figure 9.3. We, therefore, see that a simple rescaling sufficed to lower the force levels down to reasonable values. Note that the "impulse" and "momentum" equation again yield identical answers, whereas the "flux" equation seems to behave very differently. Nevertheless, the signal amplitudes are very similar (RMS lift of 0.36 for the "flux" equation, and 0.25 for the other two equations).

We decided to perform a similar rescaling to the smaller domains.

[2]Personal communication.

For the jerking cylinder, the results remained unaffected when the origin of coordinates was placed on the downstream edge (see Figure 9.4 and Figure 9.5). It can be argued that such a displacement of the origin along the stream direction should not affect the drag value since the moment enters as $\mathbf{x} \wedge \boldsymbol{\omega}$. If the moment arm has an effect at all, it should appear with the origin displaced normally to the stream direction. In Figure 9.7, the drag was computed with the origin of coordinates placed on the bottom edge (see Figure 9.6), and here a slight discrepancy of order 0.1 did appear.

For the cylinder in steady motion with the grid placed on the downstream edge, the agreement was far from being perfect (see Figure 9.8 and Figure 9.9). The RMS lift coefficient value was preserved, but the mean profile was strongly altered. Again, the results were tested to be only slightly dependent on the equation used as shown in Figure 9.10. Intuitively, we expect the results to be more reliable with the origin placed on the dowmstream edge of the domain (where the wake crosses the domain) because the moments $\mathbf{x} \cdot \delta\mathbf{u}/\delta t$ are then minimized (at least for the "flux" equation).

A more rigorous justification for the rescaling is as follows. In the "impulse" equation, the only two moments are $\mathbf{x} \wedge \boldsymbol{\omega}$ over the volume and $\hat{\mathbf{n}} \cdot \mathbf{u}(\mathbf{x} \wedge \boldsymbol{\omega})$ on the surface. By placing the origin on the downstream edge, the second moment does not contribute to the lift coefficient anymore, and only the first moment remains. This procedure thus eliminates a possible conflict between large numbers.

It was noticed by Dave Jeon[3] that for a cylinder oscillating transversely to a cross-flow, the integral of the two moments $\mathbf{x} \wedge \boldsymbol{\omega}$ and $\hat{\mathbf{n}} \cdot \mathbf{u}(\mathbf{x} \wedge \boldsymbol{\omega})$ are indeed in mutual conflict, both being *very* large and opposite. A simple shift of origin would probably eradicate the problem.

We decided to apply this idea to the case of the cylinder in steady motion, with the grid origin placed on the downstream edge of three domain sizes (see Figure 9.11). The agreement between the lift coefficient obtained with the different domains was reasonable (within an error of 0.2) as suggested by Figure 9.12 and Figure 9.13. From the arguments presented above, it is probable that a shift in grid origin improves the accuracy of the results, but not the precision. As a last remark, it should be noted that as the domain size got smaller, so did the amplitude of the lift signal.

## 9.3 Future work

In our experiments, fluid-dynamic forces were estimated by observing the flow in an arbitrary and finite domain surrounding the body. A very succinct parametric study was performed to confirm the viability of the method. It yielded satisfactory results, which can be summarized as follows.

1. For the cylinder in forced motion, the results were consistently repeatable for every procedure that was undertaken. Thus, it seems that the method is very effective in the case of *bodies in*

[3]Personal communication.

*unsteady motion* for which the vortex shedding pattern is very well accentuated and the force signals are very high.

Since only self-consistency was checked in these experiments, the experiments should be repeated with a force balance in order to produce independent measurements and thus determine the precision of the method.

2. For the case of a body in steady motion (natural shedding) at low Reynolds number, the RMS values compared reasonably well with those from numerical computations. However, it was not possible to obtain self-consistent results with a change in domain size. The moment arm of the velocity field measurement error seemed to have a large effect on these low level signals.

   Also, the "vortex shedding" process at these low Reynolds numbers may not be pronounced enough to deduce forces from it. It is true that vortices appear distinctively in the cylinder wake. However, the shedding process *per se* close to the base of the cylinder is a very "sluggish" phenomenon with very elongated vorticity fields instead of well defined vortex cores (see Figure 7.3 for example). The determination of forces from these poorly defined vortex structures may thus not be a simple task.

   Nonetheless, we believe that the experimental procedure can be strongly improved by increasing the particle seeding and using smaller DPIV processing windows (16-pixel $\times$ 16-pixel window). Also, a spatial central differencing procedure (instead of plain simple differencing algorithm) should improve the results.

3. The effects of flow *three-dimensionality* were not treated in this work. It is known that *intrinsic* three-dimensionality does lower force coefficients as compared to force coefficients obtained from two-dimensional computations.

   In the equations, we did not only set the space dimension $\mathcal{N}$ equal to 2, but we also assumed the vorticity field to be normal to the plane of measurement. By doing so, we arbitrarily removed terms in the equations which may have a strong effect when three-dimensionality is present.

   Since the essence of this work was aimed towards flows about bodies in unsteady motion, we reasoned that such flows are very close to being two-dimensional and that the present method should apply satisfactorily to them.

   Nevertheless, the effects of three-dimensionality should certainly be considered seriously in future work.

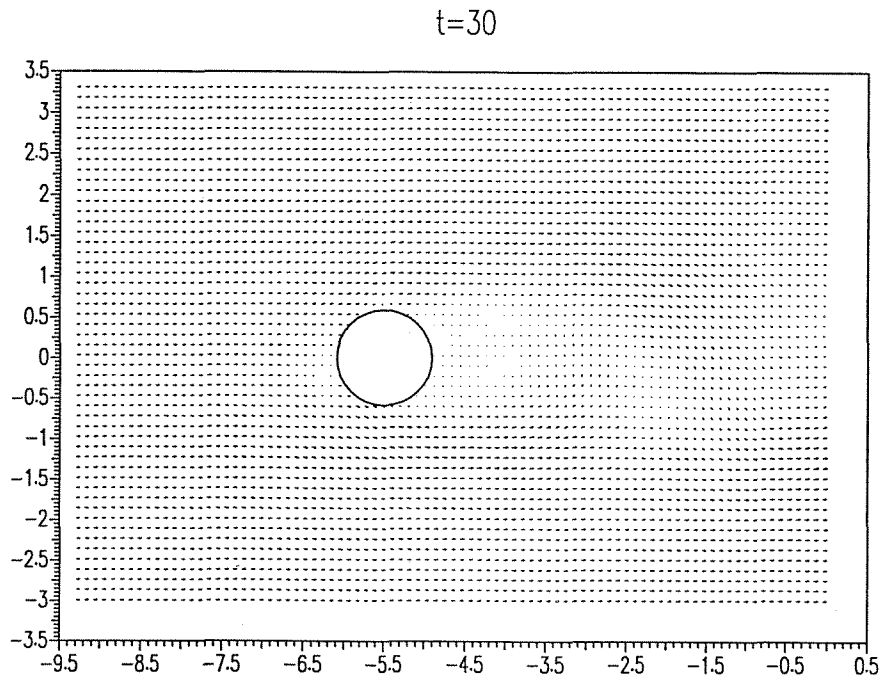


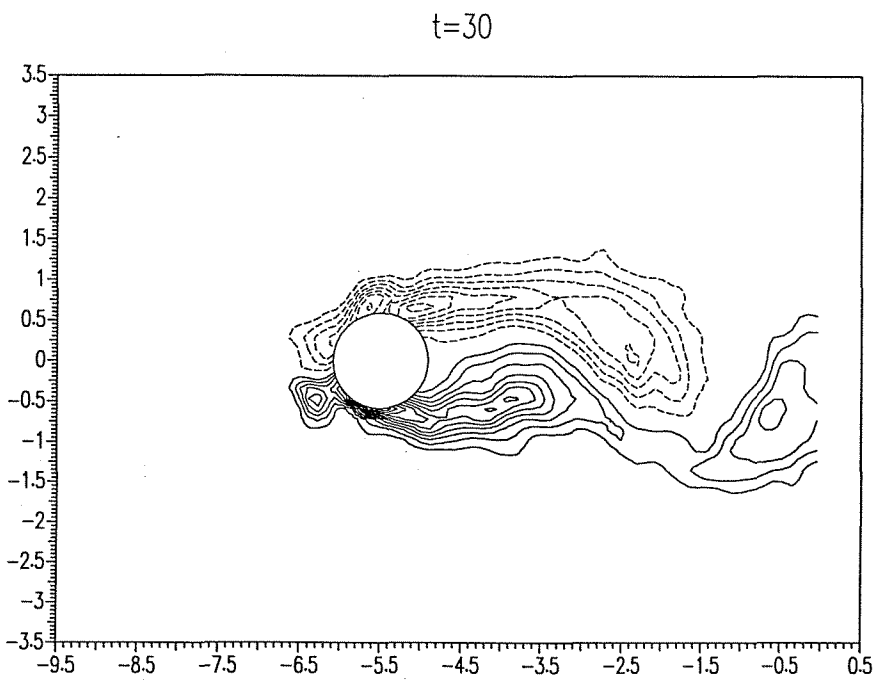


Figure 9.1: Velocity field and vorticity field for a circular cylinder at $Re \sim 100$, with the grid origin placed on the downstream surface of the control volume.

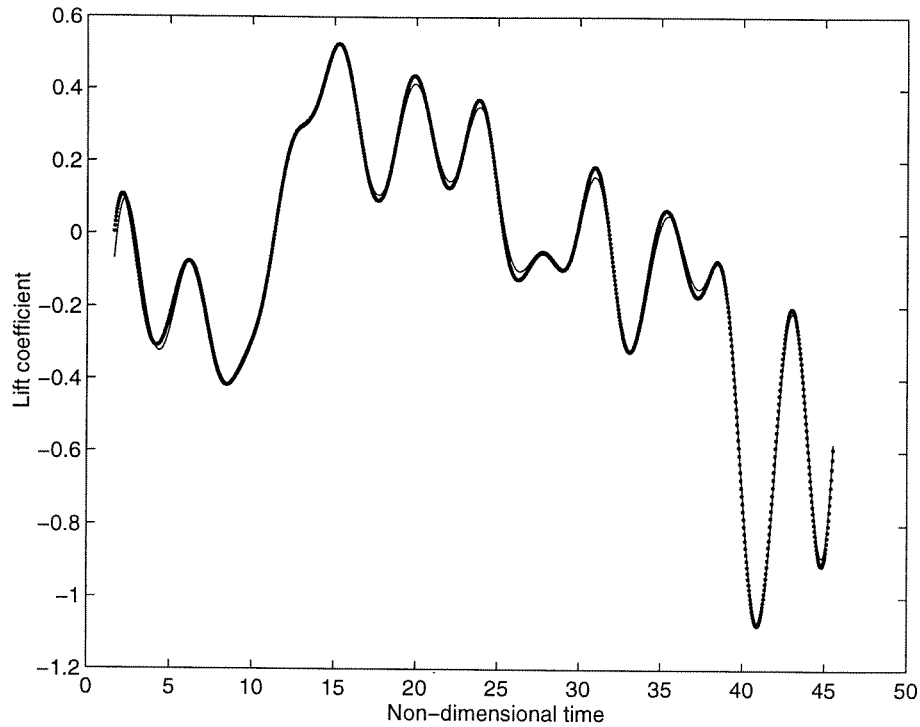


Figure 9.2: Lift coefficient vs. time, obtained with lowpass cutoff at a frequency of 0.3: ——, "impulse" equation; • • •, "momentum" equation.

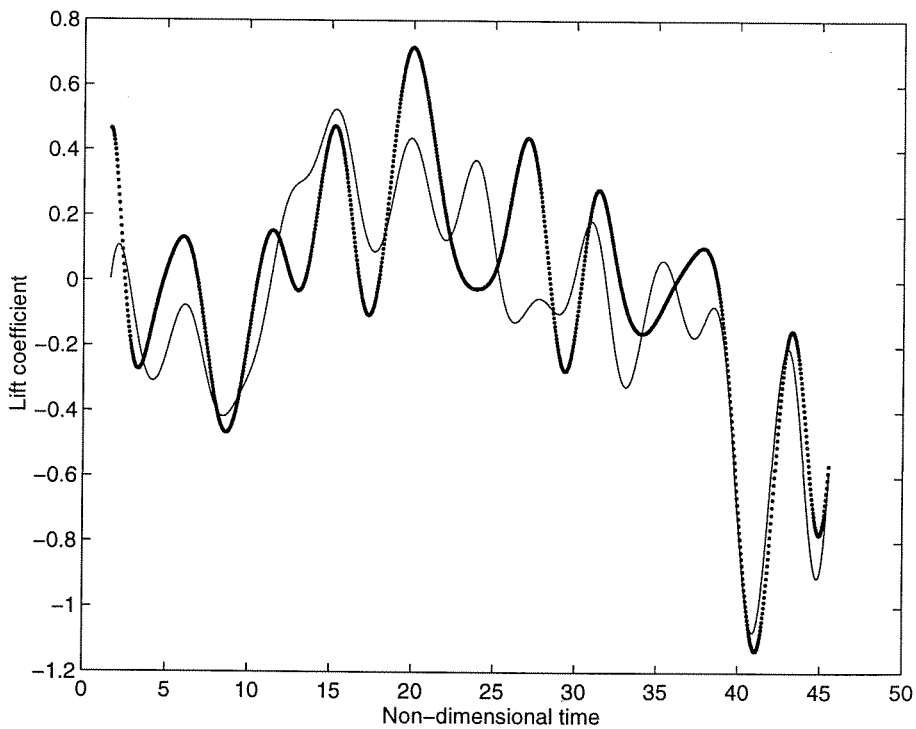


Figure 9.3: Lift coefficient vs. time, obtained with lowpass cutoff at a frequency of 0.3: ——, "momentum" equation; • • •, "flux" equation.

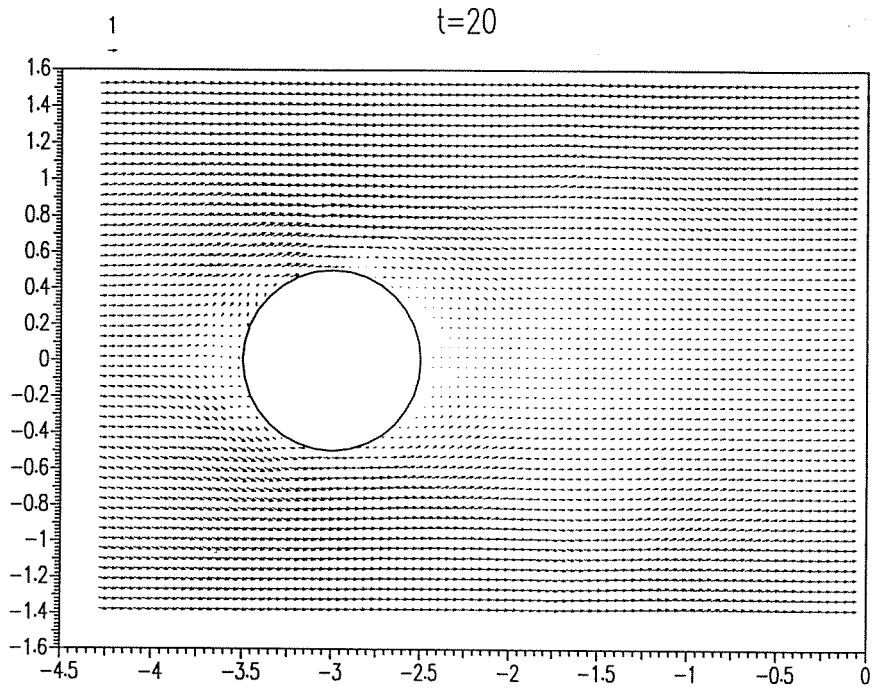


Figure 9.4: Velocity field for a jerking circular cylinder at $Re \sim 100$, with the grid origin placed on the downstream edge of the control volume.

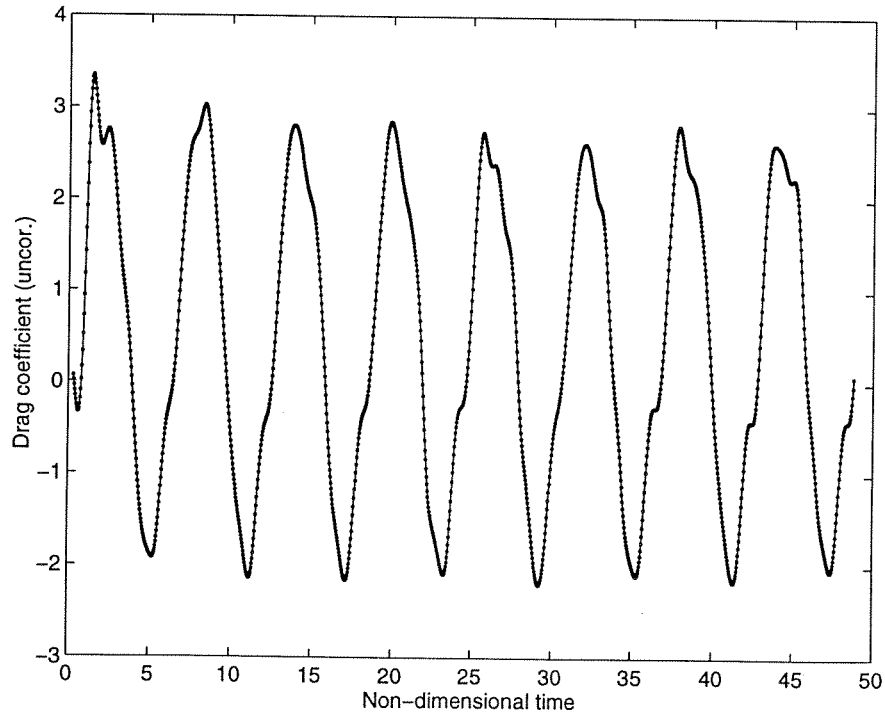


Figure 9.5: Drag coefficient vs. time for the jerking cylinder, obtained with lowpass cutoff at a frequency of 1.0 and the "momentum" equation: ——, origin at the downstream edge; · · ·, origin at the cylinder center.

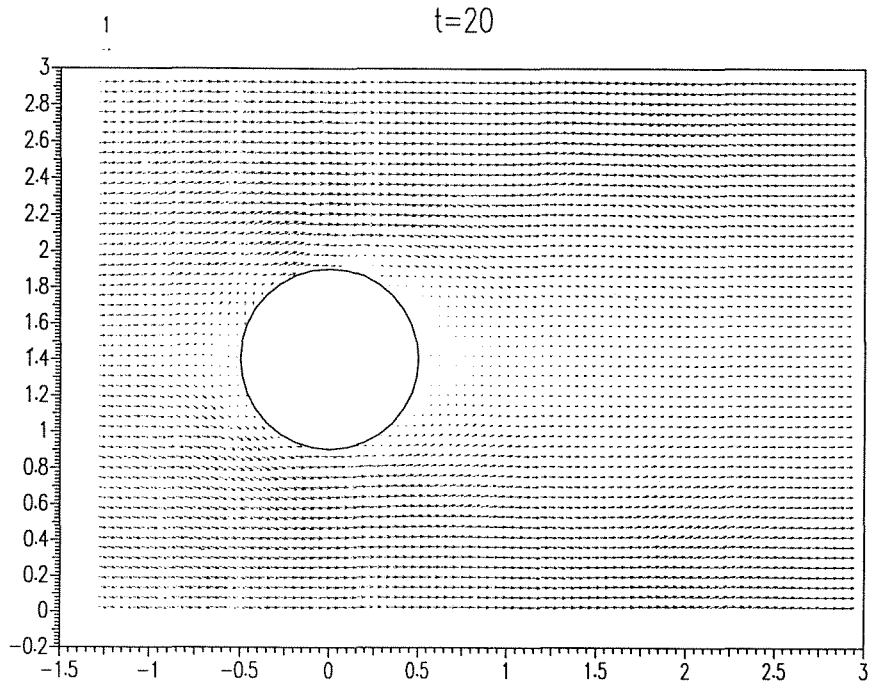


Figure 9.6: Velocity field for a jerking circular cylinder at $Re \sim 100$, with the grid origin placed on the bottom edge of the control volume.

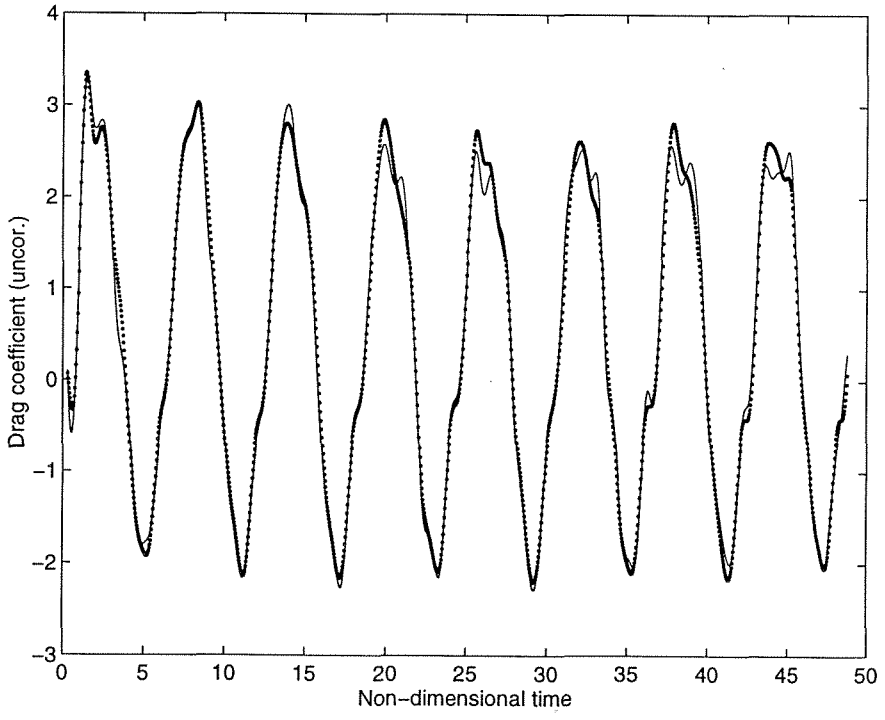


Figure 9.7: Drag coefficient vs. time for the jerking cylinder, obtained with lowpass cutoff at a frequency of 1.0 and the "momentum" equation: ——, origin at the bottom edge; · · ·, origin at the cylinder center.

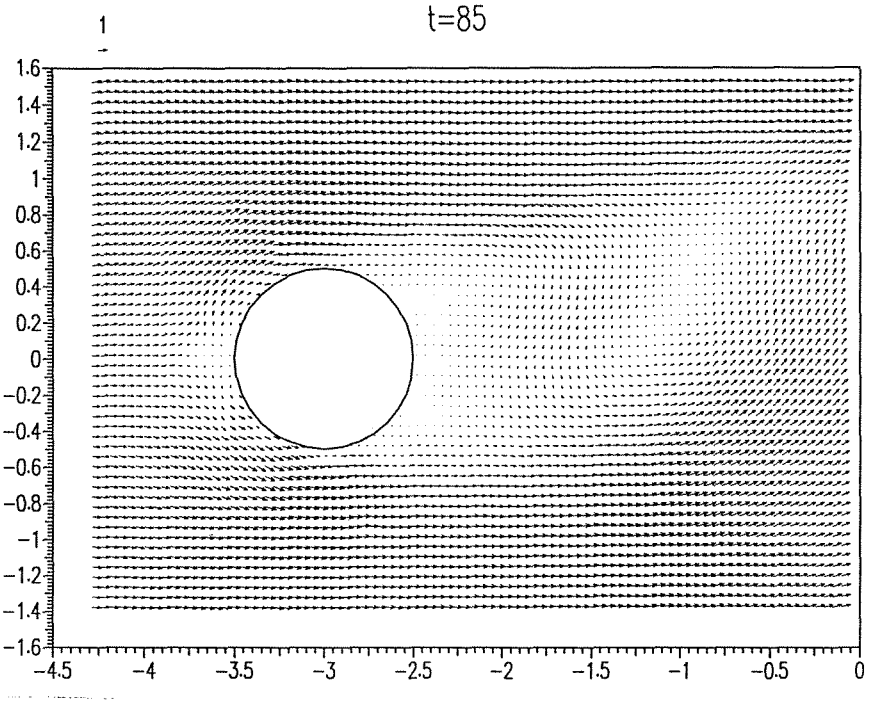


Figure 9.8: Velocity field for a circular cylinder in steady motion at $Re \sim 100$, with the grid origin placed on the downstream edge of the control volume.

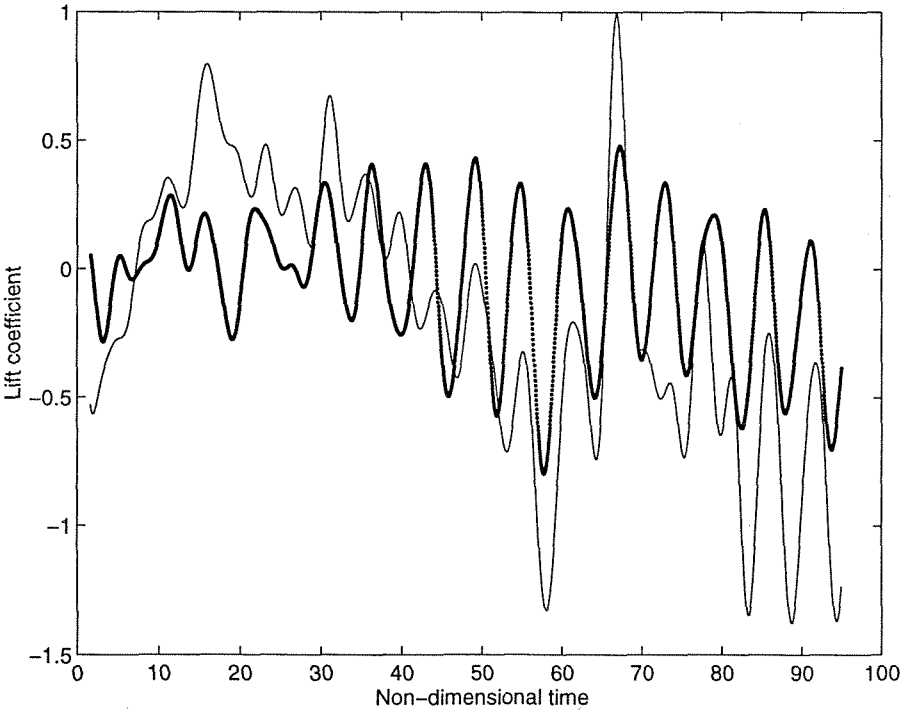


Figure 9.9: Lift coefficient vs. time for the cylinder in steady motion ($Re \sim 100$), obtained with lowpass cutoff at a frequency of 0.3 and the "momentum" equation: ——, origin at the downstream edge; · · ·, origin at the cylinder center.

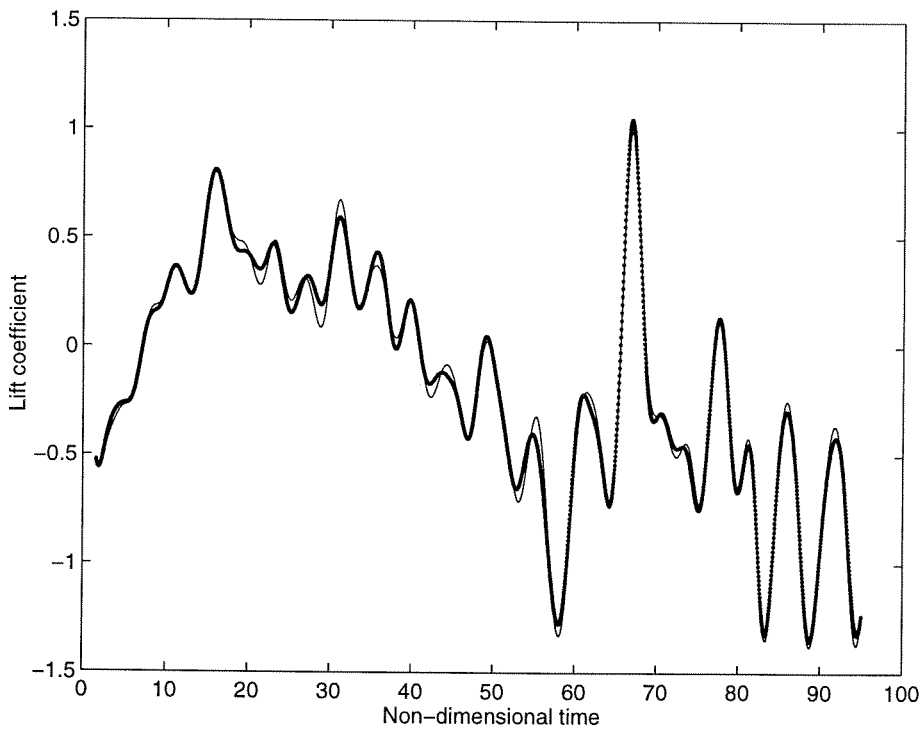


Figure 9.10: Lift coefficient vs. time for the cylinder in steady motion ($Re \sim 100$), obtained with lowpass cutoff at a frequency of 0.3 and the grid origin on the downstream edge: ——, "momentum" equation; • • •, "flux" equation.

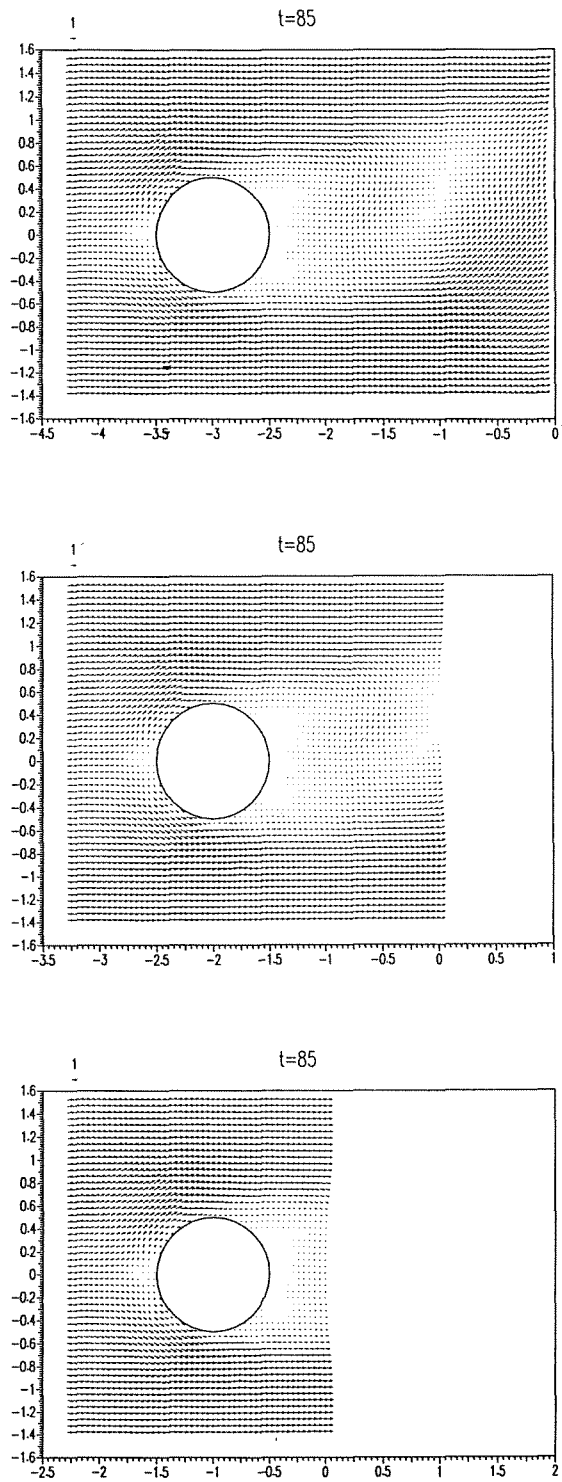


Figure 9.11: Domain sizes used for integration with grid origin on the downstream edge, from top to bottom: large domain, intermediate domain, small domain (circular cylinder in steady motion at $Re \sim 100$).

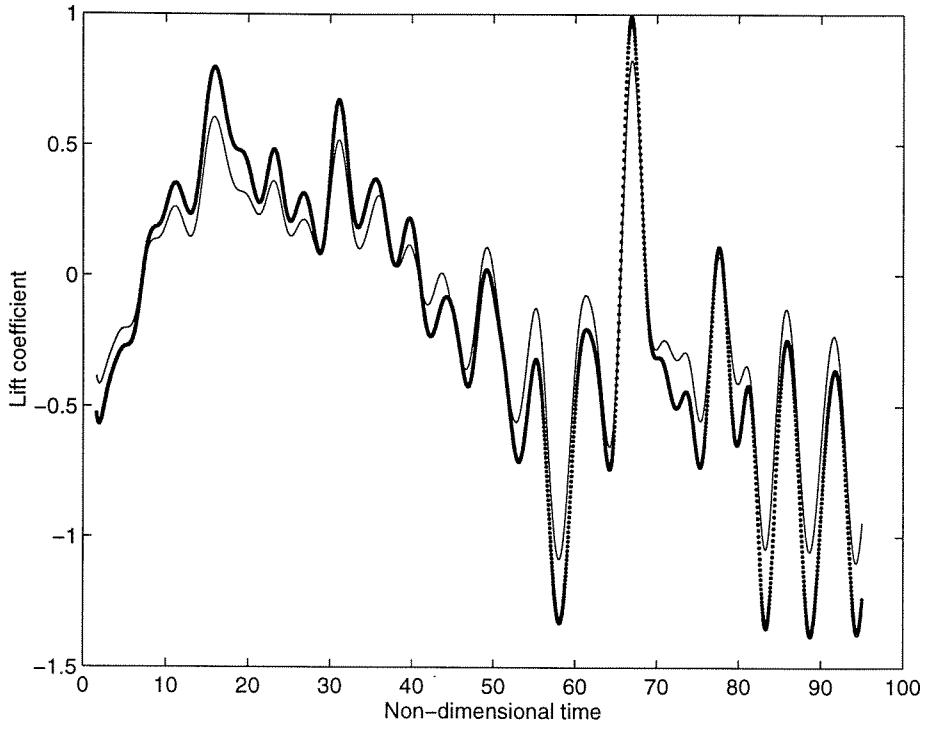


Figure 9.12: Lift coefficient vs. time, obtained with lowpass cutoff at a frequency of 0.3 and the "momentum" equation: ——, intermediate domain; • • •, large domain.

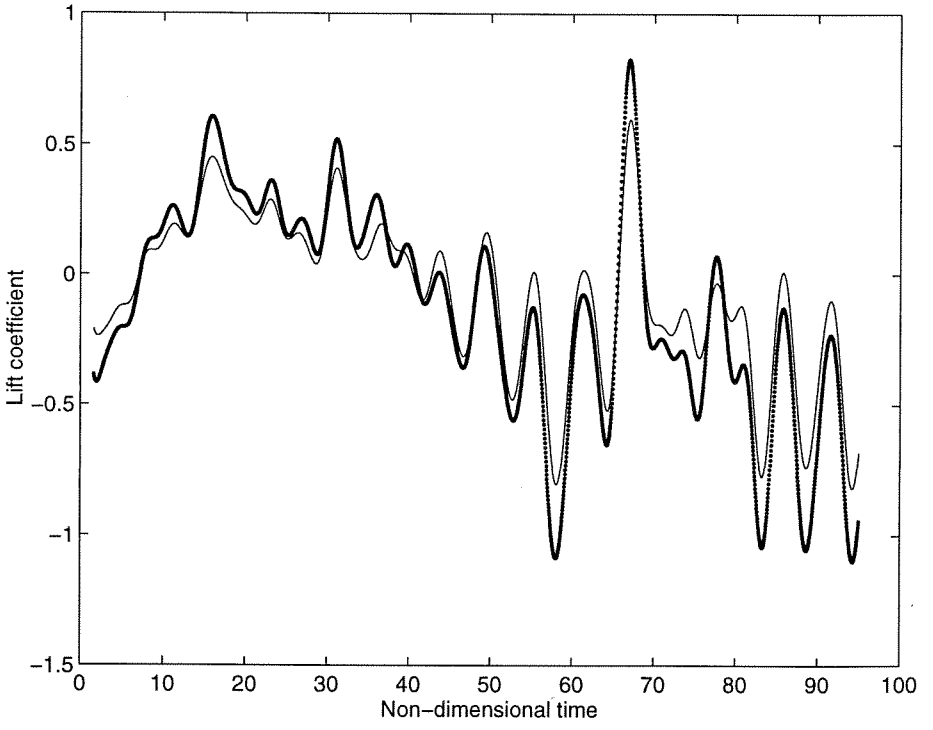


Figure 9.13: Lift coefficient vs. time, obtained with lowpass cutoff at a frequency of 0.3 and the "momentum" equation: ——, small domain; • • •, intermediate domain.

# Appendix A Vector and tensor identities

## A.1 Operations with vectors

$$\mathbf{a} \cdot \mathbf{b} \equiv a_i b_i \tag{A.1}$$

$$[\mathbf{a} \wedge \mathbf{b}]_i \equiv \epsilon_{ijk} a_j b_k \tag{A.2}$$

$$\boldsymbol{\nabla} \cdot \mathbf{a} \equiv \frac{\partial}{\partial x_i} a_i \tag{A.3}$$

$$[\boldsymbol{\nabla} \wedge \mathbf{a}]_i \equiv \epsilon_{ijk} \frac{\partial}{\partial x_j} a_k \tag{A.4}$$

$$[\boldsymbol{\nabla} \alpha]_i \equiv \frac{\partial}{\partial x_i} \alpha \tag{A.5}$$

$$\mathbf{a} \wedge \mathbf{b} = -\mathbf{b} \wedge \mathbf{a} \tag{A.6}$$

$$\mathbf{a} \cdot (\mathbf{b} \wedge \mathbf{c}) = \mathbf{b} \cdot (\mathbf{c} \wedge \mathbf{a}) \tag{A.7}$$

$$\mathbf{a} \wedge (\mathbf{b} \wedge \mathbf{c}) = (\mathbf{a} \cdot \mathbf{c})\mathbf{b} - (\mathbf{a} \cdot \mathbf{b})\mathbf{c} \tag{A.8}$$

$$(\mathbf{a} \wedge \mathbf{b}) \cdot (\mathbf{c} \wedge \mathbf{d}) = (\mathbf{a} \cdot \mathbf{c})(\mathbf{b} \cdot \mathbf{d}) - (\mathbf{a} \cdot \mathbf{d})(\mathbf{b} \cdot \mathbf{c}) \tag{A.9}$$

$$\boldsymbol{\nabla} \cdot (\alpha \mathbf{a}) = \boldsymbol{\nabla} \alpha \cdot \mathbf{a} + \alpha \boldsymbol{\nabla} \cdot \mathbf{a} \tag{A.10}$$

$$\boldsymbol{\nabla} \cdot (\boldsymbol{\nabla} \wedge \mathbf{a}) = 0 \tag{A.11}$$

$$\boldsymbol{\nabla} \wedge (\boldsymbol{\nabla} \alpha) = 0 \tag{A.12}$$

$$\boldsymbol{\nabla} \wedge (\alpha \mathbf{a}) = (\boldsymbol{\nabla} \alpha) \wedge \mathbf{a} + \alpha \boldsymbol{\nabla} \wedge \mathbf{a} \tag{A.13}$$

$$\boldsymbol{\nabla} \wedge (\boldsymbol{\nabla} \wedge \mathbf{a}) = \boldsymbol{\nabla}(\boldsymbol{\nabla} \cdot \mathbf{a}) - \boldsymbol{\nabla} \cdot \boldsymbol{\nabla} \mathbf{a} \tag{A.14}$$

$$\boldsymbol{\nabla}(\mathbf{a} \cdot \mathbf{b}) = \mathbf{a} \cdot (\boldsymbol{\nabla} \mathbf{b}) + \mathbf{b} \cdot (\boldsymbol{\nabla} \mathbf{a}) + \mathbf{a} \wedge (\boldsymbol{\nabla} \wedge \mathbf{b}) + \mathbf{b} \wedge (\boldsymbol{\nabla} \wedge \mathbf{a}) \tag{A.15}$$

$$\boldsymbol{\nabla}(\mathbf{a} \cdot \mathbf{b}) = \mathbf{a}(\boldsymbol{\nabla} \cdot \mathbf{b}) + \mathbf{b}(\boldsymbol{\nabla} \cdot \mathbf{a}) + (\mathbf{a} \wedge \boldsymbol{\nabla}) \wedge \mathbf{b} + (\mathbf{b} \wedge \boldsymbol{\nabla}) \wedge \mathbf{a} \tag{A.16}$$

$$\boldsymbol{\nabla}(\mathbf{a} \cdot \mathbf{b}) = (\boldsymbol{\nabla} \mathbf{a}) \cdot \mathbf{b} + (\boldsymbol{\nabla} \mathbf{b}) \cdot \mathbf{a} \tag{A.17}$$

$$\boldsymbol{\nabla}\cdot(\mathbf{a}\wedge\mathbf{b})=(\boldsymbol{\nabla}\wedge\mathbf{a})\cdot\mathbf{b}-\mathbf{a}\cdot(\boldsymbol{\nabla}\wedge\mathbf{b}) \tag{A.18}$$

$$\boldsymbol{\nabla}\wedge(\mathbf{a}\wedge\mathbf{b})=\mathbf{a}(\boldsymbol{\nabla}\cdot\mathbf{b})-\mathbf{b}(\boldsymbol{\nabla}\cdot\mathbf{a})+\mathbf{b}\cdot(\boldsymbol{\nabla}\mathbf{a})-\mathbf{a}\cdot(\boldsymbol{\nabla}\mathbf{b}) \tag{A.19}$$

$$\boldsymbol{\nabla}\wedge(\mathbf{a}\wedge\mathbf{b})=\mathbf{a}\wedge(\boldsymbol{\nabla}\wedge\mathbf{b})-(\mathbf{a}\wedge\boldsymbol{\nabla})\wedge\mathbf{b}-\mathbf{b}\wedge(\boldsymbol{\nabla}\wedge\mathbf{a})+(\mathbf{b}\wedge\boldsymbol{\nabla})\wedge\mathbf{a} \tag{A.20}$$

$$\mathbf{a}\wedge(\boldsymbol{\nabla}\wedge\mathbf{b})-(\mathbf{a}\wedge\boldsymbol{\nabla})\wedge\mathbf{b}=\mathbf{a}(\boldsymbol{\nabla}\cdot\mathbf{b})-\mathbf{a}\cdot(\boldsymbol{\nabla}\mathbf{b}) \tag{A.21}$$

$$\boldsymbol{\nabla}(\mathbf{a}\cdot\mathbf{a})=2\,\mathbf{a}\wedge(\boldsymbol{\nabla}\wedge\mathbf{a})+2\,\mathbf{a}\cdot(\boldsymbol{\nabla}\mathbf{a}) \tag{A.22}$$

$$\boldsymbol{\nabla}(\mathbf{a}\cdot\mathbf{a})=2\,(\boldsymbol{\nabla}\mathbf{a})\cdot\mathbf{a} \tag{A.23}$$

$$(\boldsymbol{\nabla}\mathbf{a})\cdot\mathbf{a}=\mathbf{a}\cdot(\boldsymbol{\nabla}\mathbf{a})+\mathbf{a}\wedge(\boldsymbol{\nabla}\wedge\mathbf{a}) \tag{A.24}$$

## A.2 Operations with tensors

$$[\mathbf{A}\cdot\mathbf{a}]_i\equiv \mathsf{A}_{ij}a_j \tag{A.25}$$

$$[\mathbf{a}\cdot\mathbf{A}]_i\equiv a_j\mathsf{A}_{ji} \tag{A.26}$$

$$\mathsf{A}^T_{ij}\equiv \mathsf{A}_{ji} \tag{A.27}$$

$$[\mathbf{A}:\mathbf{B}]_{ij}\equiv \mathsf{A}_{ij}\mathsf{B}_{ij} \tag{A.28}$$

$$[\mathbf{A}\cdot\mathbf{B}]_{ij}\equiv \mathsf{A}_{ik}\mathsf{B}_{kj} \tag{A.29}$$

$$[\boldsymbol{\nabla}\cdot\mathbf{A}]_i\equiv\frac{\partial}{\partial x_j}\mathsf{A}_{ji} \tag{A.30}$$

$$[\boldsymbol{\nabla}\wedge\mathbf{A}]_{ij}\equiv\epsilon_{ilm}\frac{\partial}{\partial x_l}\mathsf{A}_{mj} \tag{A.31}$$

$$[\mathsf{dual}\,\mathbf{A}]_i\equiv\frac{1}{2}\epsilon_{ijk}\mathsf{A}_{jk} \tag{A.32}$$

$$\mathsf{Tr}\,\mathbf{A}=\mathsf{A}_{ii} \tag{A.33}$$

$$\mathsf{Det}\,\mathbf{A}=\frac{1}{6}\epsilon_{ijk}\epsilon_{pqr}\mathsf{A}_{ip}\mathsf{A}_{jq}\mathsf{A}_{kr} \tag{A.34}$$

$$(\mathbf{A}\cdot\mathbf{B})^T=\mathbf{B}^T\cdot\mathbf{A}^T \tag{A.35}$$

$$\mathbf{A}\cdot\mathbf{a}=\mathbf{a}\cdot\mathbf{A}^T \tag{A.36}$$

$$\mathbf{A}\cdot\mathbf{B}\cdot\mathbf{a}=\mathbf{A}\cdot(\mathbf{B}\cdot\mathbf{a})=(\mathbf{A}\cdot\mathbf{B})\cdot\mathbf{a} \tag{A.37}$$

$$(\mathbf{A}\cdot\mathbf{a})\cdot\mathbf{B}\neq\mathbf{A}\cdot(\mathbf{a}\cdot\mathbf{B}) \tag{A.38}$$

$$\boldsymbol{\nabla}\cdot(\alpha\mathbf{A})=\boldsymbol{\nabla}\alpha\cdot\mathbf{A}+\alpha\boldsymbol{\nabla}\cdot\mathbf{A} \tag{A.39}$$

$$\boldsymbol{\nabla}\wedge(\alpha\mathbf{A})=(\boldsymbol{\nabla}\alpha)\wedge\mathbf{A}+\alpha\boldsymbol{\nabla}\wedge\mathbf{A} \tag{A.40}$$

$$\boldsymbol{\nabla}\cdot(\mathbf{A}\cdot\mathbf{a})=(\boldsymbol{\nabla}\cdot\mathbf{A})\cdot\mathbf{a}+\mathbf{A}:(\boldsymbol{\nabla}\mathbf{a}) \tag{A.41}$$

$$\boldsymbol{\nabla}\cdot(\mathbf{a}\cdot\mathbf{A})=\mathsf{Tr}\,(\boldsymbol{\nabla}\mathbf{a}\cdot\mathbf{A})+\mathbf{a}\cdot\boldsymbol{\nabla}\cdot\mathbf{A}^{T} \tag{A.42}$$

$$\boldsymbol{\nabla}\wedge(\mathbf{A}\cdot\mathbf{a})=(\boldsymbol{\nabla}\wedge\mathbf{A})\cdot\mathbf{a}-2\,\mathsf{dual}\,[\mathbf{A}\cdot(\boldsymbol{\nabla}\mathbf{a})^{T}) \tag{A.43}$$

$$\boldsymbol{\nabla}\cdot(\boldsymbol{\nabla}\wedge\mathbf{A})=0 \tag{A.44}$$

$$\boldsymbol{\nabla}\cdot(\boldsymbol{\nabla}\wedge\mathbf{A})^{T}=\boldsymbol{\nabla}\wedge\boldsymbol{\nabla}\cdot(\mathbf{A}^{T}) \tag{A.45}$$

$$\boldsymbol{\nabla}\wedge(\boldsymbol{\nabla}\wedge\mathbf{A})=\boldsymbol{\nabla}(\boldsymbol{\nabla}\cdot\mathbf{A})-\boldsymbol{\nabla}\cdot\boldsymbol{\nabla}\mathbf{A} \tag{A.46}$$

$$\mathbf{A}:\mathbf{B}=\mathbf{B}:\mathbf{A} \tag{A.47}$$

$$\mathbf{A}:\mathbf{B}^{T}=\mathbf{A}^{T}:\mathbf{B} \tag{A.48}$$

$$\mathbf{A}:\mathbf{B}^{T}=\mathsf{Tr}\,(\mathbf{A}\cdot\mathbf{B}) \tag{A.49}$$

$$\mathsf{Tr}\,(\mathbf{A}\cdot\mathbf{B})=\mathsf{Tr}\,(\mathbf{B}\cdot\mathbf{A}) \tag{A.50}$$

$$\mathsf{dual}\,\mathbf{A}^{T}=-\mathsf{dual}\,\mathbf{A} \tag{A.51}$$

$$\boldsymbol{\nabla}\wedge\mathsf{dual}\,\mathbf{A}=\frac{1}{2}\boldsymbol{\nabla}\cdot(\mathbf{A}^{T}-\mathbf{A}) \tag{A.52}$$

$$\mathsf{dual}\,\boldsymbol{\nabla}\wedge\mathbf{A}=\frac{1}{2}(\boldsymbol{\nabla}\cdot\mathbf{A}^{T}-\boldsymbol{\nabla}\mathsf{Tr}\,\mathbf{A}) \tag{A.53}$$

$$\boldsymbol{\nabla}\cdot\mathsf{dual}\,\mathbf{A}=\frac{1}{2}\mathsf{Tr}\,\boldsymbol{\nabla}\wedge\mathbf{A} \tag{A.54}$$

$$\mathsf{dual}\,\mathbf{A}\cdot\mathsf{dual}\,\mathbf{B}=\frac{1}{4}\mathbf{A}:(\mathbf{B}-\mathbf{B}^{T}) \tag{A.55}$$

$$\mathsf{dual}\,\mathbf{A}\cdot\mathsf{dual}\,\mathbf{B}=\frac{1}{4}(\mathbf{A}-\mathbf{A}^{T}):\mathbf{B} \tag{A.56}$$

## A.3 Operations with anti-symmetric tensors $\mathbf{W}$

$$\mathsf{W}_{ij} \equiv -\mathsf{W}_{ji} \tag{A.57}$$

$$\mathrm{Tr}\,\mathbf{W} = 0 \tag{A.58}$$

$$\mathbf{W} \cdot \mathbf{a} = -(\mathrm{dual}\,\mathbf{W}) \wedge \mathbf{a} \tag{A.59}$$

$$\mathbf{a} \cdot \mathbf{W} = -\mathbf{a} \wedge (\mathrm{dual}\,\mathbf{W}) \tag{A.60}$$

$$\boldsymbol{\nabla} \cdot \mathbf{W} = -\boldsymbol{\nabla} \wedge (\mathrm{dual}\,\mathbf{W}) \tag{A.61}$$

$$\boldsymbol{\nabla} \cdot \mathbf{W}^T = \boldsymbol{\nabla} \wedge (\mathrm{dual}\,\mathbf{W}) \tag{A.62}$$

$$\mathrm{dual}\,\boldsymbol{\nabla} \wedge \mathbf{W} = -\frac{1}{2}\boldsymbol{\nabla} \cdot \mathbf{W} \tag{A.63}$$

$$\mathbf{W} : \boldsymbol{\nabla}\mathbf{a} = (\mathrm{dual}\,\mathbf{W}) \cdot \boldsymbol{\nabla} \wedge \mathbf{a} \tag{A.64}$$

$$\begin{cases} \mathbf{W}_\mathbf{a} \equiv \mathrm{dual}^{-1}\mathbf{a} \\ [\mathbf{W}_\mathbf{a}]_{ij} \equiv \epsilon_{ijk} a_k \end{cases} \tag{A.65}$$

$$\mathbf{a} \wedge \mathbf{b} = -\mathbf{W}_\mathbf{a} \cdot \mathbf{b} \tag{A.66}$$

$$\mathbf{a} \wedge \mathbf{b} = -\mathbf{a} \cdot \mathbf{W}_\mathbf{b} \tag{A.67}$$

$$\boldsymbol{\nabla} \wedge \mathbf{a} = -\boldsymbol{\nabla} \cdot \mathbf{W}_\mathbf{a} \tag{A.68}$$

$$\boldsymbol{\nabla} \wedge \mathbf{a} = \boldsymbol{\nabla} \cdot \mathbf{W}_\mathbf{a}^T \tag{A.69}$$

$$\mathbf{a} \cdot \boldsymbol{\nabla} \wedge \mathbf{b} = \mathbf{W}_\mathbf{a} : \boldsymbol{\nabla}\mathbf{b} \tag{A.70}$$

$$\mathbf{a} \wedge \mathbf{A} = -\mathbf{W}_\mathbf{a} \cdot \mathbf{A} \tag{A.71}$$

$$\mathbf{A} \wedge \mathbf{a} = -\mathbf{A} \cdot \mathbf{W}_\mathbf{a} \tag{A.72}$$

$$\mathbf{a} \cdot (\mathbf{b} \wedge \mathbf{A}) = (\mathbf{a} \wedge \mathbf{b}) \cdot \mathbf{A} \tag{A.73}$$

$$(\mathbf{A} \wedge \mathbf{a}) \cdot \mathbf{b} = \mathbf{A} \cdot (\mathbf{a} \wedge \mathbf{b}) \tag{A.74}$$

$$(\mathbf{a} \wedge \mathbf{A}) \cdot \mathbf{b} = \mathbf{a} \wedge (\mathbf{A} \cdot \mathbf{b}) \tag{A.75}$$

$$\mathbf{a} \cdot (\mathbf{A} \wedge \mathbf{b}) = (\mathbf{a} \cdot \mathbf{A}) \wedge \mathbf{b} \tag{A.76}$$

$$\mathbf{a} \wedge (\mathbf{A} \wedge \mathbf{b}) = (\mathbf{a} \wedge \mathbf{A}) \wedge \mathbf{b} \tag{A.77}$$

$$\boldsymbol{\nabla} \wedge (\mathbf{A} \wedge \mathbf{a}) = \mathbf{A}(\boldsymbol{\nabla} \cdot \mathbf{a}) + (\mathbf{a} \cdot \boldsymbol{\nabla})\mathbf{A} - (\boldsymbol{\nabla} \cdot \mathbf{A}^T)\mathbf{a} - (\mathbf{A} \cdot \boldsymbol{\nabla})\mathbf{a} \tag{A.78}$$

## A.4 Operations with symmetric tensors S

$$\mathsf{S}_{ij} = \mathsf{S}_{ji} \tag{A.79}$$

$$\mathsf{dual}\,\mathbf{S} = 0 \tag{A.80}$$

$$\mathsf{Tr}\,\boldsymbol{\nabla} \wedge \mathbf{S} = 0 \tag{A.81}$$

## A.5 Operations with dyadics

$$[\mathbf{ab}]_{ij} = a_i b_j \tag{A.82}$$

$$(\mathbf{ab}) \cdot (\mathbf{cd}) = \mathbf{a}(\mathbf{b} \cdot \mathbf{c})\mathbf{d} \tag{A.83}$$

$$(\mathbf{ab}) \wedge \mathbf{c} = \mathbf{a}(\mathbf{b} \wedge \mathbf{c}) \tag{A.84}$$

$$\mathbf{a} \wedge (\mathbf{bc}) = (\mathbf{a} \wedge \mathbf{b})\mathbf{c} \tag{A.85}$$

$$(\mathbf{ab}) \wedge (\mathbf{cd}) = \mathbf{a}(\mathbf{b} \wedge \mathbf{c})\mathbf{d} \tag{A.86}$$

$$\mathbf{c} \wedge (\mathbf{a} \wedge \mathbf{b}) = \mathbf{c} \cdot (\mathbf{ba} - \mathbf{ab}) \tag{A.87}$$

$$\mathbf{c} \wedge (\mathbf{a} \wedge \mathbf{b}) = (\mathbf{ab} - \mathbf{ba}) \cdot \mathbf{c} \tag{A.88}$$

$$\mathsf{dual}\,(\mathbf{ab}) = \frac{1}{2}\mathbf{a} \wedge \mathbf{b} \tag{A.89}$$

$$\mathsf{dual}\,(\mathbf{ab} + \mathbf{ba}) = 0 \tag{A.90}$$

$$\mathsf{dual}\,(\mathbf{ab} - \mathbf{ba}) = \mathbf{a} \wedge \mathbf{b} \tag{A.91}$$

$$\mathbf{W_a} \cdot \mathbf{W_b} = \mathbf{ba} - (\mathbf{a} \cdot \mathbf{b})\mathbf{I} \tag{A.92}$$

$$[\boldsymbol{\nabla}\mathbf{a}]_{ij} = \frac{\partial}{\partial x_i} a_j \tag{A.93}$$

$$\mathbf{a} \cdot (\boldsymbol{\nabla}\mathbf{b}) = (\mathbf{a} \cdot \boldsymbol{\nabla})\mathbf{b} \tag{A.94}$$

$$\nabla(\alpha\mathbf{a}) = (\nabla\alpha)\mathbf{a} + \alpha\nabla\mathbf{a} \tag{A.95}$$

$$\nabla \cdot (\nabla\mathbf{a})^T = \nabla(\nabla \cdot \mathbf{a}) \tag{A.96}$$

$$\nabla \wedge (\nabla\mathbf{a}) = 0 \tag{A.97}$$

$$\nabla \wedge (\nabla\mathbf{a})^T = (\nabla\nabla \wedge \mathbf{a})^T \tag{A.98}$$

$$\nabla(\mathbf{a} \wedge \mathbf{b}) = (\nabla\mathbf{a}) \wedge \mathbf{b} - (\nabla\mathbf{b}) \wedge \mathbf{a} \tag{A.99}$$

$$\nabla \cdot (\mathbf{ab}) = (\nabla \cdot \mathbf{a})\mathbf{b} + (\mathbf{a} \cdot \nabla)\mathbf{b} \tag{A.100}$$

$$\nabla \wedge (\mathbf{ab}) = (\nabla \wedge \mathbf{a})\mathbf{b} - (\mathbf{a} \wedge \nabla)\mathbf{b} \tag{A.101}$$

$$[(\nabla\mathbf{a})^T - \nabla\mathbf{a}] \cdot \mathbf{b} = (\nabla \wedge \mathbf{a}) \wedge \mathbf{b} \tag{A.102}$$

$$\nabla \wedge (\mathbf{a} \wedge \mathbf{b}) = \nabla \cdot (\mathbf{ba} - \mathbf{ab}) \tag{A.103}$$

## A.6 Operations with the unit tensor $\mathsf{I}$

$$\mathsf{I} \cdot \mathbf{a} = \mathbf{a} \cdot \mathsf{I} = \mathbf{a} \tag{A.104}$$

$$\mathsf{I} \wedge \mathbf{a} = \mathbf{a} \wedge \mathsf{I} = -\mathsf{W}_\mathbf{a} \tag{A.105}$$

$$\mathbf{a} \wedge \mathbf{b} = (\mathsf{I} \wedge \mathbf{a}) \cdot \mathbf{b} \tag{A.106}$$

$$(\mathsf{I} \wedge \mathbf{a})^2 = \mathbf{aa} - \mathsf{I} \tag{A.107}$$

$$(\mathsf{I} \wedge \mathbf{a})^3 = -\mathsf{I} \wedge \mathbf{a} \tag{A.108}$$

$$(\mathsf{I} \wedge \mathbf{a})^4 = \mathsf{I} - \mathbf{aa} \tag{A.109}$$

$$(\mathsf{I} \wedge \mathbf{a})^5 = \mathsf{I} \wedge \mathbf{a} \tag{A.110}$$

$$(\mathbf{a} \wedge \mathbf{b}) \wedge \mathsf{I} = \mathbf{ba} - \mathbf{ab} \tag{A.111}$$

$$\mathbf{a} \wedge \mathbf{b} = (\mathsf{I} \wedge \mathbf{a}) \cdot \mathbf{b} \tag{A.112}$$

$$\mathbf{a} \wedge \mathbf{b} = \mathbf{a} \cdot (\mathsf{I} \wedge \mathbf{b}) \tag{A.113}$$

$$\mathsf{I} \cdot \mathsf{A} = \mathsf{A} \cdot \mathsf{I} = \mathsf{A} \tag{A.114}$$

$$\mathsf{I} : \nabla\mathbf{a} = \nabla \cdot \mathbf{a} \tag{A.115}$$

## A.7 Operations with vectors, dyadics, and tensors that use the position vector

### A.7.1 Operations with one position vector

$$\nabla \cdot \mathbf{x} = \mathcal{N} \tag{A.116}$$

$$\nabla \wedge \mathbf{x} = 0 \tag{A.117}$$

$$\nabla \mathbf{x} = \mathbf{I} \tag{A.118}$$

$$\nabla \cdot (\alpha \mathbf{x}) = \mathbf{x} \cdot \nabla \alpha + \mathcal{N} \alpha \tag{A.119}$$

$$\nabla (\alpha \mathbf{x}) = (\nabla \alpha)\mathbf{x} + \alpha \mathbf{I} \tag{A.120}$$

### A.7.2 Operations with one arbitrary vector and one position vector

$$\nabla \cdot (\mathbf{x} \wedge \mathbf{a}) = -\mathbf{x} \cdot (\nabla \wedge \mathbf{a}) \tag{A.121}$$

$$\nabla \cdot (\mathbf{a} \wedge \mathbf{x}) = \mathbf{x} \cdot (\nabla \wedge \mathbf{a}) \tag{A.122}$$

$$\nabla \wedge (\alpha \mathbf{x}) = (\nabla \alpha) \wedge \mathbf{x} \tag{A.123}$$

$$\nabla \wedge (\mathbf{x} \wedge \mathbf{a}) = \mathbf{x}(\nabla \cdot \mathbf{a}) - (\mathcal{N} - 1)\mathbf{a} - (\mathbf{x} \cdot \nabla)\mathbf{a} \tag{A.124}$$

$$\nabla (\mathbf{x} \cdot \mathbf{a}) = (\mathbf{x} \cdot \nabla)\mathbf{a} + \mathbf{a} + \mathbf{x} \wedge (\nabla \wedge \mathbf{a}) \tag{A.125}$$

$$\nabla (\mathbf{x} \cdot \mathbf{a}) = \mathbf{a} + (\nabla \mathbf{a}) \cdot \mathbf{x} \tag{A.126}$$

$$(\nabla \mathbf{a}) \cdot \mathbf{x} = (\mathbf{x} \cdot \nabla)\mathbf{a} + \mathbf{x} \wedge (\nabla \wedge \mathbf{a}) \tag{A.127}$$

$$(\mathbf{a} \wedge \nabla) \wedge \mathbf{x} = -2\mathbf{a} \tag{A.128}$$

$$\nabla (\mathbf{x} \cdot \mathbf{a}) = (\mathbf{x} \wedge \nabla) \wedge \mathbf{a} + \mathbf{x} \nabla \cdot \mathbf{a} + (\mathcal{N} - 2)\mathbf{a} \tag{A.129}$$

$$\nabla \wedge (\mathbf{a} \wedge \mathbf{x}) = 2\mathbf{a} - \mathbf{x} \wedge (\nabla \wedge \mathbf{a}) + (\mathbf{x} \wedge \nabla) \wedge \mathbf{a} \tag{A.130}$$

$$\nabla (\mathbf{x} \wedge \mathbf{a}) = \mathbf{I} \wedge \mathbf{a} - (\nabla \mathbf{a}) \wedge \mathbf{x} \tag{A.131}$$

$$\nabla \cdot (\mathbf{a}\mathbf{x}) = (\nabla \cdot \mathbf{a})\mathbf{x} + \mathbf{a} \tag{A.132}$$

$$\nabla \cdot (\mathbf{x}\mathbf{a}) = \mathcal{N}\mathbf{a} + (\mathbf{x} \cdot \nabla)\mathbf{a} \tag{A.133}$$

$$\nabla \cdot (\mathbf{x}\mathbf{a} - \mathbf{a}\mathbf{x}) = \nabla \wedge (\mathbf{a} \wedge \mathbf{x}) \tag{A.134}$$

$$\nabla \cdot (\mathbf{x}\mathbf{a} + \mathbf{a}\mathbf{x}) = 2\mathbf{a} + 2(\nabla \cdot \mathbf{a})\mathbf{x} + \nabla \wedge (\mathbf{a} \wedge \mathbf{x}) \tag{A.135}$$

$$\mathbf{x} \wedge (\boldsymbol{\nabla} \wedge \mathbf{a}) = (\mathcal{N} - 1)\mathbf{a} + \boldsymbol{\nabla}(\mathbf{x} \cdot \mathbf{a}) - \boldsymbol{\nabla} \cdot (\mathbf{x}\mathbf{a}) \tag{A.136}$$

$$\mathbf{x} \wedge (\boldsymbol{\nabla} \wedge \mathbf{a}) = (\mathcal{N} - 2)\mathbf{a} + \boldsymbol{\nabla}(\mathbf{x} \cdot \mathbf{a}) - \boldsymbol{\nabla} \wedge (\mathbf{a} \wedge \mathbf{x}) - (\boldsymbol{\nabla} \cdot \mathbf{a})\mathbf{x} \tag{A.137}$$

$$\boldsymbol{\nabla} \wedge [\mathbf{x} \wedge (\boldsymbol{\nabla} \wedge \mathbf{a})] = -(\mathcal{N} - 1)\boldsymbol{\nabla} \wedge \mathbf{a} - (\mathbf{x} \cdot \boldsymbol{\nabla})\boldsymbol{\nabla} \wedge \mathbf{a} \tag{A.138}$$

### A.7.3 Operations with two arbitrary vectors and one position vector

$$\boldsymbol{\nabla} \cdot [(\mathbf{a} \wedge \mathbf{b})\mathbf{x}] = [(\mathbf{x} \cdot \boldsymbol{\nabla})\mathbf{a}] \wedge \mathbf{b} + \mathbf{a} \wedge [(\mathbf{x} \cdot \boldsymbol{\nabla})\mathbf{b}] + \mathcal{N}\mathbf{a} \wedge \mathbf{b} \tag{A.139}$$

$$\boldsymbol{\nabla} \cdot [(\mathbf{a} \wedge \mathbf{b})\mathbf{x}] = [(\boldsymbol{\nabla} \wedge \mathbf{a}) \cdot \mathbf{b} - \mathbf{a} \cdot (\boldsymbol{\nabla} \wedge \mathbf{b})]\mathbf{x} + \mathbf{a} \wedge \mathbf{b} \tag{A.140}$$

$$(\mathbf{a} \cdot \boldsymbol{\nabla})(\mathbf{x} \wedge \mathbf{b}) = \mathbf{a} \wedge \mathbf{b} + \mathbf{x} \wedge (\mathbf{a} \cdot \boldsymbol{\nabla})\mathbf{b} \tag{A.141}$$

### A.7.4 Operations with one arbitrary vector and two position vectors

$$\boldsymbol{\nabla} \cdot (\mathbf{x}\mathbf{x}) = (\mathcal{N} + 1)\mathbf{x} \tag{A.142}$$

$$\mathbf{x} \cdot [\boldsymbol{\nabla}(\mathbf{x} \wedge \mathbf{a})] = \mathbf{x} \wedge \mathbf{a} + \mathbf{x} \wedge (\mathbf{x} \cdot \boldsymbol{\nabla}\mathbf{a}) \tag{A.143}$$

$$\boldsymbol{\nabla} \cdot [\mathbf{x}(\mathbf{x} \wedge \mathbf{a})] = (\mathcal{N} + 1)(\mathbf{x} \wedge \mathbf{a}) + \mathbf{x} \wedge (\mathbf{x} \cdot \boldsymbol{\nabla}\mathbf{a}) \tag{A.144}$$

$$\boldsymbol{\nabla} \cdot [(\mathbf{x} \wedge \mathbf{a})\mathbf{x}] = (\mathbf{x} \wedge \mathbf{a}) - (\mathbf{x} \cdot \boldsymbol{\nabla} \wedge \mathbf{a})\mathbf{x} \tag{A.145}$$

$$\mathbf{x} \wedge [\boldsymbol{\nabla} \wedge (\mathbf{x} \wedge \mathbf{a})] = -(\mathcal{N} - 1)\mathbf{x} \wedge \mathbf{a} - \mathbf{x} \wedge (\mathbf{x} \cdot \boldsymbol{\nabla}\mathbf{a}) \tag{A.146}$$

$$\mathbf{x} \wedge [\boldsymbol{\nabla} \wedge (\mathbf{x} \wedge \mathbf{a})] = (\mathcal{N} - 1)\mathbf{x} \wedge \mathbf{a} - \boldsymbol{\nabla} \cdot [\mathbf{x}(\mathbf{x} \wedge \mathbf{a})] \tag{A.147}$$

$$\mathbf{x} \wedge [\boldsymbol{\nabla} \wedge (\mathbf{x} \wedge \mathbf{a})] = 2\mathbf{x} \wedge \mathbf{a} - \boldsymbol{\nabla} \cdot [\mathbf{x}(\mathbf{x} \wedge \mathbf{a})] \tag{A.148}$$

$$\boldsymbol{\nabla} \wedge [(\mathbf{x} \wedge \mathbf{a}) \wedge \mathbf{x}] = \mathcal{N}\mathbf{x} \wedge \mathbf{a} + (\mathbf{x} \cdot \boldsymbol{\nabla} \wedge \mathbf{a})\mathbf{x} + \mathbf{x} \wedge (\mathbf{x} \cdot \boldsymbol{\nabla}\mathbf{a}) \tag{A.149}$$

$$\boldsymbol{\nabla} \wedge [(\mathbf{x}\mathbf{x}) \cdot \mathbf{a}] = (\mathbf{x} \cdot \boldsymbol{\nabla}\mathbf{a}) \wedge \mathbf{x} + \mathbf{a} \wedge \mathbf{x} - \mathbf{x} \wedge [\mathbf{x} \wedge (\boldsymbol{\nabla} \wedge \mathbf{a})] \tag{A.150}$$

### A.7.5 Operations with tensors and one position vector

$$\boldsymbol{\nabla} \cdot (\mathbf{S} \wedge \mathbf{x}) = -\mathbf{x} \wedge (\boldsymbol{\nabla} \cdot \mathbf{S}) \tag{A.151}$$

$$\boldsymbol{\nabla} \cdot (\mathbf{W} \wedge \mathbf{x}) = -2\mathbf{w} + \mathbf{x} \wedge (\boldsymbol{\nabla} \wedge \mathbf{w}) \tag{A.152}$$

$$\boldsymbol{\nabla} \cdot (\mathbf{x} \wedge \mathbf{A}) = -\mathbf{x} \cdot (\boldsymbol{\nabla} \wedge \mathbf{A}) \tag{A.153}$$

# Bibliography

These references are listed as footnotes in the text.


Aris R., *Vectors, tensors, and the basic equations of fluid mechanics*, Dover, 1962.

Batchelor G. K., *An introduction to fluid dynamics*, Cambridge University Press, 1967.

Burgatti P., *Bolletino della Unione Matematica Italiana*, **10** (1931) 1-5.

Candel S.: *Mécanique des fluides*, Dunod, 1990.

Dimotakis P., *Laser Doppler velocimetry momentum defect measurements of cable drag at low to moderate Reynolds numbers*, NCBC Report R541, 1977.

Gharib M., lecture notes from *Fluid mechanics in Nature*, Ae 240, Caltech, 1997.

Hammache M. & Gharib M., An experimental study of the parallel and oblique vortex shedding from circular cylinders, *Journal of Fluid Mechanics* **232** (1991) 567-590.

Henderson R. D., Details of the drag curve near the onset of vortex shedding, *Physics of Fluids* **7** (1995) 2102-2104.

Koumoutsakos P. & Leonard A., High-resolution simulations of the flow around an impulsively started cylinder using vortex methods, *Journal of Fluid Mechanics* **296** (1995) 1-38.

Lamb H., *Hydrodynamics*, Dover, 1945.

Leonard A., Computing incompressible flows with vortex elements, lecture notes from *Numerical methods in fluid mechanics*, Ae 232, Caltech, 1989.

Leonard A., *Particle methods in fluid mechanics*, Ecole d'été d'analyse numérique, Le Breau sans Nappe, France, 1987.

Lighthill M. J., Waves and hydrodynamic loading, *Proc. Int. Conf. Behav. Off-Shore Struct.*, 2nd, **1** (1979) 1.

Lin J. C. & Rockwell D., Force identification by vorticity fields: techniques based on flow imaging, *Journal of Fluids and Structures* **10** (1996) 663-668.

Lisoski, D. L. A., *Nominally 2-dimensional flow about a normal flat plate*, PhD Thesis, California Institute of technology, 1993.

Moreau J. J., Bilan dynamique d'un écoulement rotationnel, *J. Math. Pures Appl.* **32** (1953) 1-78.

Noca F., Shiels D., & Jeon D., Measuring instantaneous fluid dynamic forces on bodies, using only velocity fields and their derivatives, *Journal of Fluids and Structures*, in press, 1997.

Saffman P.E., *Vortex dynamics*, Cambridge University Press, 1993.

Schlichting H., *Boundary Layer Theory*, McGraw Hill, 1987.

Shiels D., *Ae 200 Report*, California institute of Technology, Spring 1996.

Slaouti A. & Gerrard J. H., An experimental investigation of the end effects on the wake of a circular cylinder towed through water at low Reynolds number, *Journal of Fluid Mechanics* **112** (1981) 297-314.

Szepessy S. & Bearman P. W., Aspect ratio and end plate effects on vortex shedding from a circular cylinder, *Journal of Fluid Mechanics* **234** (1992) 191-217.

Thomson J. J., *On the motion of vortex rings*, Adams prize Essay, London, 1883.

Truesdell C., *Kinematics of vorticity*, Indiana University Press, 1954.

Willert C. & Gharib M., Digital Particle Image Velocimetry, *Experiments in Fluids* **10** (1991) 181-193.

Williamson C. H. K., Oblique and parallel modes of vortex shedding in the wake of a circular cylinder at low Reynolds numbers, *Journal of Fluid mechanics* **206** (1989) 579-627.

Williamson C. H. K. & Roshko A., Vortex formation in the wake of an oscillating cylinder, *Journal of Fluids and Structures* **2** (1988) 355.

Wu J. Z. & Wu J. M., Vorticity dynamics on boundaries, *Advances in Applied Mechanics* **32** (1996) 119-275.